November 2018

Investigating the Role of Topological Frustration on Morphology of Novel Multiblock Copolymers

Rohit Gupta

Investigating the Role of Topological Frustration on Morphology of Novel Multiblock Copolymers

A Dissertation Presented

By

ROHIT GUPTA

SUBMITTED TO THE GRADUATE SCHOOL OF THE

UNIVERSITY OF MASSACHUSETTS IN PARTIAL FULLFILLMENT

OF THE DEGREE REQUIREMENTS FOR THE DEGREE OF

DOCTOR OF PHILOSOPHY

September 2018

Polymer Science and Engineering

Investigating the Role of Topological Frustration on Morphology of Novel Multiblock Copolymers

A Dissertation Presented

By

ROHIT GUPTA

Approved as to style and content by:

_____

E. Bryan Coughlin, Chair

_____

Samuel P. Gido, Member

_____

Jonathan P. Rothstein, Member

_____

E. Bryan Coughlin, Head

Polymer Science and Engineering

DEDICATION

To my parents and my wife for their unconditional love and support throughout this journey

ACKNOWLEDGMENTS

I would like to express my deepest gratitude to my advisor Prof. E. Bryan Coughlin for his continuous guidance and support throughout these five years. He has been someone who always listened patiently to my all problems and gave the best advice possible. I will always be grateful for his encouragement, advise and trust during my Ph.D. especially during my cumulative exams. He has been a great advisor who has been inspiring both professionally and personally, and has helped me become a better scientist and most importantly a better person in life.

I would like to acknowledge Prof. Samuel P. Gido for serving on my committee and providing constructive suggestions and comments on my work especially the morphology section of my thesis. I thank Prof. Jonathan Rothstein for his guidance and helpful suggestions in designing experiments and analyzing my data.

My sincere gratitude to Dr. Alex Ribbe for his helping me analyze my TEM samples and patiently answering all my morphology questions. I thank my collaborators Dr. Mayank Mishra and Prof. Fernando Escobedo for helping me with the computational simulations. I feel privileged for collaborating with Professors Edwin Ned Thomas and Prof. Greg Grason, from whom I have learned a lot about block copolymers in general. I would also like to acknowledge the faculty and staff in the Polymer Science and Engineering Department for their excellent teaching, insight and advice.

I appreciate the help provided by Louis Raboin with the microtoming and TEM and Dr. Sekar Dhanasekaran for his initial help with X-ray and AFM facilities. I thank Dr. Weiguo for the NMR training and Dr. Stephen Eyles and Rinat Abzalimov for teaching and performing mass spectroscopy experiments. Special Thanks to Lisa Groth, Maria Farrington and Jessica Skrocki for being so kind and helpful with all the administrative work.

I would like to thank my undergraduate advisors Prof. Savita Ladage, Prof. Lakshmy Ravishankar, DR. G.S.S. Rao and Dr. Dawid D'Mello for introducing the idea of research to me and motivating me to pursue chemistry. They had been the most inspiring persons I have ever seen in Science and I am thankful that I got to learn from you.

I would like to thank all the past group members Dr. Huseyin Tas, Dr. Kinkini Roy, Dr. Xiaohui Liu, Dr. Chya-Yan Liaw, Dr. Ying Jin, Dr. Wenxu Zhang, Dr. Brian Cromer, Dr. Patrick Homyak, Dr. Piril Ertem, Dr. Haomiao Yuan and Katie Williams who have taught me different lab techniques and helped me solve all my experimental problems. I thank all the current group members; Dr. Chinumso Nwosu, my lunch partner- Joshua Enokida, Ria Ghosh and the three "Kids" – Christian, Huyen and Yifeng who have made the group full of fun and lively. I will miss our Friday group lunches and the Ramen Tuesdays. It was great sharing everything with you guys and I will dearly miss each one of you.

I would like to thank all my friends in and out of the department, particularly the Class of 2013. Special thanks to Hyeyoung, Satyan and Di for their continuous support and friendship as we traveled this journey together and shared many difficulties and accomplishments.

I cherish the good times that I had with all my friends in Amherst and across the world, especially Parijat, Amit, Gyan and Anurag who have patiently listened to all my frustration and always gave the energy and motivation to continue working towards my Ph.D.

I would like to express my gratitude to my family; my mother, father, and my sister for all the for believing in me and supporting all my decisions throughout this journey. I sincerely hope that I have made you proud. Lastly, I would like to thank my girlfriend and now my wife, Puja for the unconditional love and support you have given me. Thank you for always standing by me through thick and thin and it would not have been possible without you.

ABSTRACT

INVESTIGATING THE ROLE OF TOPOLOGICAL FRUSTRATION ON MORPHOLOGY OF NOVEL MULTIBLOCK COPOLYMERS

SEPTEMBER 2018

ROHIT GUPTA

B.S., INDIAN INSTITUTE OF SCIENCE EDUCATION AND RESEARCH, KOLKATA

M.S., INDIAN INSTITUTE OF SCIENCE EDUCATION AND RESEARCH, KOLKATA

M.S., UNIVERSITY OF MASSACHUSETTS AMHERST

Ph.D., UNIVERSITY OF MASSACHUSETTS AMHERST

Directed by: Professor E. Bryan Coughlin

Multiblock copolymers have gained considerable attention due to their ability to offer immense potential for designing soft materials with complex architectures for diverse applications. The enlarged parameter space offered by these multiblock copolymers gives access to a wide variety of multiply continuous morphologies which can be used to produce highly ordered nanostructures. The investigation on multiblock copolymers has been subjected to two critical limitations: (i) A suitable synthetic strategy for accessing these structures and (ii) computational tools which can help in application driven design of these molecules. In this dissertation, the goal was to develop methodologies for the synthesis of multiblock copolymers with different architectures and understand how the variations in molecular architecture can influence macromolecular self-assembly.

In chapter 2, the concept of single molecule insertion (SMI) for precise insertion of functional molecules is presented. The molecule precisely inserts once within the polymer chain with high chain fidelity and provides functionalities for post-insertion modifications. A series of molecules

satisfying the criteria for SMI based on their reactivity ratios with styrene and methyl methacrylate were examined and used to synthesize a series of multiblock polymers with complex architectures. In chapter 3, a highly efficient synthetic methodology for synthesis of graft copolymers which lie along the continuum of a 3-arm star and A-B-C linear triblock copolymer has been described. The morphological characterization of the synthesized continuum graft copolymers is performed using SAXS, TEM, and DPD simulations. Interesting morphologies are observed for these continuum copolymers and projects them as interesting candidates to access new morphologies. Contrary to most of the work done on block copolymers, these structures are novel as their morphologies can be tuned keeping the φ and χ constant. This study helps in understanding of the effect of polymer architecture on the phase behavior of these graft copolymers and provides a novel pathway to tune the block copolymer morphologies.

In chapter 4, a series of PMMA-*b*-PtBS-*b*-P2VP and PtBA-*b*-PtBS-*b*-P2VP triblock copolymers with extending P2VP arm has been synthesized. The study helps in extending the concept of high χ-low N block copolymer system from diblock to triblock copolymers. The morphologies of the synthesized triblock copolymers were characterized using SAXS and TEM and morphologies with multiple domains and smaller feature size were observed. Also, the effect of extending chain length of P2VP arm on the phase diagram on these highly frustrated triblock copolymer systems was studied and the observed morphologies using SAXS and TEM were mapped with the theoretical predictions.

TABLE OF CONTENTS

Page

LIST OF TABLES

LIST OF FIGURES

Figure Page

LIST OF ABBREVIATIONS

^{o}C	degree Celsius
Đ	Molecular Weight Dispersity, Mw/Mn
δ	Chemical shift
χ	Flory-Huggins Parameter
φ	Volume Fraction
ω	Graft position
2VP	2-Vinylpyridine
4VP	4-Vinylpyridine
AA	Allyl Alcohol
AIBN	2,2′-Azobis(2-methylpropionitrile)
ATRP	Atom Transfer Radical Polymerization
BCPs	Block Copolymer
CTA	Chain Transfer Agent
DM	Dimethyl Malonate
DPD	Dissipative Particle Dynamics
d-spacing	Domain Spacing
DCC	N,N'-Dicyclohexylcarbodiimide
DCM	Dichloromethane
DMAP	4-Dimethylaminopyridine
DMF	N,N-Dimethylformamide
equiv.	Molar equivalent
ESI-MS	Electrospray Ionization Mass Spectroscopy

GPC	Gel Permeation Chromatography
kg	Kilogram
M	Molecular Mass
MeOH	Methanol
mg	Milligram
mL	Milliliter
Mn	Number average molecular weight
mmol	Millimole
mol	Mole
MD	Molecular Dynamics
MS	Mass Spectroscopy
MW	(Number Average) Molecular Weight
Mw	Weight Average Molecular Weight
mPEG	Methyl Ether Terminated Poly Ethylene Glycol
MMA	Methyl Methacrylate
Nor-An	Norbornene Anhydride
N	Degree of Polymerization
nm	Nanometer
NMR	Nuclear Magnetic Resonance Spectroscopy
NMP	Nitroxide Mediated Polymerization
ODT	Order-to-Disorder Transition
PFPMI	Pentaflurophenyl Maleimide Ester
PEG	Poly(Ethylene Glycol)

PMDETA	N,N,N’,N”,N”-Pentamethyldiethylenetriamine
PMMA	Poly(Methyl Methacrylate)
ppm	Parts Per Million
PS	Polystyrene
q	Scattering Wave Factor
RAFT	Reversible Addition-Fragmentation Chain Transfer Radical Polymerization
SCFT	Self-Consistent Field Theory
SMI	Single Molecule Insertion
SAXS	Small Angle X-ray Scattering
tBA	t-Butyl Acrylate
tBS	*t*-Butyl Styrene
TEM	Transmission Electron Microscopy
Tg	Glass transition temperature
THF	Tetrahydrofuran

CHAPTER I

INTRODUCTION

1.1 Block Copolymers

Block copolymers (BCPs) have drawn significant attention in past few decades for their wide variety of applications, such as ultrafiltration,[1] drug delivery,[2] photolithography,[3] high density storage media,[4] energy conversion[5], scaffolds and templates to fabricate nanostructured materials[4] and advanced plastics.[6] The most distinguishing characteristics of block copolymers, which are responsible for their aforementioned potential applications is the ability of the two incompatible blocks to spontaneously segregate into self-assembled structures with controllable dimensions and functionalities. The versatility of block copolymers in terms of their compositional variation, architecture, and the choice of monomers can lead to dramatic changes in self-assembly and allows us to tailor their mechanical, electrical, optical and other physical properties based on the targeted application.[7–9]

1.2 Introduction to Diblock Copolymers

The simplest and most studied architecture for block copolymers is the linear A-B diblock, consisting of a long sequence of type A monomers covalently bonded to a chemically incompatible chain of type B monomers. The phase behavior, or self –assembly, of A-B diblock copolymers is dependent on three experimentally controllable factors: the overall degree of polymerization ($\boldsymbol{N}$), or the volume fraction of the A component ($\boldsymbol{\varphi_A}$) and the Flory-Huggins interaction parameter $\boldsymbol{\chi_{AB}}$ between the monomers A and B. The regulation of the first two factors can be achieved through

the polymerization stoichiometry, whereas the magnitude of χ is determined by the selection of the A-B monomer pair.

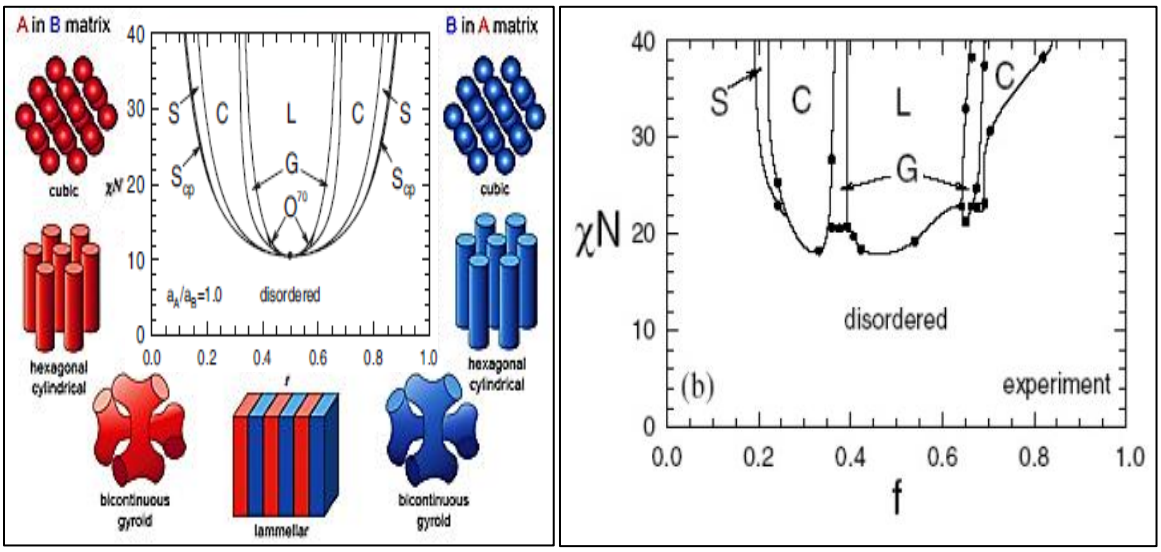

Figure 1.1: The generic phase diagram and typical micro-phase separated morphologies of a diblock copolymer (from references 8,10–12).

Based on the χN value, the phase diagram is divided into three different regimes: the weak segregation limit, the intermediate segregation limit and the strong segregation limit.[13] For values of χN < 10.5, the interactions between the two blocks is weak and non- favorable and the block copolymer is in the disordered state. In the *WSL*, the block copolymer is microphase separated with the period of the microstructure **(D**) formed dependent on **N** as $\mathbf{D \sim N^{1/2}}$ and is independent of the interaction parameter χ. The Flory- Huggins interaction parameter χ is inversely proportional to temperature (**T**); as the temperature decreases, χ increases and BCP enters into the *ISR* and can microphase separate better with $\mathbf{D \sim N^{1/3}}$. On further decreasing the temperature, the BCP enters into the *SSL* where the individual blocks stretch at the interface to minimize contact between the segments of each block, with the microdomain period **(D)** dependent on **N** and χ *as* $\mathbf{D \sim N^{2/3}\chi^{1/6}}$.[9,13]

Depending on the overall volume fraction of the component A ($\boldsymbol{\varphi_A}$) and the product $\boldsymbol{\chi_{AB}N}$ (which is the measure of the incompatibility between the two blocks), the diblock copolymer can self-assemble into different ordered microstructures with a domain spacing ranging from 10-100 nm.[7–9] The different equilibrium morphologies observed are lamellae, hexagonally packed cylinders, body-centered cubic or complex bicontinous gyroid morphologies and orthorhombic phase with Fddd symmetry (O^{70}) as shown in Figure 1.[9,12,14,15] On increasing volume fraction of one block, the BCP can undergo phase transition to form different morphologies with the inversion of major and minor components for $\boldsymbol{\varphi_A}$>0.5. These morphologies are primarily governed by the balance between enthalpic contributions from the incompatibility between two blocks and the translational and conformational entropy of the two chains.[9]

Various methods have been used to manipulate the bulk and thin morphologies of block copolymers. The most common and effective way of inducing a BCP phase transition in bulk films is by changing the annealing temperature. With increase in temperature most BCPs undergo order-to-disorder transition (ODT), due to decrease the segmental interactions and when the value of $\boldsymbol{\chi_{AB}N}$ decreases below 10.5, a disordered state is achieved.[6,9,14] On further increase in temperature, the entropic forces tend to dominate the phase behavior as the thermal expansion and compressibility effects come into play and the BCPs remain in the disordered state.

Unlike in bulk films, the interfacial interactions of the two blocks, surface energy and the commensurability between the film thickness (h) and the natural period of the micro domain morphology (L_o) are important factors which governs the thin film morphology in BCPs.[16] Several techniques such solvent annealing,[17] thermal annealing,[18] electro-magnetic fields,[19] shear,[20] zone-annealing,[21] and topographically and/or chemically patterned substrates, have been reported to manipulate BCPs thin film morphologies[22–26] for specific applications. Among all the above

mentioned methods, solvent and thermal annealing are most widely used since they can be easily combined with other external forces for synergetic effects.

1.3 General Introduction to Multiblock Copolymers

As discussed in the earlier section, linear A-B diblock copolymers have been most extensively investigated and detailed experimental and theoretical understanding of their bulk and solution phase behavior has been achieved. On extension of linear diblock copolymers to linear alternating multiblock copolymers (ABA, ABABA, etc.), substantial enhancement in the physical properties such as elasticity and fracture toughness has been reported without significantly influencing the associated phase behavior.[27] It has been recognized that linear diblock copolymers and alternating multiblock copolymers can typically adopt four equilibrium microphase structures (lamellae, gyroid, cylinders, and spheres) in the ordered state depending on their composition and chemical interaction. None of these morphologies expect the gyroid morphology have multiple domains that continuously percolate across the specimen in three dimensions. A multiply continuous, percolating domain structure would provide physical attributes which can be utilized for wide variety of technological applications.

By means of incorporating more chemically distinct blocks into a chain, or adapting unique properties such as chiral, crystalline or rod-like structures for one of the block; can offer unparalleled opportunities for designing new nanostructured materials with enhanced functionality and properties.[8] The complexity of block copolymers can be greatly enlarged in different ways, including increasing the number of blocks (n) (A_nB_n type block copolymers), bonding chemically distinct blocks (A-B-C type triblock copolymers) and introducing a certain type of branching (cyclic, graft-type, H-type and star-shaped, miktoarm block copolymers *etc.*).[28] Figure 2 shows the

different architectures which can achieved by increasing the number of blocks and the chemical distinctiveness of each block.

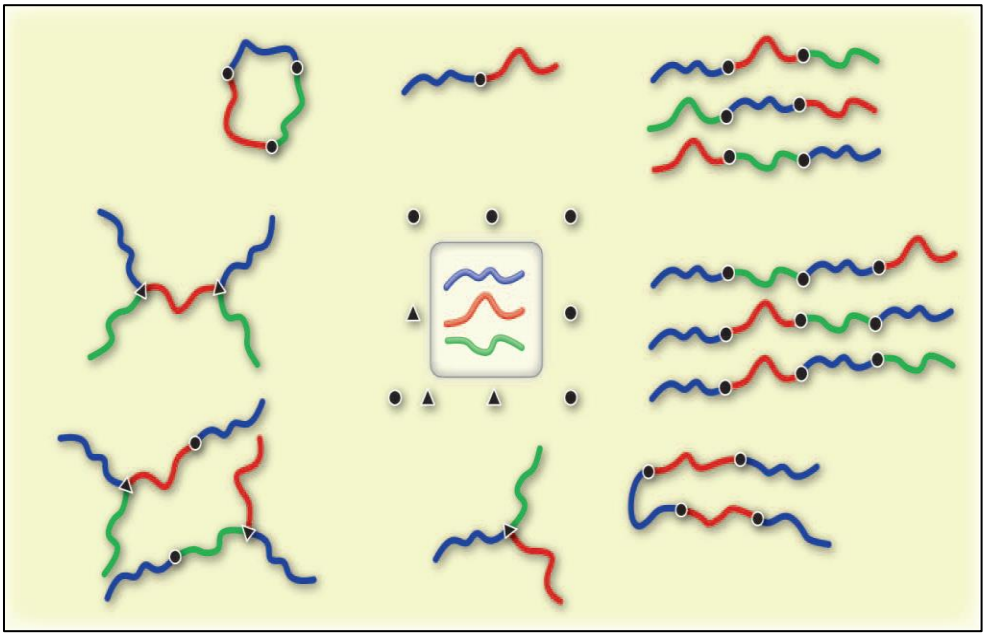

Figure 1. 2: Structural complexity of block copolymers by varying the number of blocks and the functionality of the connector at each block-block juncture (difunctional, circles; trifunctional, triangles) (taken from reference 29).

Multiblock copolymers displaying different multiply continuous morphologies can find their use in variety of applications.[30] Multiply continuous morphology has a major advantage from a mechanical property standpoint as it permits each domain to contribute directly to the modulus of the material which can significantly improve toughness, stress at failure, and creep resistance of the material.[31,32] These multi-domain structures have high interfacial area per specimen volume which can be used in gas separation membranes, the separation and extraction of excitons in solar cells to improve the overall cell efficiency.[33–38] Percolating domain structures can be strong candidates for materials used in water purification. A good example for this application includes the use of poly(lactic acid-dimethylacrylamide-styrene) triblock copolymers forming aligned cylinders as water filtration membranes.[39,40] The advantage of using the percolating domains of multiply continuous morphologies is them being less likely to terminate at the grain boundaries

and therefore does not require any alignment. This helps in minimizing the dead end pores which in turn maximizes the flux through the membrane.[41] Various 3-D structures observed for multiblock copolymers can be applied to significantly enhance the conductivity in different energy applications such as fuel cells and batteries.[42] In addition to these applications, these multiple domain morphologies has been found to play an important role in the emerging technology of 3-D photonic crystals.[43,44]

1.3.1 Linear Triblock Copolymers

By adding another component, block C to A-B diblock copolymer produces A-B-C triblock copolymers. The study of A-B-C triblock copolymers becomes challenging as the synthesis of triblock copolymers with high chemical purity is difficult using sequential living polymerization. These techniques yield triblock copolymers with possible containments such as homopolymers and diblock copolymer byproducts. Apart from the synthetic challenge, the number of parameters which defines the microphase separation of the triblock copolymers increases considerably by the addition of the third component C. In comparison to diblock copolymers, where the morphology is mainly controlled by the volume fraction of one block and the interaction parameter between the two blocks; the morphology of triblock copolymers is critically affected by different factors such as the independent volume fractions of two blocks, three different interaction parameters and the sequence of the three blocks.[45] This enlarged parameter space of A-B-C triblock copolymers makes them a promising candidate for exploring a range of intriguing nanostructures. In addition to these factors, different chain architecture i.e. linear, star,[46] or ring[47] can contribute significantly to the complex array of morphologies that can be observed for triblock copolymers system.

The simplest case of the A-B-C triblock is the A-B-C linear triblock copolymer. For this system, three different states are possible: one phase state (which is the disordered state for the A-B-C

system), two phase state (A/mixed BC, B/mixed AC and C/mixed AB, which is similar to a diblock system) and the three phase state with A, B and C forming different domains. Based on the relative strength of the interaction parameters between the three blocks, linear triblock copolymers are mainly divided into two classes: "frustrated" and "non-frustrated".[48] The classification refers to the 'non-frustrated' system if χ_{AC}, the interaction parameter between the two end-blocks is comparable or higher than the interaction parameter between the neighboring blocks i.e. χ_{AB} and χ_{BC}. Therefore, in this particular case the two end-blocks A and C phase separate and forms two distinct interfaces A/B and B/C. The other class refers to the 'frustrated' system, where χ_{AC} is much smaller than the interaction parameter of the neighboring blocks χ_{AB} and χ_{BC}. Thus, the triblock will tend to form structures with lower A/C interfacial energy than interfaces A/B and B/C. But since the formation of A/C interface is not commensurate with the chain topology, the system is 'frustrated'. The subtle balance between the benefit from interfacial energy and the energy penalty due to the topological chain constraints is primarily responsible for the complex non-equilibrium ordered phases formed, so as to relieve the topological frustration.

1.3.1.1 Frustrated Linear Triblock Copolymers

In the past decade, there has been a great deal of experimental reports on the spectrum of morphologies observed in frustrated triblock copolymer systems. Some of these systems includes: poly-(styrene-*b*-butylene-*b*-methyl methacrylate) (SBM),[49–55] poly-(styrene-*b*-ethylene-co-butylene-*b*-methyl methacrylate) (SEBM),[49–51,53–58] poly-(styrene-*b*-2-vinylpyridine-*b*-tert-butyl methacrylate) (SVT),[59–62] poly-(styrene-*b*-butadiene-*b*-caprolactone) (SBC)[63], poly-(isoprene-*b*-styrene-*b*-dimethyl siloxane)[38], poly-(styrene-*b*-isoprene-*b*-ethylene oxide)[64], poly-(styrene-*b*-butadiene-*b*-2-vinylpyridine)[65], poly-(styrene-*b*-isoprene-*b*-lactide)[66] and poly-(styrene-*b*-(ethylene-*alt*-propylene)-*b*-methyl methacrylate) (SEPM)[67]. All of these systems show more than

two dozen complex structures which includes helical, core-shell versions of gyroid, spheres, cylinders, structures-within-structure phases corresponding to three-domain lamellae (L_3), cylinders-within-lamellae (LC), spheres-within-lamellae, cylinders-on-cylinders, helices-on-cylinders, rings-on-cylinders, spheres-on-cylinder and spheres-on-spheres; cubic network phases, perforated structures, ladder morphology and knitting patterns. These complex phases are typical hierarchical structures because at least two lengths are required to characterize them. Some of the most interesting morphologies mentioned are shown in Figure 3, 4.

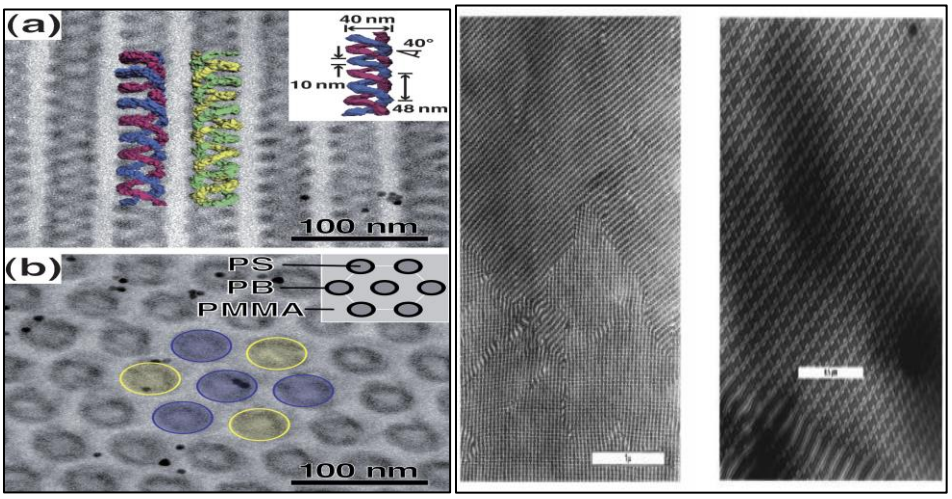

Figure 1. 3: TEM micrographs for (a) a double helical structure in PS-PB-PMMA triblock copolymers (images from reference 55)(b) knitting pattern observed for PS-PE-PMMA triblock copolymers (reproduced from reference 56).

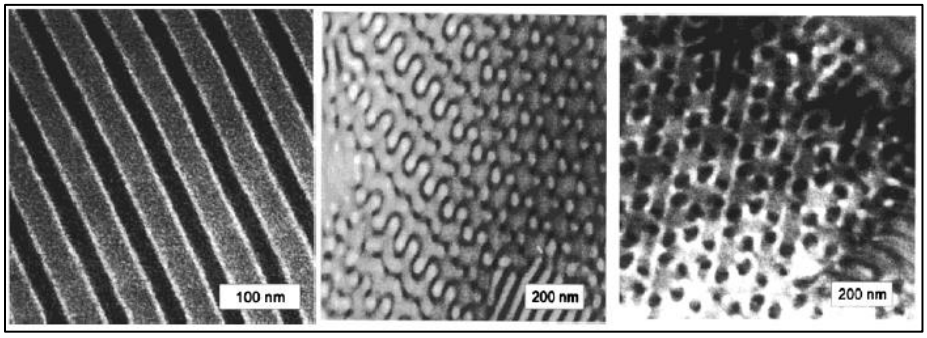

Figure 1. 4: Different morphologies observed for PS-PB-P2VP triblock copolymers (taken from reference 65).

The use of computer simulations can help predict and understand the phase behavior and morphology of complex block copolymer systems. In addition to experimental studies, the phase behavior of the frustrated A-B-C triblock copolymer system has been investigated using theoretical calculations and simulations. Using the strong segregation theory, Zheng and Wang studied the dependence of morphology on the sequence of the triblock chain and the relative strength of the various interaction parameters.[45] Most of the simulated morphologies were in agreement with the observed morphologies for the SEBM system, along with the prediction of three frustrated phases; cylinders within lamellae, spheres within lamellae and rings on cylinders. Using self-consistent mean field theory (SCFT) Tang and coworkers constructed the phase diagram for the possible 2D structures for the frustrated triblock copolymer system.[68] Since major theoretical studies were restricted to the 2D phase, Shi and coworkers expanded the phase diagram for the frustrated A-B-C linear triblock copolymer system using SCFT and predicted a number of new phases including the 2D knitting pattern and 3D gyroid with spheres.[69] Since the basis functions used in the construction of the phase diagram were limited, the accuracy of the phase boundaries obtained were imprecise. Later on, the study by Nagpal and coworkers predicted the bulk morphologies for both frustrated and non-frustrated A-B-C triblock copolymer systems in three dimensions using the coarse grain Monte Carlo (MC) simulations (Figure 5).[70] Some of these simulations were representative of the PS-PI-PMMA triblock copolymer system.

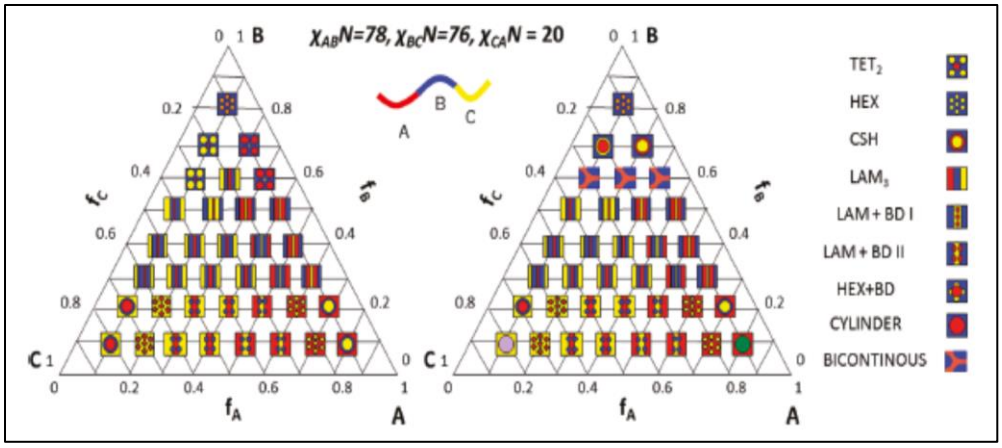

Figure 1. 5: Morphologies predicted for A-B-C linear triblock copolymers using SCFT (left) and by MC simulations (right) (reproduced from reference 70).

Using the full 3D psuedospectral method of SCFT, Shi and coworkers recently studied the phase behavior of super-cylinder forming A-B-C triblock copolymers.[71] They used SCFT to investigate the emergence, and stability, of the Knitting Pattern (KP) phase observed experimentally in SEBM system. They constructed the phase diagram for the frustrated triblock copolymer systems taking into account about 10 candidate structures as shown in Figure 6. Their study involved the investigation of the stable region of the KP phase with a uniform segment size considering the impact of the conformational parameters and the interaction asymmetry between neighboring blocks. They also examined the stability region of the KP phase when surrounded by LC, perforates lamellae (PL), L3, core-shell cylinders (CSC), perforated circular layer-on cylinders (PC), and quadruple cylinders-on cylinders (C4) phases for the SEBM model system.[48]

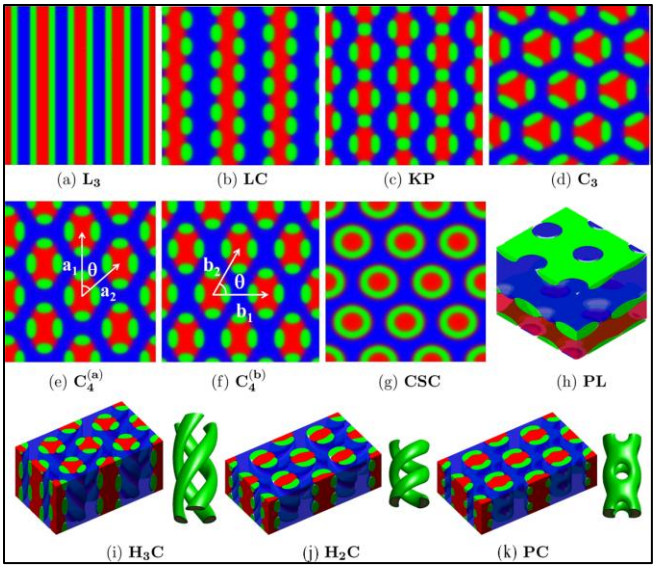

Figure 1. 6: Density iso-surface plots of morphologies formed by A-B-C linear triblock copolymers: (a) three-color lamellae (L_3), (b) cylinders-within-lamellae (LC), (c) knitting pattern (KP), (d) triple cylinders-on-cylinders (C_3), (e) and (f) quadruple cylinders-on cylinders ($C_4^{(a)}$ and C_4 $^{(b)}$, (g) core−shell cylinders (CSC), (h) perforated lamellae (PL), (i) triple helices-on-cylinders (H_3C), (j) double helices-on-cylinders (H_2C), and (k) perforated circular layer-on cylinders (PC). In C_4 $^{(a)}$ and C_4 $^{(b)}$, their basis vectors are indicated. The red, green, and blue colors denote the regions where the majority components are A, B, and C, respectively.(images taken from reference 48).

1.3.1.2 Non-Frustrated Linear Triblock Copolymers

Another class of triblock copolymers, is the non-frustrated A-B-C triblock copolymers which corresponds to the system with χ_{AC} being the largest/comparable with the other two interaction parameters χ_{AB} and χ_{BC}. Such systems typically form structures with no A/C interface with the observed morphologies being the core-shell versions of the diblock copolymers morphologies; including core-shell spheres, cylinders, gyroid, and lamellae. They are also known to show the alternating versions of the sphere, cylinder, and gyroid phases, in which the A and C domains form alternating equivalent sub-lattices within the B matrix. In addition, these systems also form two orthorhombic network phases (with space groups *Fddd* and *Pnna*).The experimental systems which belongs to this class of linear triblock copolymers include, poly-(butadiene-*b*-styrene-*b*-

vinylpyridine) (PB-PS-P2VP) (Figure 7),[72] poly-(methyl methacrylate-*b*-styrene-*b*-butadiene) (PMMA-PS-PB)[73], poly(isoprene-*b*-styrene-*b*-vinylpyridine) (PI-PS-P2VP)[74–77] (Figure 8), and poly(isoprene-*b*-styrene-*b*-ethylene oxide) (PI-PS-PEO)[78–80].

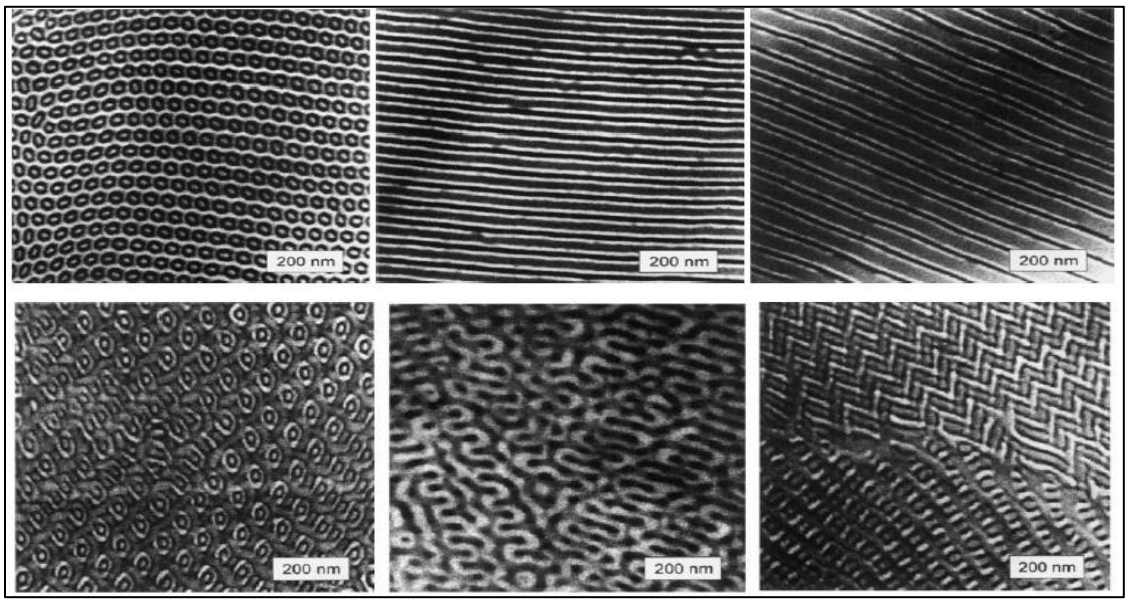

Figure 1. 7: TEM micrographs for different compositions of PS-PB-P2VP linear triblock copolymers (reproduced from reference 72).

Mogi, Matsushita and coworkers first demonstrated the systematic change in morphology for non-frustrated triblock copolymers from three phase four layer lamellae to alternating gyroid to tetragonally packed A and C cylinders in a B matrix and A and C spheres packed in *bcc* lattice embedded in B matrix with increasing PS volume fraction for the PI-PS-P2VP system (Figure 8). They also obtained the morphological phase diagram for the PI-PS-P2VP system and compared it to the PS-PI diblock copolymer system.[74–77] The other pioneering work on the non-frustrated A-B-C triblock copolymers is on the formation of network morphologies which was first demonstrated by Bates and coworkers for the PI-PS-PEO system[78–80]. Three different kinds of network morphologies have been reported for the A-B-C linear triblock copolymers; O^{70}, Q^{214} and Q^{230}. The notation is based on the crystallographic symmetry of the repeat units, in which O stands

for orthorhombic unit cell, Q stands for the cubic unit cell and the superscripts refer to the number of space group. Both Q^{214} and Q^{230} are related to the gyroid minimal surface and the two interconnected gyroids are embedded in the matrix of the major component, whereas in O^{70} there is a core shell network with one of the terminal block and the middle block are embedded in the other terminal block that is the major component. Later on, Cochran and Bates also identified a non-equilibrium network phase denoted as O^{52} for the hydrogenated PS-PB-PI system.[81] To understand the complex nature of these morphologies, multiple techniques such as Transmission Electron Microscopy (TEM), Small Angle X-ray Scattering (SAXS), rheology and computational calculations have been used to confirm their existence in different systems.[30]

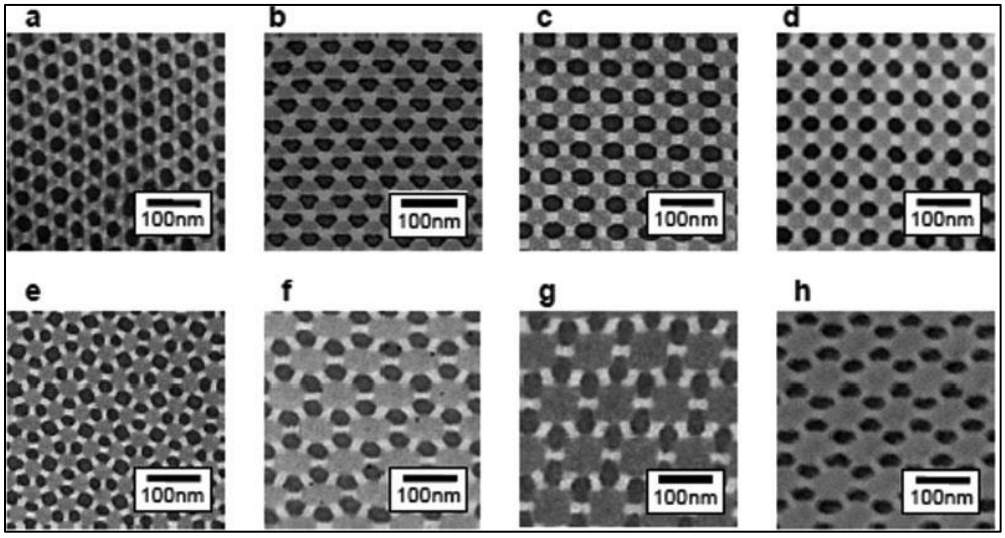

Figure 1. 8: Different morphologies observed for ISP system using TEM (images taken from reference 77).

Register and coworkers studied the extent of microphase separation in non-frustrated A-B-C linear triblock copolymers forming a "three domain, four-layer" lamellar morphology.[82] They particularly examined the extent of microphase separation between the B and C blocks, when the two blocks are sufficiently compatible and do not tend to microphase separate. It was noted that the A-block plays an important role in inducing the phase separation between the B and C blocks

and drives the localization of A−B block junction to the A−B lamellar interface. This was confirmed using both SAXS and distinct glass transitions observed for the B block at low B−C segregation strengths, and for both the B and C blocks at higher segregation strengths.

Recently, Mays and coworkers synthesized linear A-B-C triblock terpolymers containing poly(1,3-cyclohexadiene), PCHD, as an end-block and polystyrene (PS), polybutadiene (PB), and polyisoprene (PI) as the other blocks. They systematically characterized these terpolymer morphologies by varying the ratio of 1,2- /1,4-microstructures of poly(1,3-cyclohexadiene) and investigated the effect of conformational asymmetry on the microphase separation using SCFT calculations, TEM and SAXS.[83]

The experimental observations for the non-frustrated linear A-B-C triblock copolymer system has been well supported by theoretical simulations. A major share of the simulations studies done for this system has been focused on the thermodynamically symmetric A-B-C triblock copolymer, with χ_{AB} equal to χ_{BC} and assuming equal statistical segment lengths for all monomer types. Most theories for linear A-B-C triblock copolymers are mainly approximations using different strong segregation theories. Nakazawa and Ohta used the strong segregation limits of the density functional theory similar to the one developed for diblock copolymers by Ohta and Kawasaki to study the phase behavior of non-frustrated triblock copolymer systems.[84,85] They considered the competition between lamellae, alternating cylinders, alternating spheres and alternating diamond network for systems with $f_a = f_b$ and $\chi_{AB} = \chi_{AC}$.[86] They also explained, that the packing of alternating cylinders in A-B-C triblock copolymers corresponds to the square unit cell rather than the hexagonal packing which was later confirmed by Stadler and Fredrickson.[53,87] Zheng and Wang constructed the phase diagrams for both frustrated and non-frustrated systems with varying

compositions for six different sets of χ values, considering 11 different morphologies but no network morphologies.[45]

Motivated by the work from Mogi, Matsushita and coworkers on PI-PS-P2VP triblock copolymer system, Matsen and coworkers used the SCFT to predict different morphologies for symmetric system with $f_a = f_c$ and $\chi_{AB} = \chi_{BC}$.[74–76,88] The parameter space of SCFT calculations for these symmetric triblock systems is dependent on the ratio $k = \frac{\chi_{AC}}{\chi_{AB}}$, which is a dimensionless measure of segregation $\chi_{AC}*N$ and the individual volume fractions φ_A, φ_B and φ_C. The Yang and Shi groups also took advantage of SCFT and showed the stability of several lamellae and cylindrical phases, which includes two and three domain lamellae morphology, alternating and core shell cylinders and various decorated lamellae phases.[89,90]

Inspired from Leibler's theory[14] on diblock copolymer phase system, Erukhimovich and coworkers constructed a Weak Segregation theory (WST) for thermodynamically symmetric A-B-C triblock copolymers.[91,92] Their theory was only valid in the vicinity of a critical point at which the SCFT can yield a continuous order-disorder transition (ODT). They showed that for thermodynamically symmetric systems, with $\chi_{AB} = \chi_{BC}$, the critical point of interest lies along the line for which $f_a = f_c$. They mainly dealt with the systems which obeyed the Hildebrandt (solubility parameter) approximation $\chi_{ij} \sim (\delta_i - \delta_j)^2$, where δ is the solubility parameter for the particular monomer. Following this approximation, a symmetric system with $\chi_{AB} = \chi_{BC}$ and $\delta_A \neq \delta_C$ must have $\delta_B = (\delta_A+\delta_C)/2$; which using the Hildebrand approximation yields $\chi_{AC} = 4*\chi_{AB}$, or $k = 4$. Therefore, they used the WST to predict numerical results for a symmetric system with $k = 4$ in the vicinity of this critical point. Using numerical SCFT, Matsen and coworkers later on focused on $k < 4$ and demonstrated two-dimensional phase diagrams for different values of f_B and $\chi_{AC}*N$

for $k = 1$ and over a range of values of f_B and k, with $0<k<2$ for systems with a fixed value of $\chi_{AB}*N = 50$.[88]

Morse and coworkers used SCFT to study two models related to ISO triblock copolymer system. In their first model they used the symmetric system with $\chi_{AC}*N = 35$ and $\chi_{AB*}N = \chi_{BC*}N = 13$, or $k = 2.7$, and predicted the ternary phase diagram for different composition with fixed values of $\chi_{ij}*N$.[93] The second model, which was a more realistic asymmetric model, they used the reported values for the statistical asymmetric lengths and interaction parameters approximate to the ISO system to predict the phase diagram. Later on, they used the WST and the SCFT calculations for A-B-C triblock copolymers with $\chi_{AB} \approx \chi_{BC} < \chi_{AC}$. For symmetric systems with $\chi_{AB} = \chi_{BC}$ and volume fractions $f_A=f_C$ they studied the phase diagram over different values of $\chi_{AC}*N$ and k to address the issues in their previous study where the SCFT calculations were performed for very different values of k.[94] They took the same ISO system and presented a triangular phase diagram for the two models using values of $\chi_{ij}*N$ twice that to those used in their previous study. They observed the stability of an alternating diamond phase, with interpenetrating A and C diamond networks for a small region near the ODT in symmetric systems. The F*ddd* (O^{70}) phase was found to be stable in the intermediate segregation regime. In addition, Mays and coworkers also used the SCFT to emphasize the importance of conformation symmetry in tuning the interaction parameter to observe different morphologies.[83]

Millett *et al.* proposed a time-dependent Ginzburg-Landau (TDGL) model to simulate the ordering of linear non-frustrated A-B-C triblock copolymers with $\chi_{AB} \approx \chi_{BC} << \chi_{AC}$.[95] They demonstrated that different morphologies can evolve with time including tetragonal, core-shell hexagonal, three-phase lamellar, and beads-in-lamellar phases using their model (Figure 9). They also used an interaction term to study templated substrates for directed self-assembly and showed that large-

scale simulations can be performed using their model, which can play an important role in investigation of self-assembly and directed self-assembly.

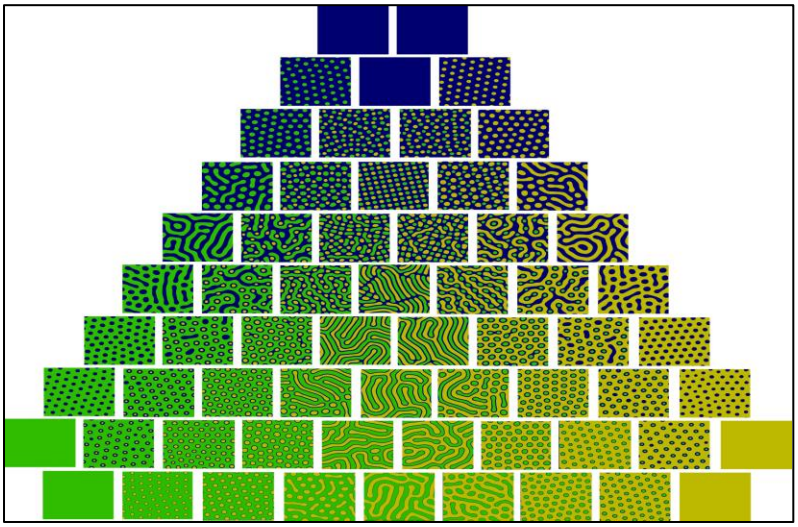

Figure 1. 9: Simulated morphologies of A-B-C triblock terpolymers obtained from the TDGL model. The blocks along each of the three edges represent diblock copolymers with green, blue, and yellow regions correspond with density distributions of A, B, and C monomers respectively (reproduced from reference 95).

1.3.2. Miktoarm Block Copolymers

With improved polymerization techniques and synthetic capabilities, diverse architectures of di and triblock copolymer system have been explored. These mainly include miktoarm star, branched and graft copolymers. These diverse architectures induce entropic constraints due to the asymmetry present in these copolymers, and led to interesting physical properties while providing access to various morphologies which cannot be achieved using linear architectures.

Among the various architectures mentioned, miktoarm star copolymers have been studied in detail both experimentally and theoretically. These refer to the class of copolymers in which different arms originate from a central core with different chemical compositions or chain lengths. These mainly include A_mB_n type which consists of ***m*** arms of homopolymer A and ***n*** arms of homopolymers B attached to the central core, A-B-C star copolymer which has blocks A, B and C

linked to the central core and $(A\text{-}b\text{-}B)_n$ type of star- shaped copolymers which refers to copolymers with ***n*** arms of A-B diblock copolymer emanating from the center, with the A block being the inner core and B block being the outer shell of the star shaped copolymer as shown in Figure 10.[96]

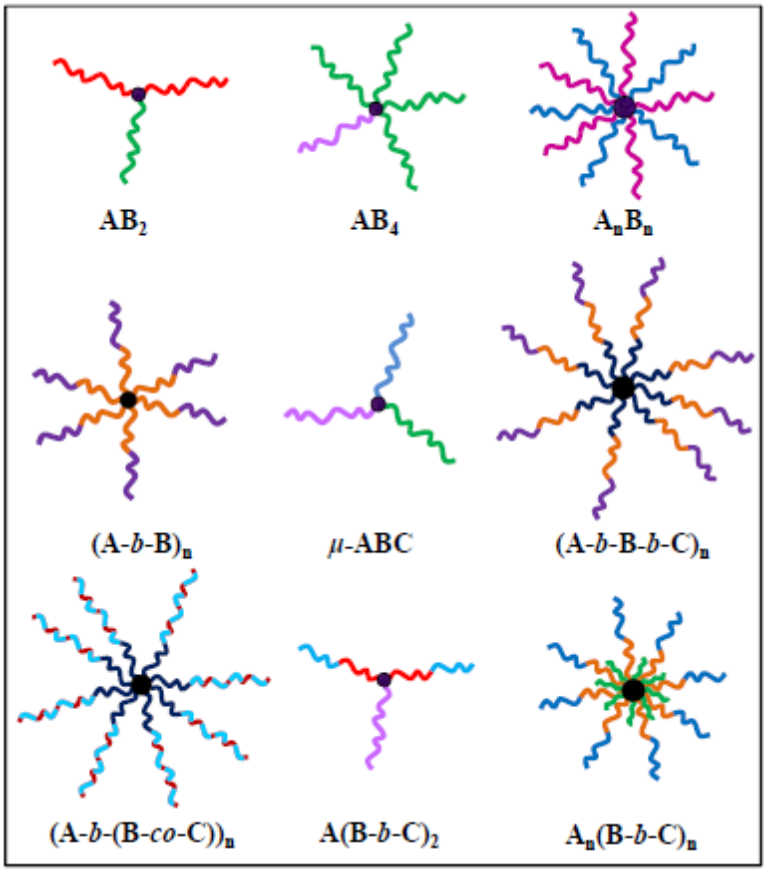

Figure 1. 10: Schematic representation of different architectures of miktoarm star copolymers (image reproduced from reference 97).

1.3.2.1 Theoretical Investigations for A-B-C Miktoarm Triblock Copolymers

The effect of different architectures on the self-assembly of various miktoarm star copolymers has been studied in detail. The first study which gave a theoretical phase diagram for the A_nB_n type miktoarm star copolymers was done by Milner (Figure 11).[98] He employed calculations for these miktoarm copolymer phase behavior appropriate to the strong segregation limit in which the A-B

interface is sharp and the chains are in stretched conformation to reduce the interfacial area per chain of A/B contact along the interface. He mentioned that the morphology and the length scale of microphase separation is determined by the competition between the increase in stretching free energy as each arm stretches away from the interface and the reduction of interfacial tension. The phase diagram of A_nB_n miktoarm star copolymers in the strong segregation limit as a function of asymmetry parameter (ε) and volume fraction (φ) of B monomer was plotted and it was observed that with increasing $\boldsymbol{\varepsilon = (n_A/n_B)(l_A/l_B)^{1/2}}$, (where $\boldsymbol{n}$ refers to the number of each block and $\boldsymbol{l}$ refers to the characteristic length) the phase boundary between the microdomains shifts towards higher volume fraction of B.

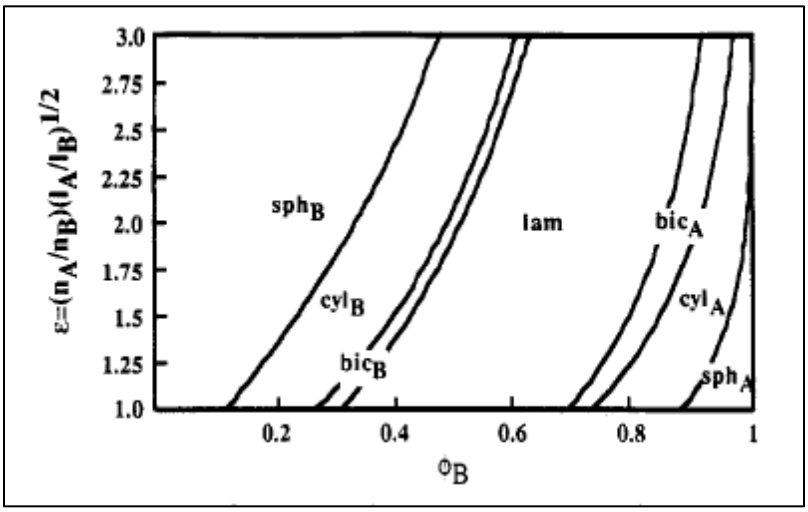

Figure 1. 11: Phase diagram for the A_nB_n star copolymers with varying volume fraction of block B (images taken from reference 98).

In principle the microphase separation for AB_n miktoarm star copolymers becomes more difficult compared of linear diblock copolymers, because the critical value $\boldsymbol{\chi^* N_t}$ $\boldsymbol{(N_t = N_a + n.N_b)}$ is higher for miktoarm copolymers than linear diblock copolymers (Figure 12). Using Mean Field Theory, Erukhimovich and coworkers provided the phase stability criteria and the static structure factor in the disordered phase for these miktoarm copolymers.[99] They studied the spinodal curves for AB_n miktoarm star copolymers for n values up to 100, and observed asymmetry in the spinodal curves

against one of the volume fractions and related it to the asymmetry induced by the architecture of miktoarm star copolymers. The critical value of $\chi^* N_t$ for the AB_n miktoarm copolymers was found be at $n = 3$ which was attributed to the delicate balance of stretching free energies of A and B arms. The interpretations of the phase behavior were found to be consistent with the SAXS measurements performed for PS-PI_3 miktoarm star copolymers.

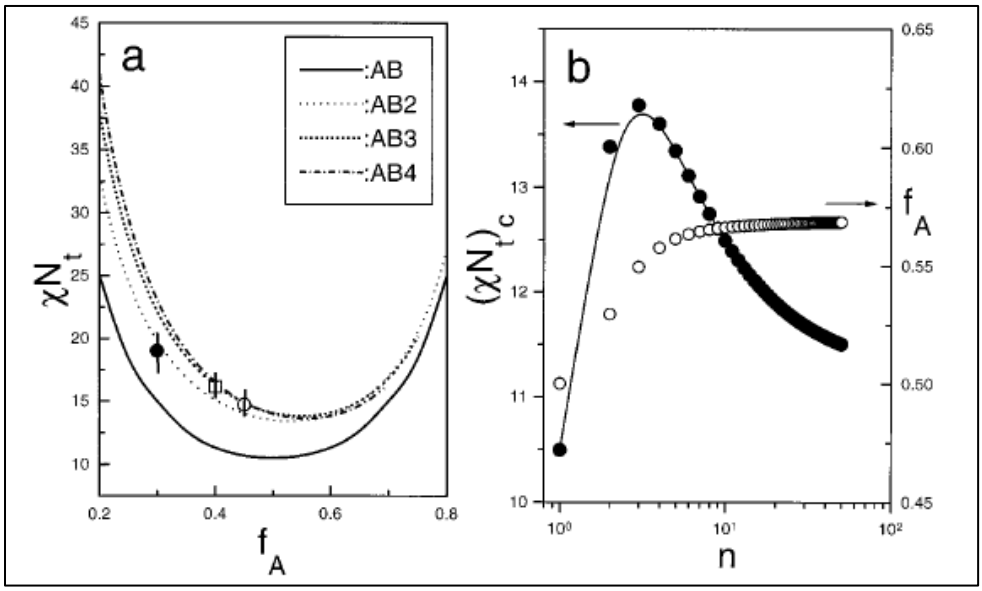

Figure 1. 12: (a) Behavior of the spinodal curves for diblock and different ABn miktoarm copolymers with n =1,2, 3, and 4. The experimental results from an AB_2 (solid sphere) and the two AB_3 (hollow square, hollow sphere) miktoarm stars have been marked. (b) Critical values of χN_t plotted as a function of the number of arms of the B-blocks (images taken from reference 99).

Grason and coworkers investigated the phase behavior of AB_n miktoarm star copolymers using the SCFT in the strong segregation limit.[100] They mainly focused on the role of A-B interface in determining the overall phase behavior of these miktoarm copolymers. They found that the phase diagrams were not symmetric at $\varphi = 0.5$ unlike diblock copolymers and are shifted towards higher volume fractions of A. It was noticed that the shape of the A-B interface is extremely sensitive to molecular asymmetry and is highly distorted for $n > 3$. They observed an increase in the stability of the A15 phase of spherical micelles with increase in the value of n, which was not observed for

linear diblock copolymers. Later on, the phase diagram for AB_2 miktoarm star copolymer was constructed by Matsen and coworkers and different morphologies, such as perforated lamellae (PL) and Fddd (O^{70}, orthorhombic and single-network structure) near the gyroid phase were observed.[78,101] The phase diagram of AB_2 miktoarm copolymers was also predicted using dissipative particle dynamics, by varying the composition and the interaction parameters.[102] These simulations considered hydrodynamic interactions and fluctuations and the results were found to be consistent with the SCFT calculations. Although in contrast to SCFT predictions, according to which the samples with low volume fraction of B can easily form ordered microstructures; tube like microstructures were predicted by dissipative particle dynamics. The overall radius of gyration for the AB_2 miktoarm copolymer was found to increase with an increase in the interaction parameter between the two blocks.

The A-B-C miktoarm copolymers offers a diverse range of unique morphologies including quasicrystalline or Archimedean tiling pattern due to the connectivity of three incompatible arms to a single point.[103] This molecular architecture affects the microphase separation of these terpolymers into different morphologies which were not observed for linear diblock copolymers. The unique feature for the A-B-C star triblock copolymers is the arrangement of their junction points, which are located on a one dimensional line where the three kinds of the interfaces meet together.

Wang and coworkers used a coarse-grained free energy function to numerically investigate the different stable and metastable structures for A-B-C star triblock copolymers.[104] Using Monte Carlo Simulations, Gemma and coworkers plotted the phase diagram of A-B-C miktoarm star copolymers in the strong segregation limit, assuming symmetric interactions between the three arms.[105] They predicted the phase behavior with the composition ratio $\boldsymbol{f_A:f_B:f_c = 1:1:x}$ and five

kinds of 2D cylindrical phases, three lamellar-type phases, and two continuous matrix phases were observed (Figure 13). Later on, they constructed a triangular phase diagram for the miktoarm triblock copolymer system which showed 2D Archemidian tiling patterns.[106] Dynamic Density Functional Theory was also used to study the localization of junction point of the A-B-C miktoarm star terpolymers.[107] It was observed that with increase in the miscibility of one block with the other two blocks, the junction points were distributed over the inter-material dividing surfaces in contrast to lines signifying the role of interaction parameter on microphase separation and the positioning of junction points.

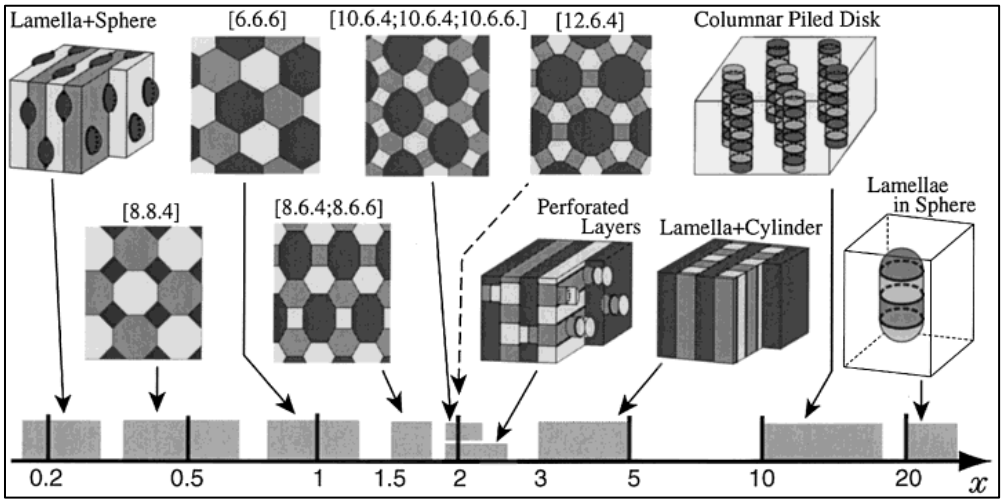

Figure 1. 13: Phase diagram of A-B-C star polymer systems with arm-length ratio 1:1:x and for symmetric interaction of the three blocks. The three blocks are depicted as A (light gray), B (medium gray), and C (dark gray) (taken from reference 105).

Kirkensgaard performed the coarse-grained Molecular Dynamics (MD) simulations on the tiling patterns for A-B-C star triblock copolymers. They predicted a rich polymorphism beyond the single [12.6.4] hexagonal mesophase and found that additional mesophases are likely to form by using selective solvents which dissolve a particular block. They stated that the complex prismatic phases related to 2D tiling patterns of the plane forms mainly due to the interfacial energy of the star triblock copolymer, irrespective of their molecular weights. The formation of lamellae morphology for A-B-C miktoarm star copolymers with $\chi_{AB} >> \chi_{AC} = \chi_{BC}$ was investigated by Abetz

and coworkers and it was found that the C microdomain separates the A and B microdomains with a small fraction of A and B chains located in the C domain because of the junction point of three arms.[65,108] Therefore, in the lamellar superstructure there is a ‘‘mixed’’ domain containing the chains for all three blocks but mainly comprises the block with the lowest degree of incompatibility. However, due to unfavorable A/C and B/C interactions the A and B chains stretch away from each other in the mixed C domain and compress the C chains to minimize the chain interactions. It was witnessed that the period of these superstructures decrease with an increase in the length of the block C (the one with the lowest interaction parameter). Although when the overall length of the three blocks increase, the domain spacing increases similarly to linear A-B-C triblock terpolymers.

Several theoretical investigations have also been done to study the phase behavior of A-B-C star triblock copolymers using SCFT. Yang and coworkers predicted nine stable microstructures for symmetric star architecture using SCFT.[109] They found that the morphology is mainly controlled by the strong topological constraints for the symmetric star and this effect vanishes when either one of the three blocks is in minority. Shi and coworkers studied the phase behavior for symmetric and asymmetric types of star triblock copolymer system using SCFT and constructed their phase diagrams.[110,111] They observed various tiling patterns which were in qualitative agreement with experimental results and previous theoretical studies using the Monte Carlo simulations. They further explored the stability of different hierarchical lamellar morphologies in A-B-C star triblock copolymers and analyzed their relative stabilities by comparing their free energies among the lamellar morphologies with various shift angles. A tricontinuous structure with monoclinic symmetry called the 3ths(5) was found using SCFT simulations for the A-B-C triblock copolymer system with an introduction of an extended molecular core.[112] The core tunes the entropic and

enthalpic free energy contributions and increases the structural length scale by destabilizing the hexagonal columnar phase to form less frustrated morphologies. Recently, Liang and coworkers investigated the phase behavior of asymmetrically interacting A-B-C star triblock copolymers using SCFT (Figure 14).[113] They expanded the previous theoretical results from equal interaction systems to unequal interaction systems and primarily focused on systems with $\chi_{AC} > \chi_{BC} \approx \chi_{AB}$. They constructed a triangular phase diagram and observed 15 ordered phases, including two- and three-dimensional structures which were found to be in good agreement with previous studies. For the triangular phase diagram constructed, it was noted that with an increase in the asymmetry, the morphologies formed are shifted more towards the B-rich corner of the triangular phase diagram.

Dissipative particle dynamics also have been adopted to simulate the phase behavior of A-B-C miktoarm star copolymers with equal interaction parameters and fixed value of N_t (N_A+ N_B+ N_C).[114] For the triblock copolymers with comparable volume fractions of the three arms, three-phase polygonal morphologies mainly [6.6.6], [8.8.4], [10.6.4;10.8.4] [3.3.4.3.4], [10.6.6;10.6.4] were observed. The polygonal morphology observed is primarily determined by the volume fractions of each arm and is independent of the interaction parameters. When two of the three blocks are in the minority, the resulting morphology is greatly influenced by the interaction parameter as the two minority components phase mix and the system forms a one-length-scale ordered morphologies. The two phase mixed blocks can later phase separate with increase in the interaction parameter between the two blocks.

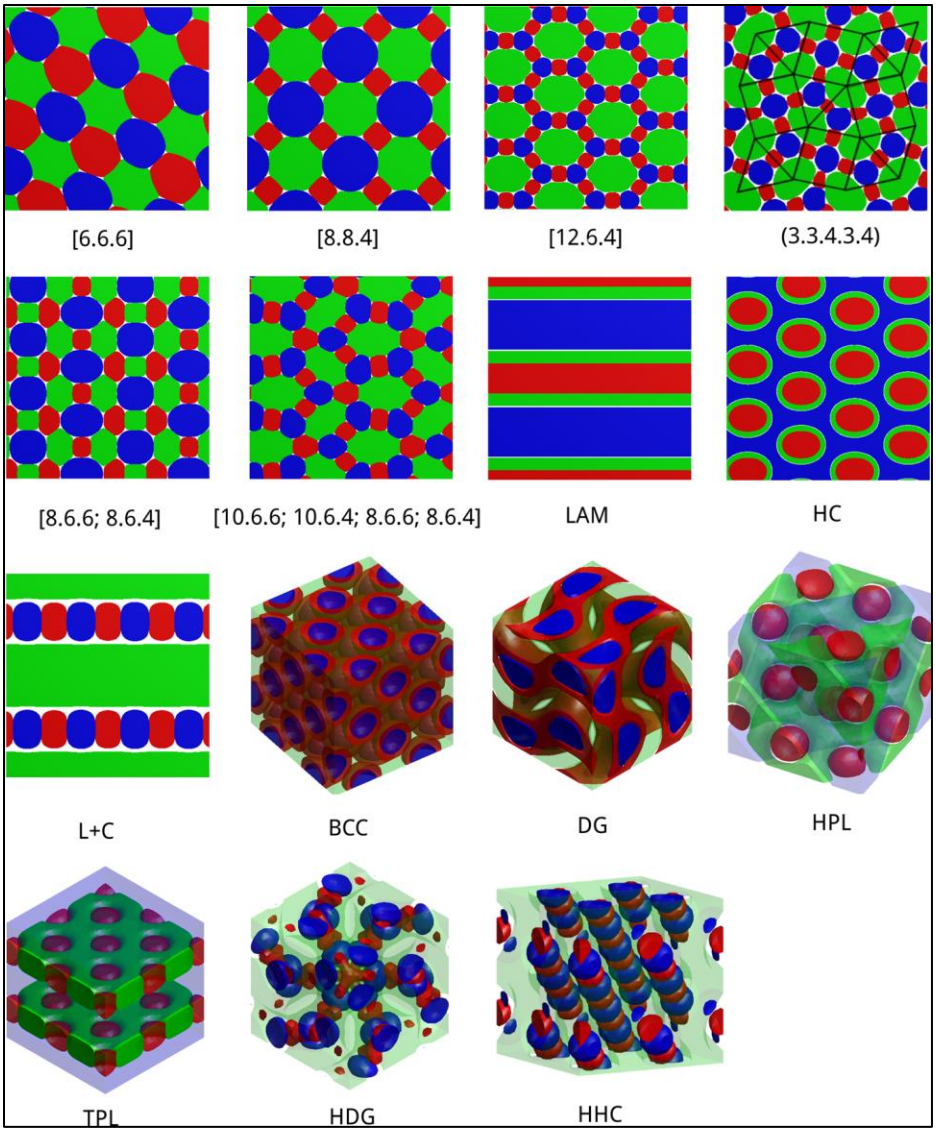

Figure 1. 14: Different ordered phases of A-B-C star triblock copolymers predicted using the SCFT calculations with $\chi_{AC}N = 50.0$, $\chi_{AB}N = \chi_{BC}N = 30.0$. The colors red, green, and blue indicates A, B, and C, respectively. The different hierarchical structures include 2D cylinders-in-lamella phases (L+C), and 3D hierarchical cylinders packed hexagonally (HHC), two kinds of cylinders in-lamella phases, with cylinders being packed hexagonally (HPL) and tetragonally (TPL), and hierarchical double-gyroid phases (HDG). The HC, BCC, and DG represent the core−shell phases of hexagonally arranged cylinders, spheres in body-centered-cubic lattice, and double-gyroid, respectively (reprinted from reference 111).

1.3.2.2 Experimental Observations for A-B-C Miktoarm Triblock Copolymers

Several groups have investigated the morphological phase diagram for different miktoarm star copolymers. Hadjichristidis and coworkers studied the influence of architecture on the microphase

separation for PS-PI miktoarm star copolymers. They observed hexagonally packed cylindrical morphology for PS-PI_2 in contrast to the lamellae or bicontinous morphology expected with similar volume fraction for the linear PS-PI diblock copolymer (Figure 15). This was related to the effect of miktoarm architecture on the curvature energy of the interface.[115,116] The phase boundary between the two microdomains for PS-PI_2 miktoarm star copolymers was found to be shifted towards higher volume fraction of PS compared with linear PI-*b*-PS diblock copolymers.[117]

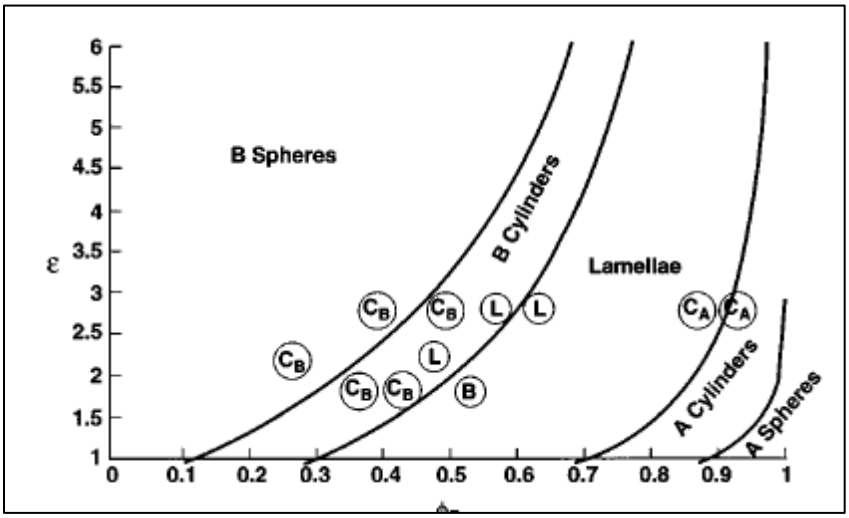

Figure 1. 15: Comparison of observed morphologies with the theoretical prediction by Milner for A_nB_n miktoarm copolymers (reprinted from reference 117).

Later on, PS-PI_2 miktoarm star copolymers system with 53% and 81% vol fraction of PS were shown to form bicontinuous cubic morphology and randomly oriented worm micelle morphology respectively.[118] Following the investigations on PS-PI_2 miktoarm star copolymers, PS-PI_3 miktoarm star copolymers were synthesized and studied for their phase behavior. It was found that the phase boundary between the two microdomains for PS-PI_3 miktoarm star copolymers was shifted more towards higher PS volume fraction. This shift in phase boundary increases with an increase in the number of PI arms. This was due to the higher curvature of the PS/PI interphase which gets curved more towards PS due to the overcrowding of PI arms and therefore providing the required space for the PI chains to pack without a severe energy penalty due to chain

stretching.[119] Studies for PS-PI_5 miktoarm star copolymer system show the formation of chevron tilt grain boundaries in lamellae forming PS-PI_5 at 58 vol % of PS. This is because of the energy penalties for curving the lamellae interface due to large packing constraints of the PI arms (Figure 16).[120]

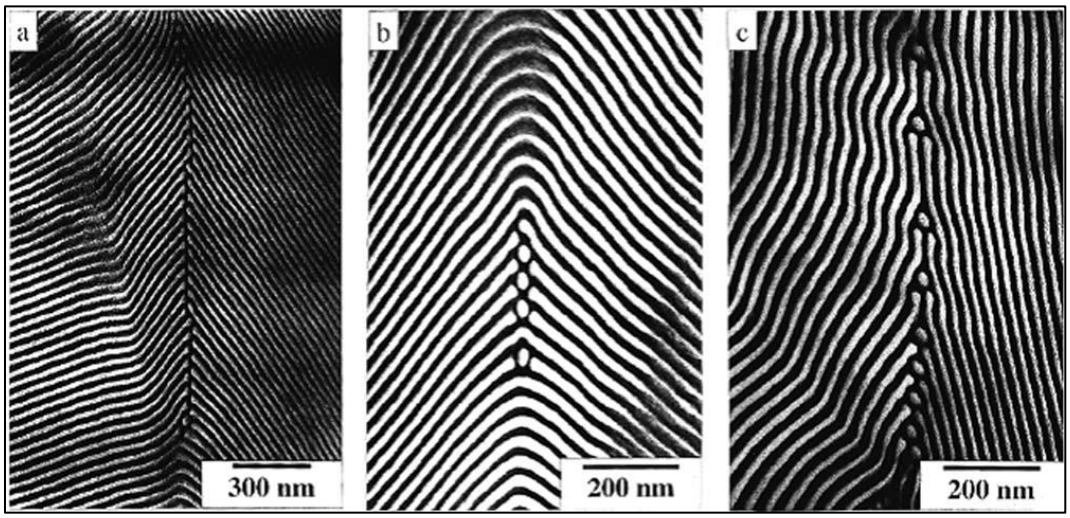

Figure 1. 16: TEM images for PS-PI_5 miktoarm copolymers showing chevron tilt boundaries for 58 % volume fraction of PS. (a) broken chevron (b) broken chevron with cylinders (c) broken **Ω** with cylinders (reprinted from reference 120)

Mavroudis and coworkers synthesized PS-$P2MP_2$ and PS-$P2MP_3$ (P2MP- poly(2-methyl-1,3-pentadiene) miktoarm star copolymers and studied their phase behavior. The morphological behavior of these PS-$P2MP_3$ miktoarm copolymers was determined using TEM, SAXS and differential scanning calorimetry (DSC) and showed more parallel boundaries between the phases compared to the curved boundaries observed PS/PI morphological system and Milner's theory. Interestingly, PS-$P2MP_3$ system showed the presence of a biphasic structure of 1D-lamellar and 3D-double gyroid structure with large grain order for 74 vol% of PS which was not predicted by Milner. These variations in the phase behavior were assigned to the large differences in characteristic ratio (C_∞) and glass transition temperature (T_g) of P2MP and PI.[121]

The AB_2 and AB_3 miktoarm star copolymers with maltoheptaose as block A and PCL as block B were investigated for their phase behavior and BCC morphologies were observed for 9 vol % and 18 vol % of A block. The *d*-spacing of these microstructures was found to be smaller than those for corresponding linear diblock copolymers and decreased with an increase in degree of branching of the PCL blocks. Sub 10 nm *d*-spacing could be achieved because of the high interaction parameter between the two blocks. It was also noted that the miktoarm copolymers with higher degree of branching exhibited smaller morphological features.[122] In contrast, the A_2B miktoarm star copolymer for the same polymer system was shown to form a lamellae morphology even with very low 16% volume fraction of the A block due to architecture induced molecular asymmetry which lowers curvature at the interface.[123]

Among the different A_nB_n type miktoarm star copolymers, Gido and coworkers synthesized PS_8PI_8 miktoarm star copolymers with 37, 44, and 47 vol % of PS and total molecular weight ranging from 330 to 894 kg/mol.[124,125] In agreement to theoretical predictions, they obtained lamellar morphologies for all the samples similar to the phase behavior predicted for linear diblock copolymers with the same relative volume fractions. These results were further compared to miktoarm copolymers with different graft point functionality and it was noted that with increase in the value of ***n*** for PS_nPI_n miktoarm star copolymers, the domain spacing increases as a result of chain stretching away from the core by each polymer segment to minimize chain crowding.

Among the different A_2B_2 type of miktoarm copolymers, PS_2PB_2 miktoarm star copolymer investigated by Turner and coworkers showed lamellar morphology and the molecular spacing was found to be higher compared to the symmetric PS-b-PB diblock copolymer. The interfacial area per molecule for $(PS)_2(PB)_2$ miktoarm star copolymer was similar to that for $(PS)_8(PI)_8$ miktoarm star copolymer studied by Gido *et al*.. Later on Gido and coworkers synthesized five

different samples of PS_2PI_2 and observed their morphology using TEM, SAXS and Small Angle Neutron Scattering (SANS). The morphologies observed were in qualitative agreement with Milner's theory as they lie in the strong segregation limit.[126,127] The PS_2PI_2 miktoarm system with 28 vol % of PS formed cylindrical morphology although lamellae was predicted and the 58 vol % of PS sample exhibited a cylindrical morphology, while a bicontinous morphology was predicted by Milner. This was related to the instability of bicontinous morphology in the strong segregation limit due to increased packing frustration.

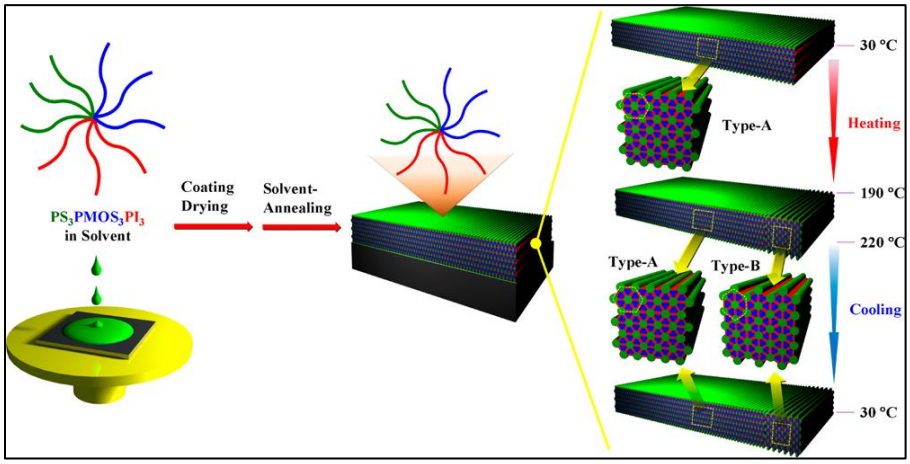

Figure 1. 17: Schematic representations of the phase separated morphologies in the solvent-annealed star polymer film showing the transition from an in-plane oriented HEX truncated PS cylinder and PMOS triangular prism structure for temperature range 25−190 °C; a mixture of the type A HEX structure and its rotational isomer (the type-B HEX structure, namely, the 30°-rotated HEX structure in the range of 190−220 °C; a mixture of the type-A and -B HEX structures formed in the range 220−30 °C.(taken from reference128)

The self-assembled morphologies of $A_3B_3C_3$ miktoarm star copolymer composed of PS, PI, and poly(4-methoxystyrene) (PMOS) were studied.[129] With individual volume fractions of the PS, PMOS, and PI being 31.4, 29.4, and 39.2% respectively, a highly ordered in-plane oriented hexagonal structure consisting of truncated PS cylinders and truncated PMOS triangular prisms in the PI matrix were observed using *in situ* Grazing Incidence Small Angle X-ray Scattering (GISAXS). This hexagonal structure was found to undergo a rotational transformation to give a

30°-rotated hexagonal structure at temperatures above 190 °C up to 220 °C, which existed even after subsequent cooling (Figure 17).

A-B-C miktoarm star copolymers have displayed interesting morphologies and the most common systems studied so far are mainly PI-PS-P2VP and PS-PB-P2VP abbreviated as ISP and SBV miktoarm copolymers. Hadjichristidis and coworkers investigated the phase behavior of ISP miktoarm star copolymers and found their morphologies similar to those of $PS(PI)_2$ miktoarm copolymers because of the similar χ values for PI and PB, which led to phase mixing of PB and PI blocks.[115] Okamoto and coworkers studied the phase behavior of PS, PDMS and PTBMA (poly(tert-butyl methacrylate)) miktoarm star copolymers using TEM, SAXS and DSC. Due to high χ values between the three blocks, special microdomains were observed for the PS-PDMS-PTBMA star copolymer with ratio of PS/PDMS/PBMA = 36/26/38 (wt %).[130] Since the chemical junction for the A-B-C star copolymer is confined to a line where the three interfaces meet, it can lead to highly complicated microdomain structures. They confirmed the presence of regular microdomain structure with three-fold symmetry, where each microdomain forms a 3D continuous network domain resulting in an ordered tricontinuous microdomain structure.

The phase behavior of PS-PI-PMMA miktoarm star copolymer was investigated by Thomas and coworkers.[131] Since the χ value between PS-PI and PMMA-PI is high as compared to PS-PMMA the system showed three-microphases and 2D periodic microstructure of an inner PI column with a surrounding PS annulus in a matrix of PMMA. No interface between the PI and PMMA was observed which implies the PS and PMMA is phase mixed and the PMMA arms passes through the PS domain to reduce the unfavorable contact with PI. The samples with the longer PMMA blocks showed cylindrical PI-PS and PS-PMMA interfaces, whereas a non-constant mean curvature concentric diamond prism shape of the PI and PS microdomains was observed for low

PMMA and high PI volume fraction. The sample with PS/PI/PMMA = 38/28/34 vol % displayed a unique morphology with the PMMA microdomain surrounded by alternating PI and PS hexagonally packed cylinders with *p6mm* symmetry (Figure 18 (I)).

The phase behavior of PS-PI-PDMS miktoarm star copolymers was studied and three dimensional microdomain structure was observed for the symmetric system.[132] The morphology was analyzed using the Energy-Filtered TEM (EF-TEM) in conjugation with 3D electron tomography and for this purpose two kinds of specimens were analyzed under the TEM, one without stain and the other sample was stained with OsO_4. Since only a single phase could be observed under the TEM, it was difficult to analyze the 3D microdomain structure for the miktoarm system. Using the EF-TEM complex microdomain morphology with three different cylindrical structures existing together was identified (Figure 18(II)).

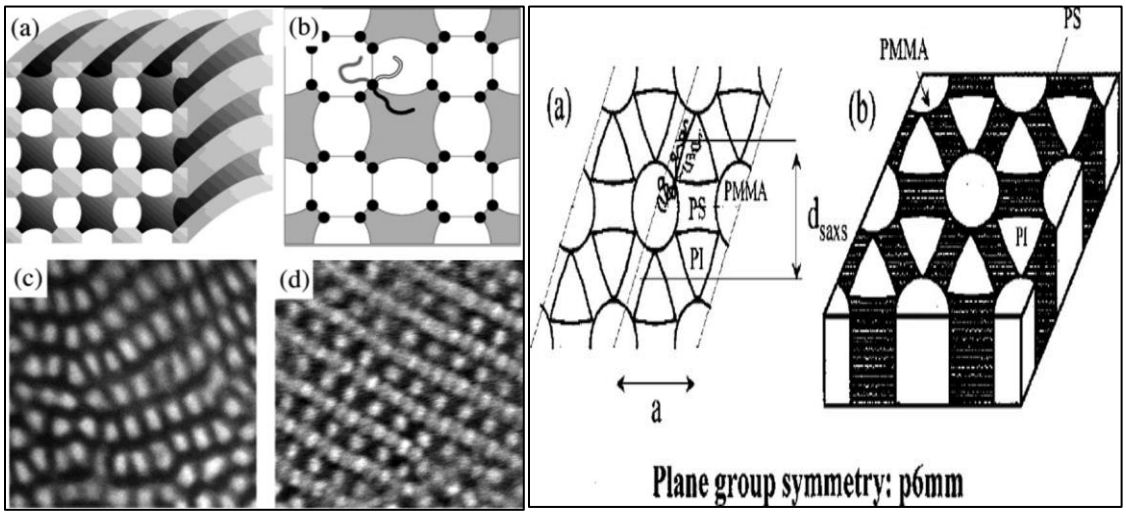

Figure 1. 18: (I) Morphologies for PI-PS-PMDS (a) projected view of alternating cylinders (b) junction point depiction of miktoarm star copolymers (c) EF-TEM image for unstained PI-PS-PDMS miktoarm star copolymer (d) EF-TEM image for PI-PS-PDMS miktoarm star copolymer stained with OsO_4 (Image taken from reference [132]).(II) Chain projections junction points for PS-PI-PMMA miktoarm copolymers (Image taken from reference131)

Stadler and coworkers synthesized PS-PB-P2VP miktoarm star copolymers and studied their phase behavior with varying volume fraction of each block.[133] Based on the composition, the system displayed three different kinds of morphologies. When the P2VP volume fraction is low, dense

packing of cylinders with tetragonal or distorted hexagonal morphologies were observed and on increasing the volume fraction to 50-60 vol %, it was shown to have a hexagonal morphology with the junction points lying along the line. With higher PB volume fraction than PS, lamellar morphologies were formed irrespective of the volume fraction of P2VP, attributed to the higher χ between PB and P2VP. There was no spatial confinement of the junction point along the one dimension and it was predicted that the shorter PS blocks shields the PB lamellae from the P2VP lamellae similar to the core-shell morphologies.

Matsushita and coworkers first reported the Archimedean tiling pattern for the A-B-C star triblock copolymers containing PI, PS and P2VP.[134] They synthesized PS-PI-P2VP Miktoarm copolymers with PS:PI:P2VP volume fractions being 1:1:0.7, 1:1:1.2, and 1:1:1.9.[135] Three-phase microdomain structures were observed for all the samples using TEM and electron tomography (Figure 19). One sample in particular, with volume fraction ratios of 1:1:0.7, showed a honeycomb-type structure having three different cylinders aligning themselves hexagonally with their junction points lying in 1D at the intersection of the three microdomains. The other two samples showed cylindrical morphology with 4-fold and 6-fold symmetry. Many defects in the morphologies were found as compared to linear copolymers due to the time taken to form a stable structure. This is mainly due to the fact that the junction point for the diblock copolymers can move in a 2D plane compared to 1D for A-B-C miktoarm copolymers. This free movement allows the diblock copolymers to attain more stable structures with less defects contrary to the A-B-C miktoarm system. They also synthesized PS-PI-P2VP Star triblock copolymers with volume ratios 1:1:X, where X varies from 0.2 to 4.9 and hierarchical nanophase-separated structures were obtained. The terpolymers with X = 0.2 showed lamellae morphology with spheres at the interface; for $0.4<X<1.9$ cylindrical structures with 2-D tiling patterns were observed; for $3.0<X<4.9$ the

system showed cylinders in lamellae morphology.[77] Recently, Almdal and coworkers synthesized a series of polydimethylsiloxane [D], poly(1,4-isoprene) [I], and poly(methyl methacrylate) [M] miktoarm copolymers and bulk morphologies with volume ratio of M/D = M/I = 0.8−13 with the ratio D/I fixed at ∼1 were explored and observed a morphological transition from [6.6.6] cylindrical tiling to [ALT.LAM] and back to [ALT.CYL] with increase in the MW of the M arm.[66]

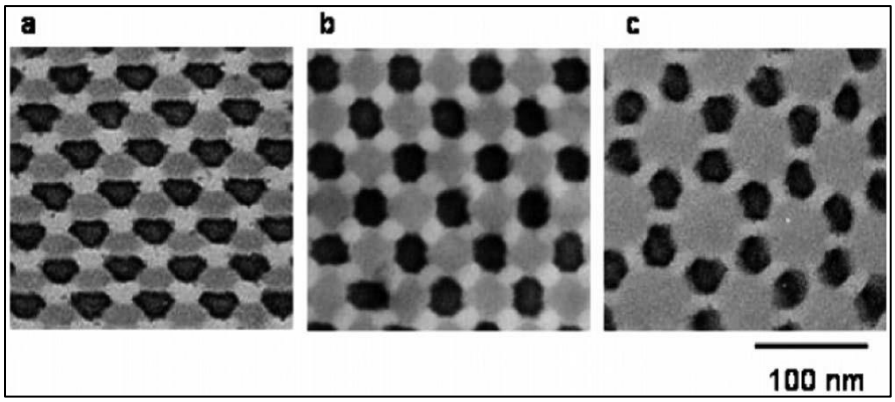

Figure 1. 19: TEM micrographs PS-PI-P2VP star triblock copolymers with different volume fractions of P2VP (image taken from reference 135).

They further explored the morphology of PS-PI-P2VP star copolymers with volume fractions of PS:PI:P2VP = 1.0:1.8:X (4.3< X <53).[136] The system was displayed three different hierarchical morphologies; cylinders-in-lamella (4.3<X<11), lamellae-in-cylinder (12<X<32), and lamellae-in-sphere structure (X = 53). For cylinders-in-lamella morphology, the PI and PS chain consists of cylindrical PI domains in lamellar PS matrix oriented perpendicular to the lamellar planes and this combined layer forms alternating lamellar morphology with layers of PS domains (Figure 20). Although various structure-in-structure morphologies has been reported but hierarchical morphology consisting of cylinders in lamellar structure were reported for the first time in contrast to the previously reported hierarchical morphology of smaller lamellae in larger lamellar structure.

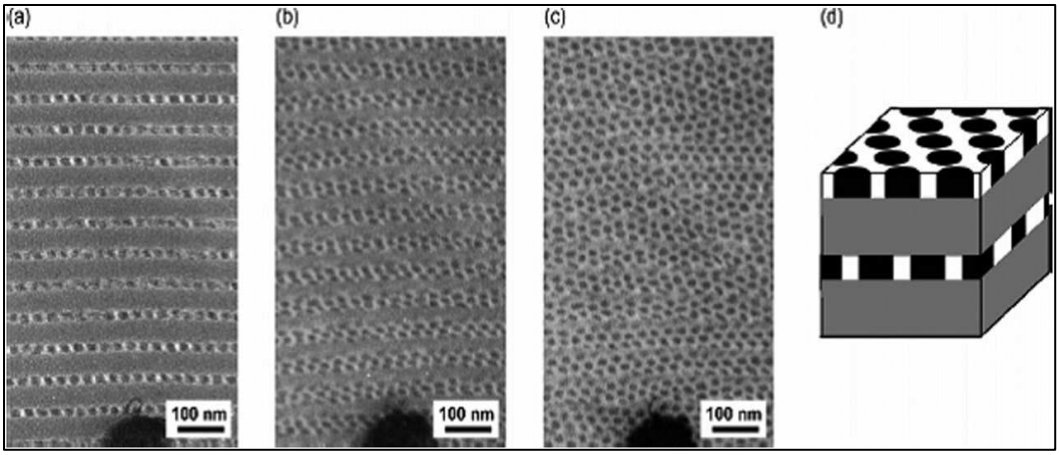

Figure 1. 20: TEM micrographs for PS-PI-P2VP samples with different tilt angles (a) 0° (b) 25° (c) 35° around the horizontal axis (d) systematic representation of the observed morphology (reproduced from reference 136).

Continuing their work on PS-PI-P2VP star triblock copolymers Matsushita and coworkers synthesized PS-PI-P2VP miktoarm star copolymers with varying volume fractions of the three arms and observed kaleidoscopic morphologies with mesoscopic length scales (Figure 21).[137] The system displayed many three phase periodic structures with changes in the overall composition of the star triblock copolymer. Four kinds of Archimedean tiling structures with individual volume fractions of the symmetric star triblock copolymer were observed along with a quasicrystalline tiling pattern with dodecagonal symmetry. With a small increase in asymmetry, a four-branched zinc-blende type morphology was noticed which was related to the strong repulsive force between PI and P2VP which reduces the contact area between PI and P2VP microdomains. Another fascinating feature of this morphology was the major component forming a double network while the minor one forming the gyroid membranes, in contrast to the usual expectation that minor component forms double networks in block copolymer systems. Further increasing the asymmetry, produced several hierarchical structures including hyperbolic tiling on a gyroid membrane, cylinders-in-lamella, lamellae-in-lamella, lamellae-in-cylinder and lamellae-in-sphere.

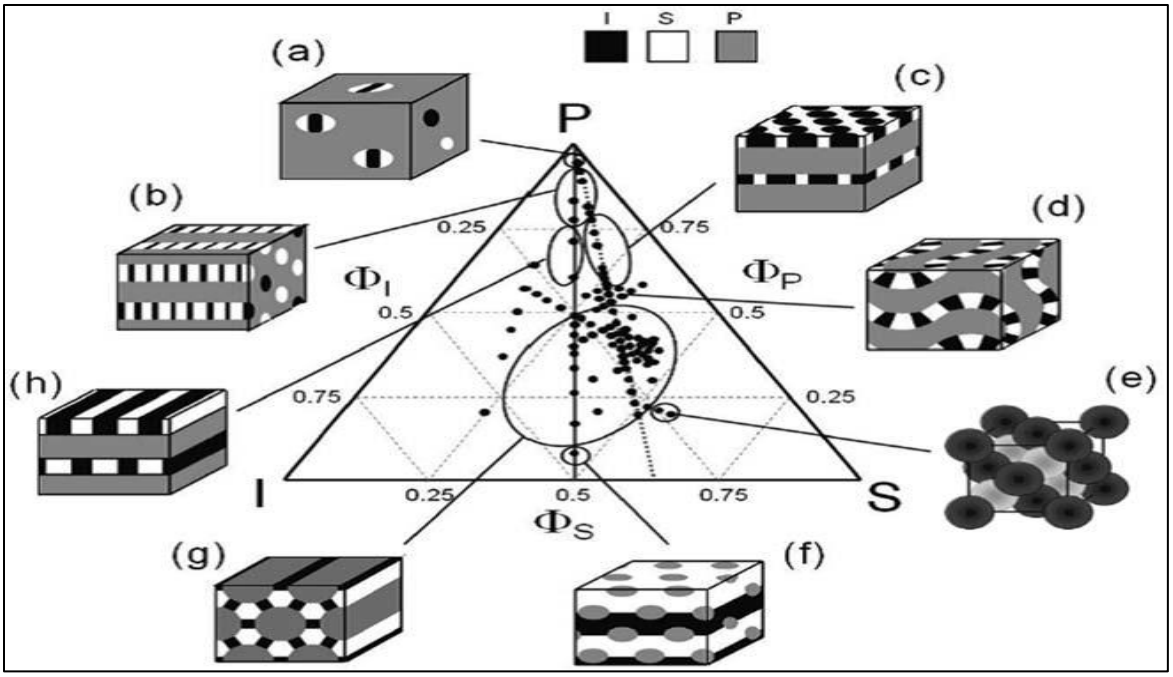

Figure 1. 21: Morphology phase diagram for PS-PI-P2VP miktoarm star copolymer system (images taken from reference 137).

More interestingly, Matsushita and coworkers observed quasicrystalline tiling pattern with 12-fold symmetry for the PS-PI-P2VP miktoarm star copolymers, which has not been displayed in any other polymeric system (Figure 22).[103] Manners and coworkers have recently studied the self-assembly behavior of PS-PI-PFS miktoarm star copolymers (where, PFS is poly(ferrocenylethylmethylsilane)). They system showed distinct morphologies with varying volume fractions of the different arms along with two different Archimedean tiling patterns, [8.8.4] and [12.6.4], and lamellae of PFS with alternating cylinders of PS and PI which was in agreement with the theoretical predictions.[138]

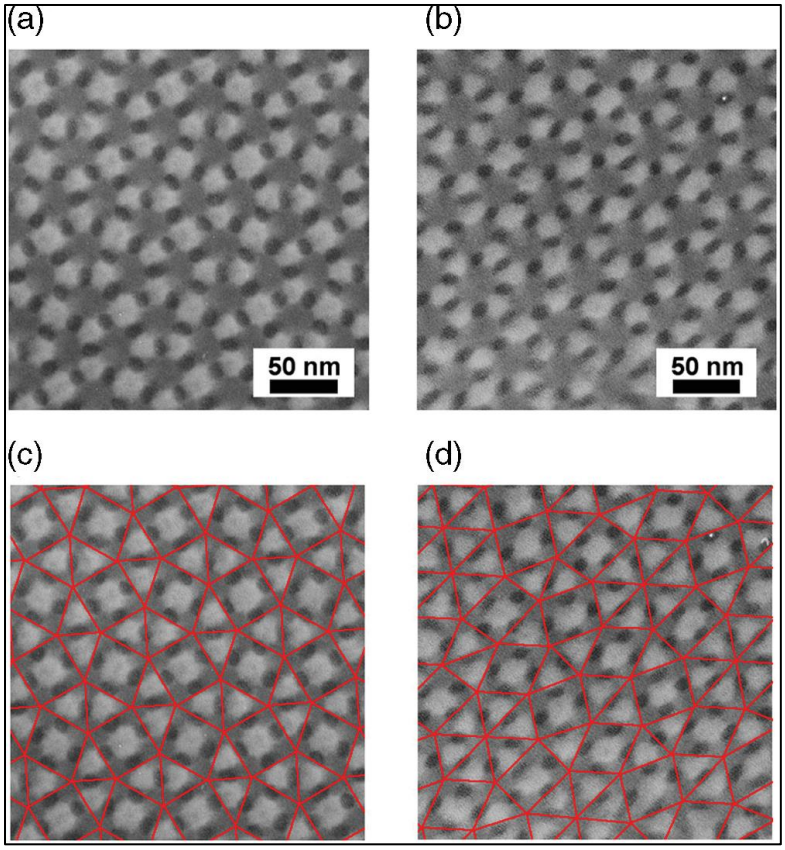

Figure 1. 22: (a,b)TEM micrographs for different compositions of *ISP* terpolymers/*S* homopolymer blend system: PI(black), PS(white), and P2VP (gray). (c,d) Imaginary equilateral triangle (Tri) and square (Sq) are superimposed on the TEM images to show the Archimedean tiling pattern (reproduced from reference 103).

Lodge and coworkers investigated the micellar morphologies of PEO-PE-PF miktoarm star copolymer (where, PE is polyethylethylene; PF is poly(perfluoropropylene)) in a dilute aqueous solution.[139] Connecting the hydrophilic PEO and the two hydrophobic and immiscible components (PE and PF) to a single junction point leads to molecular frustration when dispersed in aqueous solution. The incompatible PS and PF hydrophobic blocks tend to form cores surrounded by the PEO blocks, but both are forced to contact the PEO due to the chain architecture which leads to the formation of multicomponent micellar morphologies. They observed flat interfaces in micellar morphologies because of the super strong segregation between the hydrophobic PE and lipophobic PFs. By tuning the volume fraction of the individual blocks, these morphologies can alter

themselves to from discrete multi-compartment micelles to extended wormlike structure with segmented cores.

1.4. Dissertation Outline

In recent years multiblock copolymers have gained considerable attention due to their ability to offer immense potential for designing soft materials with complex architectures for diverse applications. The enlarged parameter space for these multiblock copolymers gives access to a wide variety of multiply continuous morphologies which can be used to produce highly ordered nanostructures. The investigation on multiblock copolymers has been subjected to two critical limitations: (i) A suitable synthetic strategy for accessing these structures and (ii) computational tools which can help in application driven design of these molecules. In this dissertation, the goal was to develop methodologies for the synthesis of multiblock copolymers with different architectures and understand how the variations in molecular architecture can influence macromolecular self-assembly.

In chapter 2, the concept of single molecule insertion (SMI) for precise insertion of functional molecules is presented. The molecule precisely inserts once within the polymer chain with high chain fidelity and provides functionalities for post-insertion modifications. A series of molecules satisfying the criteria for SMI based on their reactivity ratios with styrene and methyl methacrylate were examined and used to synthesize a series of multiblock polymers with complex architectures.

In chapter 3, a highly efficient synthetic methodology for synthesis of graft copolymers which lie along the continuum of a 3-arm star and A-B-C linear triblock copolymer has been described. The morphological characterization of the synthesized continuum graft copolymers is performed using SAXS, TEM, and DPD simulations. Interesting morphologies are observed for these continuum copolymers and projects them as interesting candidates to access new morphologies. Contrary to

most of the work done on block copolymers, these structures are novel as their morphologies can be tuned keeping the φ and χ constant. This study helps in understanding of the effect of polymer architecture on the phase behavior of these graft copolymers and provides a novel pathway to tune the block copolymer morphologies.

In chapter 4, a series of PMMA-*b*-PtBS-*b*-P2VP and PtBA-*b*-PtBS-*b*-P2VP triblock copolymers with extending P2VP arm has been synthesized. The study helps in extending the concept of high χ-low N block copolymer system from diblock to triblock copolymers. The morphologies of the synthesized triblock copolymers were characterized using SAXS and TEM and morphologies with multiple domains and smaller feature size were observed. Also, the effect of extending chain length of P2VP arm on the phase diagram on these highly frustrated triblock copolymer systems was studied and the observed morphologies using SAXS and TEM were mapped with the theoretical predictions.

1.5. References

(1) Jackson, E. A.; Hillmyer, M. A. *ACS Nano* **2010**, *4* (7), 3548–3553.

(2) Meng, F.; Zhong, Z.; Feijen, J. *Biomacromolecules* **2009**, *10* (2), 197–209.

(3) Kang, Y.; Walish, J. J.; Gorishnyy, T.; Thomas, E. L. *Nat. Mater.* **2007**, *6* (12), 957–960.

(4) Segalman, R. A. *Mater. Sci. Eng. R Reports* **2005**, *48* (6), 191–226.

(5) Orilall, M. C.; Wiesner, U. *Chem. Soc. Rev.* **2011**, *40* (2), 520–535.

(6) Bates, F. S.; Fredrickson, G. H.; Hucul, D.; Hahn, S. F. *AIChE J.* **2001**, *47* (4), 762–765.

(7) Matsen, M. *J. Phys. Condens. Matter* **2002**, *14* (2), 21–47.

(8) Bates, F. S.; Fredrickson, G. H. *Phys. Today* **1999**, *52* (2), 32–38.

(9) Bates, F. S.; Fredrickson, G. H. *Annu. Rev. Phys. Chem.* **1990**, *41* (1), 525–557.

(10) Ciach, a.; Pękalski, J.; Góźdź, W. T. *Soft Matter* **2013**, *9* (27), 6301.

(11) Cochran, E. W.; Garcia-Cervera, C. J.; Fredrickson, G. H. *Macromolecules* **2006**, *39* (7), 2449–2451.

(12) Matsen, M. W. *Eur. Phys. J. E* **2009**, *30* (4), 361–369.

(13) Borsali, R.; Pecora, R. *Soft Matter Characterization*; 2008.

(14) Leibler, L. *Macromolecules* **1980**, *13* (10), 1602–1617.

(15) Matsen, M.; Bates, F. *Macromolecules* **1996**, *29* (23), 7641–7644.

(16) Tsui, O. K. C. *Polymer Thin Films*; 2008.

(17) Park, S.; Kim, B.; Xu, J.; Hofmann, T.; Ocko, B. M.; Russell, T. P. *Macromolecules* **2009**, *42* (4), 1278–1284.

(18) Mansky, P.; Liu, Y.; Huang, E.; Russell, T. P.; Hawker, C. J. *Science* **1997**, *275* (5305), 1458–1460.

(19) Morkved, T. L.; Lu, M.; Urbas, a. M.; Ehrichs, E. E.; Jaeger, H. M.; Mansky, P.; Russell, T. P. *Science (80-.).* **1996**, *273* (5277), 931–933.

(20) Angelescu, D. E.; Waller, J. H.; Adamson, D. H.; Deshpande, P.; Chou, S. Y.; Register, R. A.; Chaikin, P. M. *Adv. Mater.* **2004**, *16* (19), 1736–1740.

(21) Berry, B. C.; Bosse, A. W.; Douglas, J. F.; Jones, R. L.; Karim, A. *Nano Lett.* **2007**, *7* (9), 2789–2794.

(22) Park, S.; Lee, D. H.; Xu, J.; Kim, B.; Hong, S. W.; Jeong, U.; Xu, T.; Russell, T. P. *Science* **2009**, *323* (February), 1030–1033.

(23) Hong, S. W.; Gu, X.; Huh, J.; Xiao, S.; Russell, T. P. *ACS Nano* **2011**, *5* (4), 2855–2860.

(24) Bita, I.; Yang, J. K. W.; Jung, Y. S.; Ross, C. a.; Thomas, E. L.; Berggren, K. K. *Science (80-.).* **2008**, *321* (August), 939–943.

(25) Kim, S. O.; Solak, H. H.; Stoykovich, M. P.; Ferrier, N. J.; De Pablo, J. J.; Nealey, P. F. *Nature* **2003**, *424* (6947), 411–414.

(26) Xu, J.; Park, S.; Wang, S.; Russell, T. P.; Ocko, B. M.; Checco, A. *Adv. Mater.* **2010**, *22* (20), 2268–2272.

(27) Hermel, T. J.; Hahn, S. F.; Chaffin, K. A.; Gerberich, W. W.; Bates, F. S. *Macromolecules* **2003**, *36* (7), 2190–2193.

(28) Christodoulou, S.; Driva, P.; Iatrou, H.; Hadjichristidis, N. *Macromolecules* **2008**, *41* (7), 2607–2615.

(29) Bates, F. S.; Hillmyer, M. a.; Lodge, T. P.; Bates, C. M.; Delaney, K. T.; Fredrickson, G. H. *Science (80-.).* **2012**, *336* (6080), 434–440.

(30) Meuler, A. J.; Hillmyer, M. a.; Bates, F. S. *Macromolecules* **2009**, *42* (19), 7221–7250.

(31) Dair, B. J.; Honeker, C. C.; Alward, D. B.; Avgeropoulos, A.; Hadjichristidis, N.; Fetters, L. J.; Capel, M.; Thomas, E. L. *Macromolecules* **1999**, *32* (24), 8145–8152.

(32) Dair, B. J.; Avgeropoulos, A.; Hadjichristidis, N.; Thomas, E. L. *J. Mater. Sci.* **2000**, *35* (20), 5207–5213.

(33) Yang, X.; Loos, J. *Macromolecules* **2007**, *40* (5), 1353–1362.

(34) Crossland, E. J. W.; Kamperman, M.; Nedelcu, M.; Ducati, C.; Wiesner, U.; Smilgies, D. M.; Toombes, G. E. S.; Hillmyer, M. A.; Ludwigs, S.; Steiner, U.; Snaith, H. J. *Nano Lett.* **2009**, *9* (8), 2807–2812.

(35) Crossland, E. J. W.; Nedelcu, M.; Ducati, C.; Ludwigs, S.; Hillmyer, M. A.; Steiner, U.; Snaith, H. J. *Nano Lett.* **2009**, *9* (8), 2813–2819.

(36) Oey, C. C.; Djurišić, a B.; Wang, H.; Man, K. K. Y.; Chan, W. K.; Xie, M. H.; Leung, Y. H.; Pandey, a; Nunzi, J.-M.; Chui, P. C. *Nanotechnology* **2006**, *17* (3), 706–713.

(37) Wang, H.; Oey, C. C.; Djurišić, A. B.; Xie, M. H.; Leung, Y. H.; Man, K. K. Y.; Chan, W. K.; Pandey, A.; Nunzi, J.-M.; Chui, P. C. *Appl. Phys. Lett.* **2005**, *87* (2), 023507.

(38) Shefelbine, T. A.; Vigild, M. E.; Matsen, M. W.; Hajduk, D. A.; Hillmyer, M. A.; Cussler, E. L.; Bates, F. S. *J. Am. Chem. Soc.* **1999**, *121* (37), 8457–8465.

(39) Yang, S. Y.; Ryu, I.; Kim, H. Y.; Kim, J. K.; Jang, S. K.; Russell, T. P. *Adv. Mater.* **2006**, *18* (6), 709–712.

(40) Phillip, W. A.; Rzayev, J.; Hillmyer, M. A.; Cussler, E. L. *J. Memb. Sci.* **2006**, *286* (1–2), 144–152.

(41) Phillip, W. A.; Amendt, M.; ONeill, B.; Chen, L.; Hillmyer, M. A.; Cussler, E. L. *ACS Appl. Mater. Interfaces* **2009**, *1* (2), 472–480.

(42) Cho, B.K.; Jain, A.; Gruner, S. M.; Wiesner, U. *Science (80-.).* **2004**, *305* (5690), 1598–1601.

(43) Lin, S. Y.; Fleming, J. G.; Hetherington, D. L.; Smith, B. K.; Biswas, R.; Ho, K. M.; Sigalas, M. M.; Zubrzycki, W.; Kurtz, S. R.; Bur, J. *Nature* **1998**, *394* (6690), 251–253.

(44) Maldovan, M.; Thomas, E. L.; Article, P.; Maldovan, M.; Thomas, E. L. *Nat. Mater.* **2004**, *3* (9), 593–600.

(45) Zheng, W.; Wang, Z. G. *Macromolecules* **1995**, *28* (21), 7215–7223.

(46) Ungar, G.; Tschierske, C.; Abetz, V.; Holyst, R.; Bates, M. A.; Liu, F.; Prehm, M.; Kieffer, R.; Zeng, X.; Walker, M.; Glettner, B.; Zywocinski, A. *Adv. Funct. Mater.* **2011**, *21* (7), 1296–1323.

(47) Lecommandoux, S.; Borsali, R.; Schappacher, M.; Deffieux, A.; Narayanan, T.; Rochas, C. *Macromolecules* **2004**, *37* (5), 1843–1848.

(48) Liu, M.; Li, W.; Qiu, F.; Shi, A. C. *Macromolecules* **2012**, *45* (23), 9522–9530.

(49) Breiner, U.; Krappe, U.; Jakob, T.; Abetz, V.; Stadler, R. *Polym. Bull.* **1998**, *40* (2–3), 219–226.

(50) Breiner, U.; Krappe, U.; Abetz, V.; Stadler, R. *Macromol. Chem. Phys.* **1997**, *198* (4), 1051–1083.

(51) Breiner, U.; Krappe, U.; Stadler, R. *Macromol. Rapid Commun.* **1996**, *17* (8), 567–575.

(52) Krappe, U.; Stadler, R.; Voigt-Martin, I. *Macromolecules* **1995**, *28*, 4558–4561.

(53) Stadler, R.; Auschra, C.; Beckmann, J.; Krappe, U.; Voigt-Martin, I.; Leibler, L. *Macromolecules* **1995**, *28*, 3080–3091.

(54) Brinkmann, S.; Stadler, R.; Thomas, E. L. *Macromolecules* **1998**, *31* (19), 6566–6572.

(55) Jinnai, H.; Kaneko, T.; Matsunaga, K.; Abetz, C.; Abetz, V. *Soft Matter* **2009**, *5* (10), 2042–2046.

(56) Breiner, U.; Krappe, U.; Thomas, E. L.; Stadler, R. *Macromolecules* **1998**, *31* (96), 135–141.

(57) Auschra, C.; Stadler, R. *Macromolecules* **1993**, *26* (9), 2171–2174.

(58) Ott, H.; Abetz, V.; Altstädt, V. *Macromolecules* **2001**, *34*, 2121.

(59) Elbs, H.; Abetz, V.; Hadziioannou, G.; Drummer, C.; Krausch, G. *Macromolecules* **2001**, *34* (23), 7917–7919.

(60) Elbs, H.; Drummer, C.; Abetz, V.; Krausch, G. *Macromolecules* **2002**, *35* (14), 5570–5577.

(61) Park, C.; Yoon, J.; Thomas, E. L. *Polymer (Guildf).* **2003**, *44* (22), 6725–6760.

(62) Ludwigs, S.; Schmidt, K.; Stafford, C. M.; Amis, E. J.; Fasolka, M. J.; Karim, A.; Magerle, R.; Krausch, G. *Macromolecules* **2005**, *38* (5), 1850–1858.

(63) Balsamo, V.; von Gyldenfeldt, F.; Stadler, R. *Macromolecules* **1999**, *32* (4), 1226–1232.

(64) Bailey, T. S.; Pham, H. D.; Bates, F. S. *Macromolecules* **2001**, *34* (20), 6994–7008.

(65) Hückstädt, H.; Goldacker, T.; Göpfert, A.; Abetz, V. *Macromolecules* **2000**, *33*, 3757–3761.

(66) Chernyy, S.; Kirkensgaard, J. J. K.; Mahalik, J. P.; Kim, H.; Arras, M. M. L.; Kumar, R.; Sumpter, B. G.; Smith, G. S.; Mortensen, K.; Russell, T. P.; Almdal, K. *Macromolecules* **2018**, *51* (3), 1041–1051.

(67) Kaneko, T.; Suda, K.; Satoh, K.; Kamigaito, M.; Kato, T.; Ono, T.; Nakamura, E.; Nishi, T.; Jinnai, H. *Macromol. Symp.* **2006**, *242*, 80–86.

(68) Tang, P.; Qiu, F.; Zhang, H.; Yang, Y. *Phys. Rev. E - Stat. Nonlinear, Soft Matter Phys.* **2004**, *69* (3 1), 1–8.

(69) Guo, Z.; Zhang, G.; Qiu, F.; Zhang, H.; Yang, Y.; Shi, A. C. *Phys. Rev. Lett.* **2008**, *101* (2), 1–4.

(70) Nagpal, U.; Detcheverry, F. a.; Nealey, P. F.; De Pablo, J. J. *Macromolecules* **2011**, *44* (13), 5490–5497.

(71) Li, Weihua; Qui, Feng; Shi, A. C. *Macromolecules* **2011**, *45*, 503–509.

(72) Huckstadt, H.; Gopfert, A.; Abetz, V. *Polymer (Guildf).* **2000**, *41* (26), 9089–9094.

(73) Abetz, V.; Goldacker, T. *Macromol. Rapid Commun.* **2000**, *21* (1), 16–34.

(74) Mogi, Y.; Mori, K.; Kotsuji, H.; Matsushita, Y.; Noda, I.; Han, C. C. *Macromolecules* **1993**, *26* (19), 5169–5173.

(75) Mogi, Y.; Nomura, M.; Kotsuji, H.; Ohnishi, K.; Matsushita, Y.; Noda, I. *Macromolecules* **1994**, *27* (23), 6755–6760.

(76) Matsushita, Y.; Suzuki, J.; Seki, M. *Phys. B Condens. Matter* **1998**, *248* (1–4), 238–242.

(77) Takano, A.; Kawashima, W.; Wada, S.; Hayashida, K.; Sato, S.; Kawahara, S.; Isono, Y.;

Makihara, M.; Tanaka, N.; Kawaguchi, D.; Matsushita, Y. *J. Polym. Sci. Part B Polym. Phys.* **2007**, *45* (16), 2277–2283.

(78) Bailey, T. S.; Hardy, C. M.; Epps, T. H.; Bates, F. S. *Macromolecules* **2002**, *35* (18), 7007–7017.

(79) Epps, T. H.; Bailey, T. S.; Waletzko, R.; Bates, F. S. *Macromolecules* **2003**, *36* (8), 2873–2881.

(80) Chatterjee, J.; Jain, S.; Bates, F. S. *Macromolecules* **2007**, *40* (8), 2882–2896.

(81) Cochran, E. W.; Bates, F. S. *Phys. Rev. Lett.* **2004**, *93* (8), 1–4.

(82) Beckingham, B. S.; Register, R. A. *Macromolecules* **2013**, *46* (9), 3486–3496.

(83) Kumar, R.; Sides, S. W.; Goswami, M.; Sumpter, B. G.; Hong, K.; Wu, X.; Russell, T. P.; Gido, S. P.; Misichronis, K.; Rangou, S.; Avgeropoulos, A.; Tsoukatos, T.; Hadjichristidis, N.; Beyer, F. L.; Mays, J. W. *Langmuir* **2013**, *29* (6), 1995–2006.

(84) Ohta, T.; Kawasaki, K. *Macromolecules* **1986**, *19* (10), 2621–2632.

(85) Ohta, T.; Kawasaki, K. *Macromolecules* **1990**, No. 5, 2413–2414.

(86) Nakazawa, H.; Ohta, T. *Macromolecules* **1993**, *26* (20), 5503–5511.

(87) Phan, S.; Fredrickson, G. H. *Macromolecules* **1998**, *31* (1), 59–63.

(88) Matsen, M. W. *J. Chem. Phys.* **1998**, *108* (1998), 785–796.

(89) Xia, J.; Sun, M.; Qiu, F.; Zhang, H.; Yang, Y. *Macromolecules* **2005**, *38* (22), 9324–9332.

(90) Jiang, Y.; Yan, X.; Liang, H.; Shi, A. C. *J. Phys. Chem. B* **2005**, *109* (44), 21047–21055.

(91) Erukhimovich, I. Y. *Eur. Phys. J. E* **2005**, *18* (4), 383–406.

(92) Erukhimovich, I.; Abetz, V.; Stadler, R. *Macromolecules* **1997**, *30* (24), 7435–7443.

(93) Tyler, C. A.; Qin, J.; Bates, F. S.; Morse, D. C. *Macromolecules* **2007**, *40* (13), 4654–4668.

(94) Qin, J.; Bates, F. S.; Morse, D. C. *Macromolecules* **2010**, *43* (11), 5128–5136.

(95) Millett, P. C. *Phys. Rev. E - Stat. Nonlinear, Soft Matter Phys.* **2015**, *92* (2), 1–9.

(96) Park, J.; Jang, S.; Kim, J. K. *J. Polym. Sci. Part B Polym. Phys.* **2015**, *53* (1), 1–21.

(97) Iatridi, Z.; Tsitsilianis, C. *Polymers (Basel).* **2011**, *3* (4), 1911–1933.

(98) Milner, S. T. *Macromolecules* **1994**, *27* (8), 2333–2335.

(99) Floudas, G; Hadjichristidis, N.; Tselikas, T.; Erukhimovich, I. *Macomolecules* **1997**, *30*, 3090–3096.

(100) Grason, G. M.; Kamien, R. D. *Macromolecules* **2004**, *37* (19), 7371–7380.

(101) Matsen, M. W. *Macromolecules* **2012**, *45* (4), 2161–2165.

(102) Huang, C. I.; Yu, H. T. *Polymer (Guildf).* **2007**, *48* (15), 4537–4546.

(103) Hayashida, K.; Dotera, T.; Takano, A.; Matsushita, Y. *Phys. Rev. Lett.* **2007**, *98* (19), 1–4.

(104) Bohbot-Raviv, Y.; Wang, Z. *Phys. Rev. Lett.* **2000**, *85*, 3428–3431.

(105) Gemma, T.; Hatano, A.; Dotera, T. *Macromolecules* **2002**, *35* (8), 3225–3237.

(106) Ueda, K.; Dotera, T.; Gemma, T. *Phys. Rev. B - Condens. Matter Mater. Phys.* **2007**, *75* (19), 1–11.

(107) He, X.; Huang, L.; Liang, H.; Pan, C. *J. Chem. Phys.* **2003**, *118* (21), 9861–9863.

(108) Birshtein, T. M.; Polotsky, A. A.; Abetz, V. *Macromol. Theory Simulations* **2004**, *13* (6), 512–519.

(109) Tang, P.; Qiu, F.; Zhang, H.; Yang, Y. *J. Phys. Chem. B* **2004**, *108* (24), 8434–8438.

(110) Zhang, G.; Qiu, F.; Zhang, H.; Yang, Y.; Shi, A. C. *Macromolecules* **2010**, *43* (6), 2981–2989.

(111) Li, W.; Xu, Y.; Zhang, G.; Qiu, F.; Yang, Y.; Shi, A. C. *J. Chem. Phys.* **2010**, *133* (6).

(112) Fischer, M. G.; de Campo, L.; Kirkensgaard, J. J. K.; Hyde, S. T.; Schröder-Turk, G. E.

Macromolecules **2014**, *47* (21), 7424–7430.

(113) Jiang, K.; Zhang, J.; Liang, Q. *J. Phys. Chem. B* **2015**, *119* (45), 14551–14562.

(114) Huang, C. I.; Fang, H. K.; Lin, C. H. *Phys. Rev. E - Stat. Nonlinear, Soft Matter Phys.* **2008**, *77* (3), 2–9.

(115) Hadjichristidis, N.; Iatrou, H.; Behal, S. K.; Chludzinski, J. J.; Disko, M. M.; Garner, R. T.; Liang, K. S.; Lohse, D. J.; Milner, S. T. *Macromolecules* **1993**, *26* (21), 5812–5815.

(116) Chrissopoulou, K.; Harville, S.; Anastasiadis, S. H.; Fytas, G.; Mays, J. W.; Hadjichristidis, N. *J. Polym. Sci. Part B Polym. Phys.* **1999**, *37* (24), 3385–3391.

(117) Tselikas, Y.; Iatrou, H.; Hadjichristidis, N.; Liang, K. S.; Mohanty, K.; Lohse, D. J. *J. Chem. Phys.* **1996**, *105* (6), 2456.

(118) Tselikas, Y.; Hadjichristidis, N.; Lescanec, R. L.; Honeker, C. C.; Wohlgemuth, M.; Thomas, E. L. *Macromolecules* **1996**, *29* (10), 3390–3396.

(119) Separation, M.; Block, I. N.; Of, T.; Architectures, N. M. **1997**, *174*, 167–174.

(120) Yang, L.; Hong, S.; Gido, S. P.; Velis, G.; Hadjichristidis, N. *Macromolecules* **2001**, *34* (26), 9069–9073.

(121) Mavroudis, A.; Avgeropoulos, A.; Hadjichristidis, N.; Thomas, E. L.; Lohse, D. J. *Chem. Mater.* **2003**, *15* (24), 1976–1983.

(122) Isono, T.; Otsuka, I.; Kondo, Y.; Halila, S.; Fort, S.; Rochas, C.; Satoh, T.; Borsali, R.; Kakuchi, T. *Macromolecules* **2013**, *46* (4), 1461–1469.

(123) Isono, T.; Otsuka, I.; Suemasa, D.; Rochas, C.; Satoh, T.; Borsali, R.; Kakuchi, T. *Macromolecules* **2013**, *46* (22), 8932–8940.

(124) Pispas, S.; Avgeropoulos, A.; Hadjichristidis, N.; Roovers, J. *J. Polym. Sci. Part B Polym. Phys.* **1999**, *37*, 1329–1335.

(125) Beyer, F. L.; Gido, S. P.; Poulos, Y.; Avgeropoulos, A.; Hadjichristidis, N. *Macromolecules* **1997**, *30* (8), 2373–2376.

(126) Turner, C. M.; Sheller, N. B.; Foster, M. D.; Lee, B.; Corona-Galvan, S.; Quirk, R. P.; Ann\'is, B.; Lin, J.-S. *Macromolecules* **1998**, *31* (98), 4372–4375.

(127) Beyer, F. L.; Gido, S. P.; Uhrig, D.; Mays, J. W.; Tan, N. B.; Trevino, S. F. *J. Polym. Sci. Part B Polym. Phys.* **1999**, *37* (24), 3392–3400.

(128) Rho, Y.; Kim, C.; Higashihara, T.; Jin, S.; Jung, J.; Shin, T. J.; Hirao, A.; Ree, M. *ACS Macro Lett.* **2013**, *2* (10), 849–855.

(129) Rho, Y.; Kim, C.; Higashihara, T.; Jin, S.; Jung, J.; Shin, T. J.; Hirao, A.; Ree, M. *ACS Macro Lett.* **2013**, *2* (10), 849–855.

(130) Okamoto, S.; Hasegawa, H.; Hashimoto, T.; Fujimoto, T.; Zhang, H.; Kazama, T.; Takano, A.; Isono, Y. *Polymer (Guildf).* **1997**, *38* (21), 5275–5281.

(131) Sioula, S.; Hadjichristidis, N.; Thomas, E. L. *Macromolecules* **1998**, *31* (97), 5272–5277.

(132) Yamauchi, K.; Takahashi, K.; Hasegawa, H.; Iatrou, H.; Hadjichristidis, N.; Kaneko, T.; Nishikawa, Y.; Jinnai, H.; Matsui, T.; Nishioka, H.; Shimizu, M.; Furukawa, H. *Macromolecules* **2003**, *36* (19), 6962–6966.

(133) Huckstadt, H.; Gopfert, A.; Abetz, V. *Macromol. Chem. Phys.* **2000**, *201* (3), 296–307.

(134) Takano, A.; Kawashima, W.; Noro, A.; Isono, Y.; Tanaka, N.; Dotera, T.; Matsushita, Y. *J. Polym. Sci. Part B Polym. Phys.* **2005**, *43* (18), 2427–2432.

(135) Takano, A.; Wada, S.; Sato, S.; Araki, T.; Hirahara, K.; Kazama, T.; Kawahara, S.; Isono, Y.; Ohno, A.; Tanaka, N.; Matsushita, Y. *Macromolecules* **2004**, *37* (26), 9941–9946.

(136) Hayashida, K.; Saito, N.; Arai, S.; Takano, A.; Tanaka, N.; Matsushita, Y. *Macromolecules* **2007**, *40* (10), 3695–3699.

(137) Matsushita, Y.; Hayashida, K.; Dotera, T.; Takano, A. *J. Physics-Condensed Matter* **2011**, *23* (28), 284111.

(138) Nunns, A.; Ross, C. a.; Manners, I. *Macromolecules* **2013**, *46* (7), 2628–2635.

(139) Li, Z.; Kesselman, E.; Talmon, Y.; Hillmyer, M.A.; Lodge, T. P. *Science (80-.).* **2004**, *306* (5693), 98–101.

CHAPTER II

SINGLE MOLECULE INSERTION AND ITS APPLICATIONS FOR SYNTHESIS OF FUNCTIONAL MATERIALS

2.1 Introduction

With development of different controlled polymerization techniques, significant advancement has been made in controlling the primary structure of synthetic polymeric materials.[1–5] However, precise control over the arrangement of different monomer units within a polymer chain is challenging and requires development of different synthetic strategies. Synthetic polymers used for a variety of applications are mainly homopolymers or copolymers with chain microstructure being either random or block. When compared to biological macromolecules, these polymers lack functional and structural complexity due to the limitation of forming precisely regulated monomer sequences. Recently, there has been increasing efforts to develop synthetic procedures capable of mimicking the precision of monomer sequence exhibited by natural polymers such as nucleic acids, carbohydrates, peptides and proteins.[6–8] The success in replicating these precise structures in synthetic polymers would be valuable in the field of nanomedicine and nanotechnology. Controlling the microstructure within a polymer chain itself can have a profound impact on the overall macroscopic properties of polymers, and can play an important role in creating functionalities for molecular targeting, recognition, biocatalysis and molecular level information storage.[9–11]

Over the past few years, notable progress has been made by synthetic chemists in developing protocols for step-growth and chain-growth polymerization to control the primary sequence of

polymers.[7] Different terminologies have been used in the literature to define these polymers, the most-common being "sequence controlled polymer" which refers to polymer with ordered monomer repeating units, segments or functionalities on the polymer chain.[12] Other nomenclatures used are "sequence regulated polymer", "sequence specific", "sequence defined" and "aperiodic polymer", but the exact nomenclature is still under debate.[13–17] Different approaches have been developed to synthesize sequence controlled polymers which includes chain-growth polymerization, step-growth polymerization, multicomponent reactions, single monomer insertion, template polymerization, solid-phase synthesis and synthesis of multiblock copolymers using built-in sequence.[18]

Since precise control over macromolecular sequence in polymeric materials involves step-growth processes, where addition of a single monomer unit on the growing chain-end by an iterative addition–activation process is performed to achieve the desired sequence. These processes primarily include esterification,[19] nitrone-mediated radical coupling,[20] amidation,[21] Horner–Wadsworth–Emmons (HWE) chemistry,[22] Wittig olefination,[23] Passerini reaction,[24] thiolactone chemistry[25] and alkyne-azide Huisgen cycloaddition.[26] You and coworkers have recently designed a one-pot method for synthesis of sequence controlled polymer consisting of a short sequence of monomers which were synthesized using sequential addition of different monomers via a combination of different organic reactions.[27] Although, the precision and reliability of these step-growth approaches for sequence control is quite high, the inability to use these for synthesis of polymers, high costs and scalability are some major concerns which limit their use.

Solid state Merrifield-Synthesis has been widely appreciated as a tool for development of macromolecular structures with precise monomer sequences of artificial peptides on a solid support.[8,21] However, synthesis of relatively short peptides limits this method, along with

consecutive protection-deprotection reactions and various purification steps. These processes make it highly time consuming and restricts its scalability. Higashimura and coworkers synthesized the sequence-controlled oligomers of vinyl ethers and styrene derivatives via living cationic polymerization.[28] Kamigaito and coworkers used atom transfer radical polymerization (ATRP) to synthesize sequence defined copolymers of styrene, acrylate and vinyl chloride from defined oligomers.[29]

Recently, Single molecule insertion (SMI) has gained considerable attention as an effective strategy to synthesize polymers with a variety of pendent functionalities and to achieve more complex architectures such as graft, branch and dendritic polymers.[30–32] In late 1980's, Zard and coworkers first performed the SMI of an N-alkylmaleide or a vinyl sulfone into a xanthate.[33] Later on, Chen and coworkers inserted a single unit of styrenic derivatives into dithiobenzoate macro-RAFT agents,[34] and since then this technique has been widely used for chain-end functionalization using different molecules including maleic anhydride,[35] N-alkyl maleimides[36] etc. Tsanaktsidis and coworkers used radical addition reversible transfer polymerization (RAFT) to sequentially insert two single monomer units into a RAFT agent.[37] They first inserted a single styrene unit which was followed by insertion of a single N-isopropyl acrylamide (NIPAM) monomer into a trithiocarbonate RAFT agent. Each insertion step was followed by purification of the macro-RAFT chain transfer agent (CTA) using column chromatography. However, due to separation limitations further single monomer insertion could not be achieved. Utilizing the concept of strong cross-polymerization behavior of maleimides and maleic anhydrides with styrene, various controlled radical polymerization techniques such as ATRP, Nitroxide Mediated Polymerization (NMP) and RAFT have been used to synthesize AB alternating monomer sequences. Lutz and coworkers have demonstrated that the addition of maleimides in small quantity at specific conversion of styrene

polymerization can vary the maleimides units from 8-10 units to 1 monomer unit insertion at precisely located position on the polystyrene backbone.[38,39] They successfully installed a series of different functionalities into a polystyrene backbone in a sequential manner and demonstrated the possibility of further controlling the sequence of the polymer using automated synthetic protocols.[40] Huang and coworkers exploited the concept of the radical addition on unconjugated double bonds as an effective strategy to perform SMI on the ATRP chain-end.[41] They added one allyl alcohol molecule on the ATRP chain-end (PMMA) using atom transfer radical addition (ATRA), and then oxidized the hydroxymethyl residue to a carboxylic acid, which was later converted to an ester to yield an active side group for further chain extension. Photo-induced copper-mediated radical polymerization has also been used to synthesize monodisperse sequence defined acrylate oligomers via consecutive SMI reactions and purifying the desired product using column chromatography or preparative Gel Permeation Chromatography (GPC).[42] Recently, Kamigaito and coworkers synthesized main and side chain sequence-regulated vinyl copolymers using a 2 step synthetic process.[43] First, the synthesis of sequenced "oligomonomers" was performed using iterative atom transfer radical addition (ATRAs) of vinyl monomers for side chain control and secondly, 1:1 or 2:1 alternating radical copolymerization of the synthesized oligomonomers and vinyl comonomers was performed for main chain control. In addition to the living radical polymerization techniques, O'Reilly and coworkers utilized the reactivity of *exo* and *endo* isomers of functional norbornenes to control the monomer sequence in ring-opening metathesis polymerization (ROMP) to give sequence controlled functionalized polynorbonenes.[44]

2.2 Molecules for Single Molecule Insertions in Different Polymers

Controlling the primary structure of the polymer chain in a chain-growth polymerization is synthetically challenging due to the difficulty in tuning the reactivity of the highly reactive

transient species (radicals or ions). Inability to control the reactivity of the two monomers A and B when copolymerized, creates undefined co-monomer sequences. The reactivity between the two co-monomers is primarily dependent on their intrinsic chemical reactivity which is quantified by the reactivity ratios between the two monomers or by the *Q–e* scheme, where *Q* expresses the monomer reactivity using resonance stabilization and *e* measures its polarization considering the functional group attached to the vinyl group. These parameters define the primary sequence in a copolymer being statistical, random, block or alternating sequences obtained in a chain-growth radical, anionic or cationic polymerization. The most fascinating among these sequences is the alternating sequence, which is the only perfectly controlled primary structures synthesized in a chain-growth process.

Utilizing several alternating monomer sequences reported in the literature, we screened molecules whose reactivity ratio with the monomer comprising the polymer chain is zero and do not homopolymerize. These molecules should insert precisely once into the polymer chain-end with high fidelity and provide functionalities for post-insertion modifications. A series of molecules satisfying the criteria for single molecule insertion mentioned in the previous section were investigated based on their reactivity ratios with styrene and methyl methacrylate and *Q–e* scheme. Different molecules were examined for SMI on polystyrene and poly (methyl methacrylate) and were used to synthesize a series of polymers which lie along the continuum of a 3-arm star and A-B-C linear triblock copolymers as described in Chapter 3. The molecule for SMI needs to insert only once within the polymer chain while maintaining its livingness for subsequent chain extension. Furthermore, the single molecule inserted should have the required functionality for grafting of the third polymer chain. With this overall approach we have the unique opportunity to move along the continuum between 3-arm star and A-B-C linear triblock copolymer.

2.3 Experimental Procedure

2.3.1 Insertion Chemistry

The insertion chemistry was performed on the PS or PMMA macro-RAFT agent using excess of the candidate molecule for SMI. PS or PMMA macro RAFT agent (1equiv.) was placed in a reaction vial and was dissolved in an appropriate amount of 1,4 dioxane. The candidate molecule (3 equiv.) and the initiator AIBN (0.1 equiv.) was added to the reaction mixture and the reaction vial was sealed. The reaction mixture was degassed by purging with nitrogen for 15 min and kept in oil bath at 60 °C for 3 days to ensure completion insertion of the candidate molecule at the PS or PMMA chain-end. The reaction mixture was then precipitated in methanol, filtered and dried under vacuum for 24 h to yield either PS-SMI or PMMA-SMI macro-RAFT agent. The insertion efficiency of the candidate structure was then analyzed using Electrospray Ionization Mass Spectroscopy (ESI-MS) and ^{1}H NMR spectroscopy.

2.3.2 Chain Extension after SMI

To further demonstrate the "livingness" of the PS-SMI or PMMA-SMI macro RAFT agent, chain extension with either styrene or MMA was performed. PS-SMI or PMMA-SMI macro-CTA was placed in a reaction vial and dissolved in an appropriate amount of 1,4 dioxane. The initiator AIBN (macro-CTA: AIBN ratio (20:1)) along with the calculated amount of styrene or MMA were added to the reaction mixture. The reaction vial was sealed and purged with nitrogen for 15 mins and placed in a preheated oil bath at 60 °C and allowed to react for a defined amount of time to achieve the desirable conversion. After completion, the reaction mixture was diluted using ethyl acetate and precipitated in methanol. The precipitated polymer was filtered and dried for 24 h under

vacuum, and was analyzed using GPC. The complete clean shift of the characteristic polymer peak towards lower retention times in GPC helped in examining the efficacy of the PS or PMMA-SMI macro CTA for chain extension, thus confirming the livingness of the polymer chains for subsequent monomer addition.

2.3.3 Grafting Chemistry

The synthesized homopolymer PS-SMI-PS was dissolved in chloroform in a 20-mL reaction vial and amine-terminated PEO (1.1 equiv.) was added. NEt_3 (0.1 equiv.) as base was added and the vial was sealed and placed in a preheated oil bath at 60 °C for 3 days. On completion, the reaction mixture was diluted with ethyl acetate, precipitated in cold diethyl ether, and dried under vacuum for 24 h. To remove the excess PEO, the dried polymer was washed with H_2O:MeOH (9:1) solution mixture to yield PS-PFPMI-PS-*g*-PEO miktoarm copolymer. Following the similar procedure, amine terminated PEO was grafted onto PMMA-SMI-PMMA to yield PMMA-PFPMI-PMMA-*g*-PEO miktoarm copolymers.

2.4 Results and Discussions

Taking advantage of different chemistries for synthesis of sequence defined polymers mentioned above, one can successfully insert interesting molecules within a polymer backbone at different positions. The techniques can be advantageous to synthesize polymers with different architectures including 3-arm star, miktoarm, graft and linear polymers where the architecture of these polymer is controlled by the location of the inserted single molecule within the polymer backbone. The different candidate molecules studied for SMI on PS chains are listed in Figure 1 and for PMMA chains are listed in Figure 2.

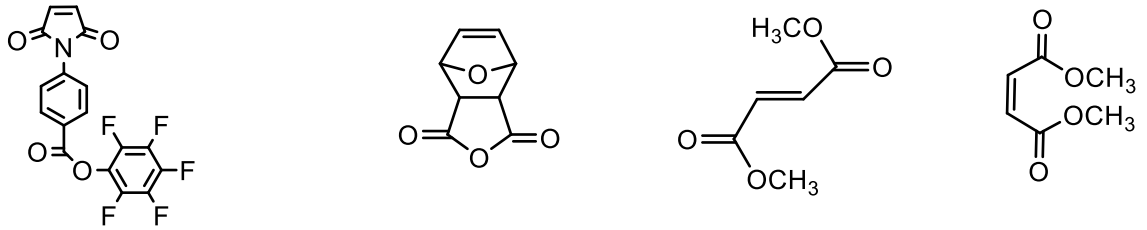

Figure 2. 1: Candidate Molecules for SMI on PS chain.

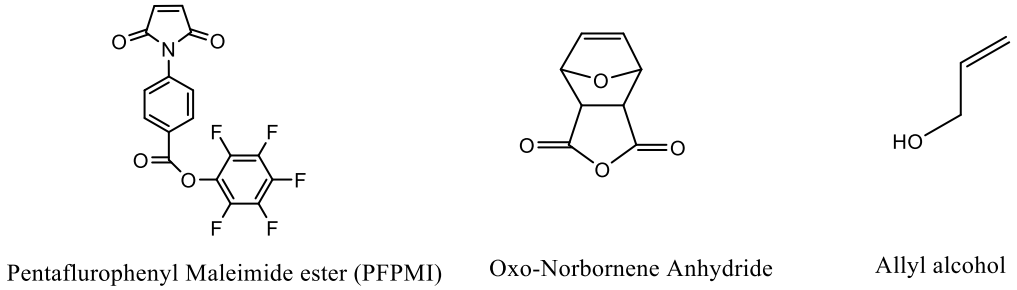

Figure 2. 2: Candidate molecules for SMI on PMMA chain.

The proficiency of these molecules to precisely insert once onto the polymer backbone was analyzed using ESI-MS. The shift in the molecular weight distribution of the polymeric chain by molecular mass of the candidate molecule after the insertion chemistry helped in determining the efficiency of the candidate molecule to insert onto the polymer chain-end.

Using RAFT methodology, the single insertion of PFPMI molecule was performed at the PS chain-end to yield PS-PFPMI macro-CTA as described in Scheme 1. Successful single insertion of PFPMI molecule was confirmed by performing the ESI-MS on both PS macro-CTA and PS-PFPMI macro-CTA. The ESI-MS of PS-PFPMI macro-CTA revealed the shift in the molecular weight distribution by 383.23 g/mol corresponding to the molecular weight of PFPMI as shown in Figure 3 validating only one insertion at the PS chain-end. The single PFPMI monomer insertion was also confirmed using ^{1}H NMR and peaks between δ 8.0-8.2 ppm corresponding to the aromatic ring of PFPMI monomer were observed (Figure 4).

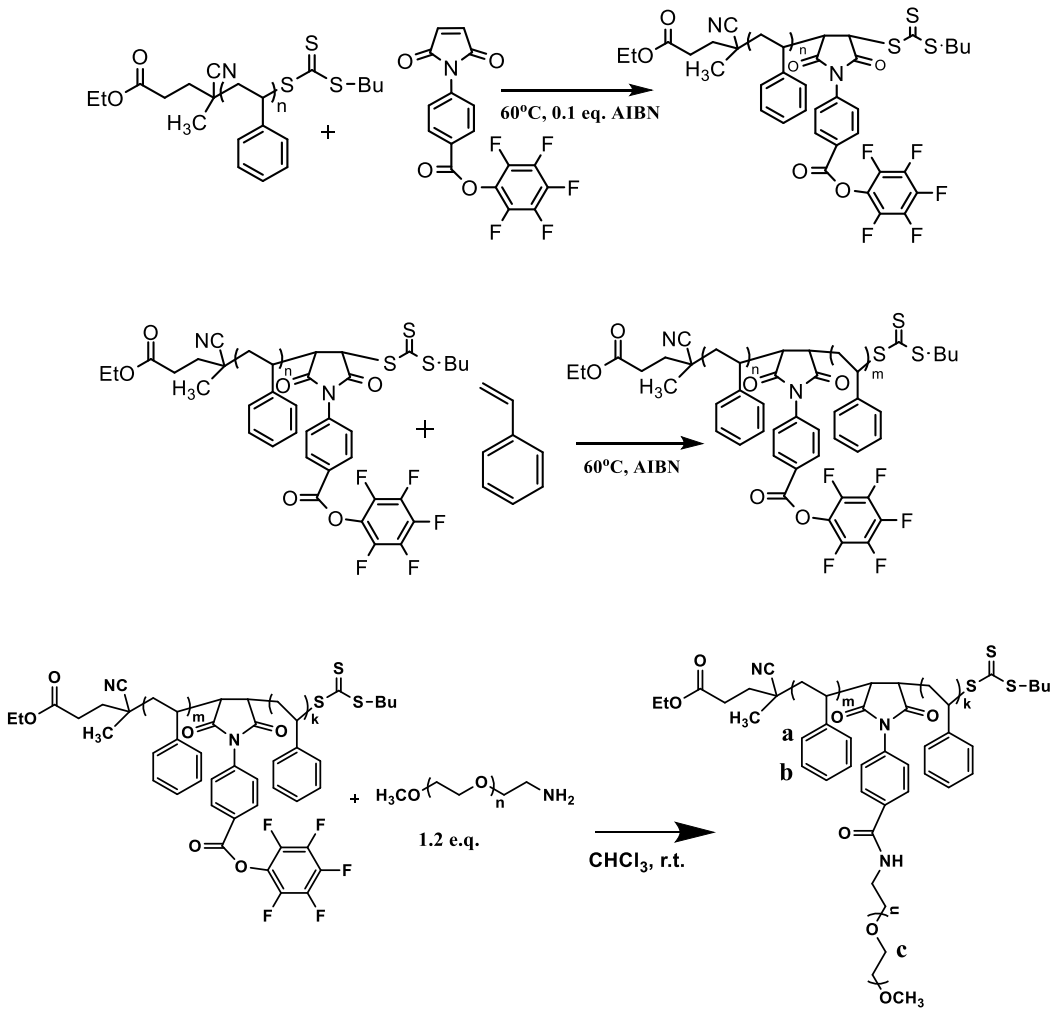

Scheme 1: Single molecule insertion of PFPMI and synthesis of PS-PFPMI-PS-*g*-PEO block copolymer.

The end-group analysis of the PS-PFPMI chains shows the presence of the tri-thiocarbonate RAFT CTA which affirms its attachment to the polymer chains after the SMI. To demonstrate the livingness of the PS-PFPMI chains, chain extension was performed using styrene and a complete shift in the GPC was observed from 3.9 Kg/mol for PS-PFPMI macro-CTA to 21 Kg/mol for PS-PFPMI-PS homopolymer (Figure 5 (a)) with the overall dispersity remaining low (<1.1). After successful insertion and chain extension, subsequent grafting of amine terminated PEO was performed utilizing activated ester chemistry (Figure 5 (b)).

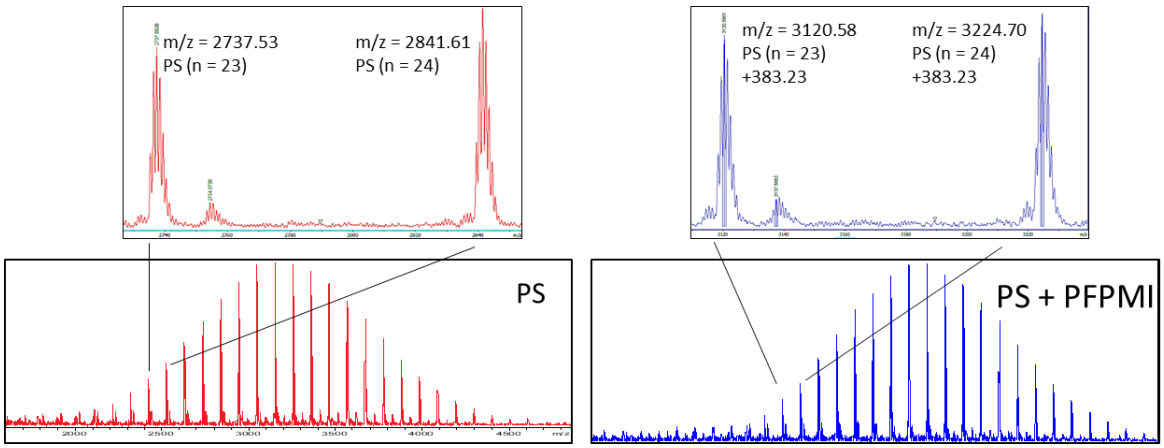

Figure 2. 3: MW distribution of PS chains before (left) and after SMI of PFPMI using ESI-MS (right).

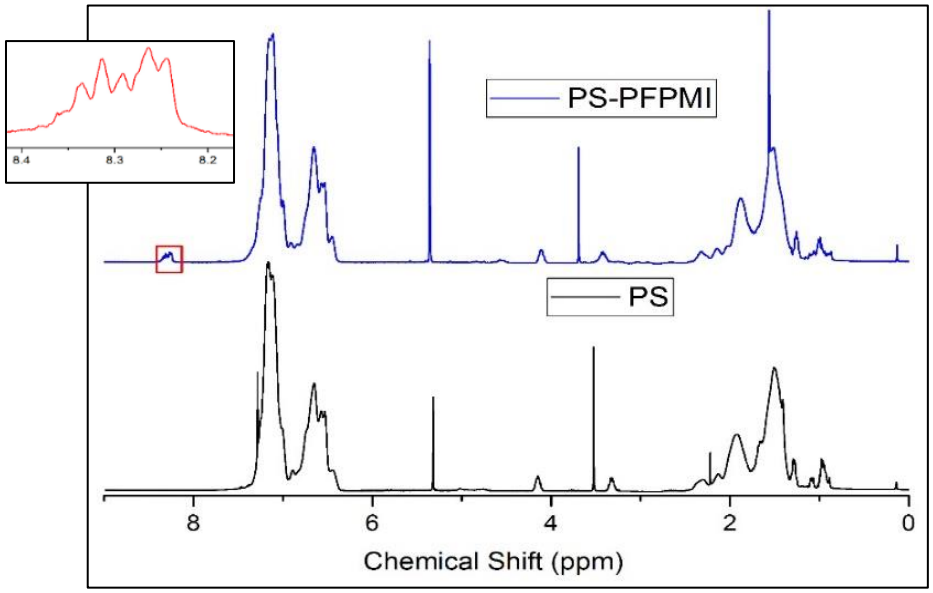

Figure 2. 4: ^{1}H NMR data for SMI of PFPMI molecule, inset is the aromatic region for PFPMI molecule (top) on PS chain-end (bottom).

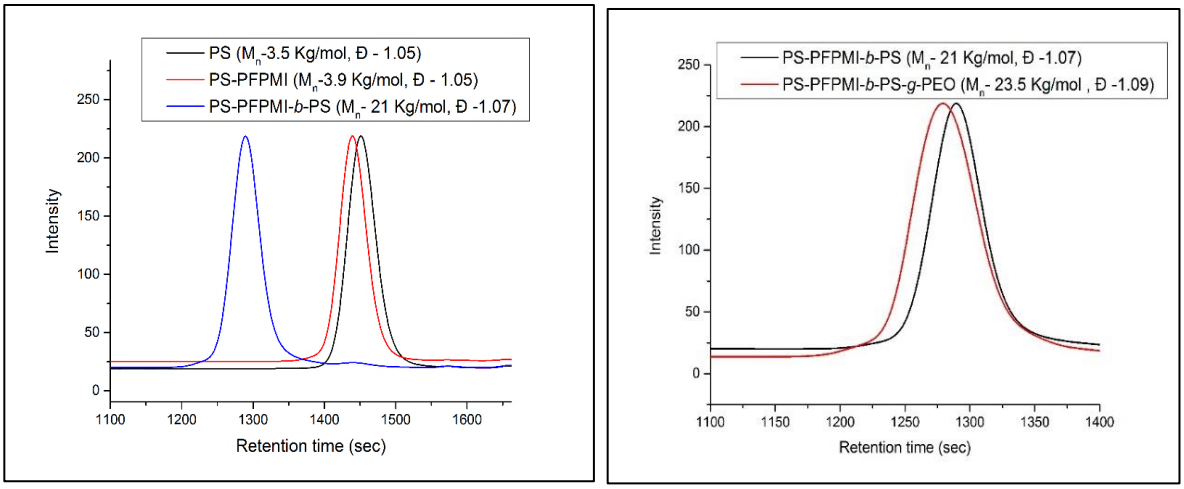

Figure 2. 5: GPC traces for PS, PS-PFPMI (left) and PS-PFPMI-PS and PS-PFPMI-PS-*g*-PEO copolymer (right).

The single molecule insertion of oxo-norbornene anhydride at the PS chain-end was performed as described in Scheme 2. A shift in molecular weight distribution for the PS chain by 122 g/mol was observed using ESI-MS after single insertion of oxo-norbornene anhydride molecule. The standard operating temperature for ESI-MS is approx. 200 °C, therefore a shift of 122 g/mol was observed as opposed to the expected 166 g/mol (MW of oxo-norbornene anhydride) (Figure 6). This can be attributed due to the tendency of anhydrides to liberate CO_2 at elevated temperatures.[45] The end-group analysis of the PS chain after SMI and the GPC data for PS chain extension confirms the livingness of the polymer chains after the SMI of oxo-norbornene anhydride (Figure 7). The grafting of amine terminated PEO onto the PS backbone at the oxo-norbornene anhydride junction clearly demonstrates the nucleophilic addition of the PEO arm to yield PS-b-PEO miktoarm copolymer with the ability to vary the location of the PEO arm on the PS backbone. When excess of PEO was used, this molecule can allow synthesis of miktoarm copolymers with the ability to insert two arms at a defined position within a polymer backbone.

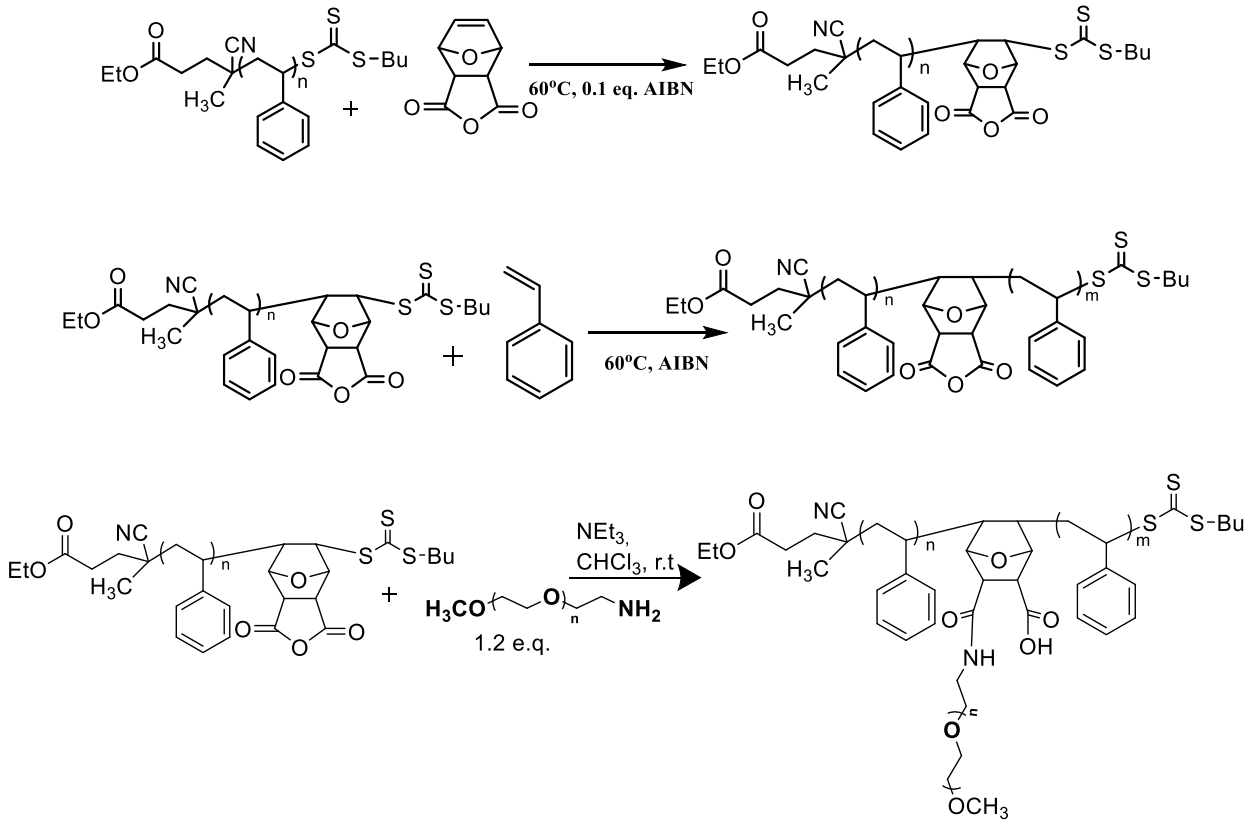

Scheme 2: Single molecule insertion of oxo-norbornene anhydride and synthesis of PS-Nor-An-PS-*g*-PEO block copolymer.

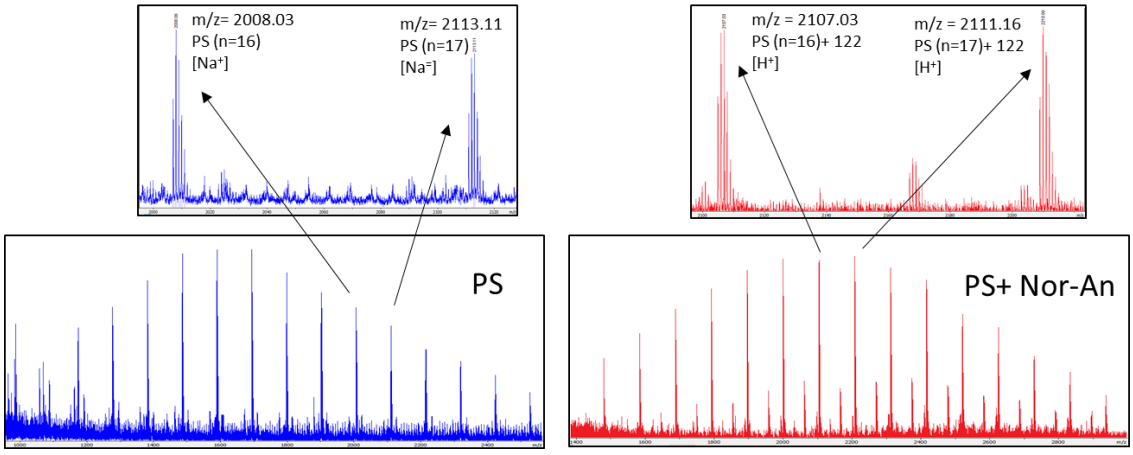

Figure 2. 6: MW distribution of PS chains before (left) and after SMI of oxo-norbornene anhydride using ESI-MS (right).

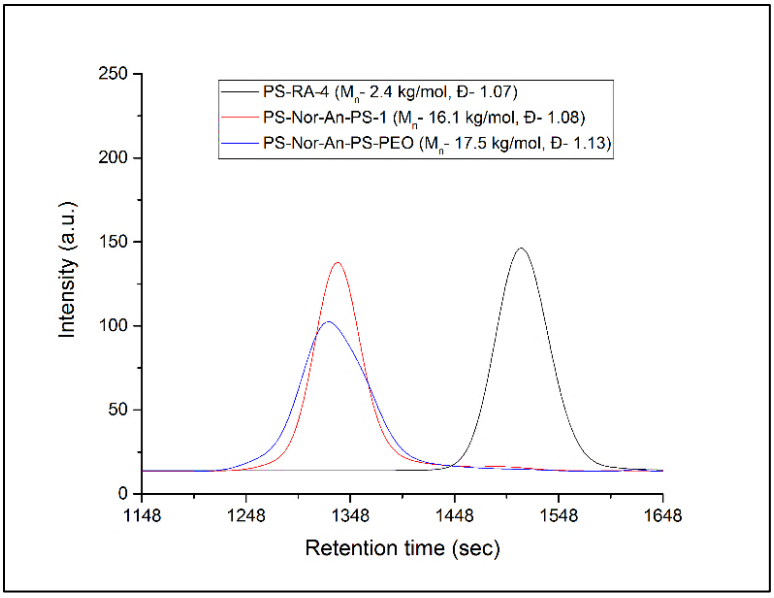

Figure 2. 7: GPC traces for PS homopolymer, PS-Nor-An-PS and PS-Nor-An-PS-*g*-PEO copolymers.

Similarly, the single molecule insertion of the two isomers dimethyl fumarate (DMFu) and dimethyl maleate (DM), were performed as described in Scheme 3. A shift in the PS molecular weight distribution by 144.12 g/mol using ESI-MS confirmed the single insertion of the two isomers at the PS chain end (Figures 8,9). The livingness of the PS chain after successful single insertion was confirmed by the end-group analysis and GPC data obtained for the PS chain extension (Figure 10). These molecules can be further modified for post-polymerization chemistries to synthesize miktoarm copolymers with the ability to insert two arms at a defined location.

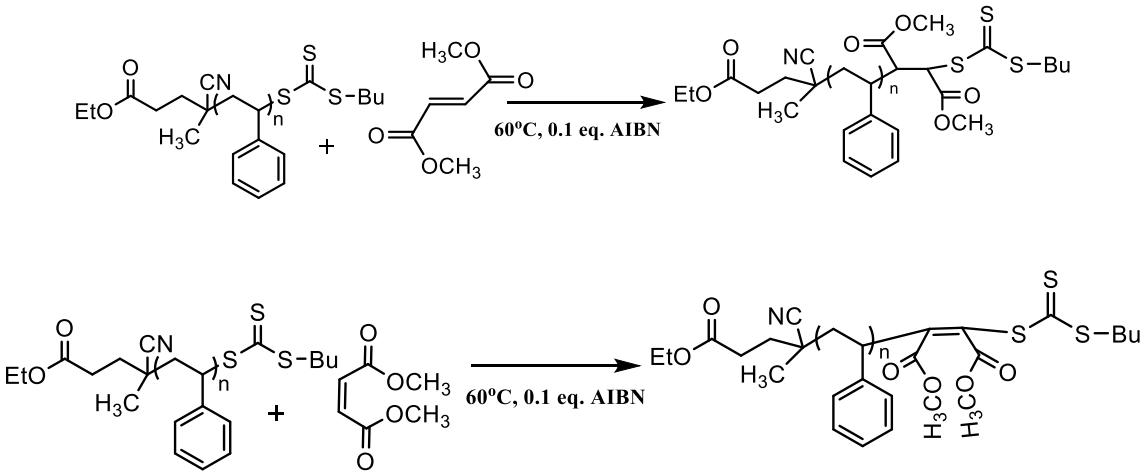

Scheme 3: Single molecule insertion of dimethyl fumarate and dimethyl maleate.

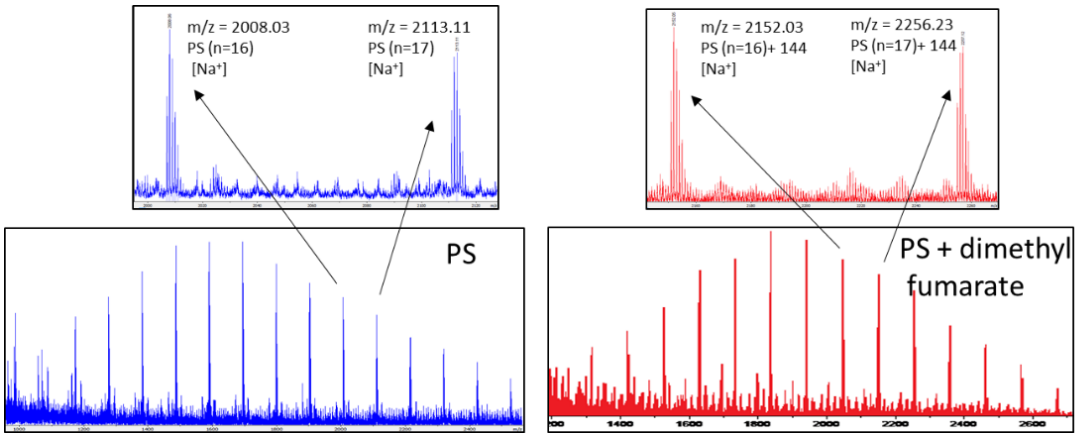

Figure 2. 8Figure 8: Molecular weight distribution using ESI-MS for PS (left) and PS-DMFu (right).

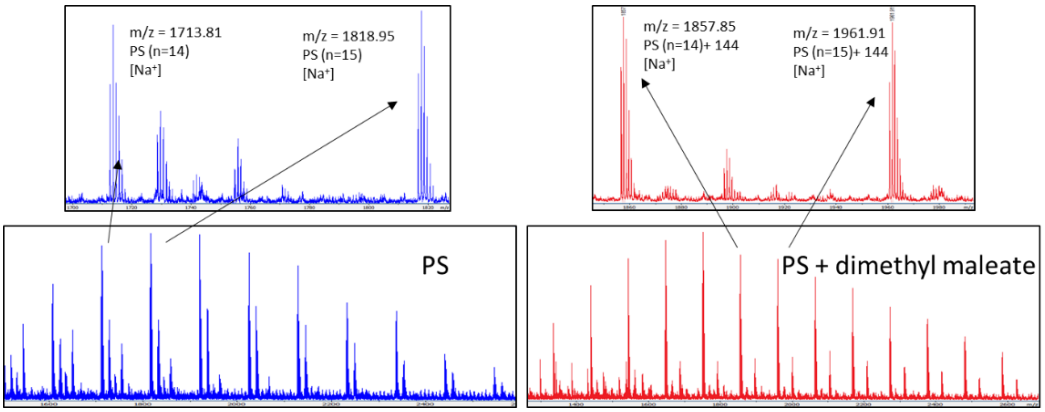

Figure 2. 9 Molecular weight distribution using ESI-MS for PS (left) and PS-DM (right).

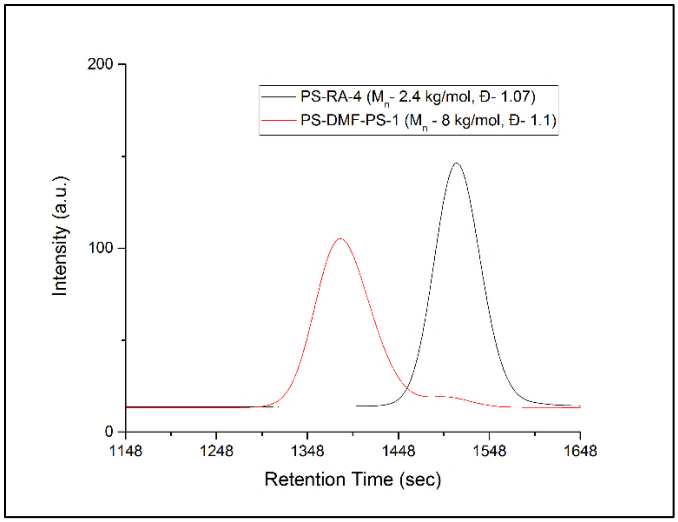

Figure 2. 10: GPC traces for PS homopolymer, and PS-DMF-PS.

Different molecules were investigated for SMI within PMMA chain including oxo-norbornene anhydride (Nor-An), pentafluorophenyl maleimide ester (PFPMI) and allyl alcohol (AA). The single molecule insertion of oxo-norbornene anhydride (Nor-An) on the PMMA chain was performed as shown in Scheme 4. The single molecule insertion at the PMMA chain-end was confirmed using ESI-MS. The MW distribution for PMMA chains was shifted by 122 g/mol instead of 166 g/mol due to the susceptibility of anhydrides towards losing CO_2 at the elevated operating temperature for ESI-MS (Figure 11). A subsequent shift in the PMMA-Nor-An GPC trace after chain extension confirmed the livingness of the PMMA-Nor-An chains after single molecule insertion. After successful insertion and chain extension, the PEO chain was grafted on the PMMA-Nor-An-PMMA homopolymer by performing nucleophilic addition using amine terminated PEO in the presence of NEt_3 as base. The shift in the GPC trace after PEO grafting clearly demonstrates the high efficiency of the reaction and the ability to synthesize miktoarm copolymers with precise grafting position within the PMMA chain (Figure 12).

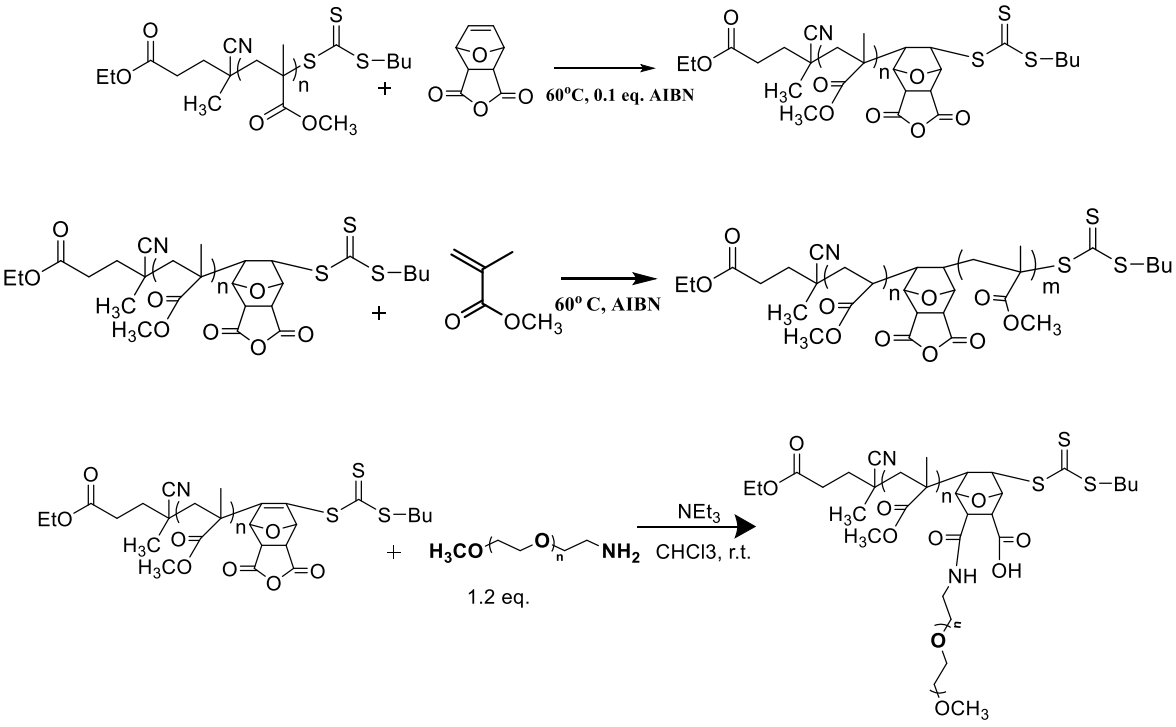

Scheme 4: Single molecule insertion of oxo-Norbornene anhydride within PMMA, chain extension and PEO grafting.

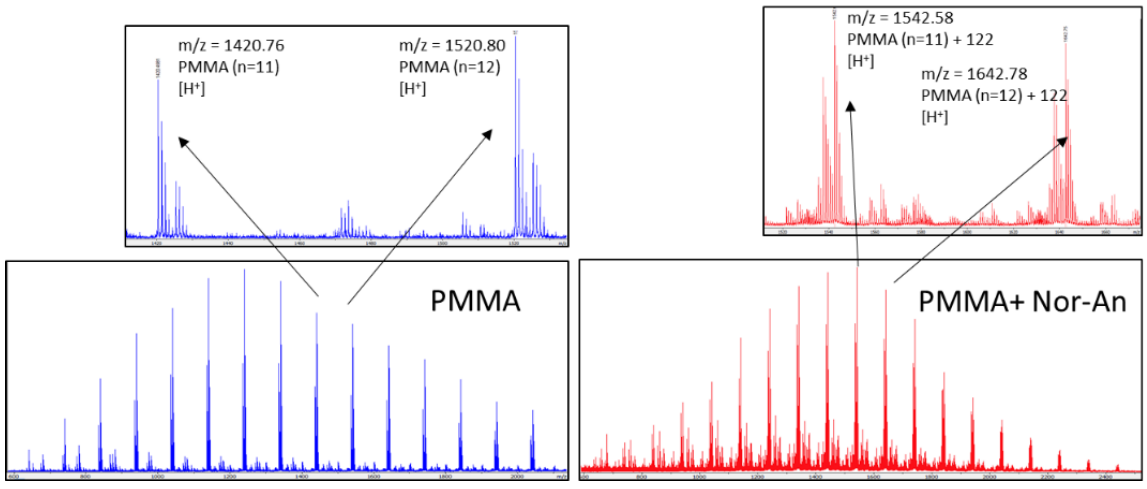

Figure 2. 11: Molecular weight distribution using ESI-MS for PMMA (left) and PMMA-Nor-An (right).

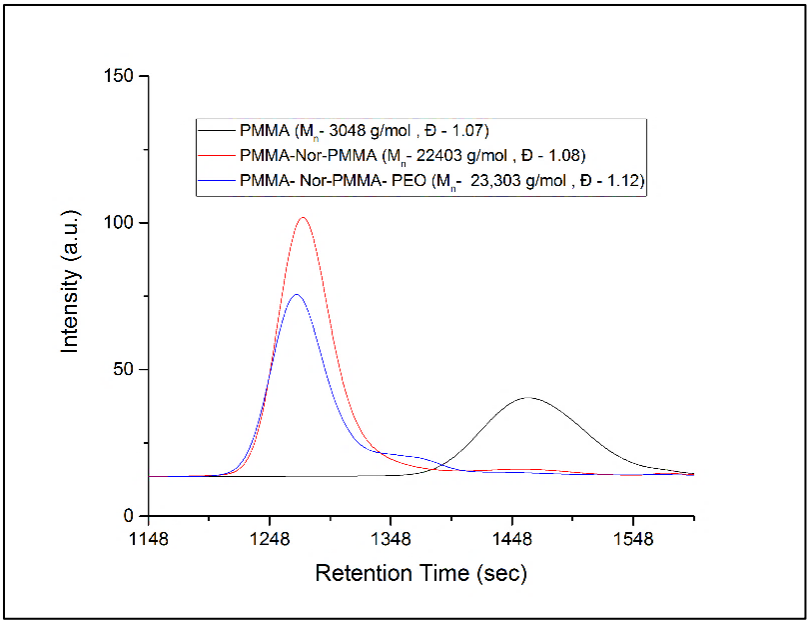

Figure 2. 12: GPC traces for PMMA homopolymer, and PMMA-Nor-An-PMMA and PMMA-Nor-An-PMMA-*g*-PEO block copolymers.

Single molecule insertion of PFPMI was performed as described in Scheme 5. The single insertion of PFPMI was confirmed using ESI-MS with a MW shift for PMMA chains by 383.23 g/mol corresponding to the MW of PFPMI (Figure 13). After single insertion, chain extension with MMA was performed which led to an uncontrolled increase in MW over short polymerization times. When the chain extension was performed using styrene, a controlled increase in the MW of styrene was observed confirming the livingness of the PMMA-PFPMI chains. Amine terminated PEO was used to graft the PEO arm on the PMMA-*b*-PS diblock to yield PMMA-*b*-PS-*g*-PEO 3-arm star copolymer (Figure 14).

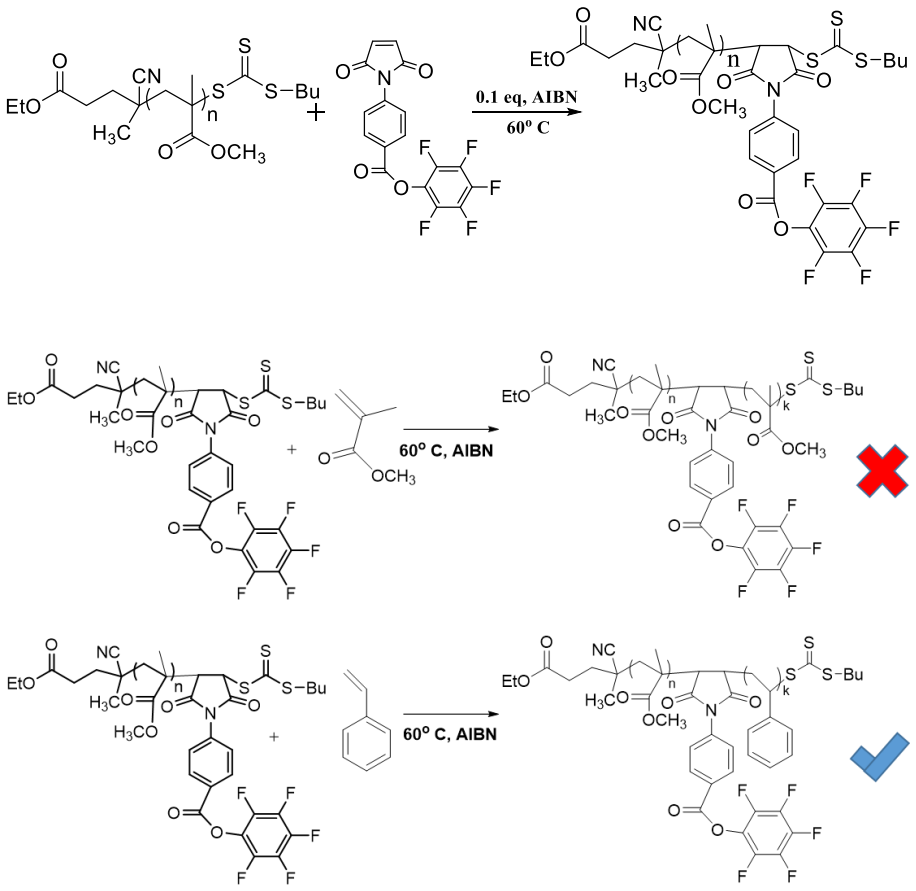

Scheme 5: Single molecule insertion of PFPMI, chain extension with MMA (top) and styrene (bottom).

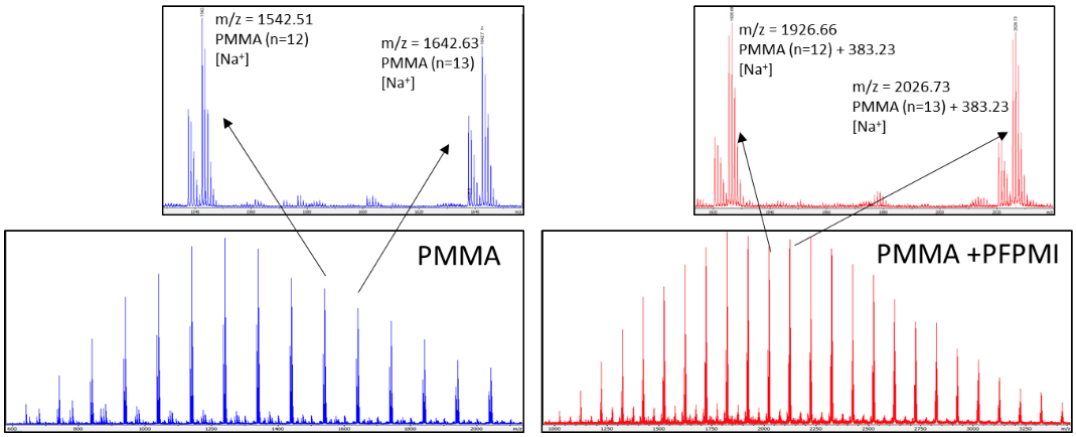

Figure 2. 13: Molecular weight distribution using ESI-MS for PMMA (left) and PMMA-PFPMI (right).

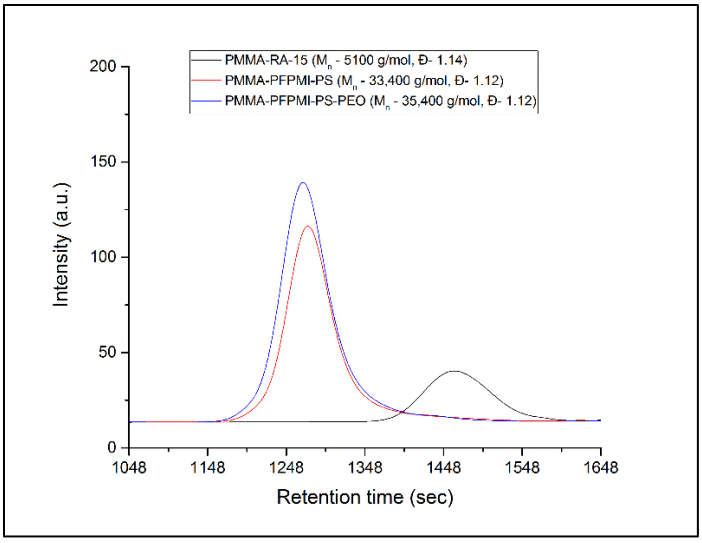

Figure 2. 14: GPC traces for PMMA homopolymer, and PMMA-PFPMI-PS and PMMA-PFPMI-PS-g-PEO block copolymers.

To investigate further, this unusual polymerization of PMMA using PMMA-PFPMI macro-CTA, a kinetic study for MMA chain extension was performed. The results suggested slower initiation and faster propagation of the PMMA chains in contrast to fast initiation and slower propagation expected for the attainment of living polymerization conditions. Similar unusual behavior with MMA chain extension was observed for all the PMMA-SMI macro-CTA's indicating the inability of the PMMA-SMI macro CTA's to efficiently initiate MMA polymerization. However, further experiments are required to completely understand this behavior particularly for MMA chain extension in detail.

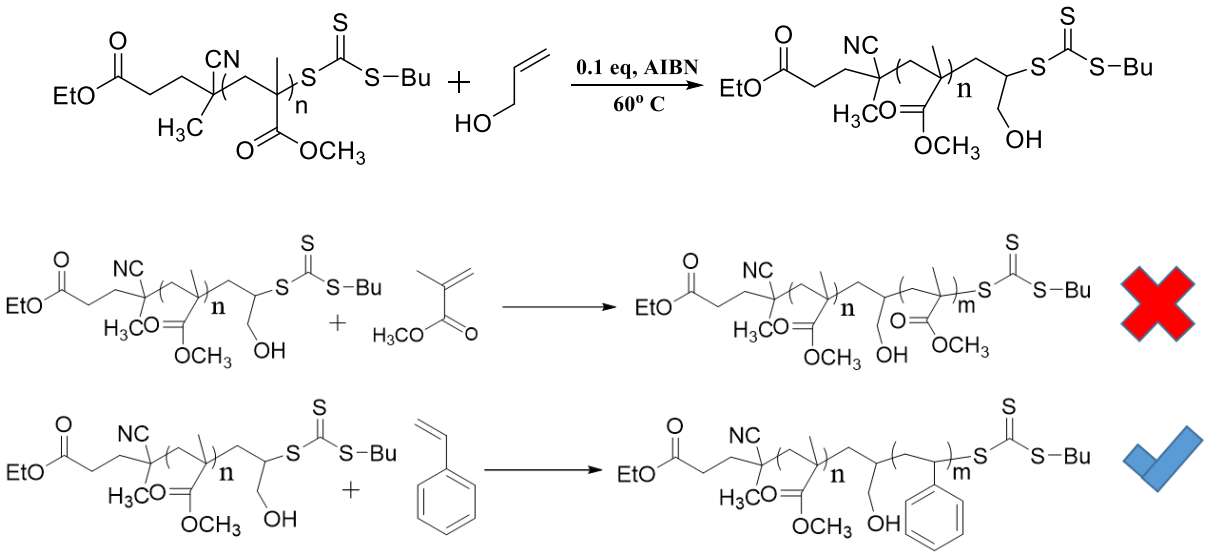

Scheme 6: Single molecule insertion of allyl alcohol and chain extension with MMA (top), and styrene (bottom).

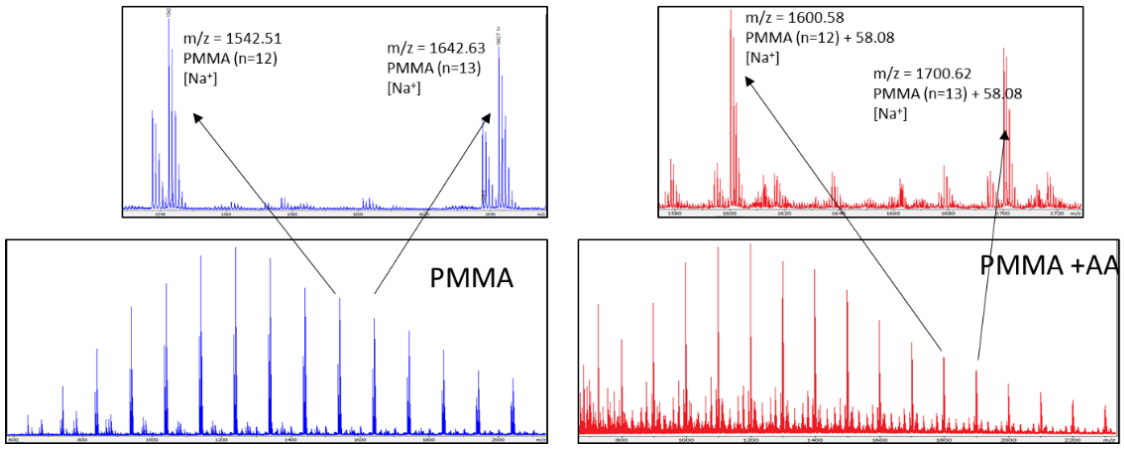

Figure 2. 15: Molecular weight distribution using ESI-MS for PMMA and PMMA-AA.

Single molecule insertion of allyl alcohol was performed as shown in Scheme 6. ESI-MS confirmed the single molecule insertion and a shift in the MW of PMMA by 58.08 g/mol was observed which confirmed the single insertion of allyl alcohol (Figure 15). To study the livingness of the PMMA-AA macro-CTA, styrene chain extension was performed. Most of the chains underwent chain extension with styrene, however a small fraction of the chains was dead as

observed by the GPC traces which might have been introduced after the single insertion of AA (Figure 16).

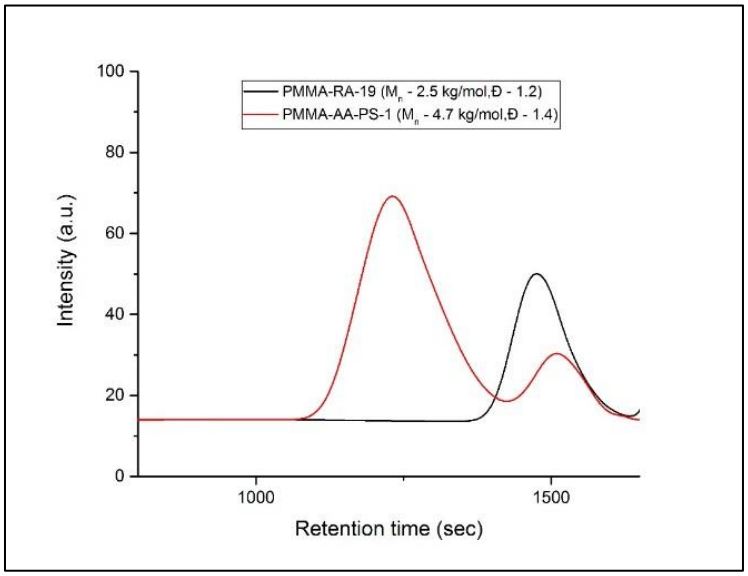

Figure 2. 16: GPC traces for PMMA homopolymer, and PMMA-AA-PS block copolymer.

2.5 Summary

We have found a range of different molecules which can insert precisely only once within the PS chain in addition to the known examples of maleimides and maleic anhydride. Also, the concept of SMI was extended to PMMA chain insertion and novel molecules for SMI within PMMA chain were studied. The concept of SMI can prove to be an efficient approach for the synthesis of polymers with different architectures such as graft, miktoarm and star copolymers. This strategy also provides exciting opportunities to end-label polymers with diverse functionalities for interesting post-polymerization chemistries.

2.6 References

(1) Lutz, J. *Angew. Chemie Int. Ed.* **2007**, *46* (7), 1018–1025.

(2) Fournier, D.; Hoogenboom, R.; Schubert, U. S. *Chem. Soc. Rev.* **2007**, *36* (8), 1369.

(3) Zhang, C.; Yang, Y.; He, J. *Macromolecules* **2013**, *46* (10), 3985–3994.

(4) Soeriyadi, A. H.; Boyer, C.; Nyström, F.; Zetterlund, P. B.; Whittaker, M. R. *J. Am. Chem. Soc.* **2011**, *133* (29), 11128–11131.

(5) Article, E.; Anastasaki, A.; Nikolaou, V.; Pappas, G. S.; Zhang, Q.; Wan, C.; Wilson, P.; Davis, T. P.; Whittaker, R.; Haddleton, D. M. *Chem. Sci.* **2014**, *5*, 3536–3542.

(6) Badi, N.; Lutz, J.-F. *Chem. Soc. Rev.* **2009**, *38* (12), 3383–3390.

(7) Lutz, J.-F.; Ouchi, M.; Liu, D. R.; Sawamoto, M. *Science (80-.).* **2013**, *341* (6146), 1238149–1238149.

(8) Merrifield, R. B. *J. Am. Chem. Soc.* **1963**, *85* (14), 2149.

(9) Mutlu, H.; Lutz, J. F. *Angew. Chemie - Int. Ed.* **2014**, *53* (48), 13010–13019.

(10) Lutz, J. F. *Acc. Chem. Res.* **2013**, *46* (11), 2696–2705.

(11) Colquhoun, H.; Lutz, J.-F. *Nat. Chem.* **2014**, *6* (June), 455–456.

(12) Chan-Seng, D.; Zamfir, M.; Lutz, J. F. *Angew. Chemie - Int. Ed.* **2012**, *51* (49), 12254–12257.

(13) Deng, X. X.; Li, L.; Li, Z. L.; Lv, A.; Du, F. S.; Li, Z. C. *ACS Macro Lett.* **2012**, *1* (11), 1300–1303.

(14) Trinh, T. T.; Oswald, L.; Chan-Seng, D.; Lutz, J. F. *Macromol. Rapid Commun.* **2014**, *35* (2), 141–145.

(15) Sun, J.; Zuckermann, R. N. *ACS Nano* **2013**, *7* (6), 4715–4732.

(16) Lutz, J. F. *ACS Macro Lett.* **2014**, *3* (10), 1020–1023.

(17) Rowan, S. J.; Barner-Kowollik, C.; Klumperman, B.; Gaspard, P.; Grubbs, R. B.; Hillmyer, M. A.; Hutchings, L. R.; Mahanthappa, M. K.; Moatsou, D.; O'Reilly, R. K.; Ouchi, M.; Sawamoto, M.; Lodge, T. P. *ACS Macro Lett.* **2016**, *5* (1), 1–3.

(18) Qu, C.; He, J. *Sci. China Chem.* **2015**, *58* (11), 1651–1662.

(19) Stayshich, R. M.; Weiss, R. M.; Li, J.; Meyer, T. Y. *Macromol. Rapid Commun.* **2011**, *32* (2), 220–225.

(20) Wong, E. H. H.; Stenzel, M. H.; Junkers, T.; Barner-Kowollik, C. *J. Polym. Sci. Part A Polym. Chem.* **2011**, *49* (10), 2118–2126.

(21) Hartmann, L.; B??rner, H. G. *Adv. Mater.* **2009**, *21* (32–33), 3425–3431.

(22) Norris, B. N.; Zhang, S.; Campbell, C. M.; Auletta, J. T.; Calvo-Marzal, P.; Hutchison, G. R.; Meyer, T. Y. *Macromolecules* **2013**, *46* (4), 1384–1392.

(23) Milnes, P. J.; McKee, M. L.; Bath, J.; Song, L.; Stulz, E.; Turberfield, A. J.; O'Reilly, R. K. *Chem. Commun.* **2012**, *48* (45), 5614–5616.

(24) Solleder, S. C.; Meier, M. A. R. *Angew. Chemie - Int. Ed.* **2014**, *53* (3), 711–714.

(25) Espeel, P.; Carrette, L. L. G.; Bury, K.; Capenberghs, S.; Martins, J. C.; Duprez, F. E.; Madder, A. *Angew. Chemie - Int. Ed.* **2013**, *52* (50), 13261–13264.

(26) Pfeifer, S.; Zarafshani, Z.; Badi, N.; Lutz, J. F. *J. Am. Chem. Soc.* **2009**, *131* (26), 9195–9197.

(27) Yan, J.-J.; Wang, D.; Wu, D.-C.; You, Y.-Z. *Chem. Commun. (Camb).* **2013**, *49* (54),

6057–6059.

(28) Minoda, M.; Sawamoto, M.; Higashimura, T. *Macromolecules* **1990**, *23* (23), 4889–4895.

(29) Satoh, K.; Ozawa, S.; Mizutani, M.; Nagai, K.; Kamigaito, M. *Nat. Commun.* **2010**, *1*, 6.

(30) Kakuchi, R.; Zamfir, M.; Lutz, J.-F.; Theato, P. *Macromol. Rapid Commun.* **2012**, *33* (1), 54–60.

(31) Pfeifer, S.; Lutz, J. F. *Chem. - A Eur. J.* **2008**, *14* (35), 10949–10957.

(32) Schmidt, B. V. K. J.; Fechler, N.; Falkenhagen, J.; Lutz, J.-F. *Nat. Chem.* **2011**, *3* (3), 234–238.

(33) Delduc, P.; Tailhan, C.; Zard, S. Z. *J. Chem. Soc. Chem. Commun.* **1988**, *1988* (4), 308.

(34) Chen, M.; Ghiggino, K. P.; Mau, A. W. H.; Rizzardo, E.; Sasse, W. H. F.; Thang, S. H.; Wilson, G. J. *Macromolecules* **2004**, *37* (15), 5479–5481.

(35) Sasso, B.; Dobinson, M.; Hodge, P. *Macromolecules* **2010**, *43* (18), 7453–7464.

(36) Henry, S. M.; Convertine, A. J.; Benoit, D. S. W.; Hoffman, A. S.; Stayton, P. S. *Bioconjug. Chem.* **2009**, *20* (6), 1122–1128.

(37) Houshyar, S.; Keddie, D. J.; Moad, G.; Mulder, R. J.; Saubern, S.; Tsanaktsidis, J. *Polym. Chem.* **2012**, *3* (7), 1879.

(38) Zamfir, M.; Lutz, J.-F. *Nat. Commun.* **2012**, *3* (18), 1138.

(39) Pfeifer, S.; Lutz, J. F. *J. Am. Chem. Soc.* **2007**, *129* (31), 9542–9543.

(40) Vandenbergh, J.; Reekmans, G.; Adriaensens, P.; Junkers, T. *Chem. Commun. (Camb).* **2013**, *49* (88), 10358–10360.

(41) Tong, X.; Guo, B.; Huang, Y. *Chem. Commun. (Camb).* **2011**, *47* (5), 1455–1457.

(42) Vandenbergh, J.; Reekmans, G.; Adriaensens, P.; Junkers, T. *Chem. Commun. (Camb).* **2013**, *49* (88), 10358–10360.

(43) Soejima, T.; Satoh, K.; Kamigaito, M. *J. Am. Chem. Soc.* **2016**, *138* (3), 944–954.

(44) Moatsou, D.; Hansell, C. F.; O'Reilly, R. K. *Chem. Sci.* **2014**, *5* (6), 2246–2250.

(45) Ashida, R.; Painter, P.; Larsen, J. W. *Energy and Fuels* **2005**, *19* (5), 1954–1961.

CHAPTER III

EXPLORING THE CONTINUUM BETWEEN A 3-ARM STAR AND A-B-C LINEAR TRIBLOCK COPOLYMER

3.1 Introduction

Block copolymers represent a class of materials composed of two or more covalently attached incompatible blocks which can spontaneously segregate into self-assembled structures with controllable dimensions and functionalities.[1–3] The versatility of block copolymers in terms of their compositional sequence, architecture, and the choice of monomers can lead to dramatic changes in self-assembly and can allow for tailoring mechanical, electrical, optical and other physical properties for the targeted application.[4,5] The simplest and most studied architecture for block copolymers is the linear A-B diblock, whose morphological behavior is dependent on three experimentally controllable factors: the overall degree of polymerization (N), the volume fraction of the A component (φ_A) and the Flory-Huggins interaction parameter χ_{AB} whose magnitude is determined by the selection of the A-B monomer pair. Depending on the values of φ_A and $\chi_{AB}N$, a diblock copolymer can self-assemble into different equilibrium morphologies with a domain spacing ranging from 10-100 nm[1,2,6–10] By means of incorporating more chemically distinct blocks into a chain, or adapting unique properties such as chiral, crystalline or rod-like structures for one of the blocks; more complex morphologies can be observed which can offer opportunities in designing novel nanostructured materials with improved functionality and properties.[6,11] Alternatively, the complexity of block copolymers can be greatly enlarged by increasing the number of blocks (n) (A_nB_n block copolymers), bonding more than two chemically distinct blocks (A-B-C triblock copolymers), and by introducing architectural asymmetry (cyclic, graft-type, H-

type and star-shaped, and miktoarm block copolymers, *etc.*).[12–17] These block copolymers, referred to as multi-block copolymers are promising candidates for exploring a range of intriguing nanostructures due to the increase in the number of parameters governing their phase behavior. In comparison to diblock copolymers, where the morphology is controlled by the volume fraction of one block and the interaction parameter between the two blocks; the morphology of triblock terpolymers is critically affected by different factors such as the volume fraction of each individual block, three different interaction parameters and the sequence of the three blocks.[18] Furthermore, different chain architectures—linear, star, branched or ring—can significantly contribute to the morphological complexity observed for multiblock copolymer systems.[19,20]

Controlling the large parameter space offered by multiblock copolymers, allows access to novel co-continuous and multi-component-continuous morphologies which are inaccessible using conventional diblock copolymer architectures. Various multiply continuous morphologies observed for multiblock copolymers have been shown to enhance different mechanical properties such as toughness, stress at failure, and creep resistance.[21–23] These multi-domain structures have high interfacial area per specimen volume which can be used to enhance the efficiency of gas separation membranes and solar cell membranes that separate and extract excitons.[24–29] Percolating domain structures can be promising candidates for materials used in water purification.[30–32] Several 3-D structures observed for multiblock copolymers can be utilized to significantly increase the ion conductivity in different energy applications such as fuel cells and batteries.[33–35] In addition to these applications, these multiple domain morphologies have also been found to play an important role in the emerging technology of 3-D photonic crystals.[36,37]

Among the numerous multiblock architectures, the linear triblock terpolymer and the star architecture have been studied extensively both experimentally and theoretically. Many complex

morphologies have been observed for the linear triblock architectures which includes structure-within-structure phases, such as cylinders-within-lamellae, spheres-within-lamellae, cylinders-on-cylinders, helices-on-cylinders, rings-on-cylinders, spheres-on-cylinders, spheres-on-spheres, and knitting patterns.[18,38,47–56,39–46] Meanwhile, for the A-B-C 3-arm star architecture several hierarchical structures including lamellae-in-cylinder, cylinders-in-lamella, lamellae-in-sphere, and hierarchical double gyroid structures have been discovered.[57,58,67–75,59–66] Both the A-B-C linear triblock and the A-B-C 3-arm star architectures have the same constitutional blocks but depending on the position of the C block, the two different architectures can be accessed. The C block at the junction of A-B block leads to 3-arm architecture, while the C block at the chain end leads to the linear triblock architecture. Conceptually, the shifting of the position of the C block along the B block can provide access to novel polymer architectures which would lie along the continuum between a 3-arm star and A-B-C linear triblock copolymer (Figure 1). This continuum of polymers has not been previously investigated, and is a challenge for the development of synthetic methodologies and morphological characterization.

In this chapter, a versatile strategy is reported to synthesize a series of PMMA-*b*-PS-*g*-PEO and PtBA-*b*-PS-*g*-PEO continuum graft copolymers which lie along the continuum between a 3-arm star and A-B-C linear triblock copolymer. Because of these investigations, a unique approach has been developed to explore systematic changes in the morphology solely as a consequence of topological frustration while keeping both χN and φ constant.

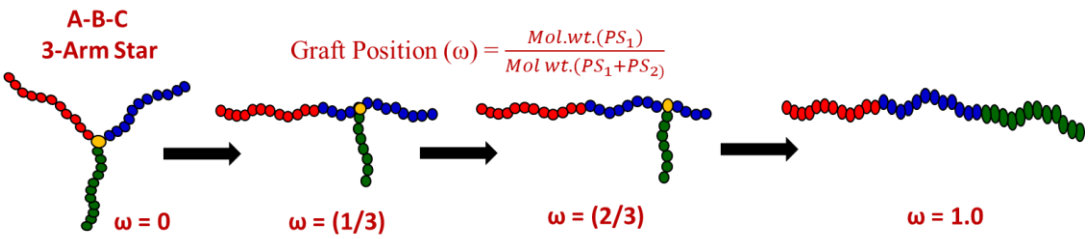

Figure 3. 1: Representative figure for different continuum graft copolymers.

3.2 Materials and Methods

3.2.1 Materials

Methyl Methacrylate (99%, Alfa Aesar) and Styrene (99%, Alfa Aesar), tert-butyl acrylate monomers were passed through a column of basic alumina prior to use to remove the inhibiter. Azobisisobutyronitrile (AIBN) was recrystallized from methanol and stored at 0^{o} C before use. Pentafluorophenyl maleimide ester (PFPMI) was synthesized as per the reported literature.[76] Poly (ethylene glycol) methyl ether was purchased from Sigma Aldrich and was modified to amine-terminated Poly (ethylene glycol) using reported literature methods.[77]

3.2.2 Instrumentation

^{1}H NMR spectroscopy was performed on 500 MHz Bruker 500 Ascend NMR spectrometer. Gel permeation chromatography (GPC) was performed in THF at a flow rate of 1.0 mL/min using a refractive index detector on a Polymer Laboratories PL-GPC 50 Integrated GPC. Small-angle X-ray scattering (SAXS) measurements were performed using a GANESHA 300 XL SAXS instrument. For SAXS measurements, the samples were prepared by dissolving the polymer in anhydrous benzene at a concentration of 50 mg/mL and casting to produce solid films in 1 mL Teflon beakers. The beakers were covered with a glass hood to allow slow evaporation of the solvent at room temperature over 5 days. Then, the samples were vacuum dried overnight to remove any residual solvent in the film, followed by thermally annealing at 125 °C for 5 days for under vacuum for the PMMA-*b*-PS-*g*-PEO samples and 170 °C PtBA-*b*-PS-*g*-PEO samples respectively. For transmission electron microscopy (TEM), ultra-thin sections of approximately 40 nm thickness were cut with a Leica (Reichert & Jung) ULTRACUT Ultramicrotome using a diamond knife at room temperature. These sections were mounted on 400 mesh copper support

grids and were stained using RuO_4 for 10 min. The stained thin sections were then examined on a JEOL 2000FX TEM operated at an accelerating voltage of 200 kV.

3.3 Exploring the Continuum of a 3-arm Star and A-B-C Linear Triblock copolymer for PMMA-*b*-PS-*g*-PEO graft copolymers.

3.3.1 Methods

3.3.1.1 Synthesis of RAFT Chain Transfer Agent for MMA Polymerization.

The synthesis of RAFT CTA-1a was performed following a reported procedure.[78] CTA-1a was modified to CTA-1b using dicyclohexylcarbodimide-4-N,N dimethaminopyridine (DCC-DMAP) coupling reaction. In a round bottom flask, CTA-1a (2.55 g, 8.75 mmol) and ethanol (1.1 mL, 17.5 mmol) were added to 30 mL dichloromethane (DCM) and stirred at room temperature for 2 days (Scheme 1). The product obtained was kept overnight in the refrigerator at -30 ^oC to precipitate the dicyclohexylurea (DCU) generated during the reaction. The product was then filtered, concentrated and purified by column chromatography using Hexane: EtOAc = 9:1 as the eluting solvent mixture to afford the desired product in 95% yield.

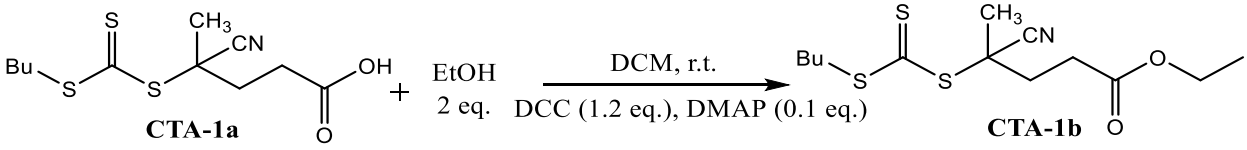

Scheme 1: DCC-DMAP coupling reaction for modification of CTA-1a to CTA-1b.

3.3.1.2 General Procedure for Polymerization of MMA using CTA-1b.

Methyl methacrylate (20 mL, 0.19 mol) was added to a 20 mL reaction vial containing CTA-1b and AIBN as the initiator in appropriate quantities based on the targeted molecular weight (Table 1). The polymerization was performed using molar ratio of AIBN/CTA as 1:20. The mixture was

degassed by N_2 for 15 mins and then heated at 60 °C for different time intervals to achieve the required conversion. On completion, the reaction was quenched in an ice bath, diluted with ethyl acetate, and precipitated in methanol. The precipitated polymer was filtered and dried overnight under vacuum to yield PMMA macro CTA as a white powder.

3.3.1.3 General Procedure for Chain Extension using Styrene (PMMA-*b*-PS_1)

The chain extension of styrene was performed using the synthesized PMMA macro CTA as the suitable RAFT agent and AIBN as the initiator. In a 20-mL reaction vial, freshly distilled styrene, AIBN, and PMMA macro CTA in 1,4 dioxane were added. Different molar ratio of styrene**:**macro-CTA were taken based on the targeted molecular weights and the AIBN:macro-CTA ratio of 1:20 was kept constant. The reaction mixture and was degassed using N_2, followed by polymerization at 60 °C for different time intervals to achieve the desired conversion. After completion, the reaction mixture was quenched in an ice bath, diluted with ethyl acetate and then precipitated in methanol. The precipitated polymer was filtered and dried overnight under vacuum to give PMMA-*b*-PS_1 as a white powder. The diblock copolymer was further purified to remove the PMMA homopolymer contamination by washing the PMMA-*b*-PS_1 using CH_3NO_2:MeOH (3:7) solution mixture.

3.3.1.4 General Procedure for Single Molecule Insertion (SMI) of Pentafluorophenyl Maleimide (PFPMI).

In a 20-mL reaction vial, PMMA macroinitiator (1 equiv.) dissolved with appropriate amount of 1,4 dioxane was added. PFPMI (3 equiv.) and AIBN (0.1 equiv.) were added. The reaction vial was sealed and degassed using N_2 and immersed in a preheated oil bath heated at 60 °C for 3 days to ensure completion insertion of the PFPMI molecule on the PS chain-end. The reaction mixture was diluted using ethyl acetate and precipitated in methanol. The precipitated polymer was filtered

and dried under vacuum for 24 h to obtain PMMA-PFPMI as a white solid. Following the similar procedure, PMMA-*b*-PS_1-PFPMI was synthesized by performing single molecule insertion using the PMMA-*b*-PS_1 macroinitiator.

3.3.1.5 General Procedure for Synthesis of PMMA-PFPMI-*b*-PS_2 and PMMA-*b*-PS_1-PFPMI-*b*-PS_2 Block Copolymers.

In a 20-mL reaction vial, PMMA-PFPMI macroinitiator, freshly distilled styrene, and AIBN dissolved in 1, 4 dioxane were added. The amount of styrene and AIBN was calculated based on the molar ratio of styrene:macro-CTA and AIBN:macro-CTA (20:1) respectively. The reaction vial was sealed and the polymerization was performed at 60 °C for a specific time interval to achieve the targeted conversion. The reaction mixture was diluted using ethyl acetate upon completion and precipitated in methanol three times. The precipitated polymer was then filtered and dried under vacuum to yield PMMA-PFPMI-*b*-PS_2 as a white solid. Similarly, PMMA-*b*-PS_1-PFPMI-*b*-PS_2 was synthesized using PMMA-*b*-PS_1-PFPMI as the macro CTA for performing the styrene chain extension. These synthesized diblock copolymers were further purified by successful removal of PS homopolymer using THF:Hexane (1:3) solution mixture, generated during the two styrenic chain extensions.

Table 3. 1: Synthesis of PMMA macro-initiator using CTA-1b.

Table 1

Sample	[CTA] (mmol/L)	[AIBN] (mmol/L)	$M_{n,GPC}$ (kg/mol)	Đ
PMMA- 30K	0.31	0.016	30.2	1.12
PMMA- 25K	0.21	0.011	25.6	1.14

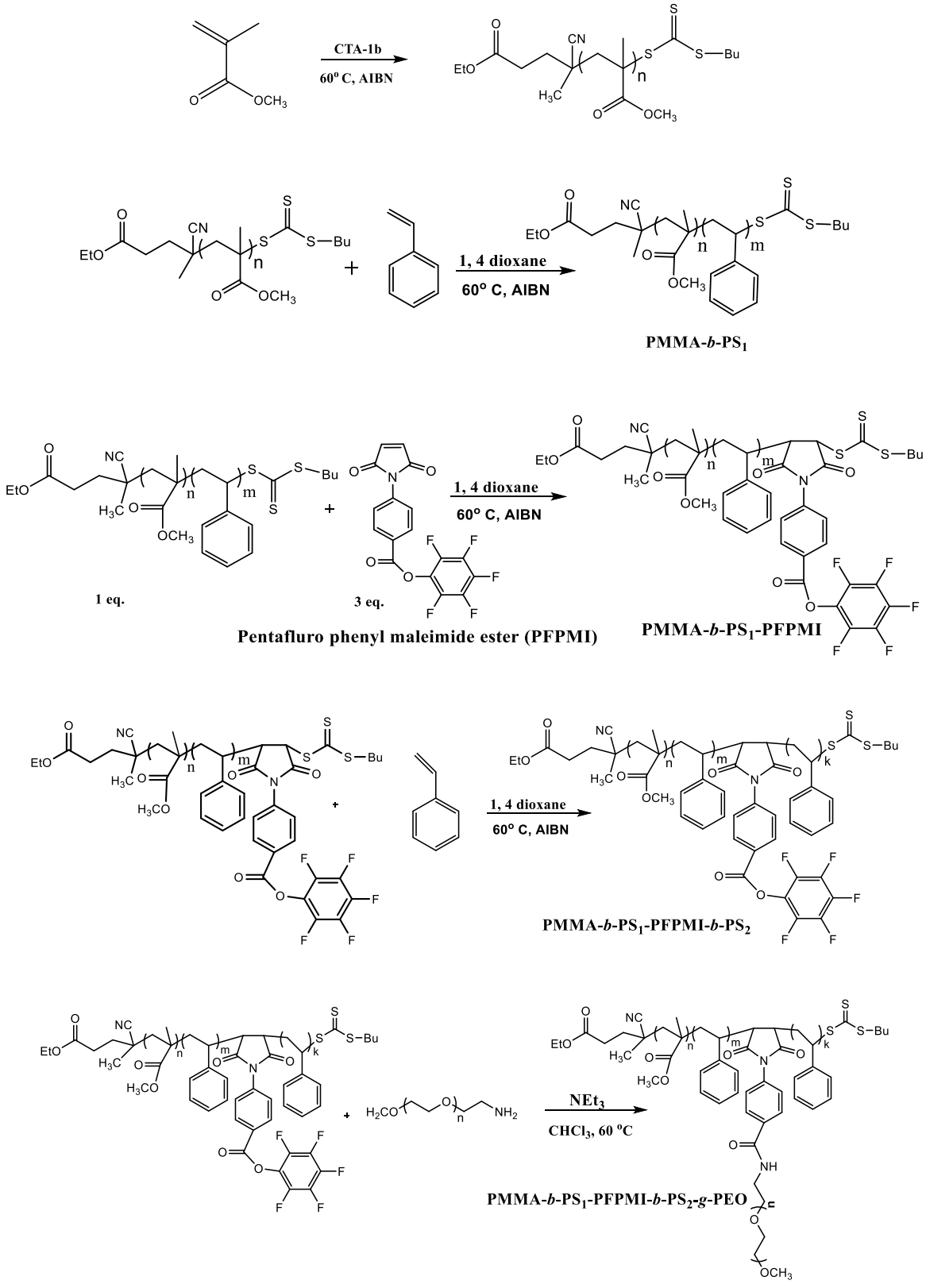

Scheme 2: Synthetic strategy for synthesis of PMMA-*b*-PS_1-PFPMI-*b*-PS_2-*g*-PEO

3.3.1.6 General Procedure for Grafting of Amine-Terminated PEO on PMMA-PFPMI-*b*-PS_2, PMMA-*b*-PS_1-PFPMI-*b*-PS_2, and PMMA-*b*-PS_1-PFPMI

The synthesized diblock copolymer PMMA-PFPMI-*b*-PS_2 was dissolved in chloroform in a 20-mL reaction vial and amine-terminated PEO (1.1 equiv.) was added. NEt_3 (0.1 equiv.) was added and the vial was sealed and placed in a preheated oil bath at 60 °C for 3 days. On completion, the reaction mixture was diluted with ethyl acetate, precipitated in cold diethyl ether, and dried under vacuum for 24 h. To remove the excess PEO, the dried polymer was washed with H_2O:MeOH (9:1) solution mixture to yield PMMA-*b*-PS-*g*-PEO star copolymer architectures. Following the similar procedure, amine terminated PEO was grafted onto PMMA-*b*-PS_1-PFPMI-*b*-PS_2 and PMMA-*b*-PS_1-PFPMI to yield PMMA-*b*-PS-*g*-PEO graft and linear triblock copolymer architectures respectively.

3.3.2 Results and Discussions

3.3.2.1 Synthesis of PMMA-*b*-PS-*g*-PEO Triblock Copolymers

Precise control over the arrangement of different monomer units within a polymer chain is challenging and requires development of various synthetic strategies. Controlling the monomer sequence within a polymer chain can have a profound impact on the overall macroscopic properties of polymers and can play an important role in creating functionalities for molecular targeting, recognition, biocatalysis and molecular information storage.[79–81] With the development of controlled polymerization techniques, notable progress has been made in developing protocols to regulate the primary sequence of polymers.[82] Recently, different approaches have been developed for synthesis of sequence controlled polymers include chain-growth polymerization,[83,84,93,94,85–92]step-growth polymerization,[95–99] multicomponent reactions,[100–103] template polymerization,[104–106] solid phase synthesis[107–110] and the synthesis of multiblock copolymers using specific block

sequence.[111–115] The concept of strong cross-polymerization behavior of maleimides and maleic anhydride with styrene, using various controlled radical polymerization techniques such as ATRP, NMP and RAFT has been studied for end-group functionalization and insertion of different functionalities within the polymer backbone. [111–115] These strategies can be advantageous to synthesize polymers with different architectures including 3-arm star, miktoarm, graft and linear polymers.[116,117]

Using multi-step RAFT polymerization and single monomer insertion (SMI) technique, a series of PMMA-*b*-PS-*g*-PEO graft copolymers were synthesized as shown in Scheme 2. The technique of SMI molecule insertion requires the functional molecule to be inserted only once within the polymer chain with high fidelity while maintaining the livingness of the polymer chain for subsequent chain extension. Furthermore, the single molecule inserted should have the required functionality for grafting the third polymer chain. The architecture of the synthesized graft copolymer is primarily dependent on the position of the SMI within the polymer backbone. Insertion of the functionalized molecule at the junction point of two blocks can lead to a 3-arm star, insertion within the polymeric backbone yields graft and miktoarm copolymers and while chain-end functionalization using SMI can generate linear triblock copolymers. With this overall approach, there is a unique opportunity to synthesize the desired graft copolymers which lie along the continuum of a 3-arm star and the A-B-C linear triblock copolymer.

To utilize this strategy to synthesize high MW graft copolymers using the SMI and activated ester chemistries, the methodology was validated by performing these reactions on low MW PS followed by detailed characterization using ESI-MS, ^{1}H NMR and GPC (Chapter 2). The SMI of PFPMI was performed on the synthesized low MW PS, and as maleimides are known to cross-propagate with styrene but do not homopolymerize, in the absence of styrene monomer, the PFPMI

molecule inserts once at the polymer chain-end with high fidelity. After successful insertion of PFPMI, the chain extension was performed using styrene and followed by subsequent grafting of amine terminated PEO utilizing the activated ester chemistry. This strategy allows the movement of the PEO arm on to the PS chain and synthesize continuum graft copolymers with different graft positions and the linear triblock copolymer architecture. Similarly, the PFPMI insertion was also performed on low MW PMMA, followed by chain extension using styrene and grafting of the PEO arm to synthesize the 3-arm star architecture.

With successful demonstration of the synthetic strategy on low MW PS and PMMA, SMI was performed on the synthesized high MW PMMA and PMMA-*b*-PS_1 chains, followed by the chain extension using styrene to give PMMA-PFPMI-*b*-PS_2, PMMA-*b*-PS_1-PFPMI-*b*-PS_2, and PMMA-*b*-PS_1-PFPMI diblock copolymers respectively with varying PFPMI grafting points. To yield diblock copolymers with high chemical purity, different solvent mixtures were used to remove the PMMA and PS homopolymer contaminants generated during the RAFT polymerization of these monomers. Amine terminated PEO was later grafted onto the PMMA-PFPMI-*b*-PS_2, PMMA-*b*-PS_1-PFPMI-*b*-PS_2, and PMMA-*b*-PS_1-PFPMI diblock copolymers using the activated ester chemistry. The excess PEO used in the final step was removed using H_2O:MeOH (9:1) solution mixture and repeated washings to yield narrow dispersed PMMA-*b*-PS-*g*-PEO graft copolymers with varying architecture lying between the continuum of a 3-arm star and A-B-C linear triblock copolymer (Figure 2). The grafting position (ω) for the PEO block is defined as:

$$\text{Graft Position } (\omega) = \frac{Mol.\,wt.(PS_1)}{Mol\,wt.\,(PS_1+PS_{2)}}$$

where, PS_1 is the PS MW prior to SMI and PS_2 refers to the PS MW after the SMI; with a value of 0 being the 3-arm star and 1 being the graft position for an A-B-C Linear triblock copolymer.

The molecular characteristics for the different series of synthesized graft copolymers is presented in Tables 2 and 3. Sample IDs for Table 2 and 3: X-Y- ω; where X denotes the equal MWs of PMMA and PS in a series, Y denotes the corresponding MW of the PEO arm and ω denotes the grafting position.

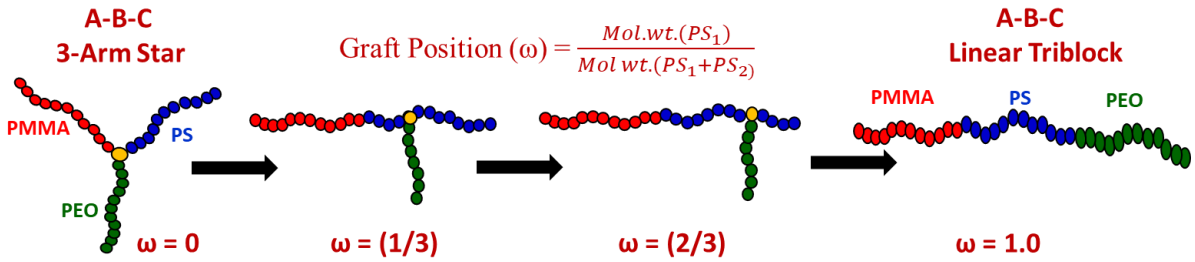

Figure 3. 2: Representative figures for different PMMA-*b*-PS-*g*-PEO continuum graft copolymers and definition of ω.

Table 3. 2: Compositions and Morphologies for the 25-8-ω, and 25-18-ω Series.

Sample ID	**PMMA (Kg/mol)**	**PS_1 (Kg/mol)**	**PS_2 (Kg/mol)**	**PEO (Kg/mol)**	**ω**	***d* (nm)**	***Morphology* (SAXS)**
25-8-0	25	0	25	8	0	35	Lamellae
25-8-1/3	25	8	16	8	1/3	29	Cylindrical
25-8-(2/3)	25	16	8	8	2/3	26	Cylindrical
25-8-(1)	25	25	0	8	1	40	Lamellae
25-18-(0)	25	0	25	18	0	39	Lamellae
25-18-(1/3)	25	8	16	18	1/3	30	Cylindrical
25-18-(2/3)	25	16	8	18	2/3	26	Lamellae
25-18-(1)	25	25	0	18	1	43	Lamellae

Table 3. 3: Compositions and Morphologies for the 30-18-ω, and 30-32-ω Series.

Sample ID	**PMMA (Kg/mol)**	**PS_1 (Kg/mol)**	**PS_2 (Kg/mol)**	**PEO (Kg/mol)**	**ω**	***d* *(nm)***	***Morphology* *(SAXS)***
30-18-(0)	30	0	30	18	0	40	Lamellae
30-18-(1/3)	30	10	20	18	1/3	29	Lamellae
30-18-(2/3)	30	20	10	18	2/3	27	Lamellae
30-18-(1)	30	30	0	18	1	24	Lamellae
30-32-(0)	30	0	30	32	0	52	Lamellae
30-32-(1/3)	30	10	20	32	1/3	35.3	Lamellae
30-32-(2/3)	30	20	10	32	2/3	33	Lamellae
30-32-(1)	30	30	0	32	1	31.1	Lamellae

The chemical and molecular weight characterization of the synthesized graft copolymers was performed using ^{1}H NMR and THF GPC. The ^{1}H NMR signals at δ 3.6 ppm corresponds to the methylene proton of the ethyl ester of PMMA and signals between δ values 6-8 ppm corresponds to the aromatic proton of styrene. After successful grafting of amine terminated PEO, a new peak appears around δ value 3.65 ppm corresponding the *–CH_2-CH_2-O-* protons for the PEO (Figure 3). The individual volume fractions for each polymer block was calculated using ^{1}H NMR by integrating the peak area for specific protons corresponding to the individual blocks. The representative GPC traces for a final PMMA-*b*-PS-*g*-PEO graft copolymers is shown in (Figure 4) shows no homopolymer and diblock contamination, thus demonstrating the high efficiency of this methodology and precise control over the molecular weight and dispersity.

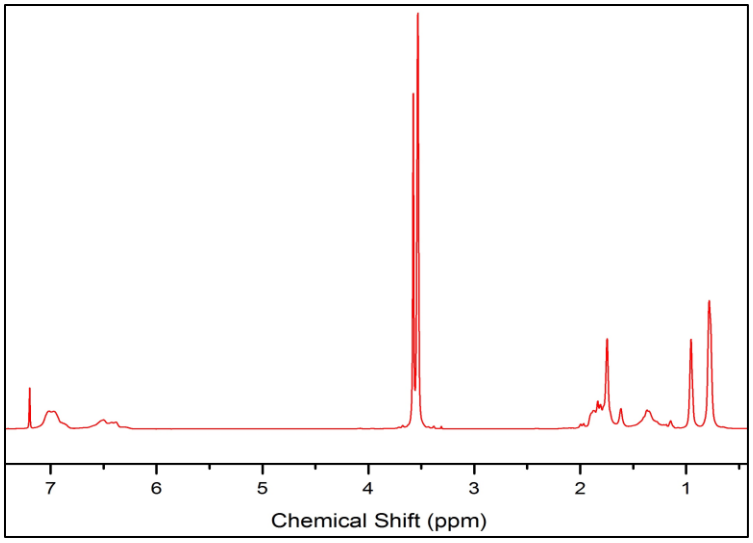

Figure 3. 3**:** Representative ^{1}H NNMR spectra for PMMA-*b*-PS-*g*-PEO graft copolymers

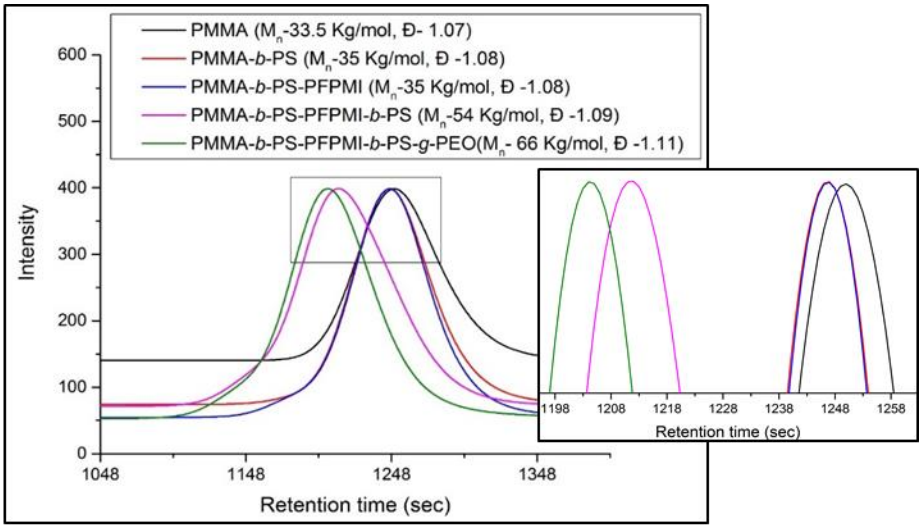

Figure 3. 4: GPC chromatograms for PMMA-*b*-PS-*g*-PEO graft copolymers.

3.3.2.2 Morphological Characterization

Morphological characterization was performed using Transmission electron microscopy (TEM) and Small Angle X-Ray scattering (SAXS). To observe the morphologies using TEM, RuO_4 staining, which primarily stains the PEO phase and lightly stains the PS phase, was employed. Since $\chi_{PMMA-PEO}$ is small and $\chi_{PMMA-PEO} < \chi_{PMMA-PS} < \chi_{PS-PEO}$, the PEO chains would prefer

mixing with the PMMA chains over PS. However, mixing with PS may be driven by topological frustration. It is expected the PS-PEO mixed phase will appear darker and the PMMA-PEO mixed domains will appear lighter under TEM. This assumption was based on the staining profile generated for these morphologies using simulations as discussed below.

An interesting change in the morphologies were observed in the SAXS profiles of the 25-8-ω series on moving along the continuum from the 3-arm to A-B-C linear triblock terpolymer architecture. Figure 5 shows the different SAXS profiles for this series: multiple higher order peaks, in integral multiples of the primary q* value, corresponding to lamellae morphology were observed for the 3-arm star copolymer. SAXS indicates a transition to the cylindrical morphology, replacement of integral reflections by those at $\sqrt{7}$ and $\sqrt{9}$ as the graft position changes to ω = 1/3. Moving further along the continuum to the graft position ω = 2/3, the morphology again changes to lamellae and stays the same for the linear triblock copolymer. Similarly, for the 25-18- ω series, the peak ratios of 1:2:3 for the 3-arm star is indicative of a lamellae morphology. Moving along the continuum to graft positions ω = 1/3 and 2/3, single peaks suggest microphase separation but a lack of long range lattice order. Finally, for the A-B-C linear triblock, the return of a secondary peak at twice the q spacing of the primary peak suggests a layered or lamellar structure, although it could also be consistent with cylinders with the $\sqrt{3}$ peak suppressed by the form factor.

For the 25-8-ω series, the domain spacing gradually decreases from 35 nm for the 3-arm star to 29 nm and 26 nm for ω = 1/3 and 2/3 respectively and then increases to 40 nm for the A-B-C linear triblock copolymer. A similar trend was observed for the 25-18-ω series, where the *d* spacing first decreased along the continuum: 38 nm for the 3-arm star to 30 nm and 26 nm for graft positions 1/3 and 2/3 respectively. It then increases to 43 nm for ω = 1 (Figure 6).

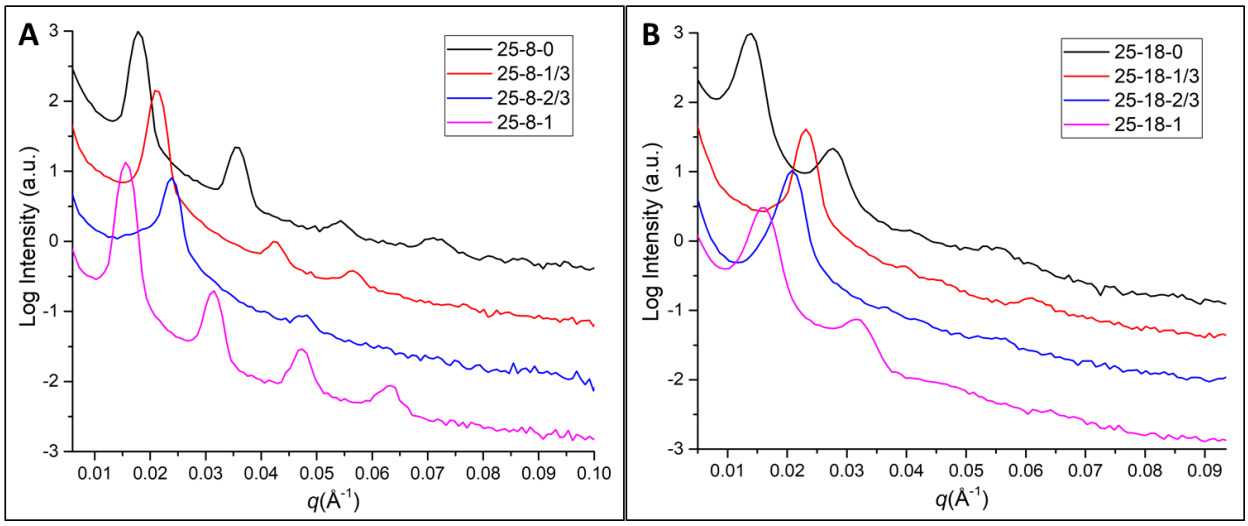

Figure 3. 5: SAXS measurements for A) 25-8-ω and B) 25-18-ω series.

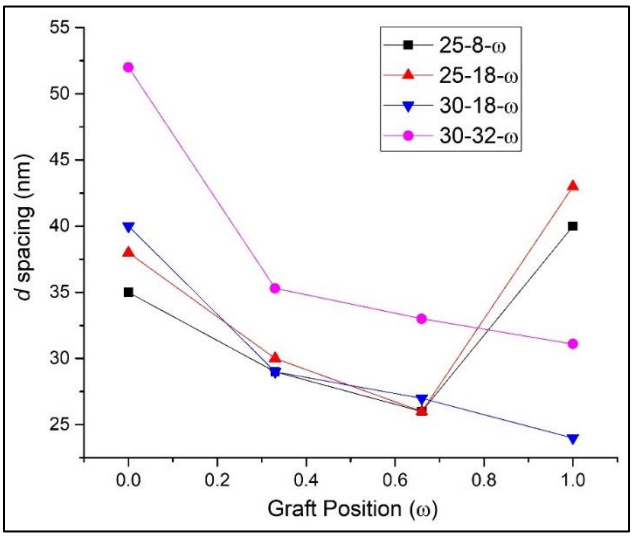

Figure 3. 6: Effect of graft position on domain spacing for 25-Y-ω and 30-Y-ω series.

Figure 7 shows TEM micrographs for the 25-8-ω series. Layering is evident in all these images. The details of image A (3-arm star) suggest that the layered structure may contain PMMA-PEO perforations running through the PS-PEO mixed domains. This would remain consistent with the overall lamellar-like SAXS observed for this sample. The SAXS data for this series suggests that B and C (ω = 1/3 and 2/3) might be cylindrical structures, and it can be difficult to distinguish cylinders from a layered structure in TEM projected images when the cylinders lie primarily in the

plane of the thin section. Images B and C do show features suggesting this possibility. For the linear triblock (ω = 1) image D of a highly ordered lamellar structure is consistent with the SAXS.

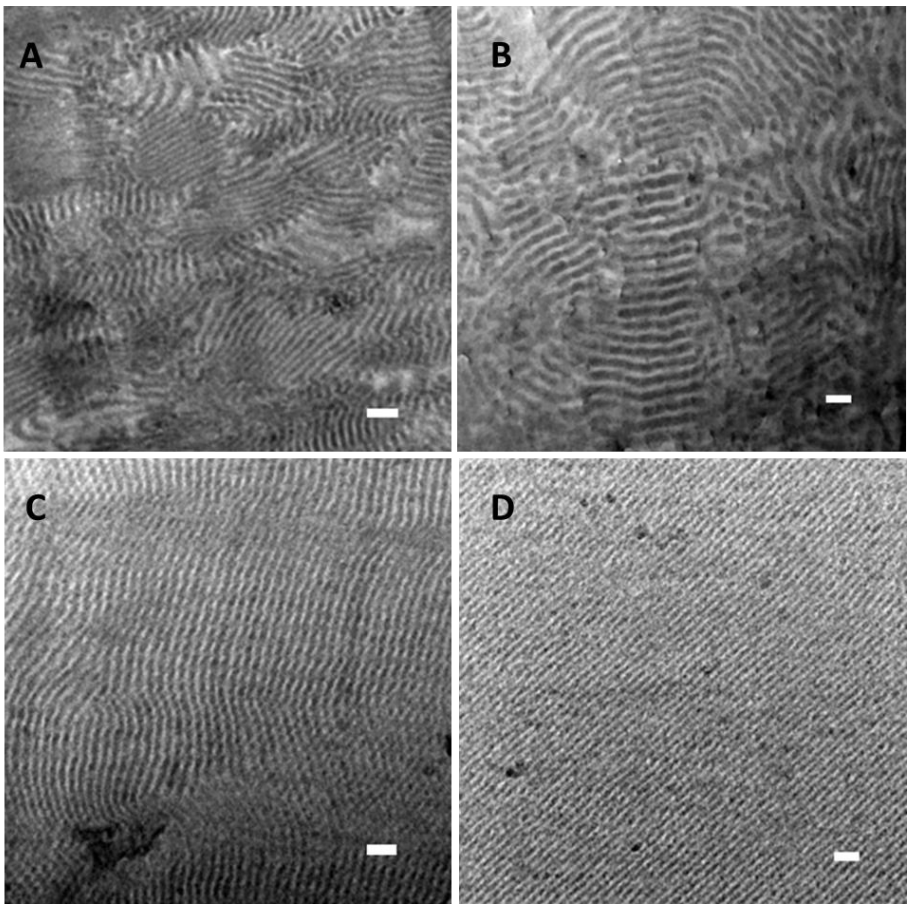

Figure 3. 7. TEM micrographs for the 25-8-ω series. A) ω = 0, B) ω =1/3, C) ω = 2/3, D) ω = 1. Scale bar: 100 nm.

Figure 8 shows the TEM images for 25-18-ω series which shows a perforated lamellae morphology for the 3-arm star with PS-PEO forming one of the lamellae domains and the PMMA-PEO mixed domain forming the other. The PMMA-PEO mixed domain forms the perforations through the PS-PEO layers. This is consistent with the SAXS data showing a lamellar or layered ordering for this sample. Moving along the continuum to ω = 1/3, the TEM image (B) is consistent with a thin section through a phase of tangled worm-like cylinders with no-long range lattice order. This is consistent with the single peak observed in SAXS. In this poorly ordered cylindrical morphology,

a PS-PEO mixed domain forms the cylinders and PMMA-PEO forms the matrix. Further moving to ω = 2/3 and 1, The TEM images are consistent with perforated lamellae with PMMA-PEO perforations running through the PS-PEO domains.

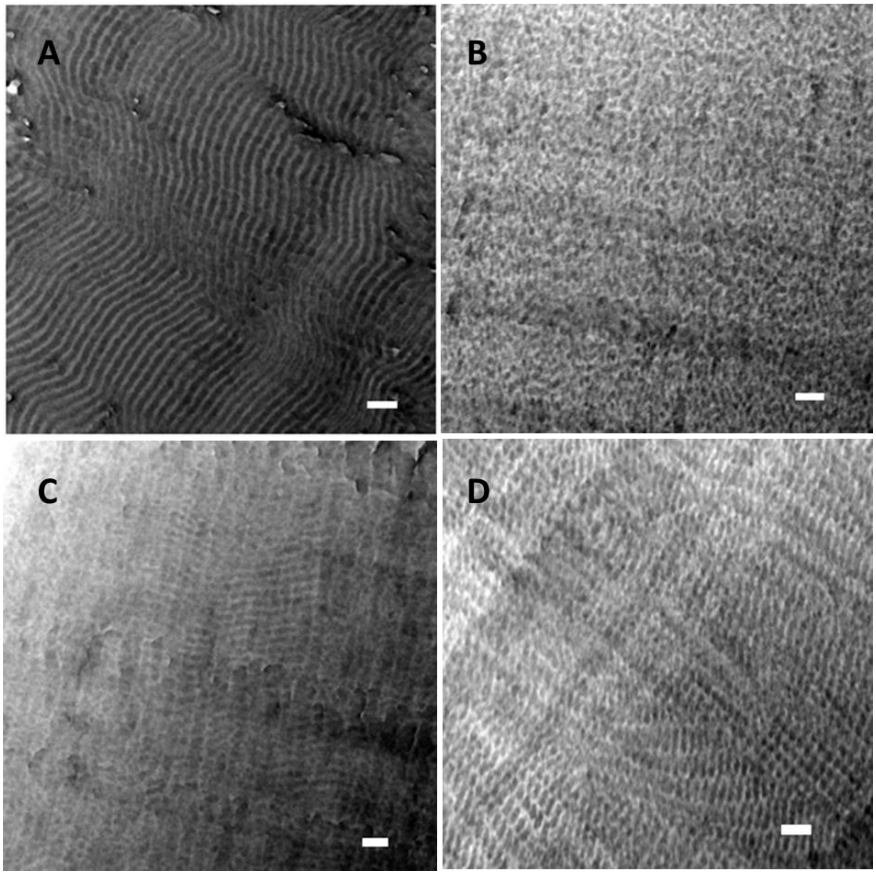

Figure 3. 8. TEM micrographs for the 25-18-ω series. A) ω = 0, B) ω =1/3, C) ω = 2/3, D) ω = 1. Scale bar: 100 nm.

Figure 9 shows the SAXS profiles for the 30-Y-ω series graft copolymers with varying length of the PEO chains. In both series, the ω = 0 and 1 SAXS data suggest a moderate degree of long range order consistent with lamellar, or otherwise layered, ordering or possibly cylinders with the $\sqrt{3}$ refection suppressed by the form factor. The 30-18- ω data for ω = 1/3 and 2/3 is consistent with microphase separation but does not provide an indication of morphology or long-range order. The 30-32- ω data for ω = 1/3 and 2/3 is shows an odd double primary peak which could indicate the

superposition of two length scales, such as might occur in perforated lamellae, with length corresponding to the layering and the other to the arrangement of perforations laterally within the layers.

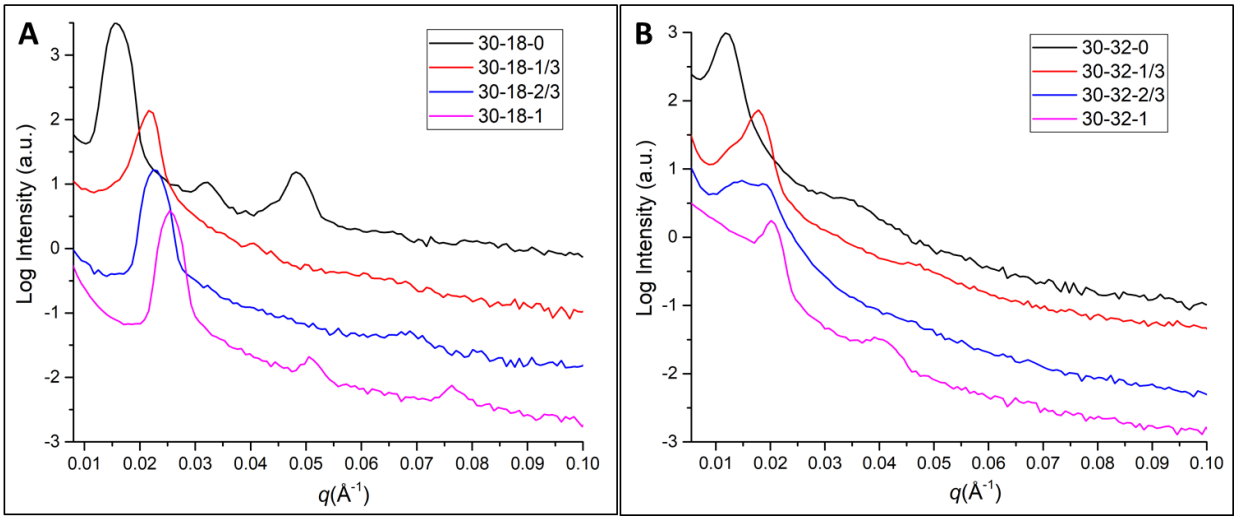

Figure 3. 9: SAXS measurements for A) 30-18-ω and B) 30-32-ω series.

The domain spacing was found to decrease monotonically on moving the graft position along the continuum from a 3-arm star to A-B-C linear triblock copolymer. The 30-18-ω series with PEO MW of 18 kg/mol showed a variation in domain spacing from 40 nm for the 3-arm star to 24 nm for the linear triblock. The 30-32-ω series with PEO MW of 32 kg/mol, exhibited a decrease in domain spacing from 52 nm for the 3-arm star to 31 nm for the linear triblock as shown in Figure 6.

TEM images for the 30-18-ω series show an undulated lamellae morphology for 3-arm star with PS-PEO forming the dark domain and the PMMA-PEO mixed domain forming the lighter one. The morphology changes to poorly ordered lamellae for ω = 1/3 and then to perforated lamellae for ω = 2/3 with PS-PEO forming one of the lamellae domains and PMMA-PEO forming the other with PMMA-PEO perforations running through the PS-PEO domain. For ω = 1, highly ordered lamellae morphology with PMMA-PEO and PS-PEO mixed domains was observed (Figure 10).

Similarly, for the 30-32-ω series, the 3-arm star architecture and ω = 1/3 showed cylindrical morphology with the darker PS-PEO forming the cylindrical domain and the PMMA-PEO mixed phase forming the matrix. For ω = 2/3, the morphology changes to perforated lamellae morphology with PMMA-PEO and PS-PEO mixed domains in lamellae morphology and PMMA-PEO forming the perforations through the PS-PEO mixed domain. As the graft reaches the end of the continuum, the morphology again changes to an ordered cylindrical morphology (Figure 11).

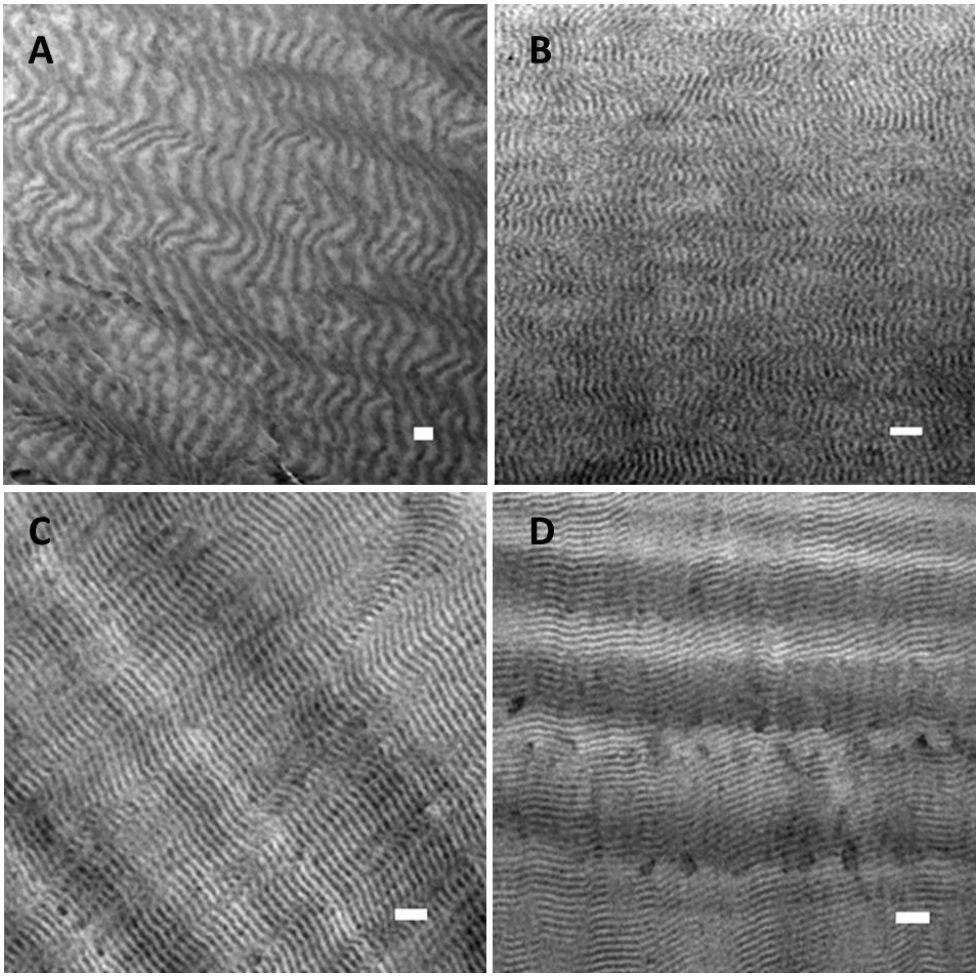

Figure 3. 10: TEM micrographs for the 30-18-ω series. A) ω = 0, B) ω =1/3, C) ω = 2/3, D) ω = 1. Scale bar: 100 nm.

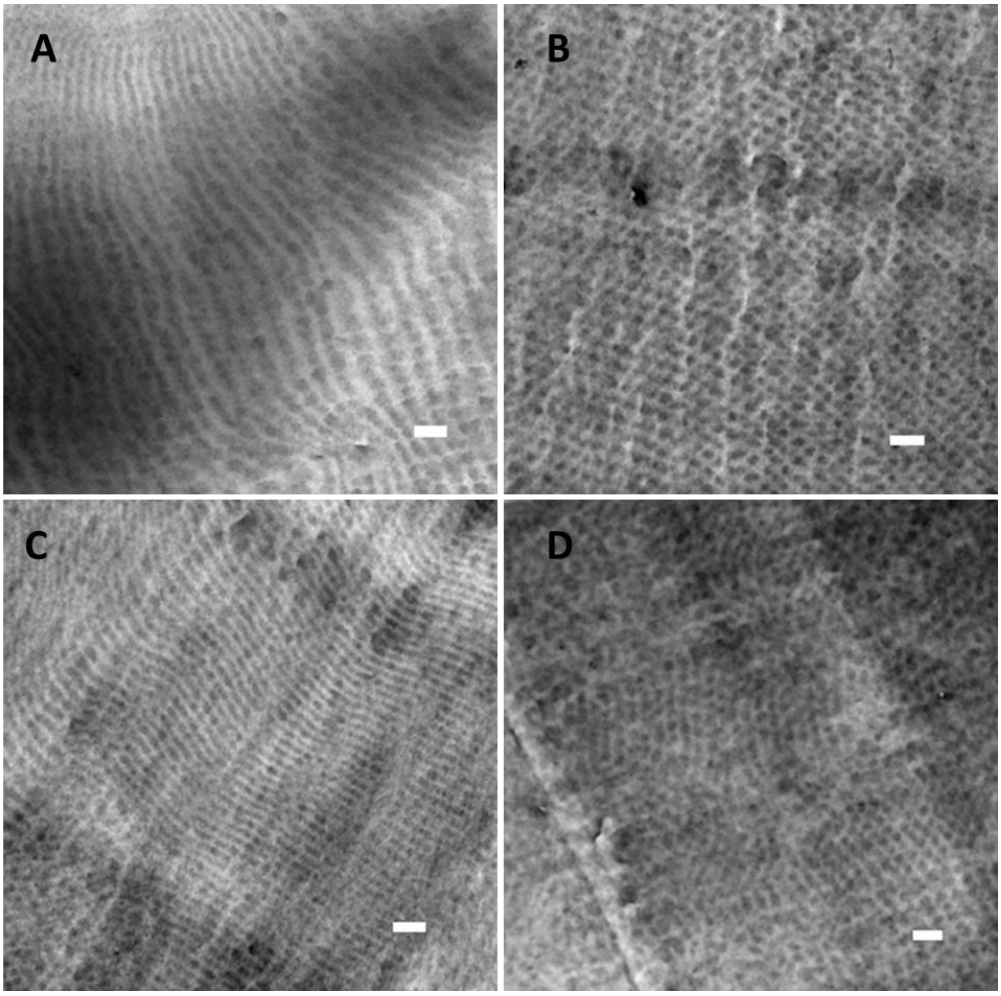

Figure 3. 11: TEM micrographs for 30-32-ω series for different graft positions. A) ω = 0, B) ω = 1/3, C) ω = 2/3 and D) ω = 1. Scale bar: 100 nm.

Comparing the two series with same MW of the PEO arm, the 25-18-ω and 30-18-ω series, it can be observed that a small increase in the χN value, can lead to a significant change in the self-assembly behavior of these continuum graft copolymers. The domain spacing observed using SAXS for the 25-18-ω decreases from ω = 0 to ω = 2/3 and then increases as the graft position reaches ω = 1.0. However, for the 30-18-ω series, a monotonic decrease in the domain spacing was observed as the graft position changes from ω = 0 to ω = 1.0. The morphologies observed using TEM for the 25-18-ω, varied from perforated lamellae (ω = 0.0) to cylindrical morphology (ω = 1/3) then changes to perforated lamellae morphology for the ω values of 2/3 and 1.0. Whereas,

for the 30-18-ω series, the morphology changes from undulated lamellae (ω = 0.0) to perforated lamellae morphology for ω values 1/3 and 2/3 and again changes to lamellae morphology for ω = 1.0. This change in the domain spacing trend using SAXS and the variation in the morphologies observed using TEM with respect to a small increase in the $\boldsymbol{\chi N}$ value could be attributed to either the presence of a morphological phase boundary of these continuum copolymers or the difference in the topological frustration for the two series of graft copolymers.

3.3.2.3 Theoretical Simulations

Further investigation of the phase morphology and evolution kinetics of the spectrum was performed using a mesoscale molecular dynamics method. Dissipative particle dynamics (DPD) is a simulation technique that has been successfully applied to study the mesophase formation of block copolymers with various molecular architectures.[118–120] Due to its coarse-grained nature, DPD can model physical phenomena occurring at larger time and spatial scales than typical molecular dynamics. The DPD particles, representing a Gaussian-like chain, interact by conservative ($\boldsymbol{F^C}$), dissipative ($\boldsymbol{F^D}$), random ($\boldsymbol{F^R}$), and bond ($\boldsymbol{F^B}$) forces which are pairwise additive. The conservative force is the primary driving force towards equilibrium, while the dissipative and random forces act as thermostat and dynamic tuning parameters. The forces on an i^{th} particle is only exerted by particles within a cut-off radius, r_c. The momentum-conserving forces are given by $F_{ij}^D = -\gamma(1 - r_{ij}/r_c)^2(\hat{r}_{ij} \cdot \vec{v}_{ij})$ and $F_{ij}^R = \sqrt{2\gamma k_B T}(1 - r_{ij}/r_c)\hat{r}_{ij}(\Delta t)^{-1/2}$, where γ is the friction coefficient, Δt is the integrating time step, k_B is the Boltzmann constant and T is the temperature. The units are scaled such that $r_c = k_B T = 1$ and $\Delta t = 0.04$. The soft repulsive conservative component is given by: $F_{ij}^C = a_{ij}(1 - r_{ij}/r_c)\hat{r}_{ij}$, where $r_{ij} = r_i - r_j$ and $\hat{r}_{ij} = r_{ij}/|r_{ij}|$. The scaling factor a_{ij} is related to Flory-Huggins χ parameter by: $a_{ij} \approx a_{ii} +$

$3.27\chi_{ij}$,when $a_{ii} = 25$ and simulation density (ρ) is 3. Accordingly, the scaling factors for our system are $a_{PMMA-PS} = 40$, $a_{PS-PEO} = 43.8$, and $a_{PMMA-PEO} = 25.7$. The bond force ($\boldsymbol{F^B}$) is added to connect bonded DPD particles with a linear spring, $F^B = -kr_{ij}$, where the stiffness constant k=4**.**

Using DPD simulations to explore the effect of both grafting position and the molecular weight of PEO on the PMMA-PS backbone, the volume fraction of PMMA and PS is always kept equal by keeping the number of backbone beads constant at N=20, where N_{PMMA} = 10 and N_{PS} = 10. Due to the coarse grain nature of the model, the grafting point for PEO is considered on the PS_2 segment, hence the ω ranges between 0 (3-arm star) and 0.9 (linear triblock). The simulations are performed in the canonical ensemble (*NVT*) with a cubic 24×24×24 box containing 41,472 particles and using periodic boundary conditions. Since the density is kept constant and molecular weight of PEO is variable, this leads to a variation in the number of molecules in the system. All simulations were initially performed by setting all the interaction parameter a_{ij} as 25, which corresponds to an athermal melt. This generates a random distribution of chains in the simulation box. Then the value of a_{ij} were instantaneously increased to the above-mentioned a_{ij} values representing the various χ parameters. The system was then allowed to relax to an equilibrated morphology for 5×10^8 time steps. The final state of the simulation was taken as a prediction of the continuum graft copolymer morphology for comparison to the experimental observations. Figure 13 shows the morphological diagram for the PMMA-*b*-PS-*g*-PEO graft copolymers with respect to changes in ω and φ_{PEO}, where φ_{PEO} is the volume fraction of PEO.

Three ordered morphologies are observed; lamellae, perforated lamellae and cylindrical. For the lamellae morphology, a PMMA-PEO mixed phase formed one domain while a PS-PEO mixed

phase formed the other domain. Similarly, for the cylindrical morphology, the PS-PEO mixed phase formed the hexagonally packed cylinders within a PMMA-PEO matrix. The formation of a PS-PEO mixed phase for these morphologies can be attributed to the forced mixing of the PS and PEO chains due to topological frustration imposed by the grafting position. In the perforated lamellae morphology, PMMA-PEO and PS-PEO mixed phases formed the lamella domains with PMMA-PEO perforations running through the PS-PEO domains. A few perforated lamellae morphologies initially had a continuous PS domain indicative of a bicontinous phase which dissapeared on equilibrating for longer time (5×10^9 time steps). Representative snapshots for the morphologies observed are shown in Figure 12. In Figs. 10 (a), (c), and (e) each block is colored differently while in Figures 12 (b), (d) and (f) the same structures are processed onto a gray scale to facilitate their comparison with the observed TEM images as follows. Since the TEM images were obtained by staining the polymer thin film using RuO_4, whose staining affinity decreases from PEO, to PS, to PMMA, we assigned a RuO_4 staining probability (P_{stain}) to each polymer bead type: $P_{stain} = \frac{1}{2n}\sum_{i=1}^{n} \alpha_i$, where n is the number of particles in the interaction sphere ($r_c = 1$) and $\alpha_i = 1, 1.5, \text{and } 2$ for PMMA, PS, and PEO, respectively. The representative simulated morphologies treated by this staining probability profile suggest that in the morphologies observed by TEM, the PMMA-PEO mixed phase should appear as the lighter phase and the PS-PEO mixed phase should as the dark phase. These results were found to be in good agreement with the experimentally observed morphologies and provided a better understanding of the behavior of the RuO_4 stain for these continuum graft copolymers.

Figure 13 shows a comparison between simulated and experimental morphologies. Since in simulations the A-B-C linear triblock is represented by ω = 0.9, the same ω was assigned for the samples obtained experimentally. The morphological transitions predicted for various systems are

in qualitative agreement with experimental results based on SAXS and TEM. Overall, experiments and model are consistent in showing the following approximate trends: morphologies with increasing interfacial curvature tend to occur for either larger φ_{PEO} at fixed ω or for decreasing ω at fixed φ_{PEO}, where in order of increasing curvature the morphologies are ranked as lamellae < perforated lamella < cylinders. The major discrepancies between simulation and experimental results are seen for the star architecture with $\varphi_{PEO} = 0.39$ and 0.43. These inconsistencies may reflect some limitation of the model DPD adopted whose large extent of coarse-graining may blur out some important molecular details; e.g., in describing the constraints around the grafting point, and in capturing the relative χN interactions.

To study the effect of moving from a 3-arm star to A-B-C linear triblock copolymers, the φ_{PEO} = 0.31 system was considered, wherein simulations a transition from cylindrical morphology to lamellae was observed, without any perforated phase to complicate the analysis. We note, however, that near this φ_{PEO}value the experimental system more generally transitioned from perforated lamellae to cylinder upon increasing ω. The calculated fraction of PMMA beads interacting with PEO, which can be seen as quantifying the extent of mixing between these blocks, reveals a slight decrease in their mixing as ω increases (Figure 14(a)). Due to the connectivity to the interphase region between PMMA-PEO, PS-rich domains have a higher concentration of PEO than PMMA-rich domains in the 3-arm stars as compared to the linear triblocks. The macroscopic morphology change occurs between ω = 0.3 and 0.4, where the cylindrical morphology changes to lamellae morphology and is microscopically marked by a significant increase in the extent of mixing of PS with PMMA and PEO (Figure 14(b)). Since this increased interaction of PS with PEO is not energetically favorable, it is clear that this phase transition is driven by the small change

in the tethering point. This effect emphasizes the idea that morphology can be controlled by changing ω.

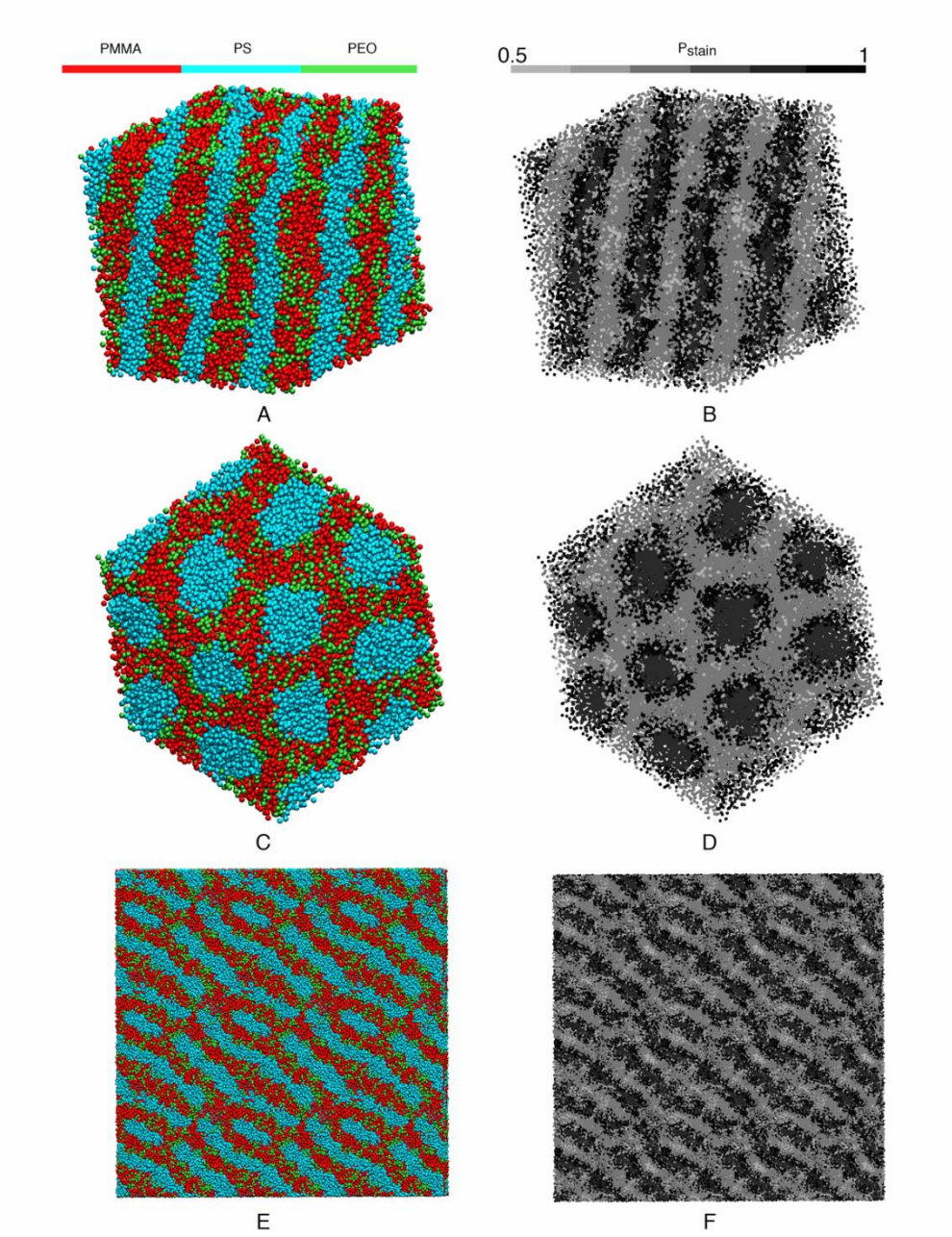

Figure 3. 12: Representative figures for the (a-b) Lamellae (c-d) Cylindrical, and (e-f) Perforated Lamellae morphologies observed using DPD simulations. Panels (b), (d), and (f) show structures mimicking TEM contrast for (a), (c), and (e), respectively.

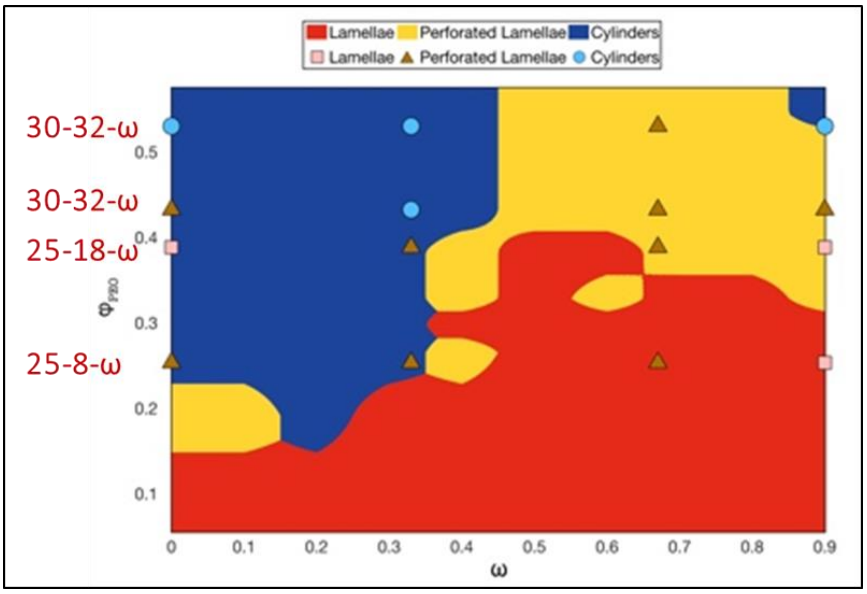

Figure 3. 13: Morphological phase diagram for the PMMA-*b*-PS-*g*-PEO graft copolymers obtained from DPD simulations. The symbols represent the experimental morphologies from observed using SAXS and TEM. The linear triblock samples are represented by ω = 0.9.

We hypothesize that the simultaneous increased mixing of PEO with both PMMA and PS is attained by chain stretching of PEO, which would imply an increased conformational frustration in the chain. The extent of chain stretching was measured as the sphericity (S) of the PEO chain[121] (reference) defined as $S = 3(\lambda_2 + \lambda_3)/2$, where the λ_1, λ_2, and λ_3 are eigenvalues of the inertial tensor and $\lambda_1 > \lambda_2 > \lambda_3$. For a stiff rod-like chain $S \approx 0$ and for an isotropic melt chain $S \approx 1$. A non-monotonic trend in S for PEO chains as a function of ω (Figure 14(c)) was observed. As ω increases the sphericity slightly decreases as the PEO stretches to mix with PMMA, however, at ω = 0.4 (1/3) a dramatic decrease in S was observed. This decrease in sphericity supports our hypothesis that the chain stretching is coupled to the increased mixing with PMMA: the chain configurational entropic loss (associated with PEO stretching) is compensated by an increase in mixing entropy, which in turn helps stabilize the emerging lamellae phase. The sphericity of PEO in the lamellae morphology starts increasing with ω exhibiting a large jump at ω = 0.7. This increase in sphericity is due to a reduced interaction between PS and PEO, hence leading to less frustration in the PEO

chain. The dramatic change in sphericity at ω = 0.7 is not accompanied by a change in morphology; instead it is linked to changes in lamellae thickness. Indeed, the lamellae thickness (calculated by calculating the average distance between each crossover point for the density profiles of PMMA and PS across the lamella) shows a minimum at ω = 0.7 (Figure 14(d)), which is accompanied by reduced mixing of PS with PMMA and PEO. For ω > 0.7, de-mixing of PS with the other components leads to a rapid increase in lamellae thickness. The minimum in domain thickness observed in the simulations at ω= 0.7 corresponds with the minimum in domain spacing observed by SAXS at ω = 2/3. Overall, the observed changes in lamellae thickness relate to the conformational changes in the constituent chains. We note that reduction in the sphericity of the PEO segments will also be associated with an increase in chain stiffness and hence affect other macroscopic properties like modulus and ionic conductivity.

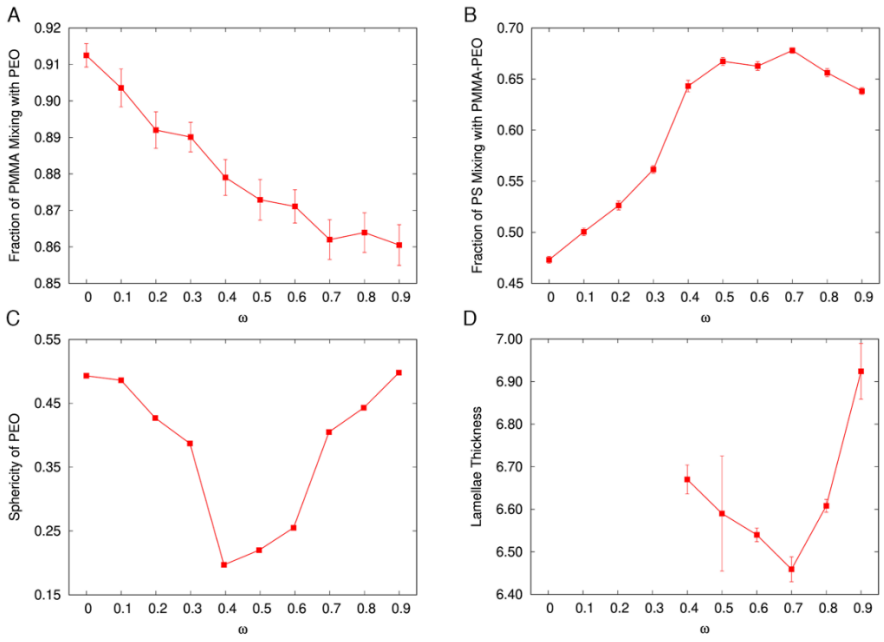

Figure 3. 14: Fraction of (a) PMMA beads interacting with PEO and (b) PS beads interacting with PMMA-PEO as a function of ω. (c) Sphericity of PEO chains and (d) Lamellae thickness for varying ω.

3.4 Exploring the Continuum of a 3-arm Star and A-B-C Linear Triblock copolymer for PtBA-*b*-PS-*g*-PEO graft copolymers

3.4.1 Methods

3.4.1.1 General Procedure for Polymerization of PtBA using CTA-1b

Tert-butyl acrylate (20 mL, 0.19 mol) was added to a 20mL reaction vial containing CTA-1b and AIBN as the initiator in appropriate quantities based on the targeted molecular weight (Table 1). The polymerization was performed using molar ratio of AIBN/CTA as 1:20. The mixture was degassed by N_2 for 15 mins and then heated at 60 °C for different time intervals to achieve complete conversion. On completion, the reaction was quenched in an ice bath, diluted with ethyl acetate, and precipitated in methanol-H_2O mixture (80:20). The precipitated polymer was filtered and dried overnight under vacuum to yield PtBA macro CTA as a light yellow solid.

3.4.1.2 General Procedure for Chain Extension using Styrene (PtBA-*b*-PS1)

The chain extension of styrene was performed using the synthesized PtBA macro CTA as the suitable RAFT agent and AIBN as the initiator. In a 20-mL reaction vial, freshly distilled styrene, AIBN, and PMMA macro CTA in 1,4 dioxane were added. Different molar ratio of styrene**:**macro-CTA were taken based on the targeted molecular weights and the AIBN:macro-CTA ratio of 1:20 was kept constant. The reaction mixture and was degassed using N_2, followed by polymerization at 60 °C for different time intervals to achieve the desired conversion. After completion, the reaction mixture was quenched in an ice bath, diluted with ethyl acetate and then precipitated in methanol-H_2O mixture (80:20). The precipitated polymer was filtered and dried overnight under vacuum to give PtBA-*b*-PS_1 as a white powder. The diblock copolymer was further purified to remove the PtBA homopolymer contamination by washing the PtBA-*b*-PS_1 using hexanes.

3.4.1.3 General Procedure for Single Molecule Insertion (SMI) of Pentafluorophenyl Maleimide (PFPMI)

In a 20-mL reaction vial, PtBA-*b*-PS_1 macroinitiator (1 equiv.) dissolved with appropriate amount of 1,4 dioxane was added. PFPMI (3 equiv.) and AIBN (0.1 equiv.) were added. The reaction vial was sealed and degassed using N_2 and immersed in a preheated oil bath heated at 60 °C for 3 days to ensure completion insertion of the PFPMI molecule on the PS chain-end. The reaction mixture was diluted using ethyl acetate and precipitated in methanol-H_2O mixture (80:20). The precipitated polymer was filtered and dried under vacuum for 24 h to obtain PtBA-*b*-PS_1-PFPMI as a pale yellow solid. Following the similar procedure, PtBA-PS_x-PFPMI was synthesized by performing single molecule insertion using the PtBA-*b*-PS_x macroinitiator where the value of x is <10 monomer units.

3.4.1.4 General Procedure for Synthesis of PtBA-PS_x-PFPMI-*b*-PS_2 and PtBA-*b*-PS_1-PFPMI-*b*-PS_2 Block Copolymers

In a 20-mL reaction vial, PtBA-PS_x-PFPMI macroinitiator, freshly distilled styrene, and AIBN dissolved in 1, 4 dioxane were added. The amount of styrene and AIBN was calculated based on the molar ratio of styrene:macro-CTA and AIBN:macro-CTA (20:1) respectively. The reaction vial was sealed, and the polymerization was performed at 60 °C for a specific time interval to achieve the targeted conversion. The reaction mixture was diluted using ethyl acetate upon completion and precipitated in methanol-H_2O water mixture (80:20) three times. The precipitated polymer was then filtered and dried under vacuum to yield PtBA-PS_x-PFPMI-*b*-PS_2 as a pale-yellow powder. Similarly, PtBA-*b*-PS_1-PFPMI-*b*-PS_2 was synthesized using PtBA-*b*-PS_1-PFPMI as the macro CTA for performing the styrene chain extension.

3.4.1.5 General Procedure for Grafting of Amine-Terminated PEO on PtBA-PSx-PFPMI-*b*-PS_2, PtBA-*b*-PS_1-PFPMI-*b*-PS_2, and PtBA-*b*-PS_1-PFPMI

The synthesized diblock copolymer PtBA-PSx-PFPMI-*b*-PS_2 was dissolved in chloroform in a 20-mL reaction vial and amine-terminated PEO (1.1 equiv.) was added. NEt_3 (0.1 equiv.) was added and the vial was sealed and placed in a preheated oil bath at 60 °C for 3 days. On completion, the reaction mixture was diluted with ethyl acetate, precipitated in cold diethyl ether, and dried under vacuum for 24 h. To remove the excess PEO, the dried polymer was washed with H_2O:MeOH (9:1) solution mixture to yield PtBA-*b*-PS-*g*-PEO star copolymer architectures. Following the similar procedure, amine terminated PEO was grafted onto PtBA-*b*-PS_1-PFPMI-*b*-PS_2 and PtBA-*b*-PS_1-PFPMI to yield PtBA-*b*-PS-*g*-PEO graft and linear triblock copolymer architectures respectively (Figure 15).

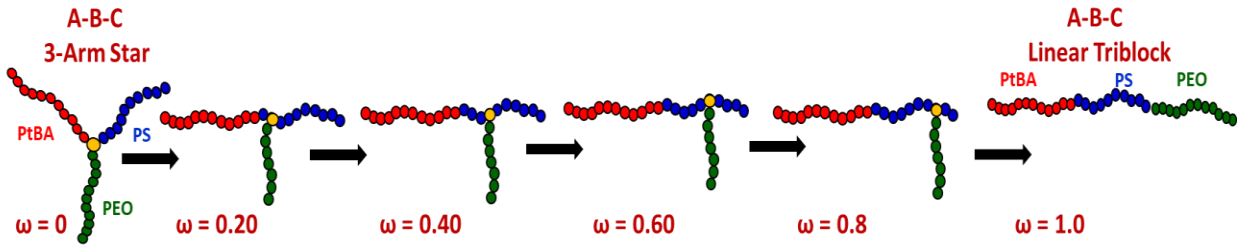

Figure 3. 15: Representative figures for different PtBA-*b*-PS-*g*-PEO continuum graft copolymers.

Table 3. 4**:** Synthesis of PtBA macro-initiator using CTA-1b

Sample	[CTA] (mmol/L)	[AIBN] (mmol/L)	$M_{n,GPC}$ (kg/mol)	Đ
PtBA- 32K	0.46	0.023	32.1	1.14
PtBA- 22K	0.69	0.034	21.9	1.10

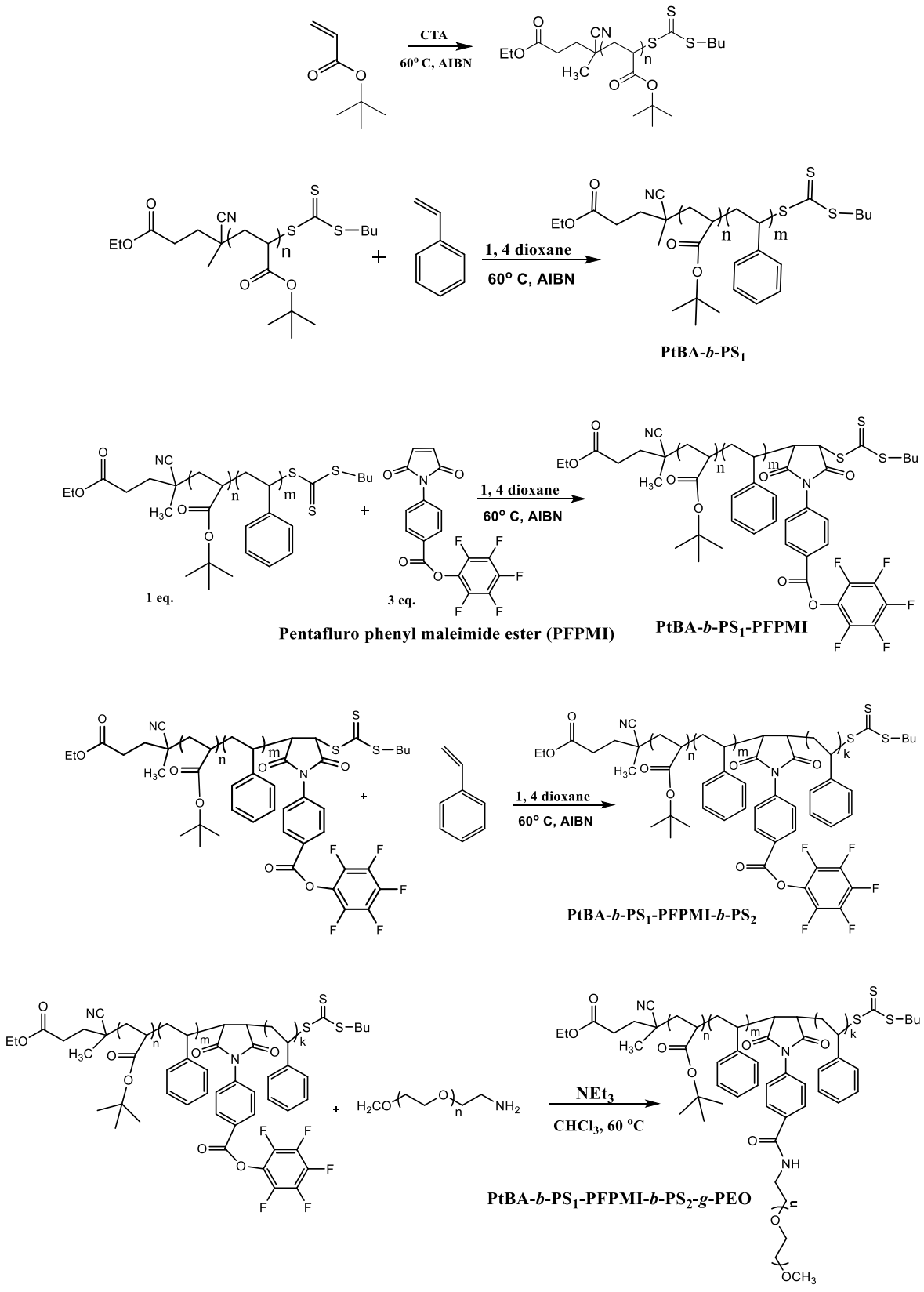

Scheme 3: Synthetic strategy for synthesis of PtBA-*b*-PS_1-PFPMI-*b*-PS_2-*g*-PEO

3.4.2 Results and Discussions:

3.4.2.1 Synthesis of PtBA-*b*-PS-*g*-PEO graft copolymers

Sequential multistep RAFT polymerization and single monomer insertion (SMI) technique was used to synthesize a series of PtBA-*b*-PS-*g*-PEO graft copolymers as described in Scheme 3. Similar approach as explained for the synthesis of the PMMA-*b*-PS-*g*-PEO graft copolymer was used to obtain these graft copolymers with precise movement of the PFPMI molecule on the PS chain to yield PtBA-*b*-PS-*g*-PEO graft copolymers which lie along the continuum of a 3-arm star and the A-B-C linear triblock copolymer. SMI was performed on the synthesized PtBA-*b*-PS_1 chains, followed by the chain extension using styrene to give PtBA-*b*-PS_1-PFPMI-*b*-PS_2, and PtBA-*b*-PS_1-PFPMI diblock copolymers respectively with varying PFPMI grafting points. However, the SMI was not successful at the PtBA chain-end and to overcome this synthetic challenge for synthesis of the 3-arm star architecture, a short PS chain (< 10 monomer units) was attached to the PtBA chain, followed by SMI and chain extension using styrene to yield PtBA-*b*-PS_x-PFPMI-*b*-PS_2 diblock copolymer. To remove the homopolymer contaminant form the synthesized graft copolymers, different solvent mixtures were used to remove the PtBA and PS homopolymer contaminants generated during the RAFT polymerization of these monomers. Amine terminated PEO was later grafted onto the PtBA-PS_x-PFPMI-*b*-PS_2, PtBA-*b*-PS_1-PFPMI-*b*-PS_2, and PtBA-*b*-PS_1-PFPMI diblock copolymers using the activated ester chemistry. The excess PEO used in the final step was removed using H_2O:MeOH (9:1) solution mixture and repeated washings were done to yield narrow dispersed PtBA-*b*-PS-*g*-PEO graft copolymers with varying architecture lying between the continuum of a 3-arm star and A-B-C linear triblock copolymer as described in Tables 5-8.

Table 3. 5: Compositions and Morphologies for the PtBA-*b*-PS-*g*-PEO-1-6 Series.

Sample #	PtBA (Kg/mol)	PS_1 (Kg/mol)	PS_2 (Kg/mol)	PEO (Kg/mol)	ω value
PtBA-PS-PEO-1	22	0	22	10	0
PtBA-PS-PEO-2	22	4.5	17.5	10	0.2
PtBA-PS-PEO-3	22	9.0	13.0	10	0.4
PtBA-PS-PEO-4	22	13.5	8.5	10	0.6
PtBA-PS-PEO-5	22	18	4.0	10	0.8
PtBA-PS-PEO-6	22	22	0	10	1.0

Table 3. 6: Compositions and Morphologies for the PtBA-*b*-PS-*g*-PEO-7-12 Series.

Sample #	PtBA (Kg/mol)	PS_1 (Kg/mol)	PS_2 (Kg/mol)	PEO (Kg/mol)	ω value
PtBA-PS-PEO-7	22	0	22	18	0
PtBA-PS-PEO-8	22	4.5	17.5	18	0.2
PtBA-PS-PEO-9	22	9.0	13.0	18	0.4
PtBA-PS-PEO-10	22	13.5	8.5	18	0.6
PtBA-PS-PEO-11	22	18	4.0	18	0.8
PtBA-PS-PEO-12	22	22	0	18	1.0

The chemical and molecular weight characterization of the synthesized graft copolymers was performed using ^{1}H NMR and THF GPC. The ^{1}H NMR signals at 2.3 ppm (1H-CH backbone) and around 1.3 ppm (12H-CH3 t-butyl) for PtBA protons and signals between δ values 6-8 ppm corresponds to the aromatic proton of styrene were used to calculate the mole fractions of the PtBA-*b*-PS diblock copolymers. After successful grafting of amine terminated PEO, a new peak appears around δ value 3.65 ppm corresponding the $-CH_2$-CH_2-O- protons for the PEO (Figure 16). by integrating the peak area for specific protons corresponding to the individual blocks, the volume fractions for each polymer block was calculated. The representative GPC traces for a final PtBA-*b*-PS-*g*-PEO graft copolymers is shown in Figure 17 which shows no homopolymer and

diblock contamination, thus demonstrating the high efficiency of this methodology and precise control over the molecular weight and dispersity.

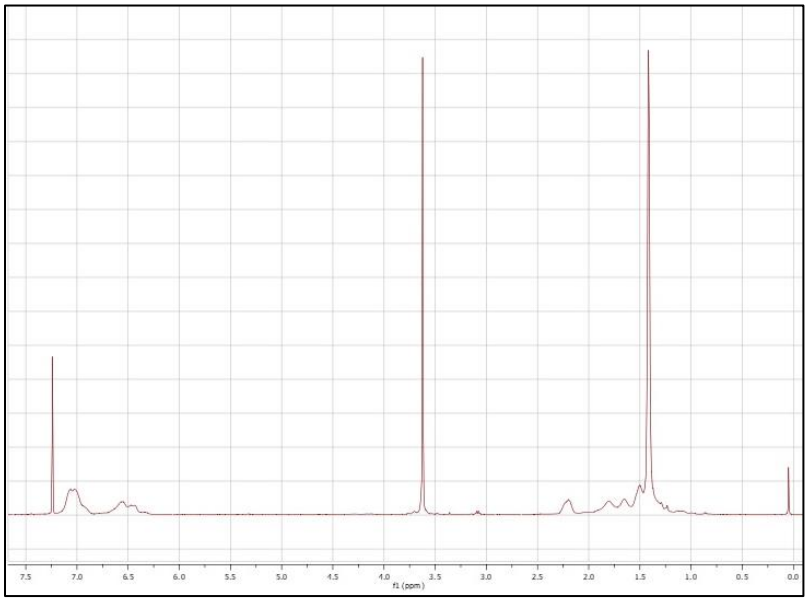

Figure 3. 16: Representative ^{1}H NMR spectra for PtBA-*b*-PS-*g*-PEO copolymer.

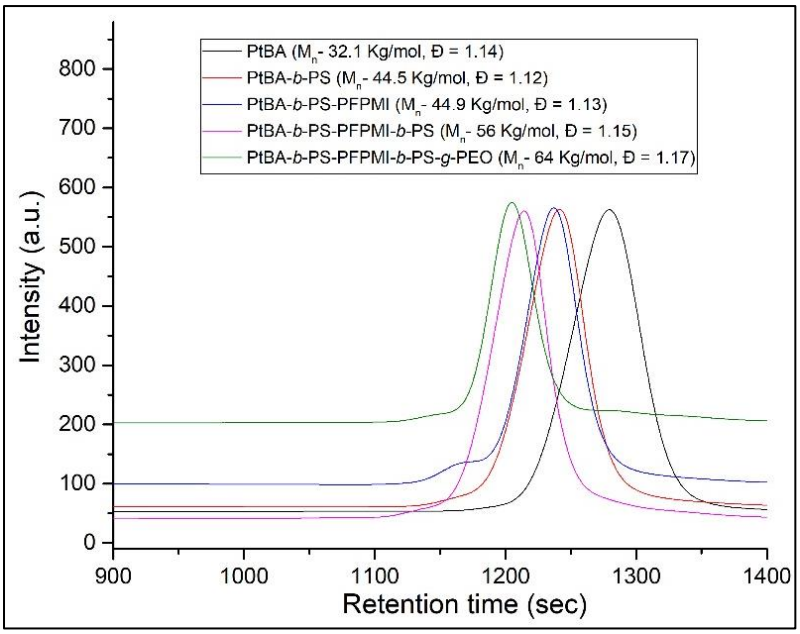

Figure 3. 17: Representative GPC chromatographs for PtBA-*b*-PS-*g*-PEO copolymers.

Table 3. 7: Compositions and Morphologies for the PtBA-*b*-PS-*g*-PEO-13-18 Series.

Sample #	**PtBA (Kg/mol)**	**PS_1 (Kg/mol)**	**PS_2 (Kg/mol)**	**PEO (Kg/mol)**	***ω* value**
PtBA-PS-PEO-13	32.0	0	32.0	10	0
PtBA-PS-PEO-14	32.0	6.4	25.6	10	0.2
PtBA-PS-PEO-15	32.0	12.8	19.2	10	0.4
PtBA-PS-PEO-16	32.0	19.2	12.8	10	0.6
PtBA-PS-PEO-17	32.0	25.6	6.4	10	0.8
PtBA-PS-PEO-18	32.0	32.0	0.0	10	1.0

Table 3. 8: Compositions and Morphologies for the PtBA-*b*-PS-*g*-PEO-25-30 Series.

Sample #	**PtBA (Kg/mol)**	**PS_1 (Kg/mol)**	**PS_2 (Kg/mol)**	**PEO (Kg/mol)**	***ω* value**
PtBA-PS-PEO-25	32.0	0	32.0	18	0
PtBA-PS-PEO-26	32.0	6.4	25.6	18	0.2
PtBA-PS-PEO-27	32.0	12.8	19.2	18	0.4
PtBA-PS-PEO-28	32.0	19.2	12.8	18	0.6
PtBA-PS-PEO-29	32.0	25.6	6.4	18	0.8
PtBA-PS-PEO-30	32.0	32.0	0.0	18	1.0

3.4.2.2 Morphological Characterization

The morphological characterization for the synthesized PtBA-*b*-PS-*g*-PEO continuum graft copolymers was performed using Transmission electron microscopy (TEM) and Small Angle X-Ray scattering (SAXS). To observe the morphologies using TEM, RuO_4 staining, which primarily stains the PEO chains and lightly stains the PS chains, was employed. The PtBA chains remains

unstained by using RuO_4 staining agent. Since $\chi_{PtBA-PEO}$ is small and $\chi_{PtBA-PEO} < \chi_{PS-PEO} < \chi_{PtBA-PS}$ the PEO chains would prefer mixing with the PtBA chains over PS. No mixing of the PtBA and PS chains is preferred due to their high interaction parameter. However, the mixing of PEO chains with PS is driven by topological frustration present in these graft copolymers. Using the RuO_4 stain and the potential mixing of the different polymers chains, it is expected that the PS-PEO mixed phase will appear darker and the PtBA-PEO mixed domains will appear lighter under the TEM.

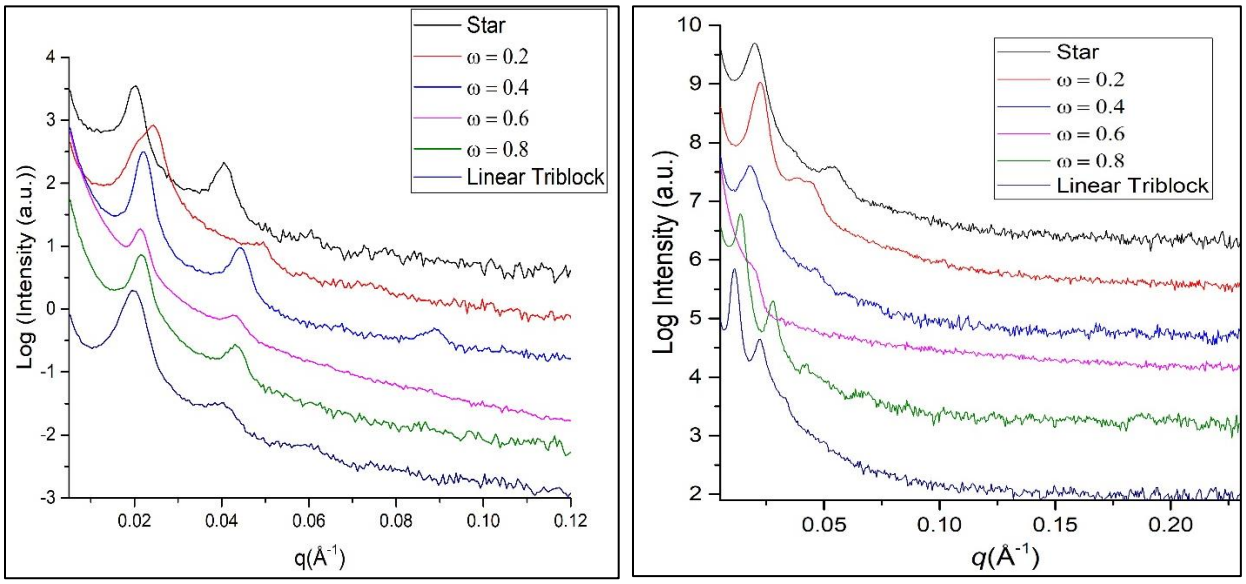

Figure 3. 18: SAXS profiles for a) PtBA-b-PS-g-PEO Series -1-6 and b) PtBA-b-PS-g-PEO Series-7-12.

An interesting change in the morphologies were observed in the SAXS profiles of PtBA-*b*-PS-*g*-PEO-1-6 and 7-12 series with corresponding MWs of PtBA, PS and PEO being 22, 22 and 10 kg/mol was observed on moving along the continuum from the 3-arm to A-B-C linear triblock copolymer architecture (Figure 18). The different SAXS profiles for the PtBA-*b*-PS-*g*-PEO-1-6 series shows the presence of multiple higher order peaks in integral multiples of the primary q* value indicates the presence of lamellae morphology for these samples. A decrease in the *d*-spacing

from 31.4 nm to 26.1 nm was observed on moving the graft position from ω = 0 to ω = 0.2. This decrease in the *d*-spacing may be attributed to the mixing of PEO arm with the PtBA, which results in looping the PS segment before the PFPMI junction point and therefore reduction in the domain spacing is observed. On moving the graft to ω = 0.4, an increase in the domain spacing is observed which can ascribed to the inability of the PEO arm to fold the PS_1 segment which leads to the forced mixing of the PEO with the PS rather than mixing with the PtBA chains. This effect continues for ω = 0.6 and 0.8 and the domain spacing remains constant. An increase in the *d*-spacing when the graft position reaches the chain end (ω = 1), which may be attributed to the release in the topological frustration for the linear triblock copolymer architecture (Figure 19 (A)).

For the PtBA-*b*-PS-*g*-PEO-7-12 series with PEO MW-18kg/mol, highly ordered cylindrical morphology was observed for ω = 0, as confirmed by the presence higher order peaks with ratios of $\sqrt{4}$ and $\sqrt{7}$ with respect to the primary peak q_*, and the possibility of the $\sqrt{3}$ peak being suppressed by the form factor. For ω = 0.2 and 0.4, the morphology remains cylindrical as confirmed by the observed higher order peaks corresponding to the ratios of 1: $\sqrt{3}$: $\sqrt{4}$ and 1: $\sqrt{3}$: $\sqrt{7}$ respectively. On moving the graft position to ω = 0.6, a single peak corresponding to microphase separation but lack of long range order was observed which changes to highly ordered lamellae morphology for ω = 0.8 and 1 as indicated by the integral higher order reflections. For PtBA-*b*-PS-*g*-PEO-7-13 series, the *d*-spacing first decreases on moving from ω = 0 to ω = 0.2 and then increases as the graft position changes to ω = 0.4. The *d*-spacing was observed to remain constant for ω = 0.6 and then increases for ω = 0.8 and 1. The *d*-spacing trend observed was found to be similar to the PtBA-*b*-PS-*g*-PEO-1-6 series, expect for ω = 0.8, where an increase in the domain spacing was observed in contrast to the being constant for the series with shorter length of

the PEO chain (Figure 19 (A)). This difference in the trend may be due to the bigger length of the PEO chain present this series which can further increase the topological frustration in this system.

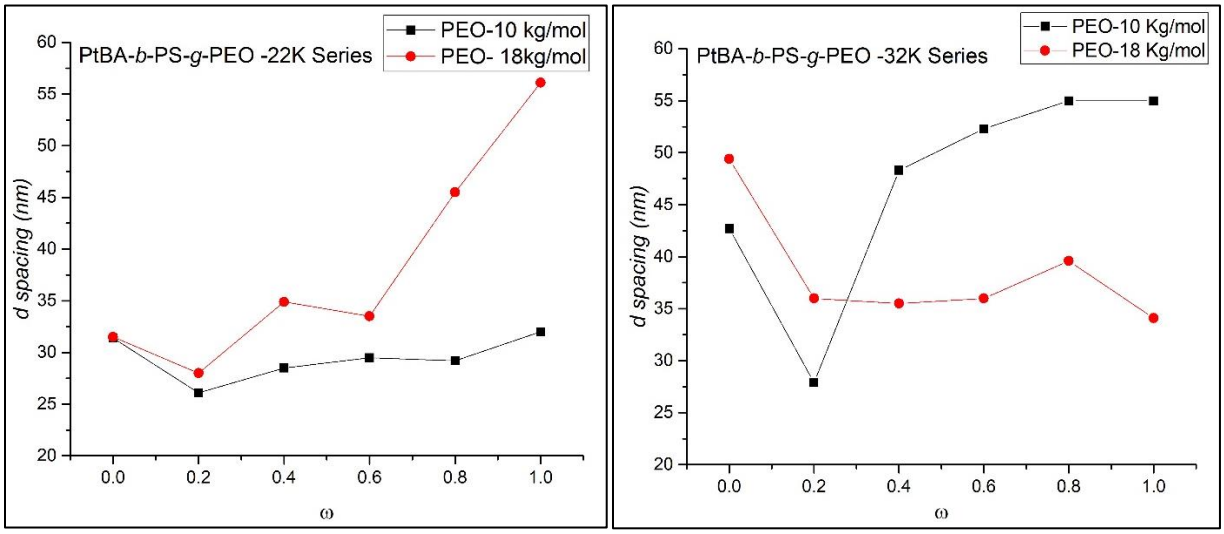

Figure 3. 19: Effect of graft position on domain spacing for different lengths of the PEO arm. A) PtBA-*b*-PS-*g*-PEO with MW of PtBA and PS = 22kg/mol B) PtBA-*b*-PS-*g*-PEO with MW of PtBA and PS = 32kg/mol.

Figure 20 shows the TEM micrographs for the PtBA-*b*-PS-*g*-PEO-1-6 series which represent a well-defined lamellae morphology for the ω value 0 and 0.2 in agreement with the SAXS data. It is expected that the PtBA-PEO mixed domain forms one of the lamellar domains and the PS-PEO forms the other. On moving along the continuum to ω = 0.4, the morphology changes to highly ordered cylindrical morphology. However, lamellae morphology was observed using SAXS which might indicative of the suppression of the $\sqrt{3}$ peak by the form factor. Moving to ω = 0.6, the morphology again changes to lamellae and remains the same throughout the continuum which was in good agreement with the SAXS data observed for these samples.

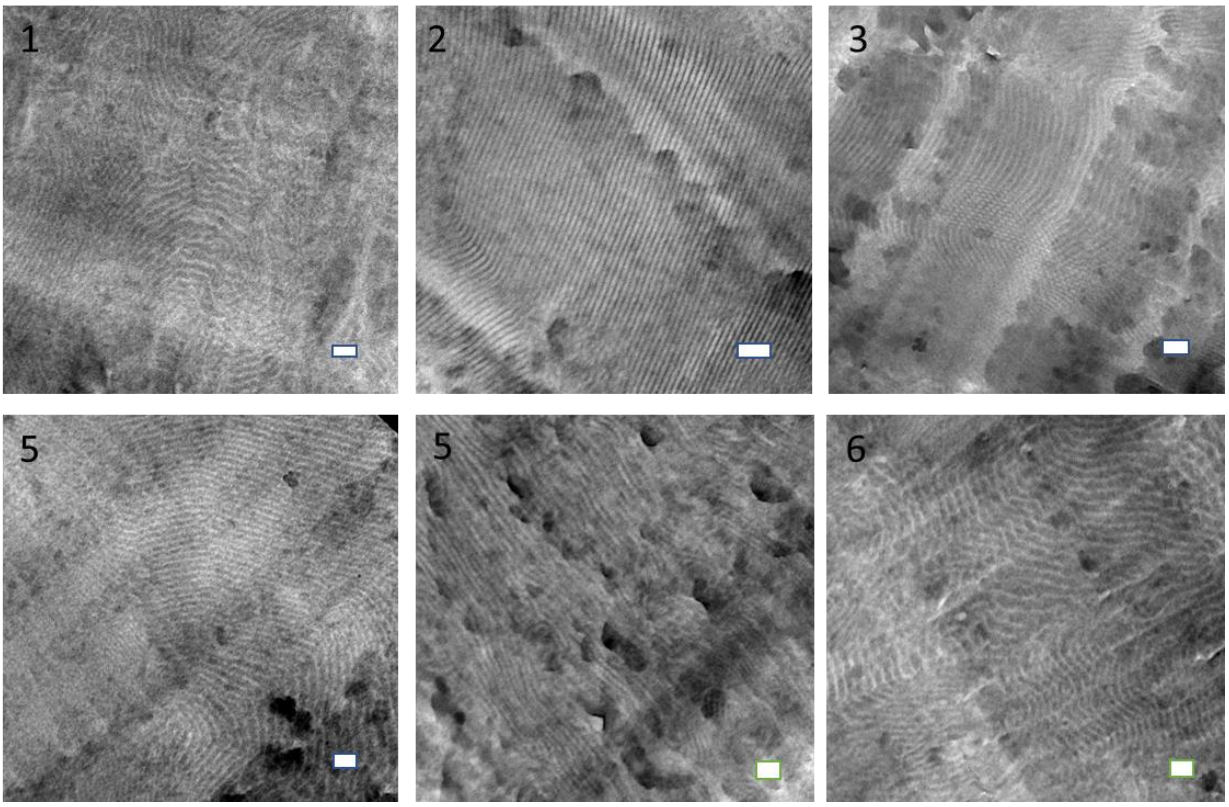

Figure 3. 20: TEM images for PtBA-*b*-PS-*g*-PEO-1-6 Series. Scale bar 100 nm.

Figure 21 shows the SAXS profile for the PtBA-*b*-PS-*g*-PEO Series-13-18 and PtBA-*b*-PS-*g*-PEO Series-25-30 with corresponding PtBA and PS MW being 32 kg/mol and PEO MW being 10 and 18 kg/mol respectively. For PtBA-*b*-PS-*g*-PEO Series -13-18, the star triblock copolymer shows higher order peaks with peak ratios being 1:2:3 indicative of a lamellae morphology. For ω = 0.2, a single peak signifying microphase separation but lack of long range order was observed. For ω = 0.4-1.0, highly ordered lamellae morphologies were observed with peak reflections ratios being 1:2:3. The *d*-spacing was observed to decrease form 42.7 nm for ω = 0 to 27.9 nm for the graft position 0.2. The domain spacing increases on moving the graft to ω = 0.4 which gradually increases to 55 nm as the graft moves toward the linear triblock copolymer architecture (Figure 19 (B)). Similarly, for the PtBA-*b*-PS-*g*-PEO Series-25-30 series, highly ordered morphologies were observed for all the samples. For ω = 0, highly ordered lamellae morphologies with peak

reflections having ratios 1:2:3:5 were observed. For ω = 0.2-1.0, integral peak ratios corresponding to lamellae morphology were observed. The *d*-spacing for the PtBA-*b*-PS-*g*-PEO-25-30 was observed to decrease form 49.4 nm for ω = 0 to 36.0 nm for the graft position 0.2 and remains constant as the graft moves to ω = 0.4 and 0.6. However, the *d*-spacing increases to 39.6 nm for ω = 0.8 and then decreases to 34.1 for the linear triblock copolymer architecture. In general, an interesting trend in the domain spacing for PtBA-*b*-PS-*g*-PEO triblock copolymers is observed, which always shows a decrease in the domain spacing on moving the PEO graft from ω = 0 to ω = 0.2. and then increases and stays constant up to a critical ω value and then depending on the length of PEO arm can either increase, decrease or remain constant as the ω changes to 1 (Figure 19 (B)).

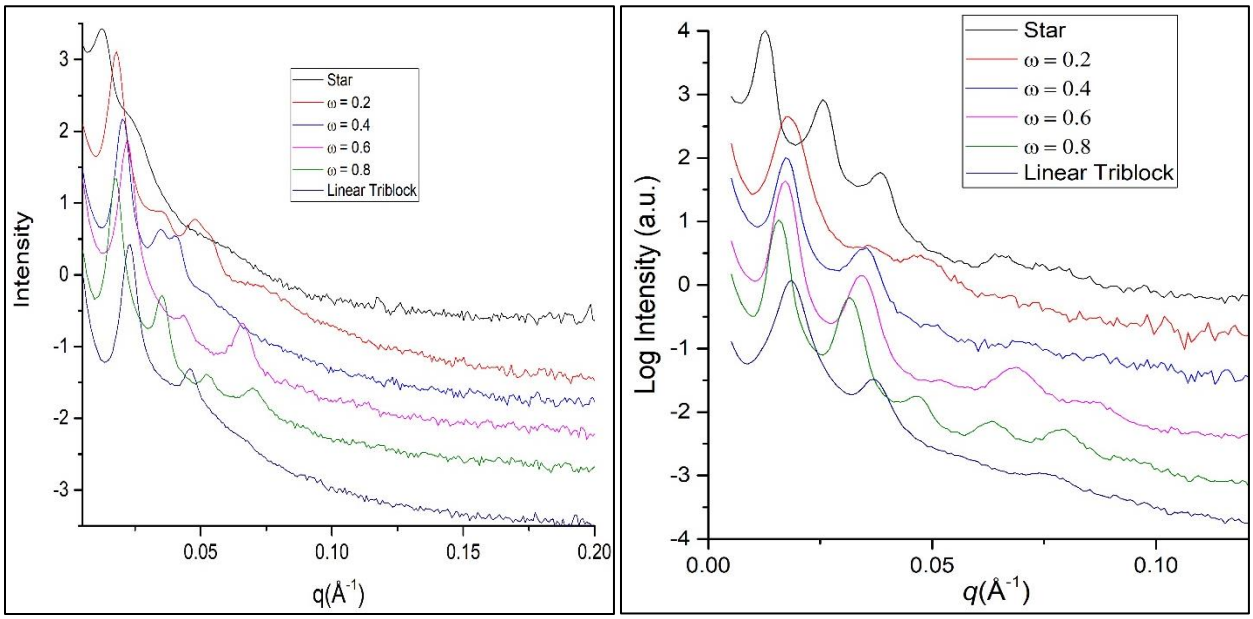

Figure 3. 21: SAXS profiles for a) PtBA-*b*-PS-*g*-PEO Series-13-18 and b) PtBA-*b*-PS-*g*-PEO Series-25-30.

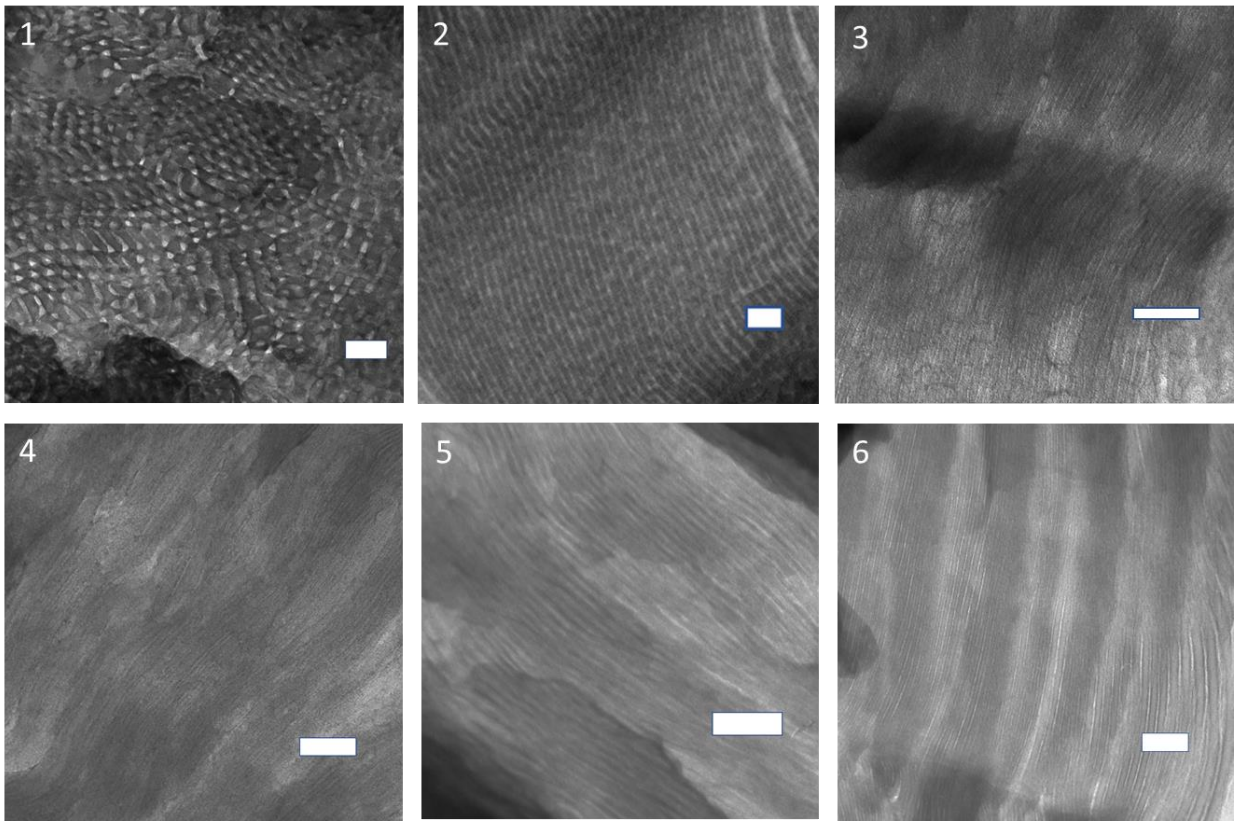

Figure 3. 22: TEM images for PtBA-*b*-PS-*g*-PEO-13-18 Series.

Figure 22 shows the TEM images for the PtBA-*b*-PS-*g*-PEO-13-18 series, which shows cylindrical morphology with PtBA-PEO forming the cylindrical domains and PS-PEO forming the matrix for the star triblock copolymer architecture. The SAXS data shows the presence of lamellae morphology, which might be indicative of the suppression of the $\sqrt{3}$ peak by the form factor. Moving to ω = 0.2, highly ordered perforated lamellae morphology was observed with PEO-PS forming one domain and the PtBA-PEO forming the other domain and the PtbA-PEO perforations running through the PS-PEO domain. As we move along the continuum to ω = 0.4-1, highly ordered three-domain lamellae morphology with PtBA as the unstained, PEO as the dark and PS as the light/grey domain was observed. The PtBA domain was observed to form PtBA-PEO interface, while the PEO formed interface with both PS and PtBA for the three-domain lamellar

morphology. This was in accordance to the SAXS data observed for these samples which indicates the presence of the lamellae morphologies for these samples.

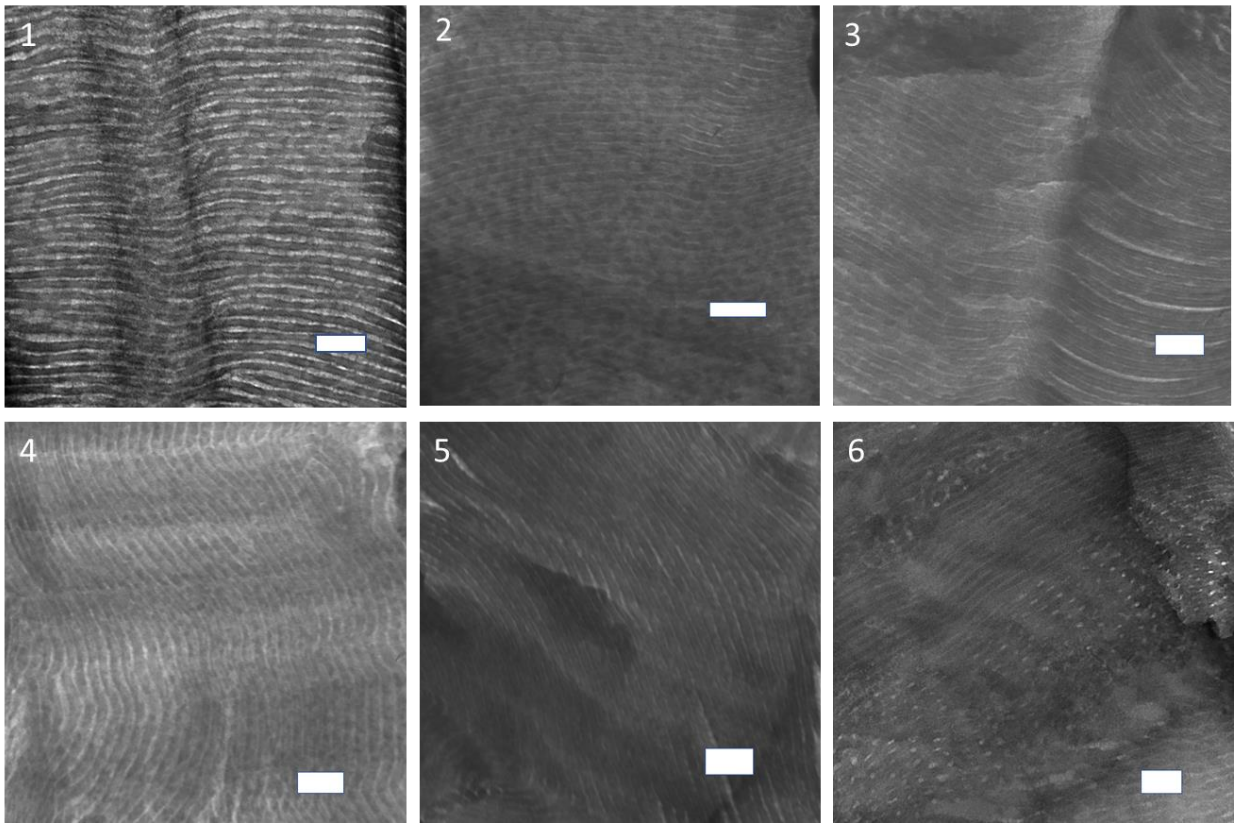

Figure 3. 23: TEM images for PtBA-*b*-PS-*g*-PEO-25-30 Series.

For the PtBA-*b*-PS-*g*-PEO-25-30 series highly ordered perforated lamellae morphologies were observed for ω = 0-0.8 with the PtBA-PEO forming one of the lamellar domain and PS-PEO forming the other with PtBA-PEO perforations running through them (Figure 23). This was in qualitative agreement with the SAXS data observed for these morphologies which was indicative for a lamellae morphology. However, on moving the graft position towards the linear triblock copolymer, highly ordered cylindrical morphology was observed, with the probability of the PEO-PtBA forming the cylindrical domains and PtBA-PS forming the matrix.

It is important to note that for some of the PtBA-*b*-PS-*g*-PEO continuum copolymers, sub-structure within the structure morphology was observed, while a co-existence of two different morphologies was observed for some of the samples. In general, a broad interface due to the mixing of the polymer chains as a result of topological frustration was observed which made these morphologies even more complicated and difficult to predict.

Since the PtBA-*b*-PS-*g*-PEO series the samples are stained using one staining agent which specifically stains the PEO and lightly stains the PS, definitive prediction of the morphological domain cannot be achieved. Therefore, computational studies are required to simulate the expected morphologies and understand the morphological behavior of these polymers.

3.5 Summary

A highly efficient synthetic methodology has been demonstrated to synthesize graft copolymers which lie along the continuum of a 3-arm star and A-B-C linear triblock copolymer. The morphological characterization of these novel continuum graft copolymers using SAXS, TEM, and DPD simulations shows exciting morphologies and projects these copolymers as interesting candidates to access new morphologies. Contrary to the majority of the work done on block copolymers, these structures are novel as their morphologies can be tuned keeping the φ and χ constant. This study also deepens our understanding of the effect of polymer architecture on the phase behavior of these graft copolymers and provides a novel pathway to tune the block copolymer morphologies.

3.6 References

(1) Leibler, L. *Macromolecules* **1980**, *13* (10), 1602–1617.

(2) Matsen, M. *J. Phys. Condens. Matter* **2002**, *14* (2), 21–47.

(3) Bates, F. S.; Fredrickson, G. H. *Annu. Rev. Phys. Chem.* **1990**, *41* (1), 525–557.

(4) Smart, T.; Lomas, H.; Massignani, M.; Flores-Merino, M. V.; Perez, L. R.; Battaglia, G. *Nano Today* **2008**, *3* (3–4), 38–46.

(5) Bates, C. M.; Bates, F. S. *Macromolecules* **2017**, *50* (1), 3–22.

(6) Bates, F. S.; Fredrickson, G. H. *Phys. Today* **1999**, *52* (2), 32–38.

(7) Ciach, a.; Pękalski, J.; Góźdź, W. T. *Soft Matter* **2013**, *9* (27), 6301.

(8) Cochran, E. W.; Garcia-Cervera, C. J.; Fredrickson, G. H. *Macromolecules* **2006**, *39* (7), 2449–2451.

(9) Matsen, M. W. *Eur. Phys. J. E* **2009**, *30* (4), 361–369.

(10) Matsen, M.; Bates, F. *Macromolecules* **1996**, *29* (23), 7641–7644.

(11) Bates, F. S.; Hillmyer, M. a.; Lodge, T. P.; Bates, C. M.; Delaney, K. T.; Fredrickson, G. H. *Science (80-.).* **2012**, *336* (6080), 434–440.

(12) Christodoulou, S.; Driva, P.; Iatrou, H.; Hadjichristidis, N. *Macromolecules* **2008**, *41* (7), 2607–2615.

(13) Georgopanos, P.; Lo, T.-Y.; Ho, R.-M.; Avgeropoulos, A. *Polym. Chem.* **2017**, *8* (5), 843–850.

(14) Wijayasekara, D. B.; Huang, T.; Richardson, J. M.; Knauss, D. M.; Bailey, T. S. *Macromolecules* **2016**, *49* (2), 595–608.

(15) Iatrou, H.; Hadjichristidis, N.; Meier, G.; Frielinghaus, H.; Monkenbusch, M.

Macromolecules **2002**, *35* (14), 5426–5437.

(16) Iatrou, H.; Willner, L.; Hadjichristidis, N.; Halperin, A.; Richter, D. *Macromolecules* **1996**, *29* (2), 581–591.

(17) Zhu, Y.; Gido, S. P.; Moshakou, M.; Iatrou, H.; Hadjichristidis, N.; Park, S.; Chang, T. *Macromolecules* **2003**, *36* (15), 5719–5724.

(18) Zheng, W.; Wang, Z. G. *Macromolecules* **1995**, *28* (21), 7215–7223.

(19) Ungar, G.; Tschierske, C.; Abetz, V.; Holyst, R.; Bates, M. A.; Liu, F.; Prehm, M.; Kieffer, R.; Zeng, X.; Walker, M.; Glettner, B.; Zywocinski, A. *Adv. Funct. Mater.* **2011**, *21* (7), 1296–1323.

(20) Lecommandoux, S.; Borsali, R.; Schappacher, M.; Deffieux, A.; Narayanan, T.; Rochas, C. *Macromolecules* **2004**, *37* (5), 1843–1848.

(21) Meuler, A. J.; Hillmyer, M. a.; Bates, F. S. *Macromolecules* **2009**, *42* (19), 7221–7250.

(22) Dair, B. J.; Avgeropoulos, A.; Hadjichristidis, N.; Thomas, E. L. *J. Mater. Sci.* **2000**, *35* (20), 5207–5213.

(23) Dair, B. J.; Honeker, C. C.; Alward, D. B.; Avgeropoulos, A.; Hadjichristidis, N.; Fetters, L. J.; Capel, M.; Thomas, E. L. *Macromolecules* **1999**, *32* (24), 8145–8152.

(24) Yang, X.; Loos, J. *Macromolecules* **2007**, *40* (5), 1353–1362.

(25) Crossland, E. J. W.; Nedelcu, M.; Ducati, C.; Ludwigs, S.; Hillmyer, M. A.; Steiner, U.; Snaith, H. J. *Nano Lett.* **2009**, *9* (8), 2813–2819.

(26) Crossland, E. J. W.; Kamperman, M.; Nedelcu, M.; Ducati, C.; Wiesner, U.; Smilgies, D.

M.; Toombes, G. E. S.; Hillmyer, M. A.; Ludwigs, S.; Steiner, U.; Snaith, H. J. *Nano Lett.* **2009**, *9* (8), 2807–2812.

(27) Oey, C. C.; Djurišić, a B.; Wang, H.; Man, K. K. Y.; Chan, W. K.; Xie, M. H.; Leung, Y. H.; Pandey, a; Nunzi, J.-M.; Chui, P. C. *Nanotechnology* **2006**, *17* (3), 706–713.

(28) Wang, H.; Oey, C. C.; Djurišić, A. B.; Xie, M. H.; Leung, Y. H.; Man, K. K. Y.; Chan, W. K.; Pandey, A.; Nunzi, J.-M.; Chui, P. C. *Appl. Phys. Lett.* **2005**, *87* (2), 023507.

(29) Shefelbine, T. A.; Vigild, M. E.; Matsen, M. W.; Hajduk, D. A.; Hillmyer, M. A.; Cussler, E. L.; Bates, F. S. *J. Am. Chem. Soc.* **1999**, *121* (37), 8457–8465.

(30) Yang, S. Y.; Ryu, I.; Kim, H. Y.; Kim, J. K.; Jang, S. K.; Russell, T. P. *Adv. Mater.* **2006**, *18* (6), 709–712.

(31) Phillip, W. A.; Rzayev, J.; Hillmyer, M. A.; Cussler, E. L. *J. Memb. Sci.* **2006**, *286* (1–2), 144–152.

(32) Phillip, W. A.; Amendt, M.; ONeill, B.; Chen, L.; Hillmyer, M. A.; Cussler, E. L. *ACS Appl. Mater. Interfaces* **2009**, *1* (2), 472–480.

(33) Ertem, S. P.; Caire, B. R.; Tsai, T.; Zeng, D.; Vandiver, M. A.; Kusoglu, A.; Seifert, S.; Hayward, R. C.; Weber, A. Z.; Herring, A. M.; Coughlin, E. B.; Liberatore, M. W. **2017**, 612–622.

(34) Cho, B.K.; Jain, A.; Gruner, S. M.; Wiesner, U. *Science (80-.).* **2004**, *305* (5690), 1598–1601.

(35) Zhang, W.; Liu, Y.; Jackson, A. C.; Savage, A. M.; Ertem, S. P.; Tsai, T.; Seifert, S.; Beyer, F. L.; Liberatore, M. W.; Herring, A. M.; Coughlin, E. B. **2016**.

(36) Lin, S. Y.; Fleming, J. G.; Hetherington, D. L.; Smith, B. K.; Biswas, R.; Ho, K. M.; Sigalas, M. M.; Zubrzycki, W.; Kurtz, S. R.; Bur, J. *Nature* **1998**, *394* (6690), 251–253.

(37) Maldovan, M.; Thomas, E. L.; Article, P.; Maldovan, M.; Thomas, E. L. *Nat. Mater.* **2004**, *3* (9), 593–600.

(38) Breiner, U.; Krappe, U.; Jakob, T.; Abetz, V.; Stadler, R. *Polym. Bull.* **1998**, *40* (2–3), 219–226.

(39) Breiner, U.; Krappe, U.; Stadler, R. *Macromol. Rapid Commun.* **1996**, *17* (8), 567–575.

(40) Breiner, U.; Krappe, U.; Abetz, V.; Stadler, R. *Macromol. Chem. Phys.* **1997**, *198* (4), 1051–1083.

(41) Stadler, R.; Auschra, C.; Beckmann, J.; Krappe, U.; Voigt-Martin, I.; Leibler, L. *Macromolecules* **1995**, *28*, 3080–3091.

(42) Breiner, U.; Krappe, U.; Thomas, E. L.; Stadler, R. *Macromolecules* **1998**, *31* (96), 135–141.

(43) Elbs, H.; Abetz, V.; Hadziioannou, G.; Drummer, C.; Krausch, G. *Macromolecules* **2001**, *34* (23), 7917–7919.

(44) Park, C.; Yoon, J.; Thomas, E. L. *Polymer (Guildf).* **2003**, *44* (22), 6725–6760.

(45) Elbs, H.; Drummer, C.; Abetz, V.; Krausch, G. *Macromolecules* **2002**, *35* (14), 5570–5577.

(46) Ludwigs, S.; Schmidt, K.; Stafford, C. M.; Amis, E. J.; Fasolka, M. J.; Karim, A.; Magerle, R.; Krausch, G. *Macromolecules* **2005**, *38* (5), 1850–1858.

(47) Balsamo, V.; von Gyldenfeldt, F.; Stadler, R. *Macromolecules* **1999**, *32* (4), 1226–1232.

(48) Bailey, T. S.; Pham, H. D.; Bates, F. S. *Macromolecules* **2001**, *34* (20), 6994–7008.

(49) Epps, T. H.; Cochran, E. W.; Bailey, T. S.; Waletzko, R. S.; Hardy, C. M.; Bates, F. S. Ordered Network Phases in Linear Poly(isoprene-b-styrene-b-ethylene oxide) Triblock Copolymers http://pubs.acs.org/doi/pdf/10.1021/ma048762s (accessed Feb 4, 2016).

(50) Epps, T. H.; Bailey, T. S.; Waletzko, R.; Bates, F. S. *Macromolecules* **2003**, *36* (8), 2873–2881.

(51) Bailey, T. S.; Hardy, C. M.; Epps, T. H.; Bates, F. S. *Macromolecules* **2002**, *35* (18), 7007–7017.

(52) Tang, P.; Qiu, F.; Zhang, H.; Yang, Y. *Phys. Rev. E - Stat. Nonlinear, Soft Matter Phys.* **2004**, *69* (3 1), 1–8.

(53) Guo, Z.; Zhang, G.; Qiu, F.; Zhang, H.; Yang, Y.; Shi, A. C. *Phys. Rev. Lett.* **2008**, *101* (2), 1–4.

(54) Nagpal, U.; Detcheverry, F. a.; Nealey, P. F.; De Pablo, J. J. *Macromolecules* **2011**, *44* (13), 5490–5497.

(55) Li, W.; Xu, Y.; Zhang, G.; Qiu, F.; Yang, Y.; Shi, A. C. *J. Chem. Phys.* **2010**, *133* (6).

(56) Liu, M.; Li, W.; Qiu, F.; Shi, A. C. *Macromolecules* **2012**, *45* (23), 9522–9530.

(57) Milner, S. T. *Macromolecules* **1994**, *27* (8), 2333–2335.

(58) Floudas, G; Hadjichristidis, N.; Tselikas, T.; Erukhimovich, I. *Macomolecules* **1997**, *30*, 3090–3096.

(59) Grason, G. M.; Kamien, R. D. *Macromolecules* **2004**, *37* (19), 7371–7380.

(60) Huang, C. I.; Yu, H. T. *Polymer (Guildf).* **2007**, *48* (15), 4537–4546.

(61) Hayashida, K.; Saito, N.; Arai, S.; Takano, A.; Tanaka, N.; Matsushita, Y. *Macromolecules* **2007**, *40* (10), 3695–3699.

(62) Bohbot-Raviv, Y.; Wang, Z. *Phys. Rev. Lett.* **2000**, *85*, 3428–3431.

(63) Gemma, T.; Hatano, A.; Dotera, T. *Macromolecules* **2002**, *35* (8), 3225–3237.

(64) Ueda, M. *Prog. Polym. Sci.* **1999**, *24* (5), 699–730.

(65) Pispas, S.; Avgeropoulos, A.; Hadjichristidis, N.; Roovers, J. *J. Polym. Sci. Part B Polym. Phys.* **1999**, *37*, 1329–1335.

(66) Tselikas, Y.; Iatrou, H.; Hadjichristidis, N.; Liang, K. S.; Mohanty, K.; Lohse, D. J. *J. Chem. Phys.* **1996**, *105* (6), 2456.

(67) Tselikas, Y.; Hadjichristidis, N.; Lescanec, R. L.; Honeker, C. C.; Wohlgemuth, M.; Thomas, E. L. *Macromolecules* **1996**, *29* (10), 3390–3396.

(68) Takano, A.; Wada, S.; Sato, S.; Araki, T.; Hirahara, K.; Kazama, T.; Kawahara, S.; Isono, Y.; Ohno, A.; Tanaka, N.; Matsushita, Y. *Macromolecules* **2004**, *37* (26), 9941–9946.

(69) Matsushita, Y.; Hayashida, K.; Dotera, T.; Takano, A. *J. Physics-Condensed Matter* **2011**, *23* (28), 284111.

(70) Rho, Y.; Kim, C.; Higashihara, T.; Jin, S.; Jung, J.; Shin, T. J.; Hirao, A.; Ree, M. *ACS Macro Lett.* **2013**, *2* (10), 849–855.

(71) Okamoto, S.; Hasegawa, H.; Hashimoto, T.; Fujimoto, T.; Zhang, H.; Kazama, T.;

Takano, A.; Isono, Y. *Polymer (Guildf).* **1997**, *38* (21), 5275–5281.

(72) Sioula, S.; Hadjichristidis, N.; Thomas, E. L. *Macromolecules* **1998**, *31* (97), 5272–5277.

(73) Yamauchi, K.; Takahashi, K.; Hasegawa, H.; Iatrou, H.; Hadjichristidis, N.; Kaneko, T.; Nishikawa, Y.; Jinnai, H.; Matsui, T.; Nishioka, H.; Shimizu, M.; Furukawa, H. *Macromolecules* **2003**, *36* (19), 6962–6966.

(74) Huckstadt, H.; Gopfert, A.; Abetz, V. *Macromol. Chem. Phys.* **2000**, *201* (3), 296–307.

(75) Takano, A.; Kawashima, W.; Noro, A.; Isono, Y.; Tanaka, N.; Dotera, T.; Matsushita, Y. *J. Polym. Sci. Part B Polym. Phys.* **2005**, *43* (18), 2427–2432.

(76) Kakuchi, R.; Zamfir, M.; Lutz, J. F.; Theato, P. *Macromol. Rapid Commun.* **2012**, *33* (1), 54–60.

(77) Mahou, R.; Wandrey, C. *Polymers (Basel).* **2012**, *4* (1), 561–589.

(78) Moad, G.; Chong, Y. K.; Postma, A.; Rizzardo, E.; Thang, S. H. **2005**, *46*, 8458–8468.

(79) Mutlu, H.; Lutz, J. F. *Angew. Chemie - Int. Ed.* **2014**, *53* (48), 13010–13019.

(80) Lutz, J. F. *Acc. Chem. Res.* **2013**, *46* (11), 2696–2705.

(81) Colquhoun, H.; Lutz, J.-F. *Nat. Chem.* **2014**, *6* (June), 455–456.

(82) Lutz, J.-F.; Ouchi, M.; Liu, D. R.; Sawamoto, M. *Science (80-.).* **2013**, *341* (6146), 1238149–1238149.

(83) Matsuda, M.; Satoh, K.; Kamigaito, M. **2013**.

(84) Hisano, M.; Takeda, K.; Takashima, T.; Jin, Z.; Shiibashi, A.; Matsumoto, A. **2013**.

(85) Liu, B.; Wang, X.; Pan, Y.; Lin, F.; Wu, C.; Qu, J.; Luo, Y.; Cui, D. **2014**.

(86) Ovitt, T. M.; Coates, G. W.; V, C. U.; York, N. **1999**, No. 16, 4072–4073.

(87) Kramer, J. W.; Treitler, D. S.; Dunn, E. W.; Castro, P. M.; Roisnel, T.; Thomas, C. M.; Coates, G. W. **2009**, No. Figure 1, 16042–16044.

(88) Few, C. S.; Wagener, K. B.; Thompson, D. L. 123–132.

(89) Li, Z.; Li, L.; Deng, X.; Zhang, L.; Dong, B.; Du, F.; Li, Z. **2012**.

(90) Zhang, J.; Matta, M. E.; Hillmyer, M. A. **2012**, 19–23.

(91) Article, E.; Moatsou, D.; Hansell, C. F.; Reilly, R. K. O. **2014**, 2246–2250.

(92) Minoda, M.; Sawamoto, M.; Higashimura, T. *Macromolecules* **1990**, *23* (23), 4889–4895.

(93) Tong, X.; Guo, B.; Huang, Y. **2011**, 1455–1457.

(94) Chem, P.; Houshyar, S.; Keddie, D. J.; Moad, G.; Mulder, R. J.; Saubern, S.; Tsanaktsidis, J. **2012**, 1879–1889.

(95) Berthet, M.; Zarafshani, Z.; Pfeifer, S. **2010**, 44–50.

(96) Yu, T.; Bai, J. Z.; Guan, Z. **2009**, 1097–1101.

(97) Chen, Y.; Guan, Z. **2010**, 4577–4579.

(98) Sumerlin, B. S.; Vogt, A. P. *Macromolecules* **2010**, *43* (1), 1–13.

(99) Badi, N. **2009**, 3383–3390.

(100) Deng, X. X.; Li, L.; Li, Z. L.; Lv, A.; Du, F. S.; Li, Z. C. *ACS Macro Lett.* **2012**, *1* (11), 1300–1303.

(101) Manuscript, A. **2015**.

(102) Online, V. A.; Lv, A.; Deng, X.; Li, L.; Li, Z.; Wang, Y.; Du, F.; Li, Z. **2013**, 3659–3662.

(103) Reaction, T.; Solleder, S. C.; Meier, M. A. R. **2014**, 711–714.

(104) Ida, S.; Terashima, T.; Ouchi, M.; Sawamoto, M. *J. Am. Chem. Soc.* **2009**, *131* (31), 10808–10809.

(105) Ida, S.; Ouchi, M.; Sawamoto, M. **2010**, 14748–14750.

(106) Brummelhuis, N. *Polym. Chem.* **2015**, *6* (5), 654–667.

(107) Pfeifer, S.; Zarafshani, Z.; Badi, N.; Lutz, J. F. *J. Am. Chem. Soc.* **2009**, *131* (26), 9195–9197.

(108) Hartmann, B. L.; Bo, H. G. **2009**, 3425–3431.

(109) Hartmann, L. **2011**, 8–13.

(110) Charles, L.; Verchin, C.; Lutz, J.; Roy, R. K.; Meszynska, A. **2015**, No. May, 1–8.

(111) Lutz, J. *Angew. Chemie Int. Ed.* **2007**, *46* (7), 1018–1025.

(112) Fournier, D.; Hoogenboom, R.; Schubert, U. S. *Chem. Soc. Rev.* **2007**, *36* (8), 1369.

(113) Zhang, C.; Yang, Y.; He, J. *Macromolecules* **2013**, *46* (10), 3985–3994.

(114) Soeriyadi, A. H.; Boyer, C.; Nyström, F.; Zetterlund, P. B.; Whittaker, M. R. *J. Am. Chem. Soc.* **2011**, *133* (29), 11128–11131.

(115) Article, E.; Anastasaki, A.; Nikolaou, V.; Pappas, G. S.; Zhang, Q.; Wan, C.; Wilson, P.; Davis, T. P.; Whittaker, R.; Haddleton, D. M. *Chem. Sci.* **2014**, *5*, 3536–3542.

(116) Zhang, W.; Sun, Z.; Jiang, Y.; Liu, X.; Gupta, R.; Russell, T. P.; Coughlin, E. B. **2017**, 1–7.

(117) Deng, G.; Chen, Y. **2004**, 18–26.

(118) Padmanabhan, P.; Martinez-Veracoechea, F. J.; Araque, J. C.; Escobedo, F. A. *J. Chem. Phys.* **2012**, *136* (23).

(119) Gavrilov, A. A.; Kudryavtsev, Y. V.; Chertovich, A. V. *J. Chem. Phys.* **2013**, *139* (22).

(120) Groot, R. D.; Warren, P. B. *J. Chem. Phys.* **1997**, *107* (11), 4423–4435.

(121) Bjorken, J. D.; Brodsky, S. J. *Phys. Rev. D* **1970**, *1* (5), 1416–1420.

CHAPTER IV

MAPPING THE PHASE DIAGRAM FOR FRUSTRATED A-B-C LINEAR TRIBLOCK COPOLYMERS

4.1 Introduction

In the past few years, linear triblock copolymers have been the most extensively studied class of multiblock copolymers. As explained in chapter 1, the number of parameters which define the microphase separation of triblock copolymers increases considerably with the addition of one more block to the diblock copolymer. This enlarges the parameter space for these block copolymers and makes them a promising candidate for exploring novel morphologies. The morphology of triblock copolymers is critically affected by the independent volume fractions of two blocks, three different interaction parameters and the sequence of the three blocks.[1] Based on the sequence and the corresponding interaction parameters of the three blocks, the triblock copolymer system can either be frustrated or non-frustrated.[2] For "frustrated" triblock copolymers, the interaction parameter between the end blocks ($\chi_{AC}N$) is much smaller than interaction parameter between the neighboring blocks ($\chi_{AB}N$) and ($\chi_{BC}N$). This leads to formation of structures with A/C interfaces, which have lower interfacial energy compared to the A/B and B/C interfaces due to the forced connectivity of the A-B and B-C block pairs with the highest relative incompatibility. However, the topology of these triblock copolymers limits the formation of A/C interfaces and thus the system is frustrated. For "non-frustrated" triblock copolymers, the domain arrangement is consistent with the topology of block sequence. $\chi_{AC}N$ is larger than the interaction parameter between the neighboring blocks, $\chi_{AB}N$ and $\chi_{BC}N$ which leads to the formation of distinct A/B and B/C interface because of the preference by A and C blocks to remain separated from each other. Many systems both frustrated

and non-frustrated triblock copolymers have been studied in the literature which includes poly(styrene-*b*-butadiene-*b*-2-vinylpyridine)(PS-*b*-PB-*b*-P2VP,SBP)[3] and PB-*b*-PS-*b*-P2VP (BSP)[3], poly (styrene-*b*-isoprene-*b*-2-vinylpyridine) (PS-*b*-PI-*b*-P2VP, SIP)[4,5] and PI-*b*-PS-*b*-P2VP (ISP)[6], and poly(styrene-*b*-isoprene-*b*-lactide) (PS-*b*-PI-*b*-PLA)[7], poly(styrene-*b*-isoprene-*b*-ethylene oxide) (PS-*b*-PI-*b*-PEO, SIO)[8] and PI-*b*-PS-*b*-PEO (ISO)[9], poly(styrene-*b*-2-vinylpyridine-*b*-tert-butyl methacrylate) (SVT)[10–12] and poly-(styrene-*b*-butadiene-*b*-caprolactone) (SBC) triblock copolymers[13]. However, the frustrated systems (SIP, SBP, SIL, SBC, SVT and SIO) have demonstrated more complicated morphologies than the corresponding non-frustrated systems as the morphologies with A/C interfaces can only be observed by utilizing the topological frustration present in the frustrated linear triblock copolymers. Due to their large parameter space many new morphologies have been observed for these frustrated triblock copolymers in the bulk, which includes the conventional morphologies observed for the diblock copolymers,[10] core−shell morphologies,[14] various complex structure-within-structure morphologies such as cylinders-within-lamellae, spheres-within-lamellae, helices-on-cylinders, rings-on-cylinders, spheres-on-cylinders, spheres-on-spheres and superstructures such as the knitting pattern have been observed.[2] Various theoretical methods and simulations have been used to predict the thermodynamically stable morphologies of frustrated A-B-C linear triblock copolymers and correlate them to the experimentally observed morphologies.[12,15–18]

In recent years, there has significant research on design and synthesis of polymeric materials with high-χ and low N due to their ability to form highly ordered microstructures with low N value allowing the formation of very small domain spacing (< 10 nm) which find their application in the microelectronics, used as templates for inorganic nanomaterials[19] and fabrication of nanoporous membranes.[20]. The typical domain spacing (d) for the conventional block polymer morphologies

are between 10–100 nm which are still higher than the preferred domain spacing of ≤ 5 nm for nanolithography.[21] Since block copolymer self-assembly is dependent on the χN value and higher N value leads to larger d-spacing, high χ–low N block polymers can be a way to access smaller d-spacing of < 5 nm.[21] In the past few years, there has been a significant progress to develop such high χ–low N systems to achieve smaller d-spacing. However, the conventional methods to increase the interaction parameter by incorporating silicon, fluorine, or metal species are not suitable for lithographic applications due to the convenience of post-processing and sustainability. Therefore, all organic polymers with high interaction parameters are required. Hillmyer and coworkers have recently demonstrated that sub-5 nm d-spacing can be achieved using poly(cyclohexylethylene-*b*-methyl methacrylate) (PCHE–PMMA) diblock copolymers.[22] Russel and co-workers could achieve sub-5 nm d-spacing by transforming the hydrophobic poly solketal methacrylate to a hydrophilic poly(glycerol monomethacrylate) for a symmetric poly(solketal methacrylate-*b*-styrene) (PSM-*b*-PS) copolymers through an acid hydrolysis.[23,24] This simple chemical transformation significantly enhances the segmental interaction parameter (χ) and thus smaller d-spacing could be achieved.

As described in chapter 1, complex multiblock copolymer architectures often lead to novel morphologies and in some cases, can lead to smaller domain spacing. Shi et al. demonstrated sub-10 nm can be obtained using PS−$(PLA)_2$ and $(PS)_2$−$(PLA)_2$ miktoarm copolymer architectures.[25] Similarly sub-10 nm d spacing was obtained by Borsali and co-workers using different multiblock copolymer architectures (AB-diblock, ABA triblock and A_2B miktoarm star) of maltoheptaose as the A block and polystyrene as the B block.[26]

Taking inspiration from these above-mentioned studies, we aim to extend the concept of high χ-low N block copolymer system from diblock to triblock copolymers to explore new morphologies

with multiple domains and smaller feature size. We have synthesized a series of high χ- low N, PMMA-*b*-PtBS-*b*-P2VP and PtBA-*b*-PtBS-*b*-P2VP triblock copolymers with extending P2VP arm to study the effect of extending chain length on the phase diagram on these highly frustrated triblock copolymer systems and the map the observed morphologies with theoretical predictions.

4.2 Experimental Section

4.2.1 General Procedure for Synthesis of PMMA-*b*-PtBS-*b*-P2VP or PtBA-*b*-PtBS-*b*-P2VP Triblock Copolymers

A series of triblock copolymers were synthesized using sequential RAFT polymerization of the three monomers; MMA, tert-butyl styrene (t-BS) and 2-vinyl pyridine (2-VP) or tert-butyl acrylate (t-BA), tert-butyl styrene (t-BS) and 2-vinyl pyridine as shown in Scheme 1. Firstly, CTA-1b was used as the RAFT agent to synthesize a relatively narrow disperse PMMA or PtBA block. The synthesized PMMA block was precipitated thrice using hexanes and PtBA using MeOH-H_2O solution (MeOH:H_2O = 8:2), and the two homopolymers were dried overnight under vacuum. The synthesized PMMA or PtBA homopolymers were then used as macro-initiator for chain extension using t-BS to yield PMMA-*b*-PtBS or PtBA-*b*-PtBS diblock copolymer with approximately equal volume fraction of the two blocks. The synthesized diblock copolymers were precipitated using cold methanol and dried under vacuum overnight. The synthesized diblock copolymers were further extended using 2-VP to yield PMMA-*b*-PtBS-*b*-P2VP or PtBA-*b*-PtBS-*b*-P2VP triblock copolymers with increasing volume fractions of the 2-VP block as described in Tables 1 and 2. The synthesized triblock copolymers were precipitated using cold diethyl ether to yield the respective triblock copolymers and dried under vacuum for further use.

Table 4. 1: Molecular characteristics of PMMA-*b*-PtBS-*b*-P2VP triblock copolymers.

Sample No.	**MW_{PMMA} (Kg/mol)**	**MW_{PtBS} (Kg/mol)**	**MW_{P2VP} (Kg/mol)**	**Φ_{P2VP}**	**d_{SAXS} (nm)**
PMMA-*b*-PtBS-3	9.0	6.0	-	-	11.9
PMMA-*b*-PtBS-*b*-P2VP-1	9.0	6.0	9.0	0.4	13.1
PMMA-*b*-PtBS-*b*-P2VP-2	9.0	6.0	18.0	0.52	27.4
PMMA-*b*-PtBS-*b*-P2VP-3	9.0	6.0	27.0	0.65	32.7
PMMA-*b*-PtBS-6	6.0	6.0	-	-	-
PMMA-*b*-PtBS-*b*-P2VP-4	6.0	6.0	6.0	0.38	11.8
PMMA-*b*-PtBS-*b*-P2VP-5	6.0	6.0	12.0	0.46	22.2
PMMA-*b*-PtBS-*b*-P2VP-6	6.0	6.0	18.0	0.57	23.7

Table 4. 2: Molecular characteristics of PtBA-*b*-PtBS-*b*-P2VP triblock copolymers.

Sample No.	**MW_{PtBA} (Kg/mol)**	**MW_{PtBS} (Kg/mol)**	**MW_{P2VP} (Kg/mol)**	**Φ_{P2VP}**	**d_{SAXS} (nm)**
PtBA-*b*-PtBS-1	4.4	3.9	-	-	9.6
PtBA-*b*-PtBS-*b*-P2VP-1	4.4	3.9	9.0	0.56	11.1
PtBA-*b*-PtBS-*b*-P2VP-2	4.4	3.9	18.0	0.64	12.5
PtBA-*b*-PtBS-*b*-P2VP-3	4.4	3.9	27.0	0.71	13.7
PtBA-*b*-PtBS-2	15	15	-	-	23.1
PtBA-*b*-PtBS-*b*-P2VP-4	15	15	15	0.3	11.8
PtBA-*b*-PtBS-*b*-P2VP-5	15	15	30	0.45	22.2
PtBA-*b*-PtBS-*b*-P2VP-6	15	15	45	0.52	23.7

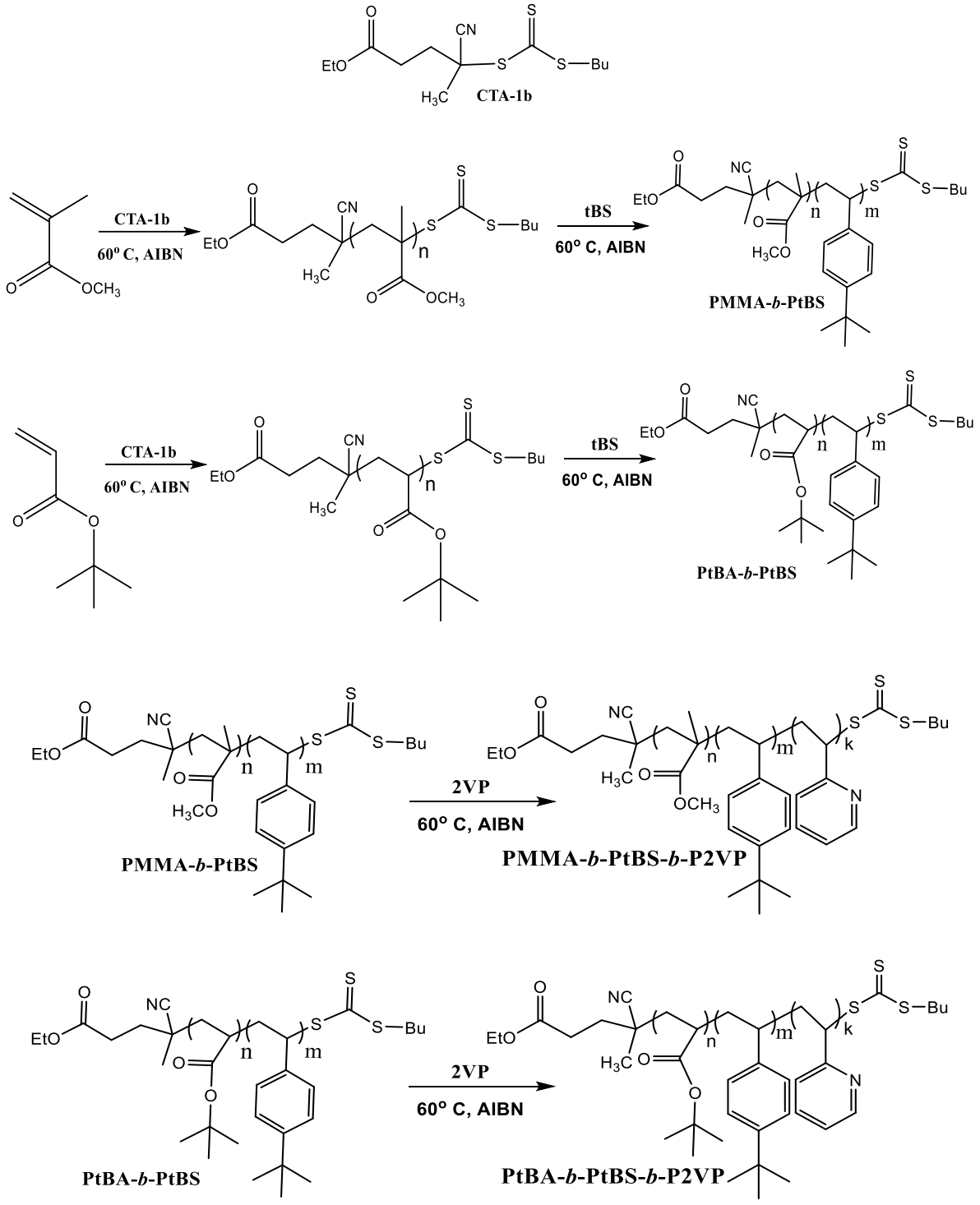

Scheme 1: Triblock copolymer synthesis of PMMA-*b*-PtBS-*b*-P2VP and PtBA-*b*-PtBS-*b*-P2VP using CTA-1b.

4.3 Instrumentation

^{1}H NMR spectroscopy was performed on 500 MHz Bruker 500 Ascend NMR spectrometer. Gel permeation chromatography (GPC) was performed in THF at a flow rate of 1.0 mL/min using a refractive index detector on a Polymer Laboratories PL-GPC 50 Integrated GPC. Small-angle X-ray scattering (SAXS) measurements were performed using a GANESHA 300 XL SAXS instrument. For SAXS measurements, the samples were prepared by dissolving the polymer in anhydrous toluene at a concentration of 50 mg/mL and were casted in 1 mL Teflon beakers. The beakers were covered with a glass hood to allow slow evaporation of the solvent at room temperature and the process was carried out for 5 days. After slow evaporation of the solvent at room temperature, the samples were vacuum dried overnight to remove any residual solvent in the film, followed by thermally annealing at 170 °C for 5 days under vacuum. For transmission electron microscopy (TEM), thin polymer sections of approximately 40 nm in thickness were prepared by Leica (Reichert & Jung) ULTRACUT Ultramicrotome using a diamond knife at room temperature. These sections were mounted on 400 mesh copper support grids and were stained using RuO_4 for 10 min and I_2 vapors for 1h. The stained thin sections were then examined on a JEOL 2000FX TEM operated at an accelerating voltage of 200 kV.

4.4 Results and Discussions

4.4.1 Synthesis of PMMA-*b*-PtBS-*b*-P2VP or PtBA-*b*-PtBS-*b*-P2VP triblock copolymers

Among the various high χ-low N diblock copolymer pairs, PMMA-*b*-PtBS and PtBS-*b*-P2VP diblock copolymers have shown to demonstrate much higher interaction parameter than the conventional PMMA-*b*-PS and PS-*b*-P2VP diblock copolymers.[27,28] This can be accounted to the increased hydrophobicity of t-BS monomer compared to styrene due to the presence of tert-butyl

group which can lead to significant increase in χ. Since the glass transition temperature (T_g) for PtBS is 40 ^{o}C higher than PS can retain the salient cross-linking photoresist properties and also compensate for the reduction in the T_g for thin films for lithographic applications.[29]

Using sequential RAFT polymerization, we have successfully synthesized a series of PMMA-*b*-PtBS-*b*-P2VP and PtBA-*b*-PtBS-*b*-P2VP triblock copolymers as shown in Scheme 1. Targeted molecular weights were achieved to yield PMMA-*b*-PtBS-*b*-P2VP and PtBA-*b*-PtBS-*b*-P2VP linear triblock copolymers with varying volume fraction of P2VP. The homopolymers at each step were removed using different solvent mixtures to remove the homopolymer contamination and were characterized for their compositions using THF GPC and ^{1}H NMR. The GPC data for the corresponding PMMA-*b*-PtBS and PtBA-*b*-PtBS diblock copolymers confirmed the synthesis of well-defined block copolymers whereas the GPC data for the triblock could not be recorded due to interaction of the P2VP block with the GPC column using THF GPC. However, single peak in the DMF GPC confirms the formation of respective triblock copolymers with narrow molecular weight distribution and dispersity. The NMR data for the triblock copolymers was also used to characterize the synthesized triblock copolymers and calculate the corresponding volume fractions of the three blocks. A representative ^{1}H NMR for PMMA-*b*-PtBS-*b*-P2VP and PtBA-*b*-PtBS-*b*-P2VP triblock copolymers is shown in Figure 1. For PMMA-*b*-PtBS-*b*-P2VP, peaks corresponding to the aryl protons of t-BS (6.00 – 7.25 ppm) and the PMMA –OCH3 protons (3.61 ppm) can be used to determine the molar ratio of these two blocks and peaks at δ 8.5−8.0 ppm (1H from 2-VP) and 7.25−6.0 ppm (3H from 2VP, 4H from t-BS), 2.5−1.0 ppm (3H from 2VP, 12H from t-BS) can be used to calculate the overall volume fraction of each individual block. Similarly, for PtBA-*b*-PtBS-*b*-P2VP, chemical shifts at 2.3 ppm (1H-CH backbone) and around 1.1 ppm (12H-CH3 t-Butyl) protons and the aryl protons of t-BS (6.00 – 7.25 ppm) were used to calculate

the mole fraction of these two blocks and peaks at δ 8.5−8.0 ppm (1H from 2-VP) and 7.25−6.0 ppm (3H from 2VP, 4H from t-BS) were used to calculate the overall volume fraction of the three blocks.

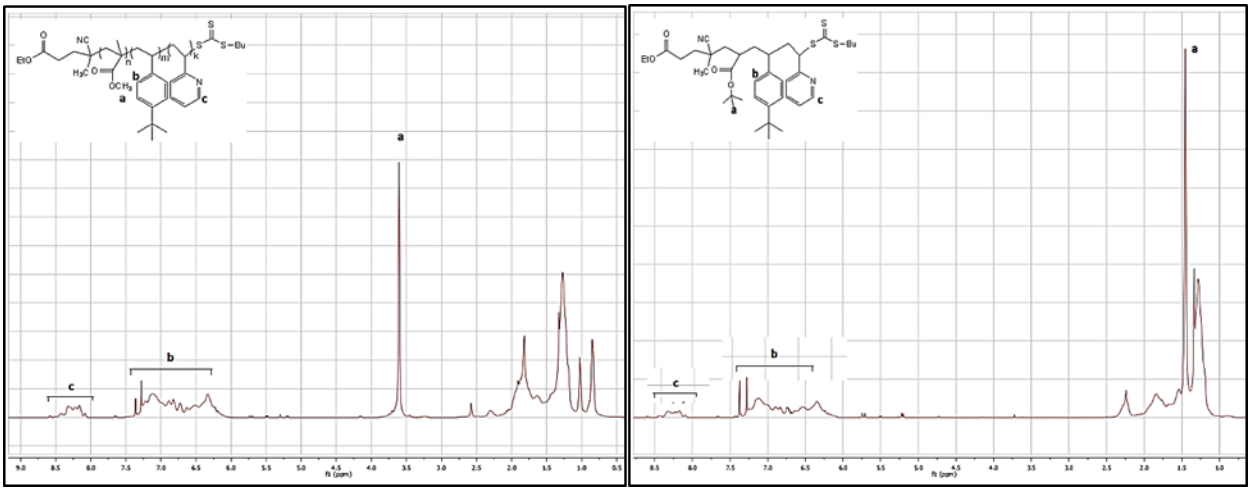

Figure 4. 1: ^{1}H NMR spectra for the synthesized PMMA-*b*-PtBS-*b*-P2VP and PtBA-*b*-PtBS-*b*-P2VP triblock copolymers.

4.4.2 Morphological Characterization

The PMMA-*b*-PtBS-*b*-P2VP and PtBA-*b*-PtBS-*b*-P2VP linear triblock copolymers were characterized for their phase behavior using SAXS and TEM. These techniques helped in providing better understanding their self-assembly behavior and investigate the effect of increase in the P2VP volume fraction on the morphology of these triblock copolymers.

4.4.2.1 Small Angle X-ray Scattering (SAXS) Measurements

The SAXS data for the synthesized PMMA-*b*-PtBS-*b*-P2VP triblock copolymers is shown in Figure 2. These patterns correspond to the PMMA-*b*-PtBS-*b*-P2VP triblock copolymers synthesized from PMMA-*b*-PtBS-3 and 6 diblock copolymers with different volume fractions of the P2VP arm. Interesting SAXS behavior was observed for the PMMA-*b*-PtBS-*b*-P2VP-1-3,

synthesized using PMMA-*b*-PtBS-3 diblock copolymer (9 kg/mol-6 kg/mol) with varying volume fraction of the P2VP from 0.4-0.6. PMMA-*b*-PtBS-3 showed a single peak in SAXS which was indicative of absence of long range lattice order for the diblock copolymer. On introducing the P2VP block, the *d*-spacing increases from 11.2 nm to 13.1 and highly ordered lamellae morphology was observed for the PMMA-*b*-PtBS-*b*-P2VP-1 corresponding to the peak ratio q_*: q_1 : q_2 = 1:2:3. On further increasing the volume fraction of P2VP φ_{P2VP} = 0.52 and 0.65, highly ordered lamellae morphology was observed for both PMMA-*b*-PtBS-*b*-P2VP-2 and 3 with corresponding *d*-spacing increasing to 27.4 and 32.7 nm respectively. The primary peak (q_*) for observed in SAXS for these samples had much lower intensity than the 2nd order peak (q_1) observed, which is contrary to the observed data for block copolymers. This might be due to presence of structure-in-structure morphologies for these triblock copolymers. The PMMA-*b*-PtBS-6 diblock copolymer showed no phase separation as indicated by absence of primary peak in SAXS, which changed to a microphase separated morphology on addition of the P2VP arm. For PMMA-*b*-PtBS-*b*-P2VP-4 with $\varphi = 0.38$, a single peak suggesting microphase separation but lack of long range lattice order was observed. Increasing the volume fraction of P2VP to 0.46 and 0.57, highly ordered cylindrical morphology were observed. The *d*-spacing was noted to change from 11.6 nm for φ_{P2VP} = 0.38 and increases to 22.2 and 23.7 nm for φ_{P2VP} = 0.46 and 0.52 respectively.

The scattering data corresponding to the PtBA-*b*-PtBS-*b*-P2VP triblock copolymers is shown in Figure 3. The triblock copolymers synthesized using PtBA-*b*-PtBS-1 (4.4 kg/mol-3.9 kg/mol) diblock copolymer showed the presence of primary peak (q_*) corresponding to the *d*-spacing varying from 9.8 nm for the diblock copolymer to 13.7 nm for the triblock copolymer with highest volume fraction of P2VP. The SAXS profiles for the triblock copolymers synthesized using PtBA-

b-PtBS-1 showed the presence of single peak indicating the microphase separation but absence of long range order for these samples. The SAXS profiles for the high molecular weight triblock copolymers synthesized using PtBA-*b*-PtBS-2 (15kg/mol -15Kg/mol) displayed highly ordered morphologies in contrast to the poorly ordered morphologies observed for triblock copolymers synthesized using PtBA-*b*-PtBS-1. The *d*-spacing was found to significantly decrease from 23.1 nm to 11.8 nm with addition of the P2VP arm to the diblock copolymer. This may be due to the formation of the hair pin loop by the middle arm to facilitate the mixing of the end blocks as their χ being the lowest. The *d*-spacing increases with increase in the volume fraction of P2VP, with corresponding lamellae *d*-spacing values of 22.2 nm to 23.7 nm for φ_{P2VP} = 0.45 and 0.52 respectively.

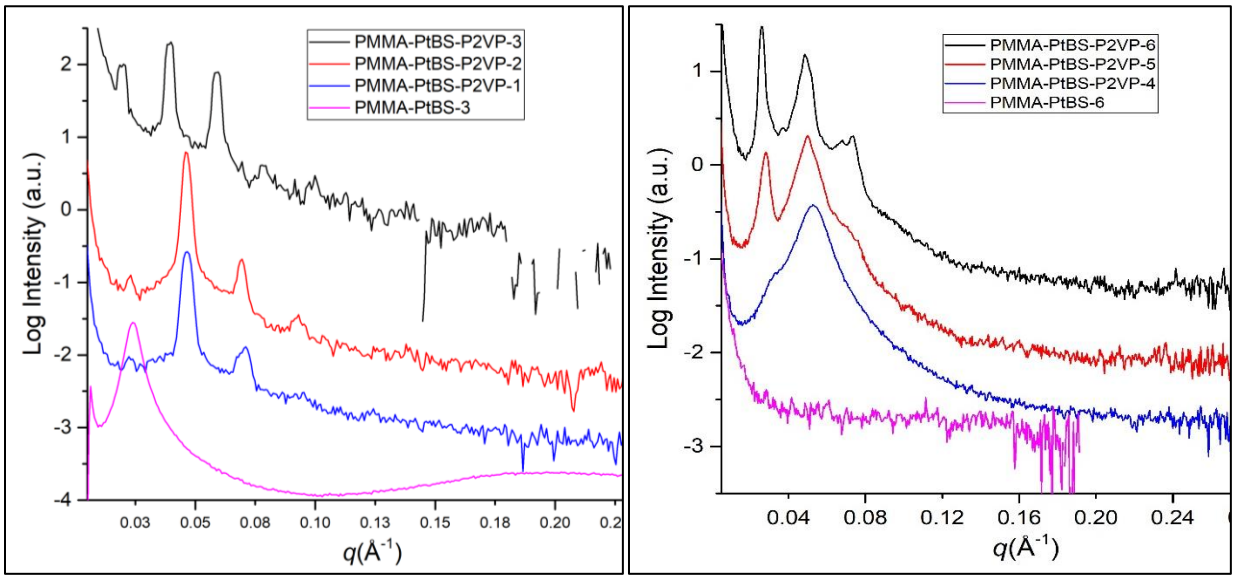

Figure 4. 2: SAXS profiles for PMMA-*b*-PtBS-*b*-P2VP triblock copolymers.

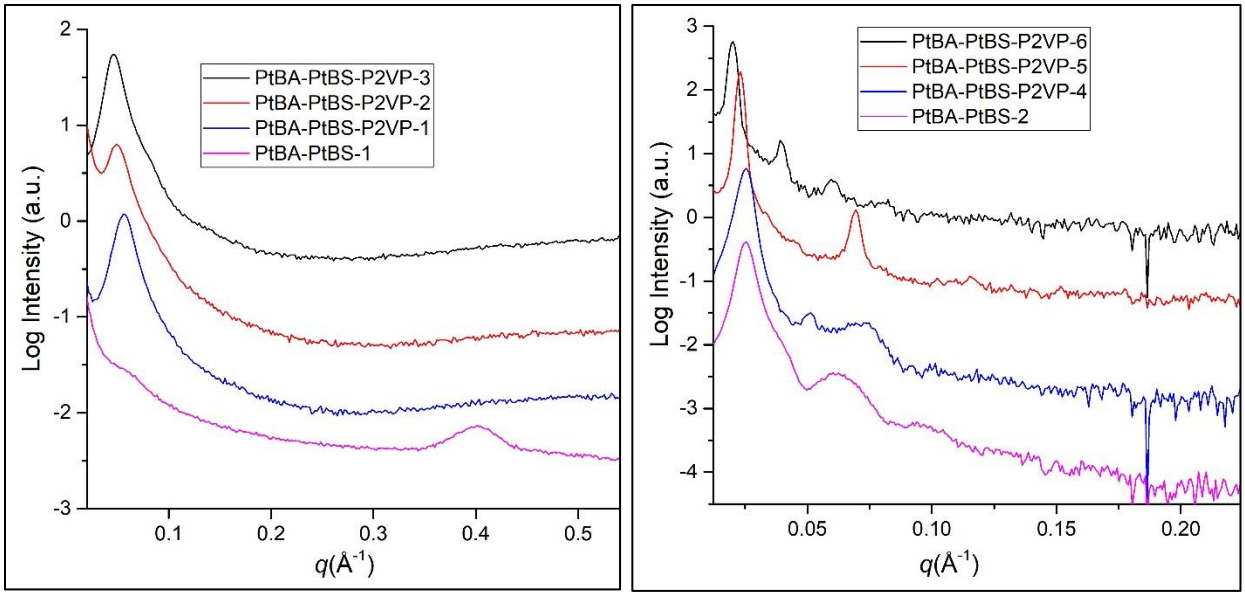

Figure 4. 3: SAXS patterns for PtBA-*b*-PtBS-*b*-P2VP triblock copolymers.

4.4.2.2 TEM studies

The PMMA-*b*-PtBS-*b*-P2VP and PtBA-*b*-PtBS-*b*-P2VP linear triblock copolymers were also characterized by TEM using OsO_4 and I_2 staining. The use of OsO_4 specifically stains the PtBS and the P2VP and PMMA or PtBA are unstained while the use of I_2 specifically stains the P2VP block and the PtBS and PMMA or PtBA remain unstained. Figures 4 shows the TEM micrographs for PMMA-*b*-PtBS-*b*-P2VP-1-6 which were stained using OsO_4. The TEM images observed PMMA-*b*-PtBS-*b*-P2VP-1-3 after OsO_4 staining shows the presence of lamellae morphology with the corresponding *d*-spacing in qualitative agreement with the SAXS data. The dark stained PtBS comprises one of the lamellae domains while the P2VP and PMMA forms the other domain. To better understand the morphology of these triblock copolymers, the samples were stained using I_2 vapors (Figure 5). The TEM micrographs obtained after I_2 staining confirms the formation of lamella morphology by these triblock copolymers which the dark P2VP forming one domain and PtBS and PMMA forming the other. Similarly, for PMMA-*b*-PtBS-*b*-P2VP- 4-6 with OsO_4

staining highly ordered lamellae morphology was observed with the PtBS as the dark domain and the PMMA and P2VP forms the lighter domain.

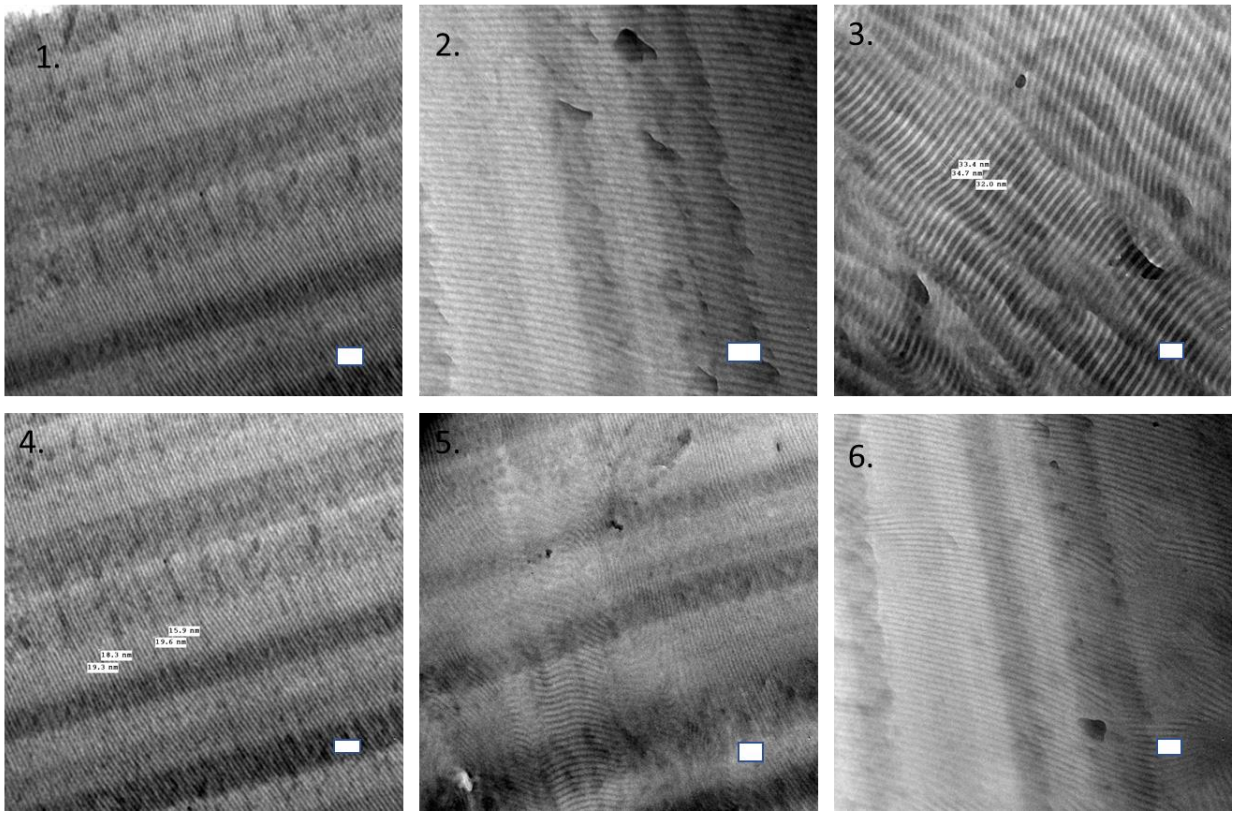

Figure 4. 4: TEM images for PMMA-b-PtBS-b-P2VP-1-6 triblock copolymers stained using OsO4.

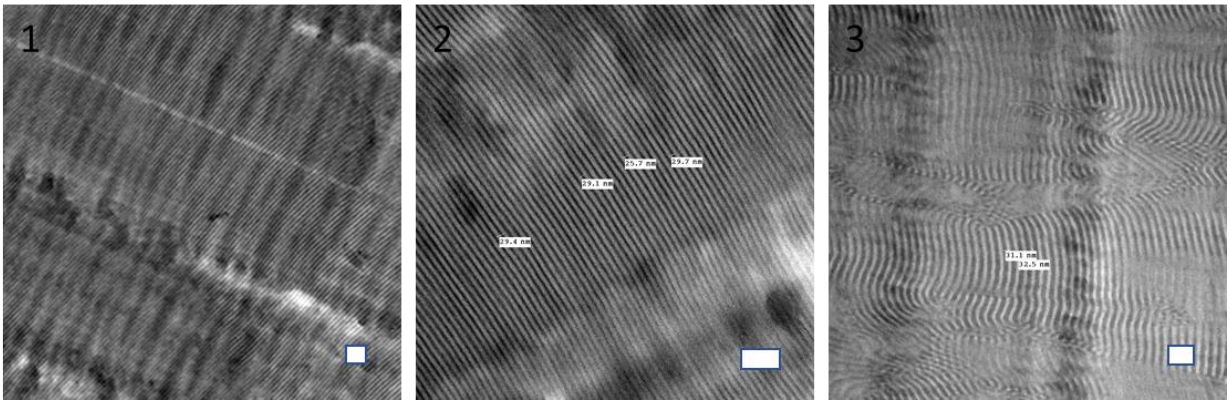

Figure 4. 5: TEM images for PMMA-b-PtBS-b-P2VP-1-3 triblock copolymers stained using I2 vapors.

PtBA-*b*-PtBS-*b*-P2VP-1-3 samples stained using OSO_4 showed the presence of poorly ordered cylindrical morphology in accordance to the absence of higher order reflections in the SAXS data (Figure 6) with PtBS as the dark cylindrical domain with the P2VP and PMMA as the matrix. For PtBA-*b*-PtBS-*b*-P2VP-4-6 highly ordered lamellae morphologies were observed with PtBS as the dark domain and P2VP and PMMA as the other domain of the lamellae. Also, the *d*-spacing for these morphologies were found to be in good agreement with the SAXS data obtained for these samples.

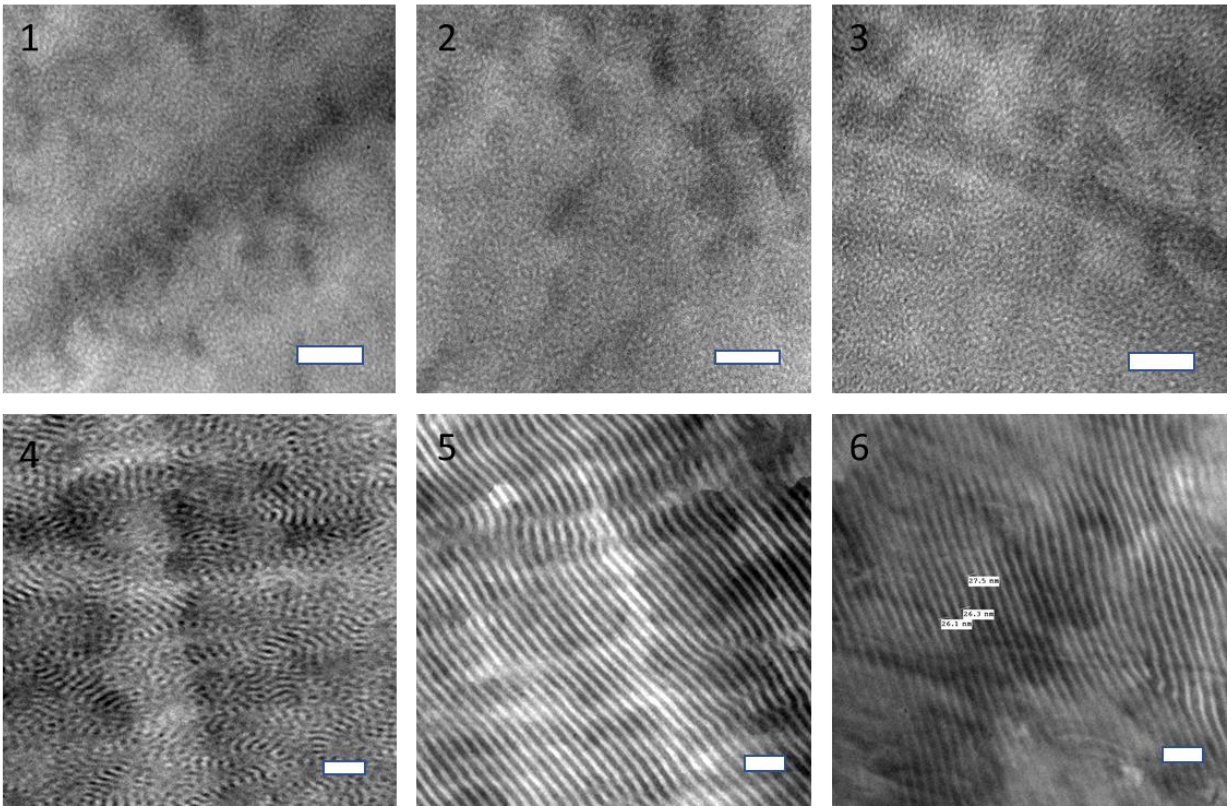

Figure 4. 6: TEM images for PtBA-*b*-PtBS-*b*-P2VP triblock copolymers stained using OsO_4.

4.5 Summary

we have successfully synthesized a series of PMMA-*b*-PtBS-*b*-P2VP and PtBA-*b*-PtBS-*b*-P2VP triblock copolymers with varying volume fraction of the P2VP arm. The PMMA-*b*-PtBS-*b*-P2VP

particularly showed highly ordered lamellae and cylindrical morphologies with *d*-spacing <15 nm for majority of the samples. On comparing the PMMA-*b*-PtBS-*b*-P2VP and PtBA-*b*-PtBS-*b*-P2VP triblock copolymers, microphase separation could be achieved with much lower *N* value for the PtBA series as compared to the PMMA series. This shows that PtBA-*b*-PtBS has a higher χ value as compared to the corresponding PMMA-*b*-PtBS diblock copolymers due to the hydrophobicity of the tert-butyl groups present in the PtBA block. Therefore, the PtBA-*b*-PtBS-*b*-P2VP triblock copolymers have a good potential to be a new high $\boldsymbol{\chi}$ – low $\boldsymbol{N}$ polymer with the capability to form morphologies with sub 10 nm *d*-spacing. However, further characterization of these samples is required to better understand their phase behavior and morphologies of these triblock copolymers. It will be exciting to explore new higher $\boldsymbol{\chi}$ – low $\boldsymbol{N}$ pair of block copolymers based on the current study and extend this study to non-frustrated system of triblock copolymers. This comparative study will provide a better understanding of the role of topological frustration in determining the self-assembly behavior of these triblock copolymers. Also, correlating the observed morphologies with theoretical predictions will help in predicting the phase diagram for these triblock copolymers and can provide a qualitative understanding of their microphase separation.

4.6 References

(1) Zheng, W.; Wang, Z. G. *Macromolecules* **1995**, *28* (21), 7215–7223.

(2) Liu, M.; Li, W.; Qiu, F.; Shi, A. C. *Macromolecules* **2012**, *45* (23), 9522–9530.

(3) Huckstadt, H.; Gopfert, A.; Abetz, V. *Polymer (Guildf).* **2000**, *41* (26), 9089–9094.

(4) Gido, S. P.; Schwark, D. W.; Thomas, E. L.; do Carmo Gonçalves, M. *Macromolecules* **1993**, *26* (10), 2636–2640.

(5) Matsushita, Y.; Tamura, M.; Noda, I. *Macromolecules* **1994**, *27* (13), 3680–3682.

(6) Mogi, Y.; Mori, K.; Matsushita, Y.; Noda, I. *Macromolecules* **1992**, *25*, 5412.

(7) Radlauer, M. R.; Sinturel, C.; Asai, Y.; Arora, A.; Bates, F. S.; Dorfman, K. D.; Hillmyer, M. A. *Macromolecules* **2017**, *50* (1), 446–458.

(8) Bailey, T. S.; Pham, H. D.; Bates, F. S. *Macromolecules* **2001**, *34* (20), 6994–7008.

(9) Bailey, T. S.; Hardy, C. M.; Epps, T. H.; Bates, F. S. *Macromolecules* **2002**, *35* (18), 7007–7017.

(10) Mogi, Y.; Nomura, M.; Kotsuji, H.; Ohnishi, K.; Matsushita, Y.; Noda, I. *Macromolecules* **1994**, *27* (23), 6755–6760.

(11) Stadler, R.; Auschra, C.; Beckmann, J.; Krappe, U.; Voigt-Martin, I.; Leibler, L. *Macromolecules* **1995**, *28*, 3080–3091.

(12) Breiner, U.; Krappe, U.; Stadler, R. *Macromol. Rapid Commun.* **1996**, *17* (8), 567–575.

(13) Balsamo, V.; von Gyldenfeldt, F.; Stadler, R. *Macromolecules* **1999**, *32* (4), 1226–1232.

(14) Krappe, U.; Stadler, R.; Voigt-Martin, I. *Macromolecules* **1995**, *28*, 4558–4561.

(15) Tang, P.; Qiu, F.; Zhang, H.; Yang, Y. *J. Phys. Chem. B* **2004**, *108* (24), 8434–8438.

(16) Guo, Z.; Zhang, G.; Qiu, F.; Zhang, H.; Yang, Y.; Shi, A. C. *Phys. Rev. Lett.* **2008**, *101* (2), 1–4.

(17) Qin, J.; Bates, F. S.; Morse, D. C. *Macromolecules* **2010**, *43* (11), 5128–5136.

(18) Nagpal, U.; Detcheverry, F. a.; Nealey, P. F.; De Pablo, J. J. *Macromolecules* **2011**, *44* (13), 5490–5497.

(19) Kim, H. C.; Park, S. M.; Hinsberg, W. D.; Division, I. R. *Chem. Rev.* **2010**, *110* (1), 146–

177.

(20) Olson, D. A.; Chen, L.; Hillmyer, M. A. *Chem. Mater.* **2008**, *20* (3), 869–890.

(21) Sinturel, C.; Bates, F. S.; Hillmyer, M. A. *ACS Macro Lett.* **2015**, *4* (9), 1044–1050.

(22) Kennemur, J. G.; Yao, L.; Bates, F. S.; Hillmyer, M. A. *Macromolecules* **2014**, *47* (4), 1411–1418.

(23) Jeong, G.; Yu, D. M.; Mapas, J. K. D.; Sun, Z.; Rzayev, J.; Russell, T. P. *Macromolecules* **2017**, *50* (18), 7148–7154.

(24) Yu, D. M.; Mapas, J. K. D.; Kim, H.; Choi, J.; Ribbe, A. E.; Rzayev, J.; Russell, T. P. *Macromolecules* **2018**, *51* (3), 1031–1040.

(25) Shi, W.; Tateishi, Y.; Li, W.; Hawker, C. J.; Fredrickson, G. H.; Kramer, E. J. *ACS Macro Lett.* **2015**, *4* (11), 1287–1292.

(26) Otsuka, I.; Zhang, Y.; Isono, T.; Rochas, C.; Kakuchi, T.; Satoh, T.; Borsali, R. *Macromolecules* **2015**, *48* (5), 1509–1517.

(27) Sweat, D. P.; Kim, M.; Larson, S. R.; Choi, J. W.; Choo, Y.; Osuji, C. O.; Gopalan, P. *Macromolecules* **2014**, *47* (19), 6687–6696.

(28) Kennemur, J. G.; Hillmyer, M. a; Bates, F. S. *Macromolecules* **2012**, *45* (17), 7228–7236.

(29) Ellison, C. J.; Mundra, M. K.; Torkelson, J. M. *Macromolecules* **2005**, *38* (5), 1767–1778.

CHAPTER V

CONCLUSIONS AND PERSPECTIVES

5.1 Conclusions

With increasing use of block copolymers for variety of applications, there is a strong need to reinvent the molecular design of modern day block copolymers which can fulfill the growing demand for specialty polymers. The design of these block copolymers needs to be more careful with the increasing focus on biocompatibility and sustainability. This increasing demand of specialized block copolymers have drawn attention towards synthesis of block copolymers with complex architectures which are shown to be promising candidates to alter the macroscopic and microscopic properties of block copolymers. Effectively several combinations of molecular architecture, (a)symmetry and connectivity among the different blocks can be envisioned, therefore an efficient synthetic strategy needs to be developed in conjugation with theory and simulations to design next generation block copolymers with targeted application. In this thesis, have successfully developed synthetic strategies to synthesize polymers with complex molecular architectures which can motivate theoretical simulations studies to design polymers which can allow us to access novel morphologies which are inaccessible by the conventional diblock copolymers.

In chapter 2, we have successfully developed the concept of single molecule insertion (SMI) which allows the insertion of functional molecules at precise location within the polymer backbone to provide functionalities for post polymer modifications and synthetize polymer architectures which are relatively difficult to synthesize using pre-existing synthetic strategies. We have investigated a series of molecules such as the maleic anhydrides, maleimides, dimethyl fumarate, dimethyl

maleate etc. which satisfy the criteria for SMI based on their reactivity ratios with styrene and methyl methacrylate, which can be used to synthesize almost all the complex macromolecular architectures such as the star, comb, graft, and dendritic polymers which were first synthesized by anionic polymerization and appropriate linking chemistries. The concept of SMI also allows us to insert structure-directing moieties (e.g., hydrogen bonding, charged) which the polymer backbone which can manipulate the self-assembly behavior of block copolymers.

In chapter 3, A versatile synthetic strategy has been designed to synthesize a series of PMMA-*b*-PS-*g*-PEO and PtBA-*b*-PS-*g*-PEO block copolymers with complex architectures which lie which lie along the continuum of a 3-arm star and A-B-C linear triblock copolymer. The synthetic methodology includes the synthesis of block copolymer using controlled polymerization technique such as RAFT polymerization, followed by a single molecule insertion (SMI) of a pentafluoro maleimide ester (PFPMI) molecule within the PS backbone. Activated ester chemistry employed allows for quantitative grafting of the PEO arm and systematically move the PEO arm on the PS chain from a 3-arm star architecture to A-B-C linear triblock copolymer. Experimental characterization of the morphologies of the synthesized graft copolymer was done using SAXS and TEM while dissipative particle dynamics was used to theoretically predict the self-assembly behavior of the synthetized copolymers. The study helps us understand the effect of the variations in molecular architecture on the macromolecular self-assembly which can be further exploited to produce highly ordered morphologies which can find their use in a variety of applications.

We have developed a robust synthetic strategy to synthesize these continuum graft copolymers using living polymerization methodology such as RAFT, ATRP and utilizing the unique SMI technique described in chapter 2. The morphological characterization of the synthesized continuum graft copolymers is performed using SAXS, TEM, and DPD simulations. Interesting

morphologies are observed for these continuum copolymers and projects them as interesting candidates to access new morphologies. Contrary to most of the work done on block copolymers, these structures are novel as their morphologies can be tuned keeping the φ and χ constant. This study helps in understanding of the effect of polymer architecture on the phase behavior of these graft copolymers and provides a novel pathway to tune the block copolymer morphologies.

In chapter 4, we have synthesized a series of novel PMMA-*b*-PtBS-*b*-P2VP and PtBA-*b*-PtBS-*b*-P2VP triblock copolymers with extending P2VP arm. These triblock copolymers are a class of frustrated linear triblock copolymers with high-χ monomer pairs which is responsible for driving phase separation in these copolymers and very low molecular weight (N) for these copolymers. The morphologies of the synthesized triblock copolymers were characterized using SAXS and TEM and morphologies with multiple domains and smaller feature size were observed. The effect of extending chain length of P2VP arm on the phase diagram on these highly frustrated triblock copolymer systems was studied and the observed morphologies using SAXS and TEM were mapped with the theoretical predictions. The study helps in extending the concept of high χ-low N block copolymer system from diblock to triblock copolymers which can be used to access novel morphologies with smaller domain spacings which can be specifically used in lithographic applications.

5.2 Future Directions

As discussed in the previous sections, with numerous advances in the field of polymer synthesis, characterization and computational theory, block copolymers have emerged as the potential materials for variety of applications which include lithographic applications, nano templates, adhesives etc. With these emerging technologies, there is a strong demand for polymers which can meet the extreme performance requirements. Polymer architecture exerts significantly impacts the

microphase behavior and accompanying physical and mechanical properties of polymer.[1] As discussed by Bates and co-workers there are numerous ways in which the three blocks can be arranged to give various architectures as shown in Figure 2, Chapter 1. Among these various architectures significant number of experimental and theoretical studies have been done on the 3-arm star and A-B-C linear triblock copolymer architectures. As described in Figure 1, there is unique opportunity to explore the continuum of architectures which lie in between the 3-arm star and linear triblock copolymer. Depending on the movement of a specific block, three different continuums are accessible on moving from the 3-arm star (center point) to either of the A-B-C, B-C-A, and C-A-B linear triblock (vertices). Also, each continuum can be accessed by two different pathways which have the same two ends -points.

In the current study, we had only been able to explore one of the 6 different pathways possible to move from a 3-arm star to the linear triblock copolymer architecture. Therefore, there is a unique opportunity from both the experimental and theoretical aspects to explore this ternary diagram.

The current work focuses on PMMA-*b*-PS-*g*-PEO and PtBA-*b*-PS-*g*-PEO graft copolymers which have relatively low-χ between the terminal blocks. This leads to poor microphase separation and leads to mixed domain morphologies. These mixed domain morphologies can be particularly advantageous in ion transport applications. However, exploring high-χ systems such as described in chapter 4 can be advantageous in exploring novel morphologies. Such high-χ systems with PtBS, P2VP, P4VP, PDMS and PLA blocks etc. can lead to better phase separation between the blocks and can further enhance the topological frustration leading to unexpected morphologies.

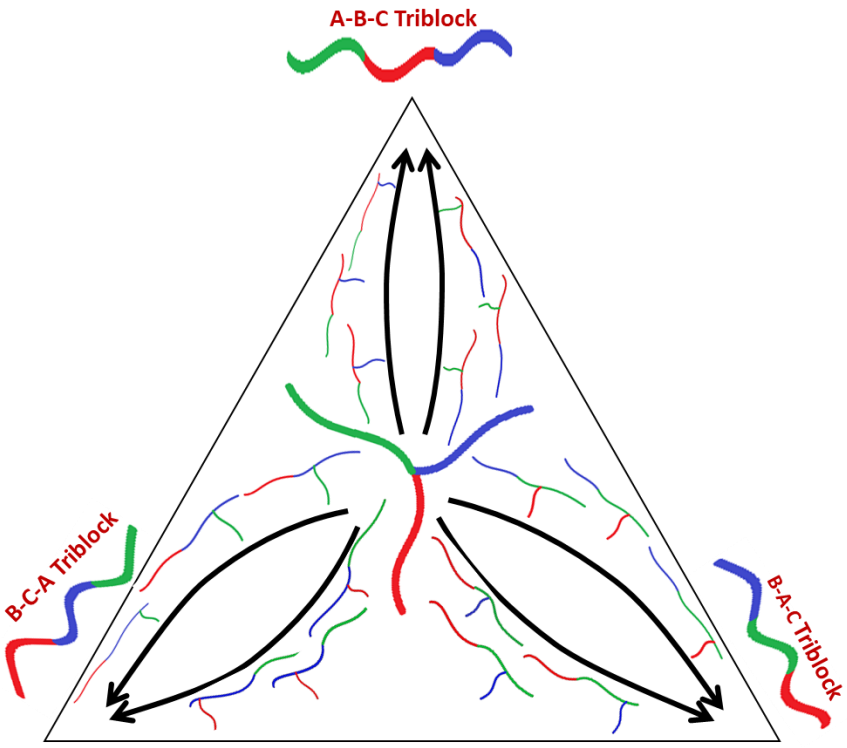

Figure 5. 1: Ternary diagram depicting the possible continuum routes from a 3-arm star to linear triblock copolymer.

Also, synthesis of such high-χ systems would require coming up with new chemistries which would enable us to obtain these multiblock copolymers. The synthesis needs to be inspired by the current work on which a theoretical model has been developed. This theoretical model can now be used to challenge the community to explore possible combinations of monomers which would enable us to synthesize polymers to achieve novel morphologies for targeted applications. The theoretical predictions would also inspire the community to come up with novel molecules which can be inserted once within polymer backbone and would provide access to other architectures in the continuum. Some of the efforts made in this direction includes exploring molecules which would specifically insert once with the PMMA backbone, which would now allow us to explore the alternate path to move from the 3-arm star to A-B-C linear triblock copolymer. This study

would help us understand how the different block combinations can affect the microphase separations for these continuum block copolymers.

So far, multiblock copolymers synthesis and characterization has been focused on flexible block polymers. Incorporating other types of polymer blocks such as semiflexible, helical, and stiff can help in synthesizing hybrid materials which can self-assemble in the bulk state for their use in technological applications, such as light-emitting diodes (LEDs),[2] organic photovoltaic devices,[3] and ion conducting membranes.[4] It will also be interesting to explore the properties or morphological behavior of these continuum copolymers by introducing charge in one the blocks or by incorporating chemical functionalities capable of hydrogen-bonding using SMI. Also, the unique non-favorable interactions between the neighboring blocks for these continuum graft copolymers can be further explored by studying their solution behavior which can allow us to access novel morphologies in solutions too.

5.3 References:

(1) Bates, C. M.; Bates, F. S. *Macromolecules* **2017**, *50* (1), 3–22.

(2) Lu, S.; Liu, T.; Ke, L.; Ma, D. G.; Chua, S. J.; Huang, W. *Macromolecules* **2005**, *38* (20), 8494–8502.

(3) Topham, P. D.; Parnell, A. J.; Hiorns, R. C. *J. Polym. Sci. Part B Polym. Phys.* **2011**, *49* (16), 1131–1156.

(4) Kreuer, K.-D. *Chem. Mater.* **2013**, *26* (1), 361–380.

APPENDIX

SYNTHESIS OF LABELED POLYMERS

A1. Synthesis of PEO-b-P4VP diblock copolymer

Synthesis of PEO macro-RAFT Chain Transfer Agent (CTA-1c)

The synthesis of RAFT CTA-1a was performed following a reported procedure.[1] CTA-1a was modified to PEO macro-CTA using dicyclohexylcarbodimide-4-N,N dimethaminopyridine (DCC-DMAP) coupling reaction. In a round bottom flask, CTA-1a (3 equiv.), DCC (1.2 equiv.) and poly ethylene glycol mono methyl ether (mPEG) (1 equiv.) were added to appropriate amount of dichloromethane (DCM) and allowed to stir for 15 mins at 0 ^{o}C. After 15 mins, DMAP was added and the solution was stirred at room temperature for 2 days (Scheme 1). The product obtained was kept overnight in the refrigerator at -30 ^{o}C to precipitate the dicyclohexylurea (DCU) generated during the reaction. The product was then filtered, and the filtrate was concentrated and precipitated using diethyl ether to yield pale yellow powder.

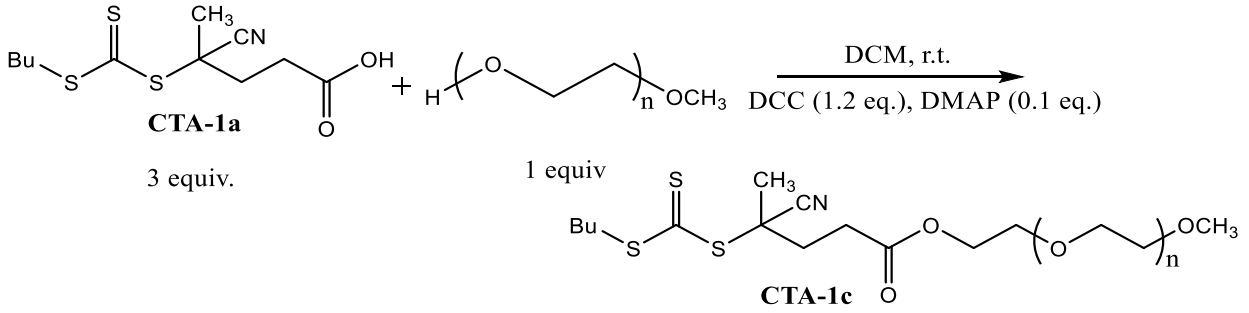

Scheme 1: DCC-DMAP coupling reaction for attachment of CTA-1a to mPEG.

General Procedure for Polymerization of 4-VP using CTA-1c

4-Vinyl pyridine (20 mL, 0.18 mol) was added to a 20mL reaction vial containing CTA-1c and AIBN as the initiator in appropriate quantities based on the targeted molecular weight (Table 1). The polymerization was performed using molar ratio of AIBN/CTA as 1:20. The mixture was degassed using N_2 and then heated at 60 °C for different time intervals to achieve the required conversion. On completion, the reaction was quenched in an ice bath, diluted with ethyl acetate, and precipitated in cold diethyl ether. The precipitated polymer was filtered and dried overnight under vacuum to yield PEO-*b*-P4VP diblock copolymer as a white powder.

Table A1. 1: Molecular characteristics of PS-*b*-P4VP diblock copolymers.

Sample ID	**PS (Kg/mol)**	**P2VP (Kg/mol)**	**M_n (Kg/mol)**
PEO-P4VP-4	4.4	4.4	7.2
PEO-P4VP-2	8	8	15
PEO-P4VP-3	16	16	29.2

Synthesis of PS-*b*-P2VP-*g*-PEO star triblock copolymers

The synthesis of PS-*b*-P2VP-*g*-PEO graft copolymers were synthesized using similar RAFT polymerization and SMI technique as described in Chapter 2 and 3. Firstly, the polymerization of styrene was performed using CTA-1b followed by single molecule insertion of the PFPMI molecule. After SMI, chain extension was performed using 2-VP monomer to yield PS-*b*-P2VP diblock copolymer with PFPMI as the junction point. Utilizing the activated ester chemistry, amine terminated PEO was used to graft the PEO chain to the PS-*b*-P2VP diblock copolymer to yield PS-b-P2VP-b-PEO diblock copolymer (Table 2).

Following the similar procedure, similar compositions of deuterated PS (d-PS)-*b*-P2VP-*g*-PEO and PS-*b*-P2VP-*g*-*d* PEO miktoarm star copolymers were also synthesized.

General Procedure for Synthesis of PS macroinitiator

In a 20-mL reaction vial, freshly distilled styrene, AIBN, and CTA-1b in 1,4 dioxane were added. Different molar ratio of styrene**:** CTA-1b were taken based on the targeted molecular weights and the AIBN: CTA-1b ratio of 1:20 was kept constant. The reaction mixture and was degassed using N_2, followed by polymerization at 60 °C for different time intervals to achieve the desired conversion. After completion, the reaction mixture was quenched in an ice bath, diluted with ethyl acetate and then precipitated in methanol. The precipitated polymer was filtered and dried overnight under vacuum to give PS as a white powder.

General Procedure for Single Molecule Insertion (SMI) of Pentafluorophenyl Maleimide (PFPMI)

In a 20-mL reaction vial, PS macroinitiator (1 equiv.) dissolved with appropriate amount of 1,4 dioxane was added. PFPMI (3 equiv.) and AIBN (0.1 equiv.) were added. The reaction vial was sealed and degassed using N_2 and immersed in a preheated oil bath heated at 60 °C for 3 days to ensure completion insertion of the PFPMI molecule on the PS chain-end. The reaction mixture was diluted using ethyl acetate and precipitated in methanol. The precipitated polymer was filtered and dried under vacuum for 24 h to obtain PS-PFPMI as a white solid.

General procedure for synthesis of PS-PFPMI-*b*-P2VP diblock copolymer

In a 20-mL reaction vial, PS-PFPMI macroinitiator, freshly distilled 2-VP and AIBN dissolved in 1, 4 dioxane were added. The amount of styrene and AIBN was calculated based on the molar ratio of 2-VP: macro-CTA and AIBN:macro-CTA (20:1) respectively. The reaction vial was sealed and the polymerization was performed at 60 °C for a specific time interval to achieve the targeted conversion. The reaction mixture was diluted using ethyl acetate upon completion and precipitated in hexanes three times. The precipitated polymer was then filtered and dried under vacuum to yield PS-PFPMI-*b*-P2VP as a white solid.

General Procedure for Grafting of Amine-Terminated PEO on PS-PFPMI-*b*-P2VP, diblock copolymer

The synthesized diblock copolymer PS-PFPMI-*b*-P2VP was dissolved in chloroform in a 20-mL reaction vial and amine-terminated PEO (1.1 equiv.) was added. NEt_3 (0.1 equiv.) was added and the vial was sealed and placed in a preheated oil bath at 60 °C for 3 days. On completion, the reaction mixture was diluted with ethyl acetate, precipitated in cold diethyl ether, and dried under vacuum for 24 h. To remove the excess PEO, the dried polymer was washed with water to yield PS-*b*-P2VP-*g*-PEO star copolymer architectures (Table 2).

Table A1. 2: Molecular characteristics for PS-*b*-P2VP-*g*-PEO miktoarm star copolymers.

Sample ID	PS (Kg/mol)	P2VP (Kg/mol)	PEO (Kg/mol)	M_n (Kg/mol)
PS-P2VP-PEO-1	4.4	4.4	4.4	11.3
PS-P2VP-PEO-2	8	8	8	22.7
PS-P2VP-PEO-3	16	16	16	45.2

A2. Synthesis of End-Labelled Polymers:

A2.1 Synthesis of α-Fe, ω-Br end-labeled polymers

Synthesis of Ferrocene-ATRP initiator (FeBr-ATRP)

Ferrocene methanol (5 g, 23 mmol, 1.0 equiv) and triethylamine (16 mL, 115 mmol, 5.0 equiv) were dissolved in 100 mL of dry dichloromethane (DCM) in a round bottomed flask under N_2 atmosphere. This flask was immersed in an ice bath for 15 min, and then α-bromoisobutyryl bromide (5.7 ml, 46 mmol, 2 equiv) was slowly added dropwise to the stirred solution over 30 mins. After stirring for 24 h at room temperature, the reaction mixture was filtered to remove the triethylamine hydrobromide by-product. The filtrate was washed with a saturated solution of sodium hydrogen carbonate (100 mL) three times followed by washing three times with deionized

water (100 mL). The purified organic solution was dried using anhydrous $MgSO_4$ and DCM was removed under reduced pressure. The crude reddish-yellow product was then purified by column chromatography using silica gel as the stationary phase and hexane-Ethyl acetate solvent mixture (9:1) as eluent (Scheme 2). The desired product FeBr-ATRP was obtained in 70% yield and was stored in the refrigerator prior to use. The representative NMR is shown in Figure 1, the chemical shifts 4-4.4 ppm correspond to the cyclopentadienyl ring protons from the ferrocene unit, while the signals at the chemical shift 4.9 ppm corresponds to the methylene proton of the ATRP agent. The protons at 1.8 ppm correspond to the $-CH_3$ protons at for the ATRP agent.

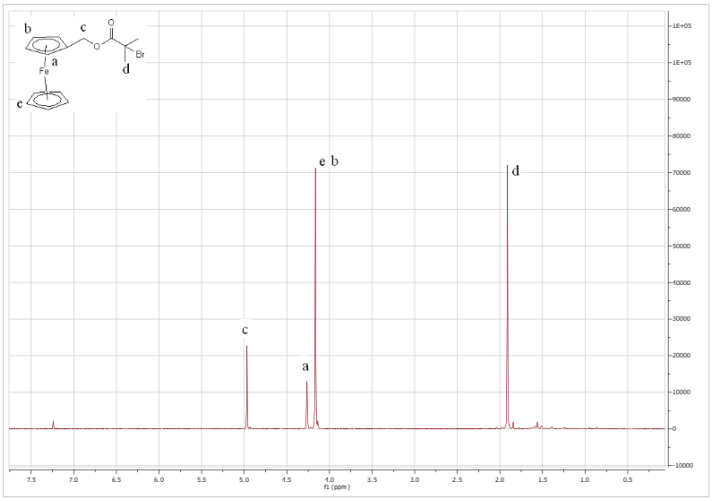

Figure A2.1.1: ^1H NMR spectra for FeBr-ATRP initiator.

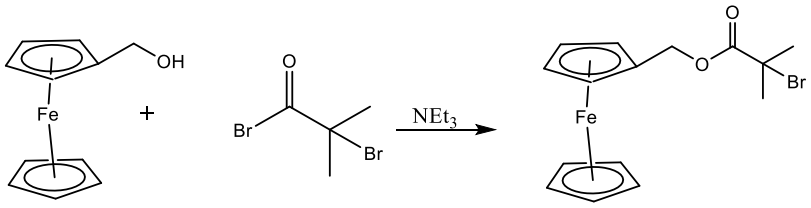

Scheme 2: Synthesis of FeBr-ATRP initiator.

Polymerization of Styrene and MMA using FeBr-ATRP initiator

The polymerization of styrene and MMA was carried out using FeOH-ATRP initiator as shown in Scheme 3. Styrene (10 mL, 9 mmol) was added to a 20-mL reaction vial containing appropriate amount of toluene as the solvent. FeBr-ATRP initiator based on the targeted MW, CuBr (1 equiv. of the initiator) and N,N,N′,N″,N″-Pentamethyldiethylenetriamine (PMDETA) (1 equiv. of CuBr) were to the vial. The mixture was degassed using N_2 and then heated at 90 °C for different time intervals to achieve the required conversion which was monitored using ^{1}H NMR. On completion, the reaction was quenched in an ice bath, diluted with ethyl acetate, and passed through a basic alumina column to remove the copper from the solution. The filtrate was concentrates and precipitated in methanol three times to yield polystyrene macroinitiator as a white powder.

Similarly, the synthesis of PMMA macroinitiator was performed using FeBr-ATRP initiator.

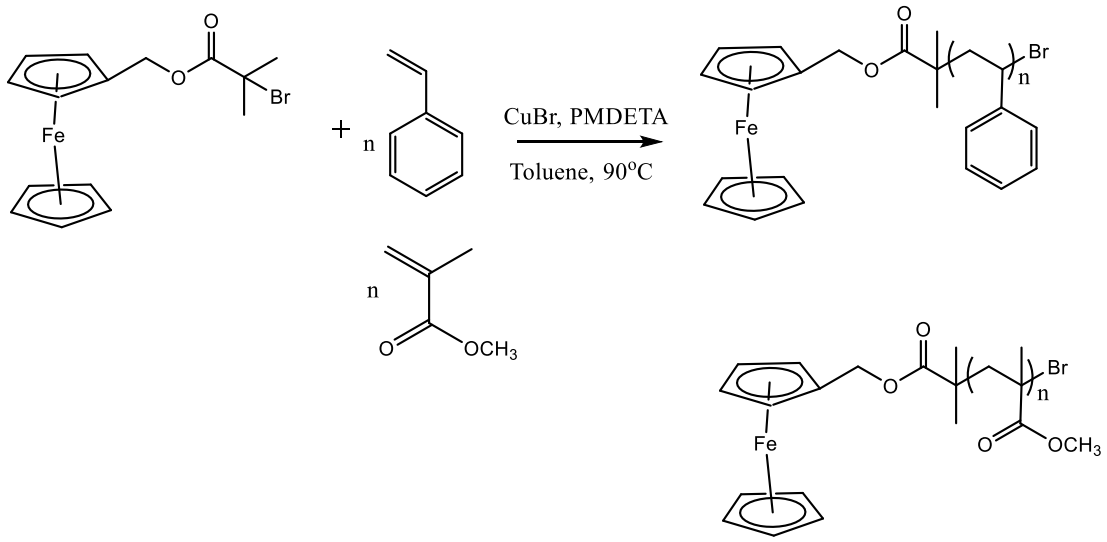

Scheme 3: Synthesis of end-labeled PS and PMMA homopolymer using FeBr-ATRP initiator.

Synthesis of Fe and Br end-labeled PS-*b*-PMMA diblock copolymer

The synthesis of end-labeled PS-*b*-PMMA diblock copolymer with the α and ω chain-ends labelled with ferrocene and bromine respectively. The synthesis was performed using ATRP living polymerization with the synthesized FeBr-ATRP as the initiator (Scheme 4).

General Procedure for synthesis of α-Fe, ω-Br end-labeled PS-*b*-PMMA diblock copolymer

The chain extension with styrene was performed using the synthesized PMMA-FeBr macro initiator for ATRP. In a 20-mL reaction vial, freshly distilled styrene and PMMA-FeBr based on the targeted molecular weight in appropriate amount of toluene were added CuBr (1 equiv. of PMMA-ATRP initiator) and PMDETA (1equiv. of CuBr) were and the reaction mixture was degassed using N_2 for 15 min, followed by polymerization at 90 °C for different time intervals to achieve the desired conversion. After completion, the reaction mixture was quenched in an ice bath, diluted with ethyl acetate and passed through a basic alumina column to remove the copper from the solution. The filtrate was concentrates and precipitated in methanol three times to yield end labeled PMMA-*b*-PS diblock copolymer as a white powder (Table 3).

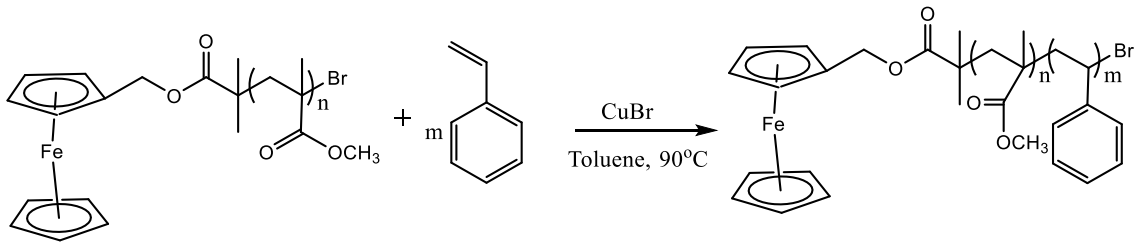

Scheme 4: Synthesis of end-labeled PMMA-*b*-PS homopolymer using FeBr-ATRP initiator.

The end-labeled PMMA-*b*-PS diblock copolymer characterization was performed using 1H-NMR and THF GPC. The peaks corresponding to signals at δ 3.6 ppm corresponds to the methylene proton of the ethyl ester of PMMA and signals between δ values 6-8 ppm corresponds to the aromatic proton of styrene were observed. The peak ratios were used to calculate the individual

volume fraction of the two blocks. The representative GPC traces for end-labeled PMMA-*b*-PS diblock copolymer is shown in (Figure 2) successful chain extension for majority of the PMMA chains with the presence of a small low MW shoulder indicating the presence of PS homopolymer. This may be due to the some of the dead chains introduced either during the polymerization or prior for the PMMA macroinitiator.

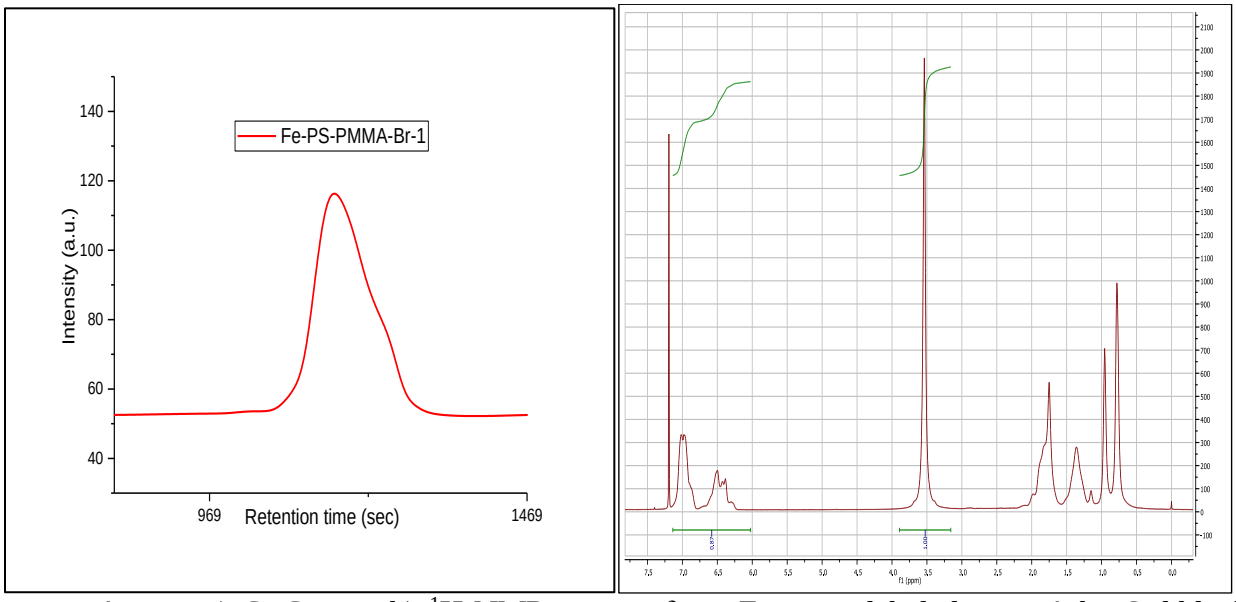

Figure A2.1.2: a) GPC trace b) ^{1}H NMR spectra for α-Fe, ω-Br labeled PMMA-b-PS diblock copolymer.

The synthesis of non-labeled PMMA-b-PS diblock copolymer was performed using CTA-1b (Chapter 2). The molecular characteristics for the synthesized polymers is described in Table 4.

Table A2.1.1: Molecular characteristics for end-labelled PS, PMMA homopolymers and PMMA-*b*-PS diblock copolymers.

S.No.	Name	M.W (Kg/mol)	Đ	Notebook entry	Mole fraction
1	Fe-PS-Br-1	27.1	1.06	N2-FeOH-PS-Br-2	
2	Fe-PS-Br-2	54	1.14	N2-FeOH-PS-Br-3	
3	Fe-PMMA-Br-1	30.5	1.11	N2-Fe-PMMA-Br-4	
4	Fe-PMMA-Br-2	47.5	1.14	N2-Fe-PMMA-Br-6	
5	Fe-PS-PMMA-1	89.2	1.19	N2-Fe-PS-PMMA-3	36:64

Table A2.1.2: Molecular characteristics for non-labelled PS, PMMA homopolymers and PMMA-*b*-PS diblock copolymers

S.No.	Name	M.W (Kg/mol)	Đ	Notebook entry	Mole fraction
1	PS-RAFT-1	27.4	1.09	N2-PS-RAFT-1	
2	PS-RAFT-2	52	1.08	N2-PS-RAFT-3	
3	PMMA-RA-1	30.5	1.1	N1-PMMA-RA-10	
4	PMMA-RA-2	42.6	1.15	N1-PMMA-RA-26	
5	PMMA-RA-PS-1	72	1.14	N1-PMMA-RA-PS-34	38:62

A2.2 Synthesis of α-5Br, ω-3S End Labeled polymers

Synthesis of 5-Br-3S RAFT agent

The synthesis of RAFT CTA-1a was performed following a reported procedure.[1] CTA-1a was modified to 5-Br-3S RAFT agent using dicyclohexylcarbodimide-4-N,N dimethaminopyridine (DCC-DMAP) coupling reaction. In a round bottom flask, CTA-1a (3 equiv.), DCC (1.2 equiv.) and 2,3,4,5,6- pentabromobenzyl alcohol (1 equiv.) were added to appropriate amount of dichloromethane (DCM) and allowed to stir for 15 mins at 0 ^{o}C. After 15 mins, DMAP was added and the solution was stirred at room temperature for 2 days (Scheme 4). The product obtained was kept overnight in the refrigerator at -30 ^{o}C to precipitate the dicyclohexylurea (DCU) generated during the reaction. The filtrate was concentrated was then purified by column chromatography using silica gel as the stationary phase and hexane-Ethyl acetate solvent mixture (7:3) as eluent to give yellow liquid as the product. 1-H NMR for the synthesized product is shown in figure 3.

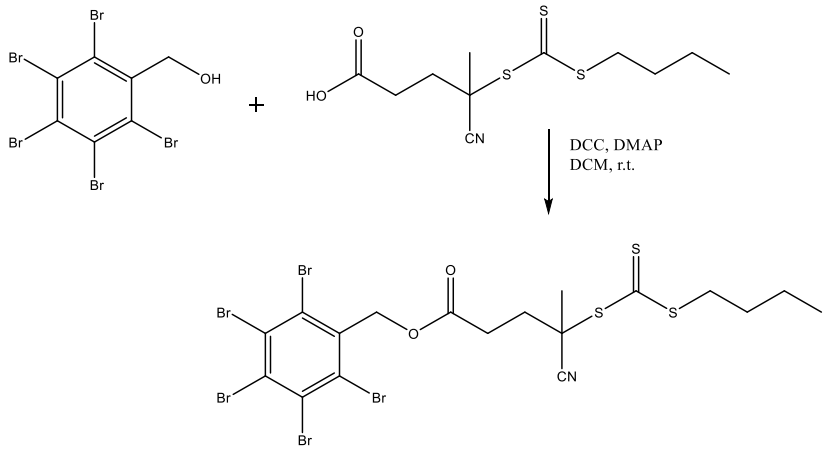

Scheme 5: Synthesis of 5-Br-3S RAFT agent.

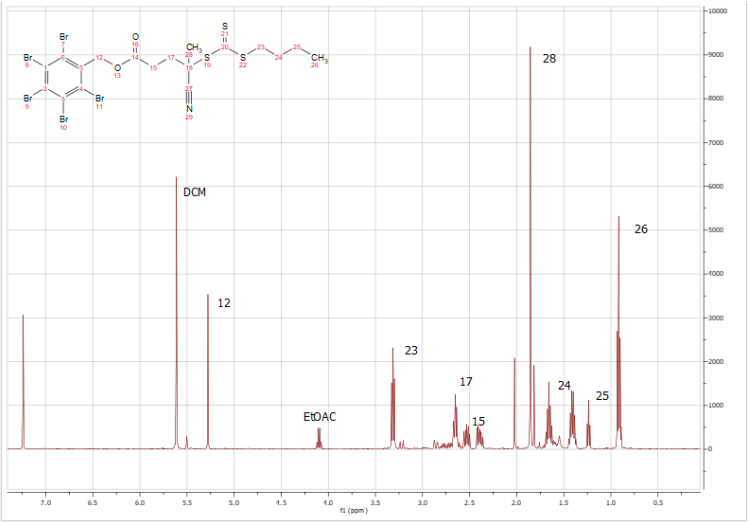

Figure 2.2.1: ^{1}H-NMR for the synthesized 5-Br-3S RAFT agent.

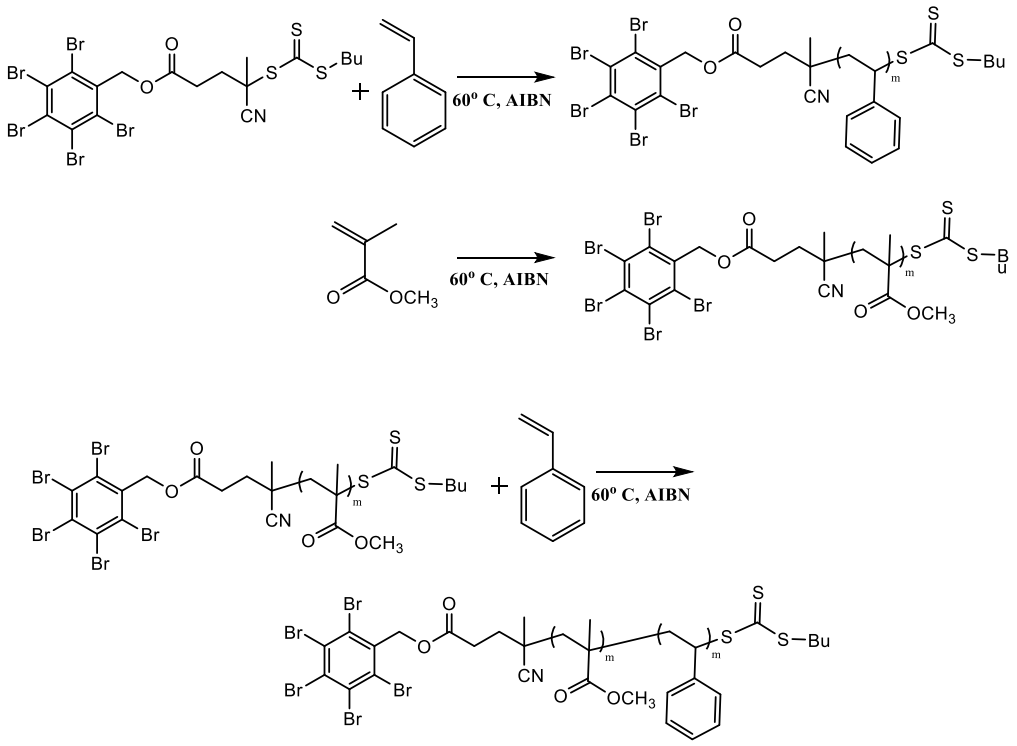

Scheme 6: Synthesis of 5-Br, 3-S labeled PS, PMMA and PMMA-*b*-PS diblock copolymers.

Synthesis of 5-Br, 3-S labeled PS, PMMA and PMMA-*b*-PS diblock copolymers

General Procedure for synthesis of 5-Br, 3-S labeled PS and PMMA homopolymers

In a 20-mL reaction vial, freshly distilled styrene, AIBN, and the synthesized 5-Br, 3-S RAFT CTA in 1,4 dioxane were added (Scheme 6). Different molar ratio of styrene**:**CTA-1b were taken based on the targeted molecular weights and the AIBN:CTA ratio of 1:20 was kept constant. The reaction mixture and was degassed using N_2, followed by polymerization at 60 °C for different time intervals to achieve the desired conversion. After completion, the reaction mixture was quenched in an ice bath, diluted with ethyl acetate and then precipitated in methanol. The precipitated polymer was filtered and dried overnight under vacuum to give PS as a white powder (Table 5). Following the similar procedure, the end-labeled PMMA homopolymer was synthesized.

General procedure for synthesis of 5-Br, 3-S labeled PMMA-*b*-PS diblock copolymer

In a 20-mL reaction vial, PMMA macroinitiator, freshly distilled styrene and AIBN dissolved in 1, 4 dioxane were added (Scheme 6). The amount of styrene and AIBN was calculated based on the molar ratio of styrene:macro-CTA and AIBN:macro-CTA (20:1) respectively. The reaction vial was sealed and the polymerization was performed at 60 °C for a specific time interval to achieve the targeted conversion. The reaction mixture was diluted using ethyl acetate upon completion and precipitated in methanol three times. The precipitated polymer was then filtered and dried under vacuum to yield 5-Br, 3-S labeled PMMA-*b*-PS diblock copolymer as a white solid.

Table 2.2.1: Molecular characteristics of synthesized 5-Br, 3-S labeled PS, PMMA homopolymers and PMMA-*b*-PS diblock copolymers.

S.No.	Name	M.W (Kg/mol) GPC	Đ	Mole fraction
1	Br_5-PS-S_3-1	26.5	1.08	
2	Br_5-PS-S_3-2	54	1.1	
3	Br_5-P4VP-S_3-1	28.5	1.17	
4	Br_5-P4VP-S_3-2	47	1.2	
5	Br_5-PS-b-P4VP-S_3-1	49	1.14	55:45
6	Br_5-PS-b-P4VP-S_3-1	110.7	1.15	50:50

References

(1) Moad, G.; Chong, Y. K.; Postma, A.; Rizzardo, E.; Thang, S. H. **2005**, *46*, 8458–8468.

BIBLIOGRAPHY

1. Jackson, E. A.; Hillmyer, M. A. ACS Nano 2010, 4 (7), 3548–3553.
2. Meng, F.; Zhong, Z.; Feijen, J. Biomacromolecules 2009, 10 (2), 197–209.
3. Kang, Y.; Walish, J. J.; Gorishnyy, T.; Thomas, E. L. Nat. Mater. 2007, 6 (12), 957–960.
4. Segalman, R. A. Mater. Sci. Eng. R Reports 2005, 48 (6), 191–226.
5. Orilall, M. C.; Wiesner, U. Chem. Soc. Rev. 2011, 40 (2), 520–535.
6. Bates, F. S.; Fredrickson, G. H.; Hucul, D.; Hahn, S. F. AIChE J. 2001, 47 (4), 762–765.
7. Matsen, M. J. Phys. Condens. Matter 2002, 14 (2), 21–47.
8. Bates, F. S.; Fredrickson, G. H. Phys. Today 1999, 52 (2), 32–38.
9. Bates, F. S.; Fredrickson, G. H. Annu. Rev. Phys. Chem. 1990, 41 (1), 525–557.
10. Ciach, a.; Pękalski, J.; Góźdź, W. T. Soft Matter 2013, 9 (27), 6301.
11. Cochran, E. W.; Garcia-Cervera, C. J.; Fredrickson, G. H. Macromolecules 2006, 39 (7), 2449–2451.
12. Matsen, M. W. Eur. Phys. J. E 2009, 30 (4), 361–369.
13. Borsali, R.; Pecora, R. Soft Matter Characterization; 2008.
14. Leibler, L. Macromolecules 1980, 13 (10), 1602–1617.
15. Matsen, M.; Bates, F. Macromolecules 1996, 29 (23), 7641–7644.
16. Tsui, O. K. C. Polymer Thin Films; 2008.
17. Park, S.; Kim, B.; Xu, J.; Hofmann, T.; Ocko, B. M.; Russell, T. P. Macromolecules 2009, 42 (4), 1278–1284.
18. Mansky, P.; Liu, Y.; Huang, E.; Russell, T. P.; Hawker, C. J. Science 1997, 275 (5305), 1458–1460.
19. Morkved, T. L.; Lu, M.; Urbas, a. M.; Ehrichs, E. E.; Jaeger, H. M.; Mansky, P.; Russell, T. P. Science (80-.). 1996, 273 (5277), 931–933.
20. Angelescu, D. E.; Waller, J. H.; Adamson, D. H.; Deshpande, P.; Chou, S. Y.; Register, R. A.; Chaikin, P. M. Adv. Mater. 2004, 16 (19), 1736–1740.

21. Berry, B. C.; Bosse, A. W.; Douglas, J. F.; Jones, R. L.; Karim, A. Nano Lett. 2007, 7 (9), 2789–2794.

22. Park, S.; Lee, D. H.; Xu, J.; Kim, B.; Hong, S. W.; Jeong, U.; Xu, T.; Russell, T. P. Science 2009, 323 (February), 1030–1033.

23. Hong, S. W.; Gu, X.; Huh, J.; Xiao, S.; Russell, T. P. ACS Nano 2011, 5 (4), 2855–2860.

24. Bita, I.; Yang, J. K. W.; Jung, Y. S.; Ross, C. a.; Thomas, E. L.; Berggren, K. K. Science (80-.). 2008, 321 (August), 939–943.

25. Kim, S. O.; Solak, H. H.; Stoykovich, M. P.; Ferrier, N. J.; De Pablo, J. J.; Nealey, P. F. Nature 2003, 424 (6947), 411–414.

26. Xu, J.; Park, S.; Wang, S.; Russell, T. P.; Ocko, B. M.; Checco, A. Adv. Mater. 2010, 22 (20), 2268–2272.

27. Hermel, T. J.; Hahn, S. F.; Chaffin, K. A.; Gerberich, W. W.; Bates, F. S. Macromolecules 2003, 36 (7), 2190–2193.

28. Christodoulou, S.; Driva, P.; Iatrou, H.; Hadjichristidis, N. Macromolecules 2008, 41 (7), 2607–2615.

29. Bates, F. S.; Hillmyer, M. a.; Lodge, T. P.; Bates, C. M.; Delaney, K. T.; Fredrickson, G. H. Science (80-.). 2012, 336 (6080), 434–440.

30. Meuler, A. J.; Hillmyer, M. a.; Bates, F. S. Macromolecules 2009, 42 (19), 7221–7250.

31. Dair, B. J.; Honeker, C. C.; Alward, D. B.; Avgeropoulos, A.; Hadjichristidis, N.; Fetters, L. J.; Capel, M.; Thomas, E. L. Macromolecules 1999, 32 (24), 8145–8152.

32. Dair, B. J.; Avgeropoulos, A.; Hadjichristidis, N.; Thomas, E. L. J. Mater. Sci. 2000, 35 (20), 5207–5213.

33. Yang, X.; Loos, J. Macromolecules 2007, 40 (5), 1353–1362.

34. Crossland, E. J. W.; Kamperman, M.; Nedelcu, M.; Ducati, C.; Wiesner, U.; Smilgies, D. M.; Toombes, G. E. S.; Hillmyer, M. A.; Ludwigs, S.; Steiner, U.; Snaith, H. J. Nano Lett. 2009, 9 (8), 2807–2812.

35. Crossland, E. J. W.; Nedelcu, M.; Ducati, C.; Ludwigs, S.; Hillmyer, M. A.; Steiner, U.; Snaith, H. J. Nano Lett. 2009, 9 (8), 2813–2819.

36. Oey, C. C.; Djurišić, a B.; Wang, H.; Man, K. K. Y.; Chan, W. K.; Xie, M. H.; Leung, Y. H.; Pandey, a; Nunzi, J.-M.; Chui, P. C. Nanotechnology 2006, 17 (3), 706–713.

37. Wang, H.; Oey, C. C.; Djurišić, A. B.; Xie, M. H.; Leung, Y. H.; Man, K. K. Y.; Chan, W. K.; Pandey, A.; Nunzi, J.-M.; Chui, P. C. Appl. Phys. Lett. 2005, 87 (2), 023507.

38. Shefelbine, T. A.; Vigild, M. E.; Matsen, M. W.; Hajduk, D. A.; Hillmyer, M. A.; Cussler, E. L.; Bates, F. S. J. Am. Chem. Soc. 1999, 121 (37), 8457–8465.

39. Yang, S. Y.; Ryu, I.; Kim, H. Y.; Kim, J. K.; Jang, S. K.; Russell, T. P. Adv. Mater. 2006, 18 (6), 709–712.

40. Phillip, W. A.; Rzayev, J.; Hillmyer, M. A.; Cussler, E. L. J. Memb. Sci. 2006, 286 (1–2), 144–152.

41. Phillip, W. A.; Amendt, M.; ONeill, B.; Chen, L.; Hillmyer, M. A.; Cussler, E. L. ACS Appl. Mater. Interfaces 2009, 1 (2), 472–480.

42. Cho, B.K.; Jain, A.; Gruner, S. M.; Wiesner, U. Science (80-.). 2004, 305 (5690), 1598–1601.

43. Lin, S. Y.; Fleming, J. G.; Hetherington, D. L.; Smith, B. K.; Biswas, R.; Ho, K. M.; Sigalas, M. M.; Zubrzycki, W.; Kurtz, S. R.; Bur, J. Nature 1998, 394 (6690), 251–253.

44. Maldovan, M.; Thomas, E. L.; Article, P.; Maldovan, M.; Thomas, E. L. Nat. Mater. 2004, 3 (9), 593–600.

45. Zheng, W.; Wang, Z. G. Macromolecules 1995, 28 (21), 7215–7223.

46. Ungar, G.; Tschierske, C.; Abetz, V.; Holyst, R.; Bates, M. A.; Liu, F.; Prehm, M.; Kieffer, R.; Zeng, X.; Walker, M.; Glettner, B.; Zywocinski, A. Adv. Funct. Mater. 2011, 21 (7), 1296–1323.

47. Lecommandoux, S.; Borsali, R.; Schappacher, M.; Deffieux, A.; Narayanan, T.; Rochas, C. Macromolecules 2004, 37 (5), 1843–1848.

48. Liu, M.; Li, W.; Qiu, F.; Shi, A. C. Macromolecules 2012, 45 (23), 9522–9530.

49. Breiner, U.; Krappe, U.; Jakob, T.; Abetz, V.; Stadler, R. Polym. Bull. 1998, 40 (2–3), 219–226.

50. Breiner, U.; Krappe, U.; Abetz, V.; Stadler, R. Macromol. Chem. Phys. 1997, 198 (4), 1051–1083.

51. Breiner, U.; Krappe, U.; Stadler, R. Macromol. Rapid Commun. 1996, 17 (8), 567–575.

52. Krappe, U.; Stadler, R.; Voigt-Martin, I. Macromolecules 1995, 28, 4558–4561.

53. Stadler, R.; Auschra, C.; Beckmann, J.; Krappe, U.; Voigt-Martin, I.; Leibler, L. Macromolecules 1995, 28, 3080–3091.

54. Brinkmann, S.; Stadler, R.; Thomas, E. L. Macromolecules 1998, 31 (19), 6566–6572.

55. Jinnai, H.; Kaneko, T.; Matsunaga, K.; Abetz, C.; Abetz, V. Soft Matter 2009, 5 (10), 2042–2046.

56. Breiner, U.; Krappe, U.; Thomas, E. L.; Stadler, R. Macromolecules 1998, 31 (96), 135–141.

57. Auschra, C.; Stadler, R. Macromolecules 1993, 26 (9), 2171–2174.

58. Ott, H.; Abetz, V.; Altstädt, V. Macromolecules 2001, 34, 2121.

59. Elbs, H.; Abetz, V.; Hadziioannou, G.; Drummer, C.; Krausch, G. Macromolecules 2001, 34 (23), 7917–7919.

60. Elbs, H.; Drummer, C.; Abetz, V.; Krausch, G. Macromolecules 2002, 35 (14), 5570–5577.

61. Park, C.; Yoon, J.; Thomas, E. L. Polymer (Guildf). 2003, 44 (22), 6725–6760.

62. Ludwigs, S.; Schmidt, K.; Stafford, C. M.; Amis, E. J.; Fasolka, M. J.; Karim, A.; Magerle, R.; Krausch, G. Macromolecules 2005, 38 (5), 1850–1858.

63. Balsamo, V.; von Gyldenfeldt, F.; Stadler, R. Macromolecules 1999, 32 (4), 1226–1232.

64. Bailey, T. S.; Pham, H. D.; Bates, F. S. Macromolecules 2001, 34 (20), 6994–7008.

65. Hückstädt, H.; Goldacker, T.; Göpfert, A.; Abetz, V. Macromolecules 2000, 33, 3757–3761.

66. Chernyy, S.; Kirkensgaard, J. J. K.; Mahalik, J. P.; Kim, H.; Arras, M. M. L.; Kumar, R.; Sumpter, B. G.; Smith, G. S.; Mortensen, K.; Russell, T. P.; Almdal, K. Macromolecules 2018, 51 (3), 1041–1051.

67. Kaneko, T.; Suda, K.; Satoh, K.; Kamigaito, M.; Kato, T.; Ono, T.; Nakamura, E.; Nishi, T.; Jinnai, H. Macromol. Symp. 2006, 242, 80–86.

68. Tang, P.; Qiu, F.; Zhang, H.; Yang, Y. Phys. Rev. E - Stat. Nonlinear, Soft Matter Phys. 2004, 69 (3 1), 1–8.

69. Guo, Z.; Zhang, G.; Qiu, F.; Zhang, H.; Yang, Y.; Shi, A. C. Phys. Rev. Lett. 2008, 101 (2), 1–4.

70. Nagpal, U.; Detcheverry, F. a.; Nealey, P. F.; De Pablo, J. J. Macromolecules 2011, 44 (13), 5490–5497.

71. Li, Weihua; Qui, Feng; Shi, A. C. Macromolecules 2011, 45, 503–509.

72. Huckstadt, H.; Gopfert, A.; Abetz, V. Polymer (Guildf). 2000, 41 (26), 9089–9094.

73. Abetz, V.; Goldacker, T. Macromol. Rapid Commun. 2000, 21 (1), 16–34.

74. Mogi, Y.; Mori, K.; Kotsuji, H.; Matsushita, Y.; Noda, I.; Han, C. C. Macromolecules 1993, 26 (19), 5169–5173.

75. Mogi, Y.; Nomura, M.; Kotsuji, H.; Ohnishi, K.; Matsushita, Y.; Noda, I. Macromolecules 1994, 27 (23), 6755–6760.

76. Matsushita, Y.; Suzuki, J.; Seki, M. Phys. B Condens. Matter 1998, 248 (1–4), 238–242.

77. Takano, A.; Kawashima, W.; Wada, S.; Hayashida, K.; Sato, S.; Kawahara, S.; Isono, Y.; Makihara, M.; Tanaka, N.; Kawaguchi, D.; Matsushita, Y. J. Polym. Sci. Part B Polym. Phys. 2007, 45 (16), 2277–2283.

78. Bailey, T. S.; Hardy, C. M.; Epps, T. H.; Bates, F. S. Macromolecules 2002, 35 (18), 7007–7017.

79. Epps, T. H.; Bailey, T. S.; Waletzko, R.; Bates, F. S. Macromolecules 2003, 36 (8), 2873–2881.

80. Chatterjee, J.; Jain, S.; Bates, F. S. Macromolecules 2007, 40 (8), 2882–2896.

81. Cochran, E. W.; Bates, F. S. Phys. Rev. Lett. 2004, 93 (8), 1–4.

82. Beckingham, B. S.; Register, R. A. Macromolecules 2013, 46 (9), 3486–3496.

83. Kumar, R.; Sides, S. W.; Goswami, M.; Sumpter, B. G.; Hong, K.; Wu, X.; Russell, T. P.; Gido, S. P.; Misichronis, K.; Rangou, S.; Avgeropoulos, A.; Tsoukatos, T.; Hadjichristidis, N.; Beyer, F. L.; Mays, J. W. Langmuir 2013, 29 (6), 1995–2006.

84. Ohta, T.; Kawasaki, K. Macromolecules 1986, 19 (10), 2621–2632.

85. Ohta, T.; Kawasaki, K. Macromolecules 1990, No. 5, 2413–2414.

86. Nakazawa, H.; Ohta, T. Macromolecules 1993, 26 (20), 5503–5511.

87. Phan, S.; Fredrickson, G. H. Macromolecules 1998, 31 (1), 59–63.

88. Matsen, M. W. J. Chem. Phys. 1998, 108 (1998), 785–796.

89. Xia, J.; Sun, M.; Qiu, F.; Zhang, H.; Yang, Y. Macromolecules 2005, 38 (22), 9324–9332.

90. Jiang, Y.; Yan, X.; Liang, H.; Shi, A. C. J. Phys. Chem. B 2005, 109 (44), 21047–21055.

91. Erukhimovich, I. Y. Eur. Phys. J. E 2005, 18 (4), 383–406.

92. Erukhimovich, I.; Abetz, V.; Stadler, R. Macromolecules 1997, 30 (24), 7435–7443.

93. Tyler, C. A.; Qin, J.; Bates, F. S.; Morse, D. C. Macromolecules 2007, 40 (13), 4654–4668.

94. Qin, J.; Bates, F. S.; Morse, D. C. Macromolecules 2010, 43 (11), 5128–5136.

95. Millett, P. C. Phys. Rev. E - Stat. Nonlinear, Soft Matter Phys. 2015, 92 (2), 1–9.

96. Park, J.; Jang, S.; Kim, J. K. J. Polym. Sci. Part B Polym. Phys. 2015, 53 (1), 1–21.

97. Iatridi, Z.; Tsitsilianis, C. Polymers (Basel). 2011, 3 (4), 1911–1933.

98. Milner, S. T. Macromolecules 1994, 27 (8), 2333–2335.

99. Floudas, G; Hadjichristidis, N.; Tselikas, T.; Erukhimovich, I. Macomolecules 1997, 30, 3090–3096.

100. Grason, G. M.; Kamien, R. D. Macromolecules 2004, 37 (19), 7371–7380.

101. Matsen, M. W. Macromolecules 2012, 45 (4), 2161–2165.

102. Huang, C. I.; Yu, H. T. Polymer (Guildf). 2007, 48 (15), 4537–4546.

103. Hayashida, K.; Dotera, T.; Takano, A.; Matsushita, Y. Phys. Rev. Lett. 2007, 98 (19), 1–4.

104. Bohbot-Raviv, Y.; Wang, Z. Phys. Rev. Lett. 2000, 85, 3428–3431.

105. Gemma, T.; Hatano, A.; Dotera, T. Macromolecules 2002, 35 (8), 3225–3237.

106. Ueda, K.; Dotera, T.; Gemma, T. Phys. Rev. B - Condens. Matter Mater. Phys. 2007, 75 (19), 1–11.

107. He, X.; Huang, L.; Liang, H.; Pan, C. J. Chem. Phys. 2003, 118 (21), 9861–9863.

108. Birshtein, T. M.; Polotsky, A. A.; Abetz, V. Macromol. Theory Simulations 2004, 13 (6), 512–519.

109. Tang, P.; Qiu, F.; Zhang, H.; Yang, Y. J. Phys. Chem. B 2004, 108 (24), 8434–8438.

110. Zhang, G.; Qiu, F.; Zhang, H.; Yang, Y.; Shi, A. C. Macromolecules 2010, 43 (6), 2981–2989.

111. Li, W.; Xu, Y.; Zhang, G.; Qiu, F.; Yang, Y.; Shi, A. C. J. Chem. Phys. 2010, 133 (6).

112. Fischer, M. G.; de Campo, L.; Kirkensgaard, J. J. K.; Hyde, S. T.; Schröder-Turk, G. E. Macromolecules 2014, 47 (21), 7424–7430.

113. Jiang, K.; Zhang, J.; Liang, Q. J. Phys. Chem. B 2015, 119 (45), 14551–14562.

114. Huang, C. I.; Fang, H. K.; Lin, C. H. Phys. Rev. E - Stat. Nonlinear, Soft Matter Phys. 2008, 77 (3), 2–9.

115. Hadjichristidis, N.; Iatrou, H.; Behal, S. K.; Chludzinski, J. J.; Disko, M. M.; Garner, R. T.; Liang, K. S.; Lohse, D. J.; Milner, S. T. Macromolecules 1993, 26 (21), 5812–5815.

116. Chrissopoulou, K.; Harville, S.; Anastasiadis, S. H.; Fytas, G.; Mays, J. W.; Hadjichristidis, N. J. Polym. Sci. Part B Polym. Phys. 1999, 37 (24), 3385–3391.

117. Tselikas, Y.; Iatrou, H.; Hadjichristidis, N.; Liang, K. S.; Mohanty, K.; Lohse, D. J. J. Chem. Phys. 1996, 105 (6), 2456.

118. Tselikas, Y.; Hadjichristidis, N.; Lescanec, R. L.; Honeker, C. C.; Wohlgemuth, M.; Thomas, E. L. Macromolecules 1996, 29 (10), 3390–3396.

119. Separation, M.; Block, I. N.; Of, T.; Architectures, N. M. 1997, 174, 167–174.

120. Yang, L.; Hong, S.; Gido, S. P.; Velis, G.; Hadjichristidis, N. Macromolecules 2001, 34 (26), 9069–9073.

121. Mavroudis, A.; Avgeropoulos, A.; Hadjichristidis, N.; Thomas, E. L.; Lohse, D. J. Chem. Mater. 2003, 15 (24), 1976–1983.

122. Isono, T.; Otsuka, I.; Kondo, Y.; Halila, S.; Fort, S.; Rochas, C.; Satoh, T.; Borsali, R.; Kakuchi, T. Macromolecules 2013, 46 (4), 1461–1469.

123. Isono, T.; Otsuka, I.; Suemasa, D.; Rochas, C.; Satoh, T.; Borsali, R.; Kakuchi, T. Macromolecules 2013, 46 (22), 8932–8940.

124. Pispas, S.; Avgeropoulos, A.; Hadjichristidis, N.; Roovers, J. J. Polym. Sci. Part B Polym. Phys. 1999, 37, 1329–1335.

125. Beyer, F. L.; Gido, S. P.; Poulos, Y.; Avgeropoulos, A.; Hadjichristidis, N. Macromolecules 1997, 30 (8), 2373–2376.

126. Turner, C. M.; Sheller, N. B.; Foster, M. D.; Lee, B.; Corona-Galvan, S.; Quirk, R. P.; Ann\'is, B.; Lin, J.-S. Macromolecules 1998, 31 (98), 4372–4375.

127. Beyer, F. L.; Gido, S. P.; Uhrig, D.; Mays, J. W.; Tan, N. B.; Trevino, S. F. J. Polym. Sci. Part B Polym. Phys. 1999, 37 (24), 3392–3400.

128. Rho, Y.; Kim, C.; Higashihara, T.; Jin, S.; Jung, J.; Shin, T. J.; Hirao, A.; Ree, M. ACS Macro Lett. 2013, 2 (10), 849–855.

129. Rho, Y.; Kim, C.; Higashihara, T.; Jin, S.; Jung, J.; Shin, T. J.; Hirao, A.; Ree, M. ACS Macro Lett. 2013, 2 (10), 849–855.

130. Okamoto, S.; Hasegawa, H.; Hashimoto, T.; Fujimoto, T.; Zhang, H.; Kazama, T.; Takano, A.; Isono, Y. Polymer (Guildf). 1997, 38 (21), 5275–5281.

131. Sioula, S.; Hadjichristidis, N.; Thomas, E. L. Macromolecules 1998, 31 (97), 5272–5277.

132. Yamauchi, K.; Takahashi, K.; Hasegawa, H.; Iatrou, H.; Hadjichristidis, N.; Kaneko, T.; Nishikawa, Y.; Jinnai, H.; Matsui, T.; Nishioka, H.; Shimizu, M.; Furukawa, H. Macromolecules 2003, 36 (19), 6962–6966.

133. Huckstadt, H.; Gopfert, A.; Abetz, V. Macromol. Chem. Phys. 2000, 201 (3), 296–307.

134. Takano, A.; Kawashima, W.; Noro, A.; Isono, Y.; Tanaka, N.; Dotera, T.; Matsushita, Y. J. Polym. Sci. Part B Polym. Phys. 2005, 43 (18), 2427–2432.

135. Takano, A.; Wada, S.; Sato, S.; Araki, T.; Hirahara, K.; Kazama, T.; Kawahara, S.; Isono, Y.; Ohno, A.; Tanaka, N.; Matsushita, Y. Macromolecules 2004, 37 (26), 9941–9946.

136. Hayashida, K.; Saito, N.; Arai, S.; Takano, A.; Tanaka, N.; Matsushita, Y. Macromolecules 2007, 40 (10), 3695–3699.

137. Matsushita, Y.; Hayashida, K.; Dotera, T.; Takano, A. J. Physics-Condensed Matter 2011, 23 (28), 284111.

138. Nunns, A.; Ross, C. a.; Manners, I. Macromolecules 2013, 46 (7), 2628–2635.

139. Li, Z.; Kesselman, E.; Talmon, Y.; Hillmyer, M.A.; Lodge, T. P. Science (80-.). 2004, 306 (5693), 98–101.

140. Lutz, J. *Angew. Chemie Int. Ed.* 2007, *46* (7), 1018–1025.

141. Fournier, D.; Hoogenboom, R.; Schubert, U. S. *Chem. Soc. Rev.* 2007, *36* (8), 1369.

142. Zhang, C.; Yang, Y.; He, J. *Macromolecules* 2013, *46* (10), 3985–3994.

143. Soeriyadi, A. H.; Boyer, C.; Nyström, F.; Zetterlund, P. B.; Whittaker, M. R. *J. Am. Chem. Soc.* 2011, *133* (29), 11128–11131.

144. Article, E.; Anastasaki, A.; Nikolaou, V.; Pappas, G. S.; Zhang, Q.; Wan, C.; Wilson, P.; Davis, T. P.; Whittaker, R.; Haddleton, D. M. *Chem. Sci.* 2014, *5*, 3536–3542.

145. Badi, N.; Lutz, J.-F. *Chem. Soc. Rev.* 2009, *38* (12), 3383–3390.

146. Lutz, J.-F.; Ouchi, M.; Liu, D. R.; Sawamoto, M. *Science (80-.).* 2013, *341* (6146), 1238149–1238149.

147. Merrifield, R. B. *J. Am. Chem. Soc.* 1963, *85* (14), 2149.

148. Mutlu, H.; Lutz, J. F. *Angew. Chemie - Int. Ed.* 2014, *53* (48), 13010–13019.

149. Lutz, J. F. *Acc. Chem. Res.* 2013, *46* (11), 2696–2705.

150. Colquhoun, H.; Lutz, J.-F. *Nat. Chem.* 2014, *6* (June), 455–456.

151. Chan-Seng, D.; Zamfir, M.; Lutz, J. F. *Angew. Chemie - Int. Ed.* 2012, *51* (49), 12254–12257.

152. Deng, X. X.; Li, L.; Li, Z. L.; Lv, A.; Du, F. S.; Li, Z. C. *ACS Macro Lett.* 2012, *1* (11), 1300–1303.

153. Trinh, T. T.; Oswald, L.; Chan-Seng, D.; Lutz, J. F. *Macromol. Rapid Commun.* 2014, *35* (2), 141–145.

154. Sun, J.; Zuckermann, R. N. *ACS Nano* 2013, *7* (6), 4715–4732.

155. Lutz, J. F. *ACS Macro Lett.* 2014, *3* (10), 1020–1023.

156. Rowan, S. J.; Barner-Kowollik, C.; Klumperman, B.; Gaspard, P.; Grubbs, R. B.; Hillmyer, M. A.; Hutchings, L. R.; Mahanthappa, M. K.; Moatsou, D.; O'Reilly, R. K.; Ouchi, M.; Sawamoto, M.; Lodge, T. P. *ACS Macro Lett.* 2016, *5* (1), 1–3.

157. Qu, C.; He, J. *Sci. China Chem.* 2015, *58* (11), 1651–1662.

158. Stayshich, R. M.; Weiss, R. M.; Li, J.; Meyer, T. Y. *Macromol. Rapid Commun.* 2011, *32* (2), 220–225.

159. Wong, E. H. H.; Stenzel, M. H.; Junkers, T.; Barner-Kowollik, C. *J. Polym. Sci. Part A Polym. Chem.* 2011, *49* (10), 2118–2126.

160. Hartmann, L.; B??rner, H. G. *Adv. Mater.* 2009, *21* (32–33), 3425–3431.

161. Norris, B. N.; Zhang, S.; Campbell, C. M.; Auletta, J. T.; Calvo-Marzal, P.; Hutchison, G. R.; Meyer, T. Y. *Macromolecules* 2013, *46* (4), 1384–1392.

162. Milnes, P. J.; McKee, M. L.; Bath, J.; Song, L.; Stulz, E.; Turberfield, A. J.; O'Reilly, R. K. *Chem. Commun.* 2012, *48* (45), 5614–5616.

163. Solleder, S. C.; Meier, M. A. R. *Angew. Chemie - Int. Ed.* 2014, *53* (3), 711–714.

164. Espeel, P.; Carrette, L. L. G.; Bury, K.; Capenberghs, S.; Martins, J. C.; Duprez, F. E.; Madder, A. *Angew. Chemie - Int. Ed.* 2013, *52* (50), 13261–13264.

165. Pfeifer, S.; Zarafshani, Z.; Badi, N.; Lutz, J. F. *J. Am. Chem. Soc.* 2009, *131* (26), 9195–9197.

166. Yan, J.-J.; Wang, D.; Wu, D.-C.; You, Y.-Z. *Chem. Commun. (Camb).* 2013, *49* (54), 6057–6059.

167. Minoda, M.; Sawamoto, M.; Higashimura, T. *Macromolecules* 1990, *23* (23), 4889–4895.

168. Satoh, K.; Ozawa, S.; Mizutani, M.; Nagai, K.; Kamigaito, M. *Nat. Commun.* 2010, *1*, 6.

169. Kakuchi, R.; Zamfir, M.; Lutz, J.-F.; Theato, P. *Macromol. Rapid Commun.* 2012, *33* (1), 54–60.

170. Pfeifer, S.; Lutz, J. F. *Chem. - A Eur. J.* 2008, *14* (35), 10949–10957.

171. Schmidt, B. V. K. J.; Fechler, N.; Falkenhagen, J.; Lutz, J.-F. *Nat. Chem.* 2011, *3* (3), 234–238.

172. Delduc, P.; Tailhan, C.; Zard, S. Z. *J. Chem. Soc. Chem. Commun.* 1988, *1988* (4), 308.

173. Chen, M.; Ghiggino, K. P.; Mau, A. W. H.; Rizzardo, E.; Sasse, W. H. F.; Thang, S. H.; Wilson, G. J. *Macromolecules* 2004, *37* (15), 5479–5481.

174. Sasso, B.; Dobinson, M.; Hodge, P. *Macromolecules* 2010, *43* (18), 7453–7464.

175. Henry, S. M.; Convertine, A. J.; Benoit, D. S. W.; Hoffman, A. S.; Stayton, P. S. *Bioconjug. Chem.* 2009, *20* (6), 1122–1128.

176. Houshyar, S.; Keddie, D. J.; Moad, G.; Mulder, R. J.; Saubern, S.; Tsanaktsidis, J. *Polym. Chem.* 2012, *3* (7), 1879.

177. Zamfir, M.; Lutz, J.-F. *Nat. Commun.* 2012, *3* (18), 1138.

178. Pfeifer, S.; Lutz, J. F. *J. Am. Chem. Soc.* 2007, *129* (31), 9542–9543.

179. Vandenbergh, J.; Reekmans, G.; Adriaensens, P.; Junkers, T. *Chem. Commun. (Camb).* 2013, *49* (88), 10358–10360.

180. Tong, X.; Guo, B.; Huang, Y. *Chem. Commun. (Camb).* 2011, *47* (5), 1455–1457.

181. Vandenbergh, J.; Reekmans, G.; Adriaensens, P.; Junkers, T. *Chem. Commun. (Camb).* 2013, *49* (88), 10358–10360.

182. Soejima, T.; Satoh, K.; Kamigaito, M. *J. Am. Chem. Soc.* 2016, *138* (3), 944–954.

183. Moatsou, D.; Hansell, C. F.; O'Reilly, R. K. *Chem. Sci.* 2014, *5* (6), 2246–2250.

184. Ashida, R.; Painter, P.; Larsen, J. W. *Energy and Fuels* 2005, *19* (5), 1954–1961.

185. Leibler, L. *Macromolecules* 1980, *13* (10), 1602–1617.

186. Matsen, M. *J. Phys. Condens. Matter* 2002, *14* (2), 21–47.

187. Bates, F. S.; Fredrickson, G. H. *Annu. Rev. Phys. Chem.* 1990, *41* (1), 525–557.

188. Smart, T.; Lomas, H.; Massignani, M.; Flores-Merino, M. V.; Perez, L. R.; Battaglia, G. *Nano Today* 2008, *3* (3–4), 38–46.

189. Bates, C. M.; Bates, F. S. *Macromolecules* 2017, *50* (1), 3–22.

190. Bates, F. S.; Fredrickson, G. H. *Phys. Today* 1999, *52* (2), 32–38.

191. Ciach, a.; Pękalski, J.; Góźdź, W. T. *Soft Matter* 2013, *9* (27), 6301.

192. Cochran, E. W.; Garcia-Cervera, C. J.; Fredrickson, G. H. *Macromolecules* 2006, *39* (7), 2449–2451.

193. Matsen, M. W. *Eur. Phys. J. E* 2009, *30* (4), 361–369.

194. Matsen, M.; Bates, F. *Macromolecules* 1996, *29* (23), 7641–7644.

195. Bates, F. S.; Hillmyer, M. a.; Lodge, T. P.; Bates, C. M.; Delaney, K. T.; Fredrickson, G. H. *Science (80-.).* 2012, *336* (6080), 434–440.

196. Christodoulou, S.; Driva, P.; Iatrou, H.; Hadjichristidis, N. *Macromolecules* 2008, *41* (7), 2607–2615.

197. Georgopanos, P.; Lo, T.-Y.; Ho, R.-M.; Avgeropoulos, A. *Polym. Chem.* 2017, *8* (5), 843–850.

198. Wijayasekara, D. B.; Huang, T.; Richardson, J. M.; Knauss, D. M.; Bailey, T. S. *Macromolecules* 2016, *49* (2), 595–608.

199. Iatrou, H.; Hadjichristidis, N.; Meier, G.; Frielinghaus, H.; Monkenbusch, M. *Macromolecules* 2002, *35* (14), 5426–5437.

200. Iatrou, H.; Willner, L.; Hadjichristidis, N.; Halperin, A.; Richter, D. *Macromolecules* 1996, *29* (2), 581–591.

201. Zhu, Y.; Gido, S. P.; Moshakou, M.; Iatrou, H.; Hadjichristidis, N.; Park, S.; Chang, T. *Macromolecules* 2003, *36* (15), 5719–5724.

202. Zheng, W.; Wang, Z. G. *Macromolecules* 1995, *28* (21), 7215–7223.

203. Ungar, G.; Tschierske, C.; Abetz, V.; Holyst, R.; Bates, M. A.; Liu, F.; Prehm, M.; Kieffer, R.; Zeng, X.; Walker, M.; Glettner, B.; Zywocinski, A. *Adv. Funct. Mater.* 2011, *21* (7), 1296–1323.

204. Lecommandoux, S.; Borsali, R.; Schappacher, M.; Deffieux, A.; Narayanan, T.; Rochas, C. *Macromolecules* 2004, *37* (5), 1843–1848.

205. Meuler, A. J.; Hillmyer, M. a.; Bates, F. S. *Macromolecules* 2009, *42* (19), 7221–7250.

206. Dair, B. J.; Avgeropoulos, A.; Hadjichristidis, N.; Thomas, E. L. *J. Mater. Sci.* 2000, *35* (20), 5207–5213.

207. Dair, B. J.; Honeker, C. C.; Alward, D. B.; Avgeropoulos, A.; Hadjichristidis, N.; Fetters, L. J.; Capel, M.; Thomas, E. L. *Macromolecules* 1999, *32* (24), 8145–8152.

208. Yang, X.; Loos, J. *Macromolecules* 2007, *40* (5), 1353–1362.

209. Crossland, E. J. W.; Nedelcu, M.; Ducati, C.; Ludwigs, S.; Hillmyer, M. A.; Steiner, U.; Snaith, H. J. *Nano Lett.* 2009, *9* (8), 2813–2819.

210. Crossland, E. J. W.; Kamperman, M.; Nedelcu, M.; Ducati, C.; Wiesner, U.; Smilgies, D. M.; Toombes, G. E. S.; Hillmyer, M. A.; Ludwigs, S.; Steiner, U.; Snaith, H. J. *Nano Lett.* 2009, *9* (8), 2807–2812.

211. Oey, C. C.; Djurišić, a B.; Wang, H.; Man, K. K. Y.; Chan, W. K.; Xie, M. H.; Leung, Y. H.; Pandey, a; Nunzi, J.-M.; Chui, P. C. *Nanotechnology* 2006, *17* (3), 706–713.

212. Wang, H.; Oey, C. C.; Djurišić, A. B.; Xie, M. H.; Leung, Y. H.; Man, K. K. Y.; Chan, W. K.; Pandey, A.; Nunzi, J.-M.; Chui, P. C. *Appl. Phys. Lett.* 2005, *87* (2), 023507.

213. Shefelbine, T. A.; Vigild, M. E.; Matsen, M. W.; Hajduk, D. A.; Hillmyer, M. A.; Cussler, E. L.; Bates, F. S. *J. Am. Chem. Soc.* 1999, *121* (37), 8457–8465.

214. Yang, S. Y.; Ryu, I.; Kim, H. Y.; Kim, J. K.; Jang, S. K.; Russell, T. P. *Adv. Mater.* 2006, *18* (6), 709–712.

215. Phillip, W. A.; Rzayev, J.; Hillmyer, M. A.; Cussler, E. L. *J. Memb. Sci.* 2006, *286* (1–2), 144–152.

216. Phillip, W. A.; Amendt, M.; ONeill, B.; Chen, L.; Hillmyer, M. A.; Cussler, E. L. *ACS Appl. Mater. Interfaces* 2009, *1* (2), 472–480.

217. Ertem, S. P.; Caire, B. R.; Tsai, T.; Zeng, D.; Vandiver, M. A.; Kusoglu, A.; Seifert, S.; Hayward, R. C.; Weber, A. Z.; Herring, A. M.; Coughlin, E. B.; Liberatore, M. W. 2017, 612–622.

218. Cho, B.K.; Jain, A.; Gruner, S. M.; Wiesner, U. *Science (80-.).* 2004, *305* (5690), 1598–1601.

219. Zhang, W.; Liu, Y.; Jackson, A. C.; Savage, A. M.; Ertem, S. P.; Tsai, T.; Seifert, S.; Beyer, F. L.; Liberatore, M. W.; Herring, A. M.; Coughlin, E. B. 2016.

220. Lin, S. Y.; Fleming, J. G.; Hetherington, D. L.; Smith, B. K.; Biswas, R.; Ho, K. M.; Sigalas, M. M.; Zubrzycki, W.; Kurtz, S. R.; Bur, J. *Nature* 1998, *394* (6690), 251–253.

221. Maldovan, M.; Thomas, E. L.; Article, P.; Maldovan, M.; Thomas, E. L. *Nat. Mater.* 2004, *3* (9), 593–600.

222. Breiner, U.; Krappe, U.; Jakob, T.; Abetz, V.; Stadler, R. *Polym. Bull.* 1998, *40* (2–3), 219–226.

223. Breiner, U.; Krappe, U.; Stadler, R. *Macromol. Rapid Commun.* 1996, *17* (8), 567–575.

224. Breiner, U.; Krappe, U.; Abetz, V.; Stadler, R. *Macromol. Chem. Phys.* 1997, *198* (4), 1051–1083.

225. Stadler, R.; Auschra, C.; Beckmann, J.; Krappe, U.; Voigt-Martin, I.; Leibler, L. *Macromolecules* 1995, *28*, 3080–3091.

226. Breiner, U.; Krappe, U.; Thomas, E. L.; Stadler, R. *Macromolecules* 1998, *31* (96), 135–141.

227. Elbs, H.; Abetz, V.; Hadziioannou, G.; Drummer, C.; Krausch, G. *Macromolecules* 2001, *34* (23), 7917–7919.

228. Park, C.; Yoon, J.; Thomas, E. L. *Polymer (Guildf).* 2003, *44* (22), 6725–6760.

229. Elbs, H.; Drummer, C.; Abetz, V.; Krausch, G. *Macromolecules* 2002, *35* (14), 5570–5577.

230. Ludwigs, S.; Schmidt, K.; Stafford, C. M.; Amis, E. J.; Fasolka, M. J.; Karim, A.; Magerle, R.; Krausch, G. *Macromolecules* 2005, *38* (5), 1850–1858.

231. Balsamo, V.; von Gyldenfeldt, F.; Stadler, R. *Macromolecules* 1999, *32* (4), 1226–1232.

232. Bailey, T. S.; Pham, H. D.; Bates, F. S. *Macromolecules* 2001, *34* (20), 6994–7008.

233. Epps, T. H.; Bailey, T. S.; Waletzko, R.; Bates, F. S. *Macromolecules* 2003, *36* (8), 2873–2881.

234. Bailey, T. S.; Hardy, C. M.; Epps, T. H.; Bates, F. S. *Macromolecules* 2002, *35* (18), 7007–7017.

235. Tang, P.; Qiu, F.; Zhang, H.; Yang, Y. *Phys. Rev. E - Stat. Nonlinear, Soft Matter Phys.* 2004, *69* (3 1), 1–8.

236. Guo, Z.; Zhang, G.; Qiu, F.; Zhang, H.; Yang, Y.; Shi, A. C. *Phys. Rev. Lett.* 2008, *101* (2), 1–4.

237. Nagpal, U.; Detcheverry, F. a.; Nealey, P. F.; De Pablo, J. J. *Macromolecules* 2011, *44* (13), 5490–5497.

238. Li, W.; Xu, Y.; Zhang, G.; Qiu, F.; Yang, Y.; Shi, A. C. *J. Chem. Phys.* 2010, *133* (6).

239. Liu, M.; Li, W.; Qiu, F.; Shi, A. C. *Macromolecules* 2012, *45* (23), 9522–9530.

240. Milner, S. T. *Macromolecules* 1994, *27* (8), 2333–2335.

241. Floudas, G; Hadjichristidis, N.; Tselikas, T.; Erukhimovich, I. *Macomolecules* 1997, *30*, 3090–3096.

242. Grason, G. M.; Kamien, R. D. *Macromolecules* 2004, *37* (19), 7371–7380.

243. Huang, C. I.; Yu, H. T. *Polymer (Guildf).* 2007, *48* (15), 4537–4546.

244. Hayashida, K.; Saito, N.; Arai, S.; Takano, A.; Tanaka, N.; Matsushita, Y. *Macromolecules* 2007, *40* (10), 3695–3699.

245. Bohbot-Raviv, Y.; Wang, Z. *Phys. Rev. Lett.* 2000, *85*, 3428–3431.

246. Gemma, T.; Hatano, A.; Dotera, T. *Macromolecules* 2002, *35* (8), 3225–3237.

247. Ueda, M. *Prog. Polym. Sci.* 1999, *24* (5), 699–730.

248. Pispas, S.; Avgeropoulos, A.; Hadjichristidis, N.; Roovers, J. *J. Polym. Sci. Part B Polym. Phys.* 1999, *37*, 1329–1335.

249. Tselikas, Y.; Iatrou, H.; Hadjichristidis, N.; Liang, K. S.; Mohanty, K.; Lohse, D. J. *J. Chem. Phys.* 1996, *105* (6), 2456.

250. Tselikas, Y.; Hadjichristidis, N.; Lescanec, R. L.; Honeker, C. C.; Wohlgemuth, M.; Thomas, E. L. *Macromolecules* 1996, *29* (10), 3390–3396.

251. Takano, A.; Wada, S.; Sato, S.; Araki, T.; Hirahara, K.; Kazama, T.; Kawahara, S.; Isono, Y.; Ohno, A.; Tanaka, N.; Matsushita, Y. *Macromolecules* 2004, *37* (26), 9941–9946.

252. Matsushita, Y.; Hayashida, K.; Dotera, T.; Takano, A. *J. Physics-Condensed Matter* 2011, *23* (28), 284111.

253. Rho, Y.; Kim, C.; Higashihara, T.; Jin, S.; Jung, J.; Shin, T. J.; Hirao, A.; Ree, M. *ACS Macro Lett.* 2013, *2* (10), 849–855.

254. Okamoto, S.; Hasegawa, H.; Hashimoto, T.; Fujimoto, T.; Zhang, H.; Kazama, T.; Takano, A.; Isono, Y. *Polymer (Guildf).* 1997, *38* (21), 5275–5281.

255. Sioula, S.; Hadjichristidis, N.; Thomas, E. L. *Macromolecules* 1998, *31* (97), 5272–5277.

256. Yamauchi, K.; Takahashi, K.; Hasegawa, H.; Iatrou, H.; Hadjichristidis, N.; Kaneko, T.; Nishikawa, Y.; Jinnai, H.; Matsui, T.; Nishioka, H.; Shimizu, M.; Furukawa, H. *Macromolecules* 2003, *36* (19), 6962–6966.

257. Huckstadt, H.; Gopfert, A.; Abetz, V. *Macromol. Chem. Phys.* 2000, *201* (3), 296–307.

258. Takano, A.; Kawashima, W.; Noro, A.; Isono, Y.; Tanaka, N.; Dotera, T.; Matsushita, Y. *J. Polym. Sci. Part B Polym. Phys.* 2005, *43* (18), 2427–2432.

259. Kakuchi, R.; Zamfir, M.; Lutz, J. F.; Theato, P. *Macromol. Rapid Commun.* 2012, *33* (1), 54–60.

260. Mahou, R.; Wandrey, C. *Polymers (Basel).* 2012, *4* (1), 561–589.

261. Moad, G.; Chong, Y. K.; Postma, A.; Rizzardo, E.; Thang, S. H. 2005, *46*, 8458–8468.

262. Mutlu, H.; Lutz, J. F. *Angew. Chemie - Int. Ed.* 2014, *53* (48), 13010–13019.

263. Lutz, J. F. *Acc. Chem. Res.* 2013, *46* (11), 2696–2705.

264. Colquhoun, H.; Lutz, J.-F. *Nat. Chem.* 2014, *6* (June), 455–456.

265. Lutz, J.-F.; Ouchi, M.; Liu, D. R.; Sawamoto, M. *Science (80-.).* 2013, *341* (6146), 1238149–1238149.

266. Matsuda, M.; Satoh, K.; Kamigaito, M. 2013.

267. Hisano, M.; Takeda, K.; Takashima, T.; Jin, Z.; Shiibashi, A.; Matsumoto, A. 2013.

268. Liu, B.; Wang, X.; Pan, Y.; Lin, F.; Wu, C.; Qu, J.; Luo, Y.; Cui, D. 2014.

269. Ovitt, T. M.; Coates, G. W.; V, C. U.; York, N. 1999, No. 16, 4072–4073.

270. Kramer, J. W.; Treitler, D. S.; Dunn, E. W.; Castro, P. M.; Roisnel, T.; Thomas, C. M.; Coates, G. W. 2009, No. Figure 1, 16042–16044.

271. Few, C. S.; Wagener, K. B.; Thompson, D. L. 123–132.

272. Li, Z.; Li, L.; Deng, X.; Zhang, L.; Dong, B.; Du, F.; Li, Z. 2012.

273. Zhang, J.; Matta, M. E.; Hillmyer, M. A. 2012, 19–23.

274. Article, E.; Moatsou, D.; Hansell, C. F.; Reilly, R. K. O. 2014, 2246–2250.

275. Minoda, M.; Sawamoto, M.; Higashimura, T. *Macromolecules* 1990, *23* (23), 4889–4895.

276. Tong, X.; Guo, B.; Huang, Y. 2011, 1455–1457.

277. Chem, P.; Houshyar, S.; Keddie, D. J.; Moad, G.; Mulder, R. J.; Saubern, S.; Tsanaktsidis, J. 2012, 1879–1889.

278. Berthet, M.; Zarafshani, Z.; Pfeifer, S. 2010, 44–50.

279. Yu, T.; Bai, J. Z.; Guan, Z. 2009, 1097–1101.

280. Chen, Y.; Guan, Z. 2010, 4577–4579.

281. Sumerlin, B. S.; Vogt, A. P. *Macromolecules* 2010, *43* (1), 1–13.

282. Badi, N. 2009, 3383–3390.

283. Deng, X. X.; Li, L.; Li, Z. L.; Lv, A.; Du, F. S.; Li, Z. C. *ACS Macro Lett.* 2012, *1* (11), 1300–1303.

284. Online, V. A.; Lv, A.; Deng, X.; Li, L.; Li, Z.; Wang, Y.; Du, F.; Li, Z. 2013, 3659–3662.

285. Reaction, T.; Solleder, S. C.; Meier, M. A. R. 2014, 711–714.

286. Ida, S.; Terashima, T.; Ouchi, M.; Sawamoto, M. *J. Am. Chem. Soc.* 2009, *131* (31), 10808–10809.

287. Ida, S.; Ouchi, M.; Sawamoto, M. 2010, 14748–14750.

288. Brummelhuis, N. *Polym. Chem.* 2015, *6* (5), 654–667.

289. Pfeifer, S.; Zarafshani, Z.; Badi, N.; Lutz, J. F. *J. Am. Chem. Soc.* 2009, *131* (26), 9195–9197.

290. Hartmann, B. L.; Bo, H. G. 2009, 3425–3431.

291. Charles, L.; Verchin, C.; Lutz, J.; Roy, R. K.; Meszynska, A. 2015, No. May, 1–8.

292. Lutz, J. *Angew. Chemie Int. Ed.* 2007, *46* (7), 1018–1025.

293. Fournier, D.; Hoogenboom, R.; Schubert, U. S. *Chem. Soc. Rev.* 2007, *36* (8), 1369.

294. Zhang, C.; Yang, Y.; He, J. *Macromolecules* 2013, *46* (10), 3985–3994.

295. Soeriyadi, A. H.; Boyer, C.; Nyström, F.; Zetterlund, P. B.; Whittaker, M. R. *J. Am. Chem. Soc.* 2011, *133* (29), 11128–11131.

296. Article, E.; Anastasaki, A.; Nikolaou, V.; Pappas, G. S.; Zhang, Q.; Wan, C.; Wilson, P.; Davis, T. P.; Whittaker, R.; Haddleton, D. M. *Chem. Sci.* 2014, *5*, 3536–3542.

297. Zhang, W.; Sun, Z.; Jiang, Y.; Liu, X.; Gupta, R.; Russell, T. P.; Coughlin, E. B. 2017, 1–7.

298. Padmanabhan, P.; Martinez-Veracoechea, F. J.; Araque, J. C.; Escobedo, F. A. *J. Chem. Phys.* 2012, *136* (23).

299. Gavrilov, A. A.; Kudryavtsev, Y. V.; Chertovich, A. V. *J. Chem. Phys.* 2013, *139* (22).

300. Groot, R. D.; Warren, P. B. *J. Chem. Phys.* 1997, *107* (11), 4423–4435.

301. Bjorken, J. D.; Brodsky, S. J. *Phys. Rev. D* 1970, *1* (5), 1416–1420.

302. Zheng, W.; Wang, Z. G. Macromolecules 1995, 28 (21), 7215–7223.

303. Liu, M.; Li, W.; Qiu, F.; Shi, A. C. Macromolecules 2012, 45 (23), 9522–9530.

304. Huckstadt, H.; Gopfert, A.; Abetz, V. Polymer (Guildf). 2000, 41 (26), 9089–9094.

305. Gido, S. P.; Schwark, D. W.; Thomas, E. L.; do Carmo Gonçalves, M. Macromolecules 1993, 26 (10), 2636–2640.

306. Matsushita, Y.; Tamura, M.; Noda, I. Macromolecules 1994, 27 (13), 3680–3682.

307. Mogi, Y.; Mori, K.; Matsushita, Y.; Noda, I. Macromolecules 1992, 25, 5412.

308. Radlauer, M. R.; Sinturel, C.; Asai, Y.; Arora, A.; Bates, F. S.; Dorfman, K. D.; Hillmyer, M. A. Macromolecules 2017, 50 (1), 446–458.

309. Bailey, T. S.; Pham, H. D.; Bates, F. S. Macromolecules 2001, 34 (20), 6994–7008.

310. Bailey, T. S.; Hardy, C. M.; Epps, T. H.; Bates, F. S. Macromolecules 2002, 35 (18), 7007–7017.

311. Mogi, Y.; Nomura, M.; Kotsuji, H.; Ohnishi, K.; Matsushita, Y.; Noda, I. Macromolecules 1994, 27 (23), 6755–6760.

312. Stadler, R.; Auschra, C.; Beckmann, J.; Krappe, U.; Voigt-Martin, I.; Leibler, L. Macromolecules 1995, 28, 3080–3091.

313. Breiner, U.; Krappe, U.; Stadler, R. Macromol. Rapid Commun. 1996, 17 (8), 567–575.

314. Balsamo, V.; von Gyldenfeldt, F.; Stadler, R. Macromolecules 1999, 32 (4), 1226–1232.

315. Krappe, U.; Stadler, R.; Voigt-Martin, I. Macromolecules 1995, 28, 4558–4561.

316. Tang, P.; Qiu, F.; Zhang, H.; Yang, Y. J. Phys. Chem. B 2004, 108 (24), 8434–8438.

317. Guo, Z.; Zhang, G.; Qiu, F.; Zhang, H.; Yang, Y.; Shi, A. C. Phys. Rev. Lett. 2008, 101 (2), 1–4.

318. Qin, J.; Bates, F. S.; Morse, D. C. Macromolecules 2010, 43 (11), 5128–5136.

319. Nagpal, U.; Detcheverry, F. a.; Nealey, P. F.; De Pablo, J. J. Macromolecules 2011, 44 (13), 5490–5497.

320. Kim, H. C.; Park, S. M.; Hinsberg, W. D.; Division, I. R. Chem. Rev. 2010, 110 (1), 146–177.

321. Olson, D. A.; Chen, L.; Hillmyer, M. A. Chem. Mater. 2008, 20 (3), 869–890.

322. Sinturel, C.; Bates, F. S.; Hillmyer, M. A. ACS Macro Lett. 2015, 4 (9), 1044–1050.

323. Kennemur, J. G.; Yao, L.; Bates, F. S.; Hillmyer, M. A. Macromolecules 2014, 47 (4), 1411–1418.

324. Jeong, G.; Yu, D. M.; Mapas, J. K. D.; Sun, Z.; Rzayev, J.; Russell, T. P. Macromolecules 2017, 50 (18), 7148–7154.

325. Yu, D. M.; Mapas, J. K. D.; Kim, H.; Choi, J.; Ribbe, A. E.; Rzayev, J.; Russell, T. P. Macromolecules 2018, 51 (3), 1031–1040.

326. Shi, W.; Tateishi, Y.; Li, W.; Hawker, C. J.; Fredrickson, G. H.; Kramer, E. J. ACS Macro Lett. 2015, 4 (11), 1287–1292.

327. Otsuka, I.; Zhang, Y.; Isono, T.; Rochas, C.; Kakuchi, T.; Satoh, T.; Borsali, R. Macromolecules 2015, 48 (5), 1509–1517.

328. Sweat, D. P.; Kim, M.; Larson, S. R.; Choi, J. W.; Choo, Y.; Osuji, C. O.; Gopalan, P. Macromolecules 2014, 47 (19), 6687–6696.

329. Kennemur, J. G.; Hillmyer, M. a; Bates, F. S. Macromolecules 2012, 45 (17), 7228–7236.

330. Ellison, C. J.; Mundra, M. K.; Torkelson, J. M. Macromolecules 2005, 38 (5), 1767–1778.

331. Bates, C. M.; Bates, F. S. Macromolecules 2017, 50 (1), 3–22.

332. Lu, S.; Liu, T.; Ke, L.; Ma, D. G.; Chua, S. J.; Huang, W. Macromolecules 2005, 38 (20), 8494–8502.

333. Topham, P. D.; Parnell, A. J.; Hiorns, R. C. J. Polym. Sci. Part B Polym. Phys. 2011, 49 (16), 1131–1156.

334. Kreuer, K.-D. Chem. Mater. 2013, 26 (1), 361–380.

335. Moad, G.; Chong, Y. K.; Postma, A.; Rizzardo, E.; Thang, S. H. 2005, *46*, 8458–8468.